Electrochemical concentration gradients in Deep Eutectic Solvents

Thesis submitted for the degree of

Doctor of Philosophy

at the University of Leicester

by

Christopher John Zaleski (MSc) (Leicester)

Department of Chemistry

University of Leicester

2015

None of this work has been submitted for another degree in this or any other University.

Christopher John Zaleski

.....

Electrochemical concentration gradients in Deep Eutectic Solvents

Christopher John Zaleski

University of Leicester

2015

Abstract

Concentration gradients present in the solution during the redox chemistry of selected metals and conducting polymer (poly(3,4ethylenedioxythiophene) (PEDOT)) films redox cycled in Deep Eutectic Solvents (DES) were observed for the first time through the application of the Probe Beam Deflection (PBD) technique combined with the Electrochemical Quartz Crystal Microbalance (EQCM). Suitability of choline chloride (ChCl) based DES for applications as electrolytes in PEDOT based charge storage devices has also been investigated using EQCM. The combination of carefully optimized experimental parameters (temporally extended chronoamperometry and slow scan rate voltammetry) with modified design of the instrument (reduced probe's distance of approach) allowed for *in-situ* observations of electrochemically induced concentration gradients in DES based systems. During the studies of electroactive polymer films, complete determination of mobile species transfers in PEDOT/Ethaline and PEDOT/Propaline systems has been achieved. The application of PBD-EQCM technique in studies of metal electrodeposition from DES allowed for monitoring metal speciation in dynamic and quantitative fashion. EQCM study of ChCl based DES indicated Ethaline as the most promising potential electrolyte for PEDOT based charge storage devices. Additionally, an unusual mass exchange process has been detected in PEDOT/Propaline and PEDOT/Acetaline processes.

This work has shown a novel, affordable and non-invasive route for observation of electrode/electrolyte interface processes in DES. The experimental protocol developed can potentially be implemented in further studies of DES as well as Ionic Liquids.

Acknowledgments

First and foremost I would like to thank my supervisors, Prof. Karl Ryder and Prof. Robert Hillman for all of their help and support over the past 4 years.

I would also like to thank both past and present members of the Ionic Liquids group and in particular, Prof. Andrew Abbott, Dr Gero Frisch, Dr Emma Smith, Dr Andrew Ballantyne, Dr Rachel Sapstead, Dr Virginia Ferreira, Dr Alex Goddard, Dr William Wise, Dr Luka Wright and Dr Robert Harris, as well as the workshop team (Mr Praful Chauhan and Mr Carl Schieferstein) for complying with my various and endless demands.

I thank my wife Regina, who has helped me throughout my master's and doctoral studies and I thank my parents for the tremendous amount of effort in bringing me up.

Contents

Chapter I

Introduction

1.1 Electrochemistry

All matter is largely, if not entirely electrical in its nature. Thus, one can reason that all chemistry is in fact electrochemistry since all intermolecular interactions are governed by the presence and/or interactions of electrical charges.[1] However, such broad classification is inevitably very vague. On a more specific level, electrochemistry deals with the interactions of chemical systems and electricity. Electrochemical reactions are those that occur from application or result in formation of electrical charge. Faraday laid foundations of this discipline with his ground-breaking experiments relating mass and charge during electrodeposition of silver. He was the first one to prove the dependency of the electrochemically induced mass transport on the electron flux summarized in the 1^{st} and 2^{nd} law of electrolysis.[1] Electrochemical experiments allow for elucidation of kinetics and thermodynamics of the electrode/electrolyte systems. Electron transfer process is the core of any electrochemical reaction. Full understanding of this process requires the thorough analysis of the electrode/electrolyte interface. This interface is usually composed of the liquid electrolyte, solid electrode and/or adsorbed layer adhered to the electrode surface. This solid/liquid interface is of paramount importance for many physico-chemical processes such as electrodeposition, chemisorption, catalysis and biological cell transport.[2]

1.2 Materials

1.2.1 Conducting polymers

1.2.1.1 Origins

Once regarded as a mere laboratory curiosity, conducting polymers gradually became an important industrial product with a variety of applications. Traditional electrode materials (like Pb^0/Pb^{2+} in lead – acid battery) suffer from problems arising from their non-elastic nature. Conducting polymers offer the exciting possibility of overcoming these issues due to the polymers' elasticity.

Polymeric materials have historically been used as insulators. 1977 brought the first reports, of novel polymeric material, doped polyacetylene (PA) which displayed frequency dependent electrical transport.[3] This spurred an avalanche of research devoted to these materials.[4] Further investigations revealed that the origin of this unusual feature lay in the conjugated π systems formed through an overlap of carbon sp_2 (p_z) orbital which is a product of alternate single and double bonds. A notable exception from this general rule is polyaniline (PANI) where nitrogen p_z orbitals and benzene rings form the conjugation path. Intensive research resulted in developments (among others), polypyrrole and polythiophene families of polymers and a wide range of their derivatives (see figure 1).[5]

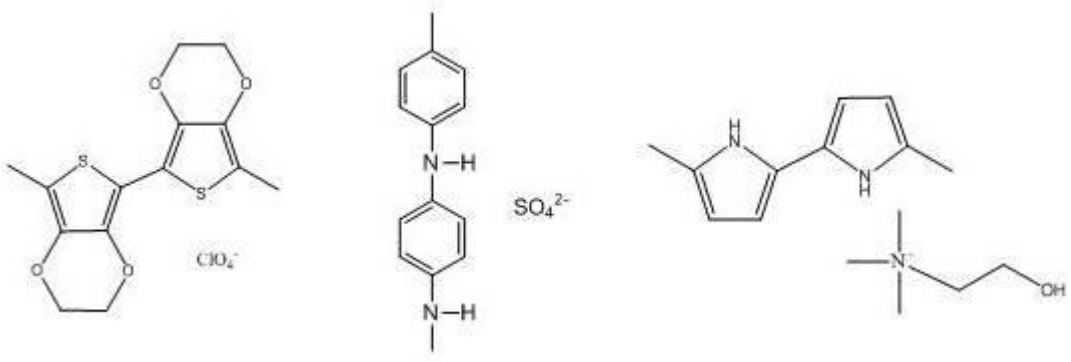

Figure 1. Selected examples of conducting polymers. From left to right: oxidised (p-doped) PEDOT doped with perchlorate anion, oxidised (p-doped) PANI doped with sulphate anion and reduced (n-doped) PPy doped with choline cation.

1.2.1.2 Electrochemistry

Redox reactions in organic materials involve both electronic and atomic motions. These processes include transport and transfer of charge, formation and dissociation of excitons and energy transfer. Generic electrical conductivity of conducting polymers is based on the presence of polarons, bi-polarons and solitons. The concept of polaron was initially developed by Holsetin et al.[6] Electron – lattice interactions result in the displacement of lattice particles forming new equilibrium conditions. Formed displacements act as wells for electrons and the electron filled well is termed the polaron. This term is usually reserved for singly (e^-) charged species with ½ spin, while doubly charged ($2e^-$) spinless species are termed bipolarons. The third species are solitons (these exist in two forms – e^- with no spin or neutral with ½ spin). Presence and characteristics of spins in these polymers was confirmed by EPR experiments**.** Species formation results in an overlap of the conduction and valence bands and formation of an organic semi-conductor. Unlike in metals where valence and conduction bands form a single overlapping band, conducting polymers require doping to form new energy levels, which act as a bridge between the valence and conduction bands. Therefore, CP are closer in their character to highly doped semi-conductors (like Boron doped Silica) than to metallic conductors like silver or copper. Band overlap is graphically presented in figure 2.

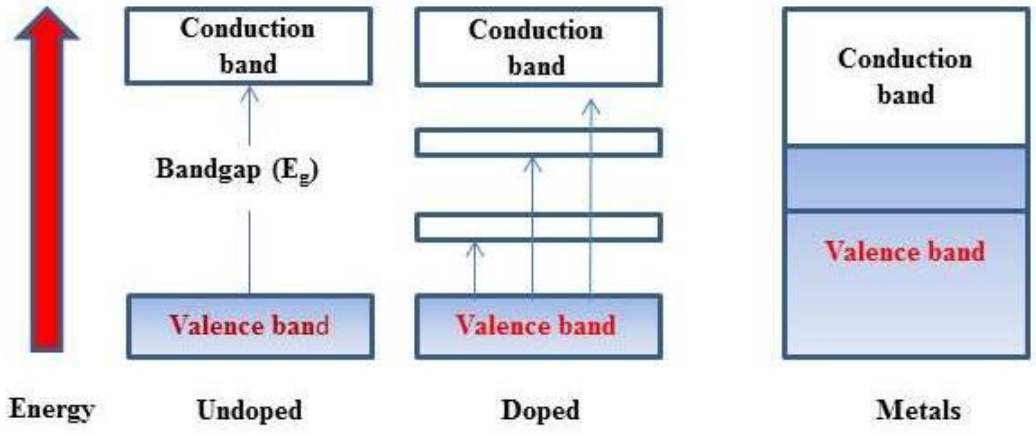

Figure 2. Electric transition of conducting polymers in undoped (left panel) and doped (centre panel) states versus metals (right panel).

Polarons, bi-polarons and solitons are only capable of providing limited electric conductivity but no significant charge storage and therefore pristine CP are still considered to be in an insulating state. Rapid change occurs during the process colloquially known as doping. Doping process is the insertion of ions: n-type (electron donating) or p-type (electron accepting) into the porous polymer film. The conductivity level rises with the doping level and at the high doping level the insulator – metal transition (IMT) occurs. This is characterized not only by the significant (circa 10 fold) rise in DC conductivity [4] but also by the polymer film attaining negative dielectric constant,[7] a Drude metallic response[8] as well as temperature – independent Pauli susceptibility. Linear correlation between thermoelectric power and temperature had also been reported.[4] Examples of I_2 doped PA reaching σ_{dc} of lead and HF_6 doped PPy having σ_{dc} of 100 – 400 S over a wide range of temperatures are not uncommon.[4]

However, till date no conducting polymer can match the conductivity of Ag (σ_{dc}= 10^5 S) or Cu (σ_{dc}= 10^5) and the electrochemical performance of these materials vary widely depending on the type of material, processing route (chemical or electrochemical deposition), dopants used and operating conditions. Nevertheless, the large range of possible polymeric configuration, elasticity and economic prospects make CP an important and very promising industrial material. Even more importantly, apart from their ever decreasing resistance, conducting polymers offer semiconducting as well as photochromic properties. This cannot be achieved at all using traditional metallic conductors and hence it is a major driving force behind CP development as it enables fabrication of a variety of novel, switchable devices (e.g. flexible displays, photoactive windows).

Failure of currently known conducting polymers to reach conductivities of silver or copper metals may at least partially have its origin in low crystalinity levels reaching only 80 – 90 % even in the most doped form of CP films. Heterogeneous nature of the polymer films comprises highly conductive metallic ‘islands’ linked by a network of 1-D disordered regions. Inevitably, the overall conductivity of the material is limited by the least conductive (1-D regions). In this respect, CP can be treated as percolating systems like an aqueous Ag/KCl solution. However, since one polymer chain can simultaneously be a part of the metallic island and a disordered 1 D structure CP system does not have sharp boundaries. The characteristics of these ‘fuzzy’ borders between the conducting (ordered) and insulating (disordered) phases are dependent on the CP morphology. Morphology in turn is heavily dependent on the formation pathway chosen

with chemically synthesised polymers generally yielding more homogeneous materials than electro synthesized ones. Morphology has also a major impact on conductivity since the 1-D regions provide conductance purely through the phonon assisted transport while metallic islands are the dopant acceptors (and therefore sites of the percolation mechanism).[4] High frequency conductivity of doped conducting polymers has also been assigned to quantum hopping. According to this model, IMT (insulator-metal transition) occurs initially in the metallic islands through charge delocalization (hopping). Once the initial polaron, bi-polaron and solitons are formed, conduction in undoped CP takes place purely through hopping process between these states. This is followed by a subsequent transition of the entire polymer through direct tunnelling between the metallic 'islands'.

Since doping itself is an electrochemical (redox) reaction, research on conducting polymers is inexorably linked to the field of electrochemistry. Both redox polymers like polyvinylferrocene and electronically conducting polymers like PPy and PEDOT possess redox moieties and are thus able to undergo reversible redox reactions. However, as already stated, the presence of bipolarons and solitons forms only the electronic part of the overall CP conductivity. Pure electronic conductivity is limited by conjugation length (determining charge propagation along the polymer chain) and presence of π dimers providing orbital's overlap (determining charge propagation between adjacent chains). Introduction of dopants into the conducting polymer network allows them to act as bridges for electronic coupling significantly increasing conductivity. CP are able to reversibly switch between at least two redox states. It must be noted that majority of them can only switch between neutral (discharged) and positive (charged) forms. Some CP, like PEDOT were observed in reduced, neutral and oxidised form.[9,10]

Polymer chain elasticity enables it to bear deformations with low elastic energy cost. This feature allows for creation of stable energy levels within the energy bandgap (which is the gap between the valence and conduction bands). Storage of significant charge amount in CP films is only possible if some form of opposite charge compensates it – this is provided by dopants. Conducting polymers electrochemistry is usually characterized by their cyclic voltammetry signal. It is significantly different from the voltammetric signal displayed by other redox systems like metal oxides. Current signal is usually broad and displays a plateau at high potentials with no distinct redox peaks. Due to the hysteresis phenomena, there are also major differences between

first and subsequent voltammetric cycles. In this context, hysteresis is classified as structural changes in the polymer film upon repetitive ingress/egress of dopants and solvent. This results in a conspicuous separation of the anodic and cathodic peak potentials also known as "redox asymmetry". The origin of these unusual characteristics lies in the severe reorganization of the polymer film structure, changes in solvation state and mass transport (ingress and egress of dopants with simultaneous solvent transport – often in opposite direction). Due to rather low density and high porosity, these materials have high surface area. Consequently, double layer charging (capacitive current = non-Faradaic current) is present to a significant amount and it overlaps in a current signal with the electrode/electrolyte electrochemical interactions (Faradaic current).

Cyclic voltammetry is also a very useful tool in a bandgap determination (calculated as a difference between oxidation and reduction potentials). Low bandgap CP (like PEDOT or PITN) are of particular interest as this property makes them useful in charge storage (among other applications). Development of the low bandgap polymer films is based on the decrease of the lower border of the conduction band (also known as Highest Occupied Molecular Orbital) and/or increase of the upper border of the valence band (also known as Lowest Unoccupied Molecular Orbital). Unfortunately, increase of the conduction band results in the material being highly susceptible to the electron loss through oxidation. Hence, many of the low bandgap CP's like poly(isothianaphthene) (PITN) oxidize readily when exposed to the atmosphere and are therefore of little practical value.[3] Examples of some low bandgap CP are presented below in figure 3:

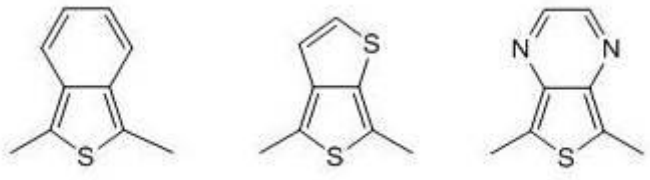

Figure 3. Selected examples of low-band gap polythiophene analogs. From left to right, poly(isothianaphthene) (PITN), thiophene ring modified PEDOT, pyrimidine ring modified PEDOT.

Regardless of the polymer type and the electrolyte used, two major processes are always associated with CP redox switching. First one is the ionic motion enforced by

the electro neutrality requirement (i.e. charge formed in the polymer through an application of the external electric field must be compensated through inclusion or expulsion of ions). Second one is the conformational change of the polymer film – this has a major impact on the solvation/desolvation process. Electric Impedance Spectra (EIS) studies conducted by Rahindramahazaka et al (among others) have confirmed that the analysed conducting polymer films are composed of two dynamic zones, namely compact and open one.[11]

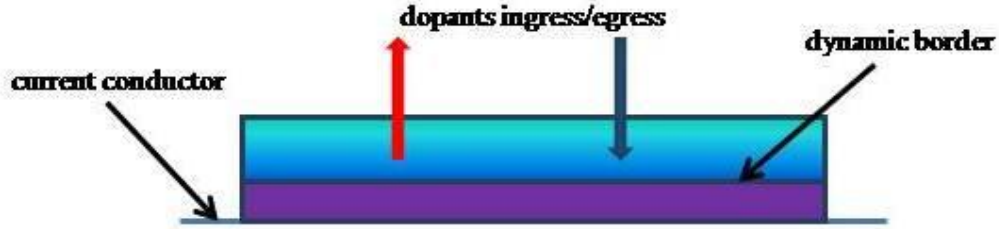

Figure 4. Graphic representation of the open and compact zones of the CP film. Red arrow indicates dopants egress, blue arrow indicates dopants ingress.

Significant effect of the CP film solvation levels on the relative sizes of compact and open zones was also observed, indicating that the zones' volumes are a dynamic quantity.

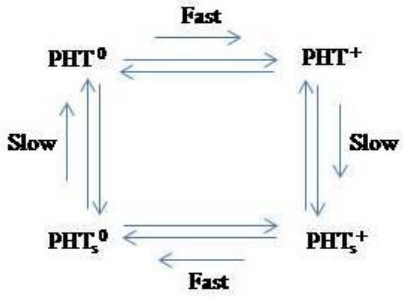

Figure 5. Scheme-of-squares model for poly(3-hexylthiophene) (PHT) film redox cycled in 0.1 M tetraethylammoniumhexafluorophosphate ($TEAPF_6$)/propylene carbonate. "0" superscript indicates film in its neutral state, "+" indicates oxidized state. "s" subscript indicates that the film is its solvated state. Horizontal vectors represent doping/undoping while the vertical ones represent solvation state changes.

Therefore, theoretical models describing CP redox switching must account for a variety of factors like capacitive and Faradaic currents, hysteresis phenomena, counterion nature, polymer film thickness, solvation type (radically different in molecular and ionic liquids), as well as type and timescale of the potential applied. Hillman et al proposed scheme of squares which offers good explanation how solvation changes influence storage and loss moduli variations in a poly(3-hexylthiophene) films redox cycled in propylene carbonate.[12]

Otero et al. proposed electrochemically simulated conformation–relaxation (ESCR) model.[13] This model correlates the direction of applied scan and its time frame with the open/compact zones proportions concluding that the compact zone growth is hindering the exchange of counterions. As it has been mentioned, doping level is the key feature in the IMT phenomenon. The conductivity/doping level relationship however is not linear but instead is a three phase process. Initially the conductivity increases sharply with the rise in doping level eventually reaching the plateau, further increase in doping results in decrease in CP conductivity.

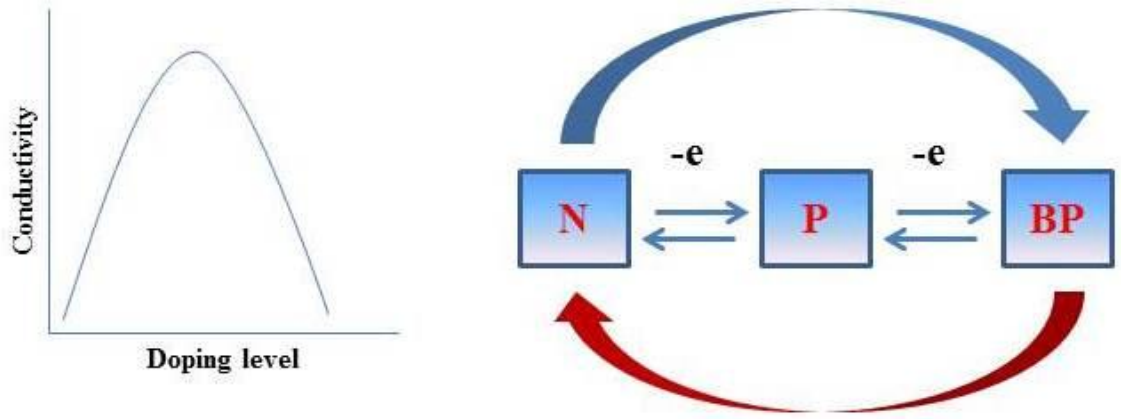

Figure 6. General model for the conductivity/doping level ratio in relation to the corresponding redox states involved (N = polymer films in its neutral state, P = polymer films in its polaronic state, BP = polymer films in its bi-polaronic state, red arrow = reduction, blue arrow = oxidation). Model is based on the behaviour displayed by polypyrrole and related molecules.

Both dopants' and polymer film natures (this broad term includes the conditions, solvent and counterions used in film electrodeposition) may induce large variations in the conductivity profile. Strikingly, in contrast to the predictions of the purely bipolaron

model, conductivity might sometimes decrease at a very high doping levels. This has been confirmed by Zotti and co-workers to originate from partial overoxidation of the CP film (which results in film's degradation) and in the case of PPy and related polymers also by the stabilization of the bipolaronic state (see Figure 6).[14]

1.2.1.3 Applications

CP family encompass a wide range of molecules with a range of applications varying from charge storage,[15,16] photovoltaic cells,[17] electro-chromic devices[18,19] and antimicrobial applications[3] to name just a few. Of particular interest in this thesis are CP applications in charge storage systems. For the sake of consistency and clarity, a brief review of charge storage processes and systems was therefore considered necessary at this point. For charge storage applications to operate, two electrodes must be connected together. A battery stores the energy mostly through Faradaic processes occurring at the electrode/electrolyte interface during the redox process. The electrode at which oxidation occurs is termed anode and the one where reduction occurs is termed cathode. In double layer capacitors charge is stored in a double layer due to the electrostatic effects (i.e. the electrical energy produced is derived from the potential difference arising from the electrical double layer between the electrolyte and electrode). CP oxidation is a process of electrons removal from the polymer backbone. Thus formed oxidised CP is then in a positively charged (p-doped) state. Addition of electrons to the neutral polymer results in the polymer reduction and formation of a negatively doped (n-doped) polymer film. Neutral film is the one in its zero charge state. Since CP films display characteristics of both electrochemical and capacitive charge storage devices, CP based charge storage systems are often called 'supercapacitors'. Different types of energy storage devices are usually quantified using Ragone plots.

These plots classify the storage devices by their available energy for an external constant active power request (i.e. device which is powered).[20] Ragone plots provide the limits of a charge storage device practical limitations as well as its optimum working energy. The desired position of supercapacitors within the Ragone plot is shown in figure 7.

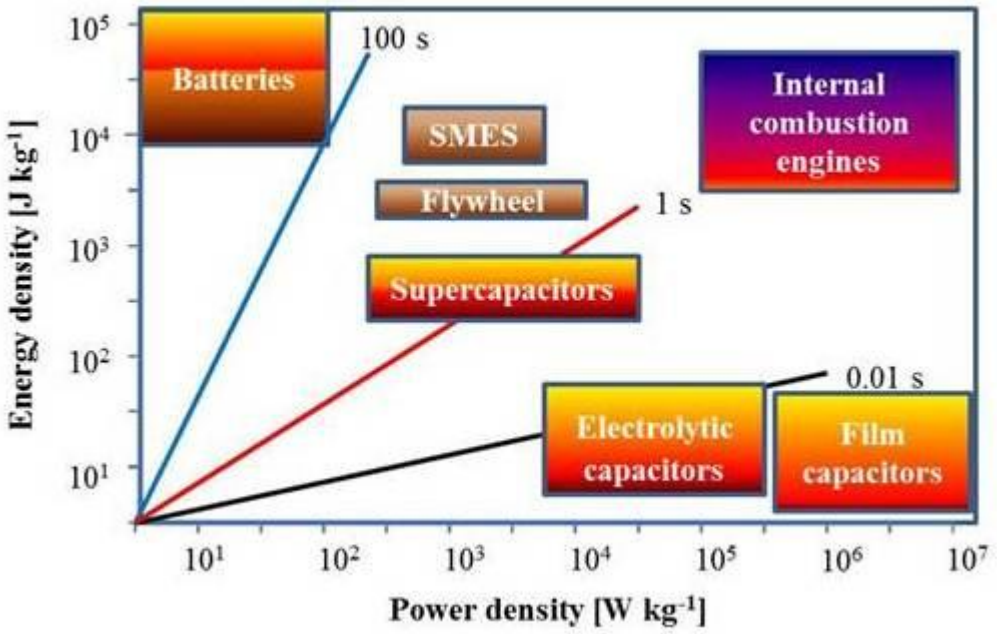

Figure 7. Ragone plot: displays available energy of a device for fixed power request. Blue, red and black lines describe typical response time for each device type. Flywheel, internal combustion engine and superconducting magnetic energy storage (SEMS) are mechanical devices. Batteries and supercapacitors are electrochemical devices. Capacitors are electrical devices.

1.2.2 Poly(3,4-ethylenedioxythiophene) remarkable properties, scientific importance and applications.

1.2.2.1 Properties and importance

Continuous development of touch screens, video displays and plastic solar cells as well as smart windows and electronic paper calls for improvements in the existing fabrication methods of transparent and flexible conductive materials. Historically, such materials were manufactured from Sn-doped indium III oxide (In_2O_3) (ITO) deposited on elastic, polymeric (usually PET) backing. This approach however suffers from serious limitations as ITO brittleness limits the coating durability. Additional concerns arise from indium metal limited availability and its salt's toxicity.[3]

Growing demand for portable systems used in a variety of civilian and military applications as well as the development of electric vehicles and charge storage facilities

for renewable energy sources prompted great interest in new generation of batteries and capacitors. The traditional metal/metal oxide or carbon based electrode materials are known to suffer from the lack of elasticity and limited capacitance (only the material's surface is used for the process of charge accumulation). Although lead-acid, nickel metal hydride and especially Li – ion based batteries are the current state of the art in charge storage technology, concerns related to these metals availability (particularly Li) as well as recycling and toxicity issues constantly grow. Additionally, lead-acid batteries have rather moderate power density due to the high density of this metal. Hence, the attention has in the recent years turned to conducting polymers (CP). PEDOT is currently (2015) widely regarded to be the most successful (in terms of industrial applications) member of the conducting polymers family.[3]

1.2.2.2 Applications in charge storage

The CP rise as a new electrode material is still hindered by these materials poor mechanical endurance and very modest stability during redox cycling. Therefore, efforts have been placed on the improvement of these properties. Frąckowiak and co-workers have reported formation of a novel electrode materials composed of PANI, PPy and PEDOT combined with multiwalled carbon nanotubes (CNTs). The electrodes were subsequently tested in solid-state supercapacitors. Among the composites tested, PEDOT/CNT displayed superior stability during the electrochemical cycling. Capacitance value of 100 F g^{-1} at 1.5 V operating window has been reached. The energy density of the electrodes was further improved by the use of activated carbon as a negative electrode. This modification widened the operating window to 1.8 V.[21]Xu and co-workers have investigated the graphene/PEDOT composite electroactive films reporting good processability in organic solvents, conductivity of up to 0.2 S cm^{-1} and excellent flexibility.[17]Conductivity of these composites was retained even when the films were bent at 90º. Very good thermal stability exceeding that of commercial PEDOT-PSS (Baytron ®) was also noted. Ryn et al reported applications of PEDOT in PEDOT/active carbon asymmetric capacitors. Constructed devices displayed very good stability and specific discharge capacitance of up to 56 F g^{-1}. Despite the use of organic solvent based electrolyte ($LiPF_6$ in EC/DMC) devices showed good stability over 100 redox cycles.[22] It must be mentioned however that both groups characterized only the

electrode performance, which not always translates into the performance of a complete device.

1.2.2.3 Applications in electrochromic devices

Both PEDOT and PEDOT-PSS found widespread application in electrochromic devices. De Longchamp and Hammonds have reported formation of layer-by-layer (LbL) PEDOT/PANI electrochromic devices. Optical contrast between the neutral and reduced state of 30% has been recorded. Upon redox cycling, the devices switched between deep blue-green coloured state (neutral PEDOT) and pale yellow coloured state (oxidised PEDOT) at a regular frequency (1.1 Hz). Remarkably, stability of these systems was monitored over 35 thousands cycles without any considerable decrease in performance.[18] Namboothiry and co-workers described the fabrication of an electrochromic material composed of PEDOT and Ag/Au nanoparticle chromophores. Materials showed enhancement in absorbance which was linked to the presence of nanoparticles (the presence of chromophores excited localized surface plasmons). Magnitude of the enhancement was found to be controlled by the nanoparticles concentration. These results indicate that Ag and Au nanoparticles have fully retained their chromophore activity when blended into the PEDOT film.[19] Electronic paper, textiles and other fully flexible electrochromic displays are of great interest due to their possible en masse applications. Widespread use of such devices requires portable, lightweight power sources. Bhattacharya et al have reported construction of a textile, PEDOT based, secondary battery.[16] PEDOT-PSS was the redox material for both the anode and the cathode while Ag-coated polyimide fibres were serving as the current collectors. Authors observed that in the constructed battery, Ag ions were the charge balancing species while PEDOT served as the electrolyte. Conducting polymers ability to store charge reliably and for a long period of time after being doped by Ag^+ ions has previously been reported by Ocypa et al**.**[23]

Many of the above PEDOT applications are based on the widespread PEDOT:PSS formulation which suffers from problems related to water absorption as well as rather low conductivity due to PSS being an insulating material. Additionally, PEDOT posses a metal extraction abilities (enhanced by PSS acidic nature) and although it can be advantageous in the charge storage process (see above) it is usually considered a hindrance in PEDOT/ITO applications due to indium elution into the

polymer layer.[3] Hence, the attention has been turned to the materials that can possibly replace the styrene sulphate. Kim et al have reported a successful application of the polymeric ionic liquids (PIL) based on imidazolium anions.[24] Formulated PEDOT-PIL films had better conductivity and lower surface roughness than commercially available PEDOT-PSS films. Upon doping with hydrophobic like $(CF_3CF_2SO_2)_2$ anions these novel polymeric films were reported to display hydrophobic nature thus eradicating water absorption issues. Hydrophobic PEDOT films were also formed through the cation exchange process. In this approach, reported by Dobbelin and co-workers, hydrogen cations from the styrene sulphate moiety were exchanged for imidazolium or tetraalkylammonium based cations.[25] Thus, organic cation modified PEDOT-PSS films showed excellent hydrophobic properties (with contact angle values of up to 100°). They have also displayed solubility in common organic solvents like DCM. The already mentioned effects of conductivity, material homogeneity and surface smoothness increase are probably a result of IL's capacity to induce supramolecular ordering. Dobbelin et al have exploited this particular IL property to form PEDOT-PSS/IL dispersions.[26] Morphology of films casted from PEDOT-PSS/(bmim)BF_4 showed clear phase segregation with PSS rich (insulating) regions embedded into the continuous network of PEDOT rich (conducting) regions. This composition resulted in the reported circa 10 fold increase in conductivity over the untreated samples.

Yet another approach to prepare electrochromic devices has recently been reported by Segura and co-workers. This group reported a chloromethyl functionalized EDOT monomer used to form PEDOT derivatives endowed with anthraquinone, perylenebisimide and tetracyanoanthraquinodimethane moieties. Cyclic voltammograms of the electropolymerized films indicated that pendant moieties retain their individual redox behaviour, which coupled with PEDOT redox behaviour is resulting in a large electrochemical window of these novel electroactive films.[27] Inganäs reported a very rare feature of modified PEDOT films, namely a reversible thermo chromic character. The thermochromic effect has been achieved using poly(3,4-ethylenedioxythiophene)-imidazolium (PEDOT-Im) although it must be mentioned that the thermochromic effect has beed reported for an aqueous solution of this polymer and not for the film itself.[28] Döbbelin and co-authors have reported electropolymerization of PEDOT-Im films from dichloromethane solutions. Upon doping with a variety of anions like BF_4^-, PF_6^- or $(CF_3SO_2)_2N^-$ this novel materials showed interesting properties

like solubility in organic solvents as well as tuneable (anion controlled) hydrophobic character.[29]

1.2.2.4 Applications in organic light emitting diodes (OLED)

Novel, ionic liquids based approach has also been implemented in the design of practical PEDOT based devices. Hole injection layer in the OLED's is used to inject electron holes from the anode into the light emitting part of the device. Kim and co-workers have reported organic light emitting diodes with hole injection layer composed of PEDOT:PIL instead of the usual PEDOT:PSS.[30] The improved OLED device displayed circa 7 fold increase of its working lifetime. Lu and co-workers pioneered the application of ionic liquids in this field when they researched the design of the electrochromic displays based on PEDOT/(bmim)BF_4.[31] A sandwich structure composed of layers of PEDOT (cathode), PANI(anode) and (bmim)BF_4 (electrolyte) system was used to build an electrochromic numeric display. The device had good optical contrast of 63% (at 560 nm wavelength).

1.2.2.5 Applications in electrochemical actuators

Electrochemical actuators have been frequently manufactured from PEDOT, however designs based on molecular solvent based electrolytes suffer from setbacks like solvent evaporation as well as the electrode material delamination**.** Chevrot and co-workers have reported the fabrication of a PEDOT-IL based actuator with excellent stability.[32] Unlike the traditional actuators composed, of redox materials attached to a conductive elastic backing, Chevrot's approach was to from a gradient structure. The device was composed of polybutadiene/poly(ethylene oxide) porous material on which PEDOT was deposited through the chemical oxidation route. Cross section analysis revealed that the outer regions of the PB/PEO network had the highest PEDOT concentration and that CP content was gradually decreasing away from the surface. (emim)TFSI ionic liquid was used as the electrolyte. The device showed no trace of degradation or deformation over 7×10^{-6} cycles at 10 Hz frequency.

1.2.2.6 Applications in dye sensitized solar cells

PEDOT has also found its way into the fabrication of dye sensitized solar cells (DSSC). Hayase et al reported a PEDOT:PSS:IL semi solid solar cell with charge transfer resistance (which is the main performance limiting factor of solar cells) reduced 10 fold as compared to classic Pt based DSSC's.[33] Shibata reported the chemical polymerization of PEDOT using IL/AuCl.[34] Formulated films were used in a prototype DSSC composed of TiO_2 working electrode, PEDOT: PSS counter electrode and 1-methyl-3-propylimidazolium iodide electrolyte (with tetrabromomethyl benzene gelator). Results indicated that PEDOT's electrocatalytic properties are comparable with those of platinum and the solar cell's charge transfer resistance decreased from 14.1 Ω cm^2 to 1.5 Ω cm^2. This effect and the overall increase in efficiency had been assigned to the interaction between the conducting polymer and the cross linking agent.

1.2.3 Deep Eutectic Solvents. Discovery and applications.

1.2.3.1 Discovery and importance of the field

Conventional molecular solvent based electrolytes are hampered by a variety of shortcomings namely volatility, flammability and electrode degradation.[36] Therefore there has been a considerable amount of interest in a fully ionic media which offer advantageous, although vastly different solvation characteristic as compared to the molecular solvents. These are ionic liquids (IL) often interchangeably classified as molten salts. Ionic liquid is a solvent, which is composed exclusively of ions and has no neutral component. Using a simplistic approach, simple metal chlorides like NaCl (melting point 806 ºC) while in molten state can be classified as IL. Invention of a solvent that offers pure ionic environment at room temperatures resulted in Room Temperature Ionic Liquid (RTIL) term being coined, to distinguish them from media like high temperature molten metal halides. Simplistically, they can be classified as salts, which are liquids below 100 ˚C, and as their name stipulates they are composed exclusively of ions.[35] The early formulations of the aluminium chloride based IL were beleaguered in their applications by their sensitivity to air and moisture. Since then, a wide range of ionic liquids based on various types of chemistry had been developed and

RTIL have attracted considerable and rapidly growing amount of research. Earliest reports of what is now known as classic IL's were centred on $AlCl_3$ salts and although they have displayed novel and interesting properties they have unfortunately suffered from high oxygen and moisture sensitivity limiting their industrial applications. Later on, RTIL research had been focused on solvents composed of Zn, Al, Sn and Fe chlorides mixed with quaternary ammonium salts. From the early 1990's the rising concerns with ecological footprint of the chemical industry in general and existing IL in particular switched the research focus to metal free IL's. Most popular synthesis path seemed to be a replacement of the metal cation by an imidazolium based one. These cations were usually combined with halide based anions (most common examples being: Cl^-, BF_4^-, PF_6^-.[35] This approach allowed for a vast increase of the possible cation-anion combinations with estimates ranging from 10^{18} to 10^{34}. However, even these new, improved IL's suffered from many drawbacks with most significant being often very poor biodegradability, toxicity as well as high manufacturing costs with the last one being a combination of required purity of the individual components and often rigorous synthetic conditions.[36]

In 2002, Abbott and co-workers have reported a new generation of ionic solvents.[37] Formation of these solvents occurs through complexation of quaternary ammonium salts with hydrogen bond donors. Hydrogen bonding between the halide anion and the hydrogen donating moiety results in a charge delocalization. This in turn results in a deep depression of the freezing point (as compared to the individual components). This effect is most prominent at the eutectic composition of the QAS:HBD mixture. Hence these novel solvents were named Deep Eutectic Solvents. In contrast to traditional IL's (for example Ethyl imidazolium chloride – $AlCl_3$), DES are generally not considered to be ionic liquids. Although they do offer a fully ionic environment, DES unlike IL's can be obtained from non–ionic species.[38] In terms of industrial applications, eutectic solvents have significant advantages over traditional IL's. Many of DES's display physico-chemical properties similar to those of imidazolium based IL's. Their other notable advantages are low price (result of usually cheap components and 100% atom economic synthesis process), inertness towards air and water (thus eliminating the application barrier of $AlCl_3$ based liquids), low toxicity and biodegradability reported for many of these solvents.[36] Abbott and co-workers had so far identified four types of DES.[39] Three of them are based on the general formula of $R_1R_2R_3R_4N^+X^- \cdot Y^-$.

Type I DES

Y = MX → solvent example = ChCl: $ZnCl_2$

Type II DES

Y = MX · n H_2O → solvent example = ChCl: $CrCl_3$× 6 H_2O

Type III DES

Y = R_5Z → solvent example = ChCl: $CONH_2$ (where Z = $CO(NH_2)_2$, COOH, ROH)

Type IV DES are composed during the complexation of metal chlorides with different hydrogen bond donors.

MX + HBD → solvent example = $CO(NH_2)_2$: $CrCl_3$ × 6 H_2O

Types I → III formulations patterns share the similar complexation pathway, which can be generally described by the following equilibrium:

cation + anion + complexing agent → cation + complex anion

or

cation + anion + complexing agent → anion + complex cation

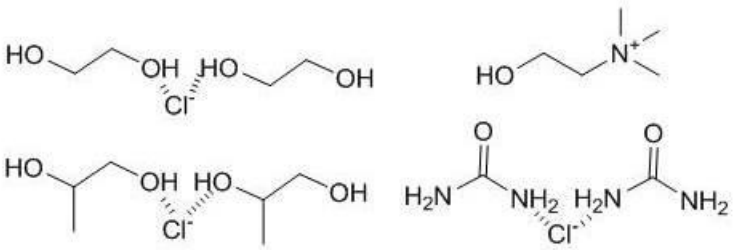

Figure 8. Selected examples of anionic and cationic species whose existence has been postulated in the DES. From top left clockwise: ethylene glycol – chloride complex anion, choline cation, propylene glycol – chloride complex anion and urea – chloride complex anion.

DES are very promising solvents with applications ranging from the design of novel catalytic processes,[36] preparations of novel structures (including nanostructures)

and materials,[36] as non-volatile solvents[40] and as soldering fluxes,[41] in energy storage [42] and in the fields of ion metallurgy, electroplating[43] and electrowinning.[44,45]

Due to this thesis subject, the following properties and application overview will focus on the last four topics. Like IL's, Deep Eutectics can be considered as *task specific chemicals* and together with traditional IL's they are often known as *designer solvents*. The sheer amount of possible hydrogen bond donors and quaternary ammonium salts makes the number of susceptible DES formulations practically unlimited. Resulting compositional flexibility (similar to that of IL's) allows DES to attain a variety of interesting properties. This not only enables formation of easier and safer routes (for example zinc and lead extraction from the Electric Arc Furnace (EAF) dust[46]) for the existing processes but also often provides pathway to completely novel processes (cast iron soldering[40]) and materials (photo luminescent and photo chromic zinc phosphate material[36]).

1.2.3.2 Physical Chemistry of DES

The freezing point depression observed in DES stems from the halide ion interaction with the HBD moiety. The eutectic composition (i.e. the one with the lowest melting point) can be obtained using a phase diagram. Figure 9 shows a generic diagram for the melting point temperature as a function of a QAS molar content.

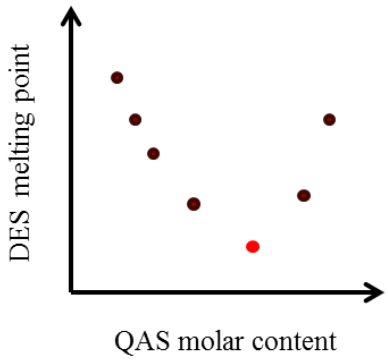

Figure 9. Generic DES phase diagram. Red point indicates the eutectic composition (i.e. molar mixture with the lowest obtainable melting point).

For example in Reline (ChCl: Urea) the interaction between the Cl^- and Urea results in possible formation of $(CO(NH_2)_2)Cl^-$ complex anion. The following charge delocalization results in a decrease of the crystal lattice energy and formation of a solvent with a freezing point (at the eutectic composition) of 12 ºC. In comparison, the

melting points of its individual components are 302 ºC (ChCl) and 133 ºC (Urea). In the case of Reline the lowest freezing point has been achieved at a composition of 46% mol urea. This is commensurate with the theory of each chloride anion being complexed to two urea molecules. It is also the case for mono carboxylic acids and glycols.[47] Ionic species present in the DES were a subject of detailed PFG-NMR[48] and EQCM-PBD studies.[49] Examples of possible cation and anion identities are shown in figure 7.

It has been proposed by Abbott and co-workers that the freezing point of the eutectic mixture depends on:

- Lattice energy of individual DES components
- Anion/cation interactions
- Entropy change induced by the formation of the liquid phase

Density, viscosity and conductivity are some of the most important properties of a solvent and they often determine its suitability for a given process. DES density usually exceeds that of water, table 1 lists the densities of some most commonly encountered eutectic solvents.[36]

QAS	HDB	QAS:HBD molar ratio	Density (g cm^{-3})
choline chloride	ethylene glycol	1:2	1.111
choline chloride	urea	1:2	1.205
$ZnCl_2$	ethylene glycol	1:2	1.449
choline chloride	malonic acid	1:2	1.136
$EtNH_3Cl$	CF_3CONH_2	1:1.5	1.273
$EtNH_3Cl$	Urea	1:1.5	1.140
$Me(Ph)_3PBr$	Glycerol	1:2	1.310
$ZnCl_2$	Urea	1:3.5	1.630

Table 1.Densities of selected DES at 298 K.

DES have generally rather high viscosities (for example: 85000 cP at 298 K for the $ChCl/ZnCl_2$ DES). Thence, the low viscosity (10 – 40 cP) eutectics constitute the main research area due to their, often direct applicability to existing industrial processes.

According to Abbott and co-workers, the molecular motions in DES are governed by the "Hole theory". This theory is commonly applied to explain molecular motions in traditional IL's. It is based on the assumption that the ionic material is filled with randomly distributed voids. The ions movement is then restricted by their availability of finding a suitably sized vacancy. Probability (P) of ions finding a void is given in the equation 1.

$$P_{dr} = \frac{16}{15\sqrt{\pi}} a^{7/2} r^6 e^{-ar^2} dr \qquad \textbf{[1]}$$

Where: $a = 4\pi\gamma/kT$, γ is the liquid surface tension, T is absolute temperature, k is the Boltzmann constant and r is the hole radius. Equation 1 displays connection between the void size and the liquid surface tension. Decrease in surface tension diminishes the ionic interactions leading to an increase in free volume.[50] DES posses' intrinsic ionic character and thus they essentially are ionic liquids with HBD added as a complexing agent. Fully ionic environment and extremely high ionic forces result in restricted availability of the voids. Predilections of Hole theory are in agreement with the experimental observations of many DES having density close to or higher than pure HBD (Urea = 1.32 g cm^{-3}, Reline 200 = 1.25 g cm^{-3}, Ethylene glycol = 1.11 g cm^{-3}, Ethaline 200 = 1.15 g cm^{-3}). Mixing quaternary ammonium salt into the hydrogen bond donor decreases the average hole radius resulting in density increase. Hole theory is further confirmed by the linear dependence of density on the HBD molar fraction observed for many DES.[39]

Viscosity

Another important property linked to liquid's molecular motions is the viscosity.[47] Equation 2 relates solvents viscosity to the void availability and thus Hole theory:

$$\eta = \frac{mc/2.12\,\sigma}{P(r > R)} \qquad \textbf{[2]}$$

Where: *r* is the ionic radius. This implies that both the viscosity and ion mobility (and hence species diffusion rates) are dependent on the hydrodynamic radius. This in turn is determined by the speciation, which originates from QAS: HBD types and molecular ratios. Average void size is related to the liquids' surface tension by the equation 3.[39]

$$4\pi(r_H^2) = 3.5\ {}^{kT}/_{\gamma} \qquad \textbf{[3]}$$

As with their other physical properties, HBD type and ratio seem to have the most significant impact on the solvent viscosity. Table 2 lists viscosities of some of the most commonly encountered DES.

QAS	HDB	QAS:HBD molar ratio	Viscosity (cP)
choline chloride	urea	1:2	1200
choline chloride	ethylene glycol	1:2	40
choline chloride	$ZnCl_2$	1:2	85000
Bu_4NBr	imidazole	3:7	810
$ZnCl_2$	urea	1:3.5	11340

Table 2. Viscosities of selected DES at 298 K.

DES high viscosity is often attributed to the presence of hydrogen bonds. These bonds are responsible for the actual formation of complex ions. Formed complex, large ions have diminished mobility resulting in moderate diffusion coefficients. Essentially, hydrogen bonds, van der Walls forces and electrostatic interactions govern the DES molecular mechanics. The importance of hydrogen bonds in determining the DES viscosity is highlighted by the fact that Glycerol based DES (Glyceline 200) has lower viscosity that that of pure HBD. This is in stark contrast to the behaviour displayed by a vast majority of the DES.[36] For example; Ethaline 200 (solvent composed of two moles of ethylene glycol and one mole of choline chloride) displays a viscosity of 40 cp at 25 °C as opposed to 16.9 cP for pure HBD. The unexpected behaviour of Glyceline is presumed to originate from glycerol's strong cohesive energy. The cohesive forces in

glycerol are a result of an extensive hydrogen bond network which is caused by the presence of three OH groups in this molecule. The significant decrease of viscosity upon the QAS (ChCl) addition is attributed to at least partial rupture of this network with the glycerol molecules complexing with chloride to form complex anions.

DES described in the literature [36, 39] exhibit the Arrhenius – like behaviour as do traditional IL's (i.e. their viscosity and temperature are inversely related).

Conductivity

Considering their various applications within the field of electrochemistry, DES conductivity is of paramount importance. Unfortunately, due to their high viscosity, most of these solvents display very modest conductivity (see table 3).

QAS	HDB	QAS:HBD molar ratio	Conductivity (mS cm^{-1})
Bu_4NBr	imidazole	3:7	0.24
choline chloride	ethylene glycol	1:2	7.61
choline chloride	glycerol	1:2	1.05
choline chloride	1,4-butanediol	1:3	1.64

Table 3. Ionic conductivities of selected DES at 20°C.

Since viscosity seems to be the limiting factor for the DES conductivity, Arrhenius equation is also applicable for predicting eutectics conductivity vs. temperature (it is directly proportional to temperature).[36] Like with other physical properties, molar fractions of QAS: HBD and their nature can dramatically alter the conductivity. It has been noted that in case of ChCl based eutectics increase in the salt content (polar component) versus the HBD (usually non-polar component) results in a conductivity increase.[36] At choline salt molar loading exceeding 25% (by weight), DES display conductivity similar to those of traditional IL's (> 1 mS cm^{-1}).[36]

Diffusion rates

Speed of diffusion is one of the main factors determining the rate of any chemical or electrochemical reaction. In DES, macroscopic transport properties are thought to be governed by the "Hole theory". This theory predicts that the hydrodynamic radius of migrating species is one of the main factors determining the species mobility. Stokes – Einstein equation relates hydrodynamic radius to the diffusion coefficient D.

$$D = \frac{kT}{6\pi\eta r} \quad \textbf{[4]}$$

In terms of DES self-diffusion rates (i.e. diffusion of anions and cations in pure DES) the values reported for choline cation reached $2.62 \times 10^{-11} m^2 s^{-1}$ to $1.28 \times 10^{-10} m^2 s^{-1}$ in Ethaline 200 (viscosity 40 cP) in the 298-333 K temperature range and 0.35×10^{-11} $m^2 s^{-1}$ to $2.10 \times 10^{-10} m^2 s^{-1}$ in Reline 200 (viscosity 1100 cP) in the same temperature range.[48] Lloyd and co-workers reported values for choline cation self-diffusion that were similar to those previously reported by for $[CuCl_4]^{2-}$ complex in the same solvent.[51] This confirms the validity of the hole theory as the radiuses of both species are similar (choline cation = 3.29 Å and $[CuCl_4]^{2-}$ = 3.14 Å). In terms of metal ion diffusion, groups conducting studies of DES in metal deposition processes reported diffusion rates of $1.75 \times 10^{-10} m^2 s^{-1}$ for $[TeCl_6^{2-}]$ in Reline 200[52] and $2.64 \times 10^{-10} m^2 s^{-1}$ for $[SnCl_4^{2-}]$ in Ethaline 200[53] (both values quoted at room temperature) further indicating that the species ionic radius might be the main factor controlling the diffusion rate.

1.2.3.3 Applications

DES in charge storage

Both primary and secondary batteries as well as electrochemical capacitors rely on the electrolyte's presence. The electrolyte act as a charge carrier during redox chemistry. It also provides the means of anode/cathode physical separation. Unlike the classic IL's, reports of DES used in actual charge storage devices are very scarce, probably due to these solvents relative novelty. The situation is now changing and recent review by Chakrabarti et al. highlights the advantages of DES when applied as the electrolyte in charge storage devices.[42] DES have on average a narrower

electrochemical window than many classic IL's, nevertheless eutectic solvents do posses some significant advantages.[42] As compared to classic IL's, during DES synthesis, there is no need for complex synthetic steps and toxicity of the final product is usually low. High manufacture costs can also be avoided**.**

A DES, when applied as an electrolyte in a charge storage device performs well in comparison to most organic solvents. Although acetonitrile (electrochemical window = 5 V) based batteries are capable of delivering open circuit potential (OCP) of up to 2.6 V, the average current efficiency is usually limited to circa 40 %.[54] Flammability, volatility and acute toxicity of these solvents are also a source of major safety and environmental concerns. Aqueous based electrolytes were the first (Baghdad battery) and are still the most commonly used (lead acid battery) technology used in charge storage systems.[55] Although water-based systems do possess some unquestionable advantages (e.g. uncomplicated formulations), their operating potential is constrained by a rather narrow electrochemical window (pH dependant, but usually limited to 2 V). Additional problems arise from parasitic losses due to hydrogen evolution.[44] Examples of practical, operable DES-based charge storage devices in the literature are still very rare, however a recent publication of Lloyd and co-workers describes a working DES Zn(II)-Fe(II) redox battery with the energy efficiency of 78%.[51]

DES in metal processing

Metal processing is so far the most popular application for DES.[36] Hydrogen bonding ability enables these solvents to act as electrons/protons donor/acceptors. This property results in the excellent dissolution properties. Formation of chlorine rich (5.4M of Chloride in Ethaline 200) environment confers them with particularly good solubility of metal halides (like LiCl, AgCl which are sparingly soluble in water) as well as aromatic acids and amino acids.[36] Even more interestingly, DES also have the ability to dissolve a wide range of metal oxides.[36,56] This DES property has already found an application in the electropolishing of stainless steel[36] and in formulation of novel (DES based) soldering fluxes.[41]

Concept of molten salts originated in the field of electrochemistry during Humphrey Davy pioneer work on electrodepostion.[1] Electrodeposition is a process, which relies on the application of an electric force (current) to reduce metal ions, CP monomers or similar reducible material onto the electrode's surface forming a stable,

neutral deposit. This form of surface modification is widely used for the purpose of corrosion protection (chrome plating, zinc plating, CP coating),[57] conductivity enhancement (for example through silver plating),[58] magnetic applications, conductive polymers manufacture, electro-catalysis as well as decorative purposes (e.g. nickel plating).[36] Since the process itself is reduction-based, any electrolyte used should display very negative reduction potential to avoid solvent degradation during the process. Sharing of similar properties to classic IL's combined with excellent air and water tolerance enabled DES to generate considerable interest in the electroplating industry. Abbott and co-workers reported deposition of Cu, Cu-Zn coatings as well as Cu/Al_2O_3 and Cu/SiC composites.[59] Their study indicated that DES display considerable variation in their ability to plate specific metal and the morphology of the deposits obtained and that the HBD type (e.g Reline allows for efficient Zn plating while Ethaline is incapable of it) governs both of these properties. Golgovaci et al described electrodeposition of Te and Te/Bi, Te/Sb from Reline 200.[52] Results indicated diffusion control of the deposition process with the diffusion coefficient being in the IL's range. Gomez et al. have reported concomitant deposition of Co and Sm.[60] Authors have obtained SmCo deposits that exceeded 70% wt. of samarium. This value is higher than of the currently produced alloys and might be useful in preparation of soft magnetic materials. Electrodeposition of tin from Ethaline, Reline and Propaline has been studied by Salome and co-workers.[53] Results revealed strong influence of DES viscosity on the Sn deposit properties with Reline (η = 1100 cP) producing a layer of uniformly distributed crystals while Ethaline (η = 40 cP) produced a layer with very few crystals present. This viscosity related effect can be translated as the difference in diffusion coefficients, which are diminishing with increasing viscosity. The electrodeposition of Gallium and its alloys is of potential interest for photovoltaic industry because this metal can act as a dopant in the photovoltaic cells. Shivagan et al reported deposition of Cu-Ga as well as Cu-In-Ga-Se films with 6 – 8 % Ga content making it potentially suitable for practical photovoltaic devices.[61] Cadmium composites[62] and chrome[63] have also been successfully electrodeposited from type III and type II DES respectively. This forms an environmentally friendly alternative for the currently existing technologies. Deposition on water sensitive metals like magnesium have also been conducted with Reline reported as an electrolyte that enables plating of Zn coatings onto Mg.[64]

Non–metallic deposits produced through electrodeposition from DES have also been reported. Mortis et al have reported deposition of nickel coated multiwalled carbon nanotubes (MWCNT) on a copper substrate. The key factor for a successful deposition was very good dispersion of MWCNT's in $NiCl_2$/Reline solution. Such a feat cannot be accomplished in an aqueous solution of metal salt due to the electrostatic and chemical interactions between MWCNT's and metal ions. Reline's ability to form stable carbon nanotubes suspensions was attributed to its high viscosity (resulting in an increased kinetic stability) and the columbic screening of the nanotubes charge.[65] Conducting polymer films like polypyrrole (PPy) can also be deposited from DES. Skopek et al reported deposition of PPy from 1:1 Ethaline/water solution.[66]

Immersion plating (also known as galvanic replacement reaction) is a deposition process, which relies on the difference in redox potentials between two or more metals. During the process, the metal ions dissolved in the electrolyte spontaneously reduce onto the cathode (made of different metal). The whole process is governed by individual metals formal electrode potentials in a given electrolyte. Abbott and co-workers[67] and Gu and co-workers[68] have both reported silver immersion coating on Cu surfaces from choline chloride based DES. Unlike aqueous solutions of silver salts, eutectics enabled the deposition of thick nanoporous Ag films. This result has been assigned to different kinetics and metal ion solvation shells, which in this chorine rich environment forms $AgCl_2^-$ as well as $AgCl_3^{2-}$complexes. This has been confirmed by an application of extended X ray absorption fine structure (EXAFS).[58] Interestingly, the deposit morphology was reported to be influenced by silver concentration.

Electropolishing is a process used for removal of the oxide layer from the metal's surface in order to obtain smooth finish. Ethaline 200 is currently being used as a base media for stainless steel electropolishing thus forming an eco-friendly alternative to phosphoric and sulphuric acid process.[69]

Since, as already mentioned, DES display HBD controlled selectivity in dissolution of metal oxides they have been applied to the extraction of specific metals from mixed metal matrixes like the dust from electric arc furnace (EAF). Application of ChCl/EG/Urea hybrid DES allowed for the selective recovery of Pb and Zn.[46] Abbott et al had also showed that metal extraction process can be accelerated by the addition of an oxidising agent like I_2 which in these chlorine rich environment forms environmentally

benign oxidising agent I_2Cl^-. Application of current allows for electroplating of the target metals on the cathode while I_2 is regenerated on the anode thus returning the electrolyte to its initial state.[45]

Most recent DES application is their use as an active ingredient in soldering fluxes. Soldering is an industrial process that relies on use of low melting point metals (usually Sn-Sb alloy) to form a joint between metals of higher melting points. To achieve good bond adhesion residual metal oxides and carbides need to be removed first. Initial tests conducted at the University of Leicester indicated that Glyceline acts very well on CuO removal while Reline displays rather unique ability to act as a soldering flux for cast iron.[41]

Biodiesel purification

Production of biodiesel is commonly conducted through alcohol/acid catalysed transesterification of vegetable oils.[36] Glycerol forms as a by-product of this reaction. It's high viscosity (1200 cP at 298 K) and non-combustible nature means that it has to be removed from the fuel for it to meet the automobile industry approval. Since glycerol is highly polar and biodiesel is not, this process is currently conducted using liquid bi-phase extraction, however this approach results in a significant amount of glycerol remaining in the mixture. Abbott et al investigated removal of glycerol from soy bean derived biodiesel by an addition of ChCl: Glycerol DES (Glyceline 100). Glyceline forms an eutectic at 1:2 QAS/HBD composition, this fact was exploited to conduct spontaneous DES saturation with glycerol which resulted in removal of 99% of it within 10 min.[70] Similar results were reported by Hayyan et al. for glycerol extraction from palm-oil derived biodiesel.[71] Recently ethylene glycol and triethylene glycol based DES were also reported as being suitable solvents for biodiesel purification purposes.[72]

CO_2 capture

Solubility of carbon dioxide in liquids is a subject of research due to potential applications in a variety of processes like gas separation, purification, chemical fixation (e.g. CO_2 storage) and catalysis.[36] Han and co-workers reported that CO_2 is soluble in Reline[73] (up to 0.2 mol l^{-1} at 313 K), while Wang et al related carbon dioxide solubility in this solvent to be inversely proportional to Reline water content.[74] Since the

concentration of CO_2 that were successfully dissolved in the DES tested so far are too low to be practically useful this field still requires a considerable development.

Drug solubilisation

Effective application of medicines requires the active ingredient to be delivered in an efficient manner. For both oral and intravenous applications this usually means dissolving the active ingredient in transport media. Morrison and co-workers investigated solubility of several medicinal active ingredients like grisefulvin, benzoic acid and itraconazole in Reline and Maline. Results indicated that these drugs were 5 to 22000 times more soluble in DES than in pure water. To confirm DES ability to act as drug transport media, aqueous solutions of malonic acid and urea were also tested with no superior drug solubility over pure water being recorded. Tested DES displayed non-toxicity combined with excellent drugs solubility. This undoubtedly will contribute to their emergence as a novel, promising pharmaceutical ingredient.[75]

DES in catalysis

The role of solvent in catalysis is crucial. They are a medium in which the reaction is conducted as they provide the means of physical contact between the catalysts and reactants. Therefore, the choice of solvent determines the reaction conditions; work–up procedures and recycling (disposal) strategy. DES are a subject of considerable amount of interest in the catalysis fields as they can potentially provide affordable and safe media.[36]

Acid catalysed reactions in DES have been so far concentrating on the industrially important process namely hexose to 5-hydroxymethylfurfural (HMF) conversion. Success in this field will mark a significant milestone in DES commercial applications as HMF is widely used in production of polymers and as a fuel additive. Konig and co-workers reported the production of HMF in ChCl/carbohydrate DES with yields ranging from 45% (glucose/ChCl) to 67% (fructose/ChCl) using $FeCl_3$ as catalyst.[76] Even more interestingly, Han and co-workers have reported 76% yield of fructose to HMF conversion without the use of metal catalyst. DES used were mixtures of ChCl with malonic, oxalic or citric acid as HBD. This particular DES application has a remarkable potential from the green chemistry point of view as it offers a new pathway for catalytic conversion of starch, lignin and cellulose into bio-based

chemicals.[77] Moreover, authors reported that these DES could be easily recycled after the process.

High added value chemicals have also been produced in DES. Davies and co-workers have reported Diels-Alder reaction conducted in acidic type II DES (ChCl/MCl_2 where M = Zn or Sn) with product yield in the 85 – 91% range.[78] Recently, del Monte and co-workers reported polymerization process from acidic DES composed of ChCl/acrylic or methacrylic acid. In these solvents, acids act not only as hydrogen bond donors but also as a monomer reservoir. Synthesis of polyacrylic acid has been afforded in the 75-85 % range.[79]

Reline is a DES, which is notable for offering basic conditions. Using this solvent, Shankarling and co-workers reported electrophilic substitution of aromatic compounds with yields ranging from 84 to 95%, a feat currently unachievable in organic solvents.[80] Such high yields were attributed to Reline's ability to stabilize transition states. This DES was also reported as a suitable solvent for a Knoevenagel reaction (chromophores synthesis) with 75-95% yields.[81] A novel approach has been presented by Coulembier and co-workers who have described a formation of novel DES, comprising lactide (LA) and 1,3 dioxan-2-one (TMC) in 1:1 ratio. Formed liquid was used as a solvent in the synthesis of poly(lactide) and varying the reaction conditions allowed for both LA and TMC to be incorporated into the product.[82] Hybrid carbohydrate/urea/inorganic salt DES were also deployed in Pd-Cu catalysed reactions like Suzuki coupling with 78 - 98 % yields.[83] Notably, d-mannose/dimethylurea DES provided the environment for the Suzuki coupling to proceed with only Pd catalyst without the need for Cu presence.[84]

Strong HBD like urea are well known to denature proteins.[36] Hence, bio-catalysis in DES was not extensively researched until in 2008 Kazlauskas and co-workers reported that various lipases were stable in Reline unlike in aqueous solutions of choline chloride or urea.[85] It is thought, that the hydrogen bonding in DES has lowered the activity of the individual components creating protein-friendly environment.

DES in organic synthesis

Continuous search for green, benign solvents has a major impact on the field of organic synthesis where, even more so than in catalysis, solvents play pivotal role. Azizi et al. have reported synthesis of alcohols from a range of aldehydes, ketones and epoxides in Reline with 75–99% yields.[86] Gore and co-workers reported Dihydropirimidinone (DHPM) synthesis using tartaric acid/urea DES thus bypassing the need for traditionally used Brønsted and Lewis acids and therefore significantly reducing the ecological footprint of the process.[87] This potentially forms new route for the synthesis of this valuable, biologically active compound widely used in the pharmaceutical industry.

DES in material preparation

Traditional methods of preparation of both organic and inorganic materials usually necessitate the use of either organic or aqueous solvents. Continuous strive towards greener chemistry resulted in DES being widely applied in this field.[36] Abbott et al reported the production of bio plastics using thermoplastic starch and Glyceline (which acted as a binding agent). Obtained polymers can have similar applications as current commercial plastics but unlike them, they are fully recyclable, biodegradable and compostable.[88]

Preparation of inorganic materials can be generally divided into two general approaches: solvothermal synthesis (relying on temperature and pressure to form the desired structure) and a more recent development of ionothermal synthesis. Solvothermal synthesis consists of growing single crystals from pressurized non-aqueous solution, followed by removal of solvent by thermal treatment. Unlike the solvothermal synthesis, the ionothermal synthesis does not require thermal step for the crystallization and structure formation process. The entire synthesis process relies instead on the solvent's being predominantly ionic (presence of molecular water disrupts the reaction) with ions providing the template around which the inorganic frameworks form. In this approach ionic liquids or increasingly eutectic solvents are used not only as solvents but both also as a structure directing agents (templates) and reactant feedstock.[36]

This route has multiple benefits with the main one being DES low volatility combined with their non-flammability (leading to safer processes) and even more importantly, their practically unlimited variety, which results in an equally large number of possible templates. In this context, Morris and co-workers have reported preparation of aluminophosphate zeolites using Reline with DES playing the pivotal role in the framework formation reportedly due to its charge balancing capacity.[89] Good moisture tolerance expressed by the eutectic solvents offers novel, improved route to obtain these water sensitive materials. Application of hybrid ChCl/R-COOH/Base eutectic mixtures was reported by the same group to allow for synthesis of novel CoAlPO structures with Co-Cl bonds (which are impossible to obtain in aqueous solvents).[90] Liao et al had reported the use of Reline in zinc phosphate frameworks and noted that the NH_4^+ released from Reline acts as a void filling reagent and is in fact directly responsible for these materials porosity.[91] Similar structure directing strategy can also be employed using cationic element of the DES as reported by Wang and co-workers in the synthesis of zincophosphate from Oxaline.[92] Using cation-template approach this group had recently synthesized zinc chlorophosphate material which exhibited both photoluminescence and photo chromic properties. Prepared material is the first ever, metal phosphate having such dual properties.

The above examples clearly highlight that the ability of DES to act as a solvent, template, reactant, void filler and charge balancer gives them almost unparalleled scope as solvents in various chemical processes and applications.

1.3 Analytical techniques

1.3.1 Electrochemical techniques

1.3.1.1 Cyclic Voltammetry

Electrochemical equilibriums are a combination of chemical and electrical energies. While chemical energies are quantified via chemical potentials, the electric potentials need to be measured as the achievement of electrochemical equilibrium

involves the transfer of charged particles. The electrochemical potential is quantified using the derivative of Nernst equation:

$$\mu_j^- = \mu_j + Z_j F \Phi \qquad \textbf{[5]}$$

Where Z is the charge on the specie j, F is the charge present in one mole of elemental particles (F = 96485.3365 C mol^{-1}), Φ is the solid (electrode) or liquid (electrolyte) phase potential and μ is the electrochemical potential. The phase potential depends on whether the species are present in the solid or in the liquid phase. Equation 5 necessitates the need for precise measurement and control of the electrode potential.[93] Typically, to obtain a quantitative result from electro-analysis a measured amount of electrical quantity (potential, current) is recorded vs. the quantity of the redox material present on the electrode. This quantity is controlled by a potentiostat (figure 10).

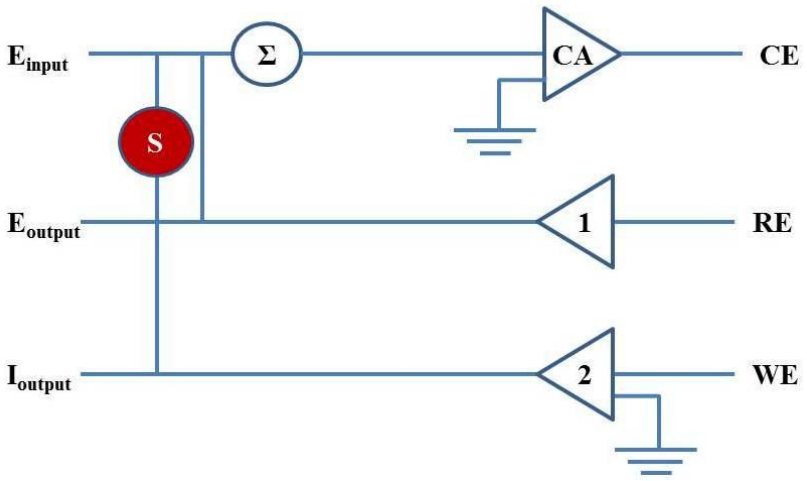

Figure 10. Simplified scheme of the potentiostat. Σ - the summation point which is used to regulate the potential and waveform, CA – control amplifier used to force current through the electrochemical cell, CE – counter electrode, S – switch between potentiostatic and galvanostatic modes, 1 – differential amplifier (measures the potential difference between the WE and RE), 2 – current meter. In potentiostatic mode CE potential is controlled versus WE so that the WE/RE potential difference correspond to the value described in the waveform. In galvanostatic mode, current difference between WE and CE is controlled so that the WE/RE potential and current differences correspond to the value described in the waveform. Adapted from reference.[94]

Potentiostats are usually equipped with 3 electrodes:

- Working electrode (WE) forms the interface under study and is the receiver of the applied current I or potential E
- Counter electrode (CE) serves as a passage for the equal electric quantity as WE but is it inert and hence it does not contribute to the overall redox reaction
- Reference electrode (RE) provides a constant measurement of WE/electrolyte potential difference. Application of RE enables the measurements of an absolute WE/CE potential difference. If a two electrode system is used, only the relative WE/CE potential difference can be measured.

Several analytical techniques are used with potentiostats with cyclic voltammetry (CV) being probably the most popular one. In this technique, the WE potential is scanned linearly (within a potential window of interest) versus time and the generated current is measured. A schematic example of applied potential and recorded current is shown below in Figure 11.

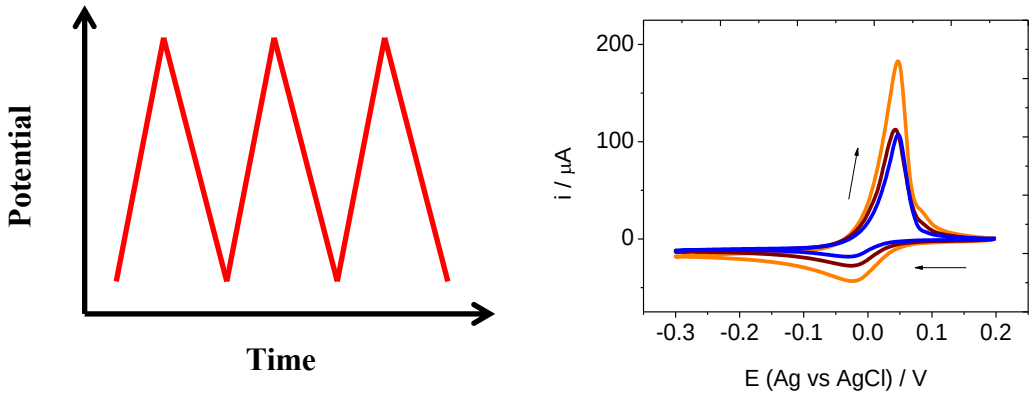

Figure 11. Left panel: Schematic representation of the application of potential during the cyclic voltammetry experiment. Right panel: An example of the experimental result: Cyclic voltammograms of 0.01 M AgCl in Ethaline 200. Potential window applied 0.2 V → – 0.3 V → 0.2 V. ν = 5 mV s^{-1} (orange line), 0.5 mV s^{-1} (brown line), 0.25 mV s^{-1} (blue line), 0.125 mV s^{-1} (pink line) and 0.0625 mV s^{-1} (black line).

As the name implies, the process is usually repeated, thus allowing to record redox system changes over time. Recorded current is plotted vs. potential (voltammogram) or current logarithm (Tafel plot).[93] Cyclic voltammetry experiments can also be used to determine diffusion coefficients using Cottrell or Randles-Sevcik equations.[93] Potentiostats allow for the studies of WE/electrolyte interactions, measured as a function of applied potential. An optional instrument which is capable of generating constant current (and measuring potential as a function of time) is called a galvanostat.

1.3.1.2 Potential step methods – chronoammperometry and chronocoulometry

These methods rely on the application of the potential step usually starting from a neutral (no electrochemical activity on the WE surface) potential to oxidation or reduction potential and measurement of the current vs. time. Integration of the current/time signal allows for charge measurement.[93] Other **v**ariants of the step techniques are potentiometry (application of a current step and measurement of potential vs. time) and chronocoulometry (application of specific E/t steps to the electrode to create controlled amount of charge). A schematic example of the applied current and recorded potential (charge) is shown below in Figure 12.

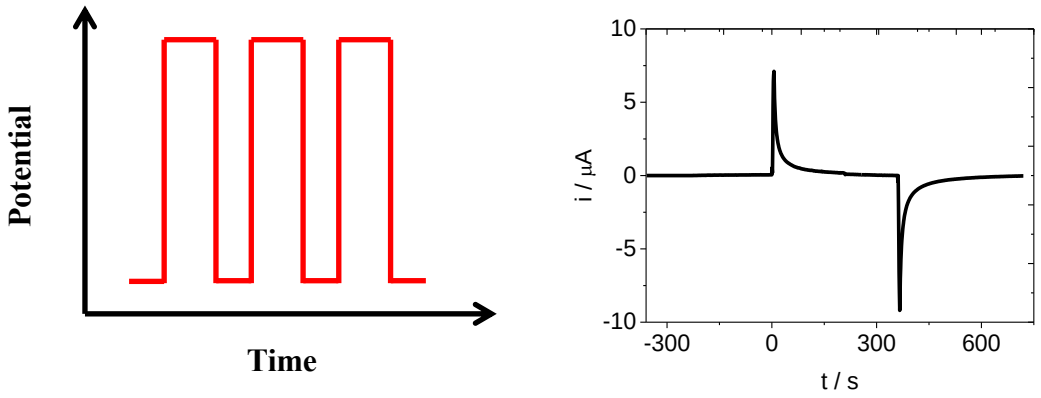

Figure 12. Left panel: Schematic representation of the application of potential during the chronoammperometric experiment. Right panel: chronoammperogram (black line) of a 0.8 µm [+/- 0.1 µm] PEDOT film (Q_{dep} = 55.1 mC cm^{-2}) potential stepped from - 0.3 V → 0.7 V → - 0.3 V in Ethaline 200. Duration of each step = 360s.

Both voltammetry and potential step methods have considerable experimental power. Voltammetry allows for determination of species diffusion coefficients, their concentrations, number of electrons transferred as well as establishing whether the

system is under diffusion or kinematic control. These electrochemical approaches are however not without some considerable limitations as the recorded signal is inevitably a sum of Faradaic and non-Faradaic processes.[93, 2]

1.3.2 Electrochemical Quartz Crystal Microbalance (EQCM)

1.3.2.1 Introduction

The effect of piezoelectricity (discovered by P. Currie in 1880) originates from specific properties of the quartz crystals. These crystals are capable of generating an electric current when subjected to external pressure and inversely, application of the electric current results in formation of an internal strain within the crystal lattice. This inverse piezoelectric effect is the key feature of the Quartz Crystal Microbalance (QCM). The internal strain (also called shear, hence QCM crystals are frequently named as Thickness Shear Mode (TSM) resonators) is a consequence of realignment of dipoles in the crystal structure induced by an externally applied electric field.[95] Direct piezoelectric effect is also widely applied with one of the more prominent examples being Atomic Force Microscopy (AFM).[95]

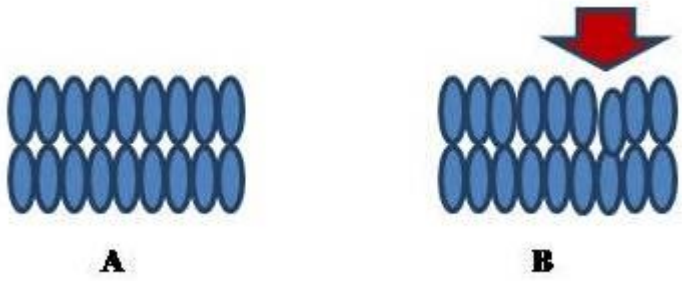

Figure 13. General concept of the piezoelectric effect. Panel A: quartz crystal not subjected to any load. Panel B: quartz crystal subjected to a load (indicated by a red arrow). Resulting dislocation generates the inverse piezoelectric effect.

The beauty of the QCM lies in the simplicity of the design and its rather unique versatility coupled with an almost unparalleled sensitivity (every object, however small, has a mass). These properties make it the most frequently used piezoelectric device. In

its most frequently encountered form, one of the crystal faces serves as a working electrode thus allowing for a simultaneous electrochemical and gravimetric analysis. In this form, the technique is called Electrochemical Quartz Crystal Microbalance.

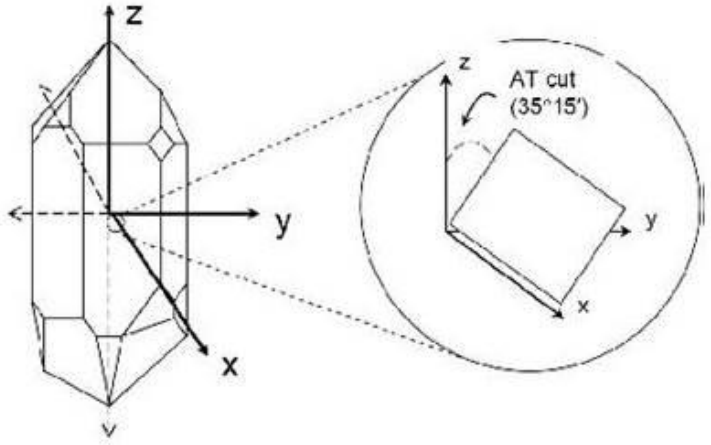

Figure 14. Generic quartz crystal and the AT-cut crystal used in the majority of EQCM applications.

Quartz is the most stable from of silica and a member of acentric materials family. Acentric materials are these which crystallize into non-centrosymmetric modules (Rochelle salt and tourmaline are another examples of these materials). Out of a variety of quartz crystals, alpha–quartz has superior piezoelectric and mechanical properties. During the electrode manufacture process the raw quartz rod is sliced at a specified angle into thin wafers. The most commonly used are the so called AT-cut (angle of cut of 35.17° with respect to the optical axis) crystals due to their negligent temperature induced frequency drift at ambient temperatures.[95]

1.3.2.2 Importance of the field

The widespread use of EQCM is undoubtedly a corollary of the fact that this particular technique has filled the longstanding gap in the (otherwise vast) array of electrochemical techniques. XX century witnessed a vast effort in the development of the electrogravimetric methods. Nevertheless, the ability to measure the mass of the electrodeposited material with high precision and in real time remained elusive until 1980's.[95] Perhaps the extended waiting period resulted in an unusually rapid development of EQCM once it was conceived and its application to virtually every

aspect of electrochemistry. Such immense impact of EQCM can be assigned to three factors. Firstly, the technique is highly sensitive, measurement of 1 Hz frequency change (out of 10 MHz operating frequency) translates into mass measurement equal to approximately 1.1 ng (i.e. 1 – 2 % of a monolayer). Secondly, unlike many other techniques (electrochemical SEM, electrochemical AFM, EXAFS) EQCM presents an affordable option. Thirdly, the ability to measure the mass variation in real time allows for direct molar calculations. EQCM popularity resulted in the technique being combined with optical techniques (PBD - EQCM),[2] spectroscopy, infrared analysis (FTIR – EQCM)[95], ellipsometry[2] as well as mass spectrometry[96] resulting in a vast library of publications. Ease of use and (superficial but often misleading) trivial data analysis result in EQCM being used in a non – specialist application which nevertheless enhance the current knowledge of this technique capabilities.

The technique origins can be traced back to the work of Glassford.[97]Although his was mostly a theoretical approach, it was the first publication where the possibility of a quartz resonator operating in a liquid environment was clearly envisaged and practically tested. Strikingly, Glassford work was not concerned with the electrochemical applications of the QCM in liquids. Instead, it concentrated on the implications of liquid's presence on the quartz sensors used in vacuum metalizing industry (as thickness monitors) and spacecraft's (contamination monitors). Nevertheless, the experimental results proved that the velocity gradient in liquid and resulting relative loss of sensitivity do not present major obstacles to QCM analysis. Frequency damping which was until then, seen as impenetrable barrier was successfully overcame through an application of the increased power to the oscillating circuit allowing it to overcome viscous losses.[95]

This was soon followed by work of Bruckenstein and Shay who described the first successful EQCM experiments conducted in a liquid electrolyte.[98] The development of the technique resulted in a constantly growing field of analysis for both parent (QCM) and daughter technique (EQCM) as applications of EQCM in biological, biosensing and biomedical applications often lead to the QCM being applied to study these systems without the electrochemical influence.[95]

On a more specific level, EQCM analysis requires careful consideration as the technique has its own incongruities. First one is the quartz crystal resonance frequency temperature dependence. However, since the overwhelming majority of the EQCM applications are at room temperature where this effect is close to zero, the temperature

influence can be safely omitted. Second is the viscoelastic effect described in more detail in the following section.[95]

1.3.2.3 Basic principles

In a typical EQCM experiment a potential applied across circuit causes the quartz crystal to resonate at a stable, set frequency (e.g. 10 MHz) henceforth called the fundamental frequency (f_0). General assumption of the gravimetric analysis is that any material deposited on the electrode moves synchronously with it. This assumption is colloquially called a *non-slip* and is graphically presented in the figure 15 below. Thus, the deposit can be treated as an extension of the quartz crystal electrode. This forms the basis of the frequency-to-mass conversion which is mathematically expressed in the Sauerbrey equation:

$$\Delta f = -\left(\frac{2}{\rho_q v_q}\right) f_0^2 \Delta M = -S\Delta M \qquad \textbf{[6]}$$

Where: ρ_q is the quartz density and υ_q is the velocity of the acoustic wave propagating through the quartz. The negative sign in the equation is related to the simple fact that any mass increase leads to the frequency decrease. For a typical f_0 = 10 MHz quartz crystal electrode with the electroactive area of 0.23 cm^2, the S constant is 4.426×10^{-9}g $cm^{-2}Hz^{-1}$. Thus, it can be approximated that the decrease of frequency (Δf) by 1 Hz is equal to a mass increase (Δm) of 1.1 ng. Sauerbrey based his equation on the original application for the QCM which was deposition from a gas phase.[99]

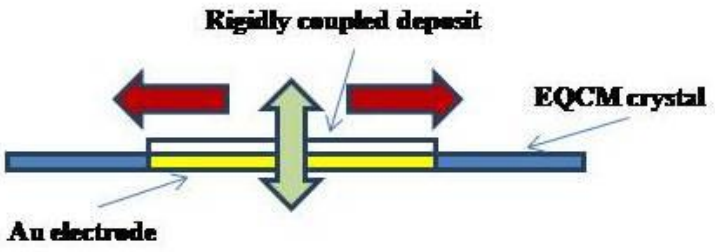

Figure 15. Non-slip condition required for the successful application of the Sauerbreys' equation (i.e. gravimetric regime). Green arrow indicates the allowed (non-slip) deposit movements, red arrow indicates forbidden (slip) movements of the deposit.

Conducting the gravimetric experiments in the liquid phase presented yet another complication which was elegantly approached by Kanazawa.[100,101] Assuming a simple case of a smooth resonator, one can envision that part of the liquid which is the closest to the electrode will oscillate synchronously with the electrode. This part of the liquid can be defined as a "viscously coupled fluid layer". The thickness of this layer is then defined by the following equation:

$$x_L = \left(\frac{\eta_L}{\pi \rho_L f_0}\right)^{1/2} = \left(\frac{2v_L}{\omega}\right)^{1/2} \quad \textbf{[7]}$$

Where: η_L is the liquid viscosity, υ_L is the liquid kinematic viscosity (which is liquid viscosity multiplied by its' density) and ω is the resonator's angular frequency. Presence of minor surface defects in the deposit morphology does not represent problems either as the liquid trapped in such crevices is unable to move in the lateral direction (slip) therefore the *non-slip* condition is still maintained. The frequency change observed while conducting both resonance experiments in liquid environment is determined by properties of both the liquid and the deposit. Both density and viscosity of the bathing liquid significantly influence the quartz crystal response thus making the QCM a very sensitive viscometer. Equation 8 relates liquid density and viscosity to the quartz resonator frequency shift:

$$\Delta f = -f_0^{3/2} \left(\frac{\rho_1 \eta_1}{\pi \rho_q \mu_q}\right)^{1/2} \quad \textbf{[8]}$$

An effective quantitative analysis requires the separation of the deposit and fluid contributions. This is particularly important in the analysis of the processes where redox-induced mass changes are on the order of, or smaller than the liquid contributions. This aspect of the QCM analysis has successfully been approached by Bruckenstein and Hillman who implemented dual quartz crystal impedance (DQCM) method.[102] This method relies on the use of two quartz resonators with one serving as the analytical probe (WE for EQCM experiments) while the other (identical) resonator monitors the liquid influence on the frequency signal.

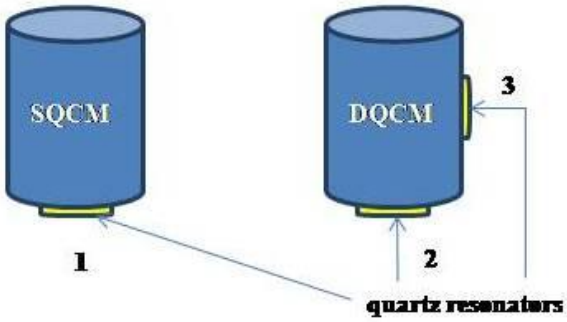

Figure 16. Configuration of the electrochemical cells used for SQCM and DQCM experiments. Blue elements represent the electrochemical cell and yellow ones represent quartz resonators. Numbers 1 and 2 represent quartz crystals used as working electrodes, number 3 represents quartz crystal used for monitoring the influence of electrolytes' viscosity on the oscillation frequency.

This approach allows compensating for viscosity and density effects. Another important aspect of the QCM analysis is the nature of the material deposited on the electrode. While Sauerbrey equation is well suited to the analysis of the rigid materials which resonate synchronously with the electrode, viscoelastic deposits require different approach. Analysis of the viscoelastic materials (e.g. conducting polymer films) was successfully approached by Kanazawa[100] who related the acoustic resonance signal of the viscoelastic films to their physical properties. The deposits degree of viscoelasticity influences on the overall resistance of the composite (quartz electrode + deposit) resonator has been explained and the viscoelasticity – resistance relationship has been described as non –monotonic. The exact resonance signal for the viscoelastic deposits is a result of a complex interplay between the deposit thickness, its mechanical properties and the shear wavelength. Moreover, the author investigated the effects of quartz resonator oscillation in Newtonian liquids (shear wave penetration depth, frequency damping) concluding that this type of analysis was indeed a viable analytical tool.

1.3.2.4 Applications

It is almost inconceivable to imagine a modern electrochemical toolbox without the EQCM. In 1981 Nomura et al reported application of EQCM in monitoring variations in silver concentrations upon electrodeposition.[103] Current applications of this

technique, either solely or in conjunction with other techniques, into the studies of a variety of electrochemical processes have been extensively reviewed elsewhere[95] and include electrodeposition, anion and neutral absorption, UPD, electrochemistry of redox, ladder and conductive polymers, electroactive oxides and solid metal complexes, self assembled monolayers and gas absorption as well as bio-sensory applications.[95,2] Since this thesis focuses mainly on the application of the EQCM in conjunction with the optical deflection technique the following review will be devoted to gravimetric analysis combined with laser techniques. Long et al reported the use of quartz oscillator in conjunction with electrochemical Kösters laser interferometer in studies of Pt films redox chemistry in H_2SO_4.[104] Combination of both techniques allowed for the simultaneous collection of interfacial stress, gravimetric and electrical signals. Data collected revealed non-monotonic correlation between mass change (Δm) and stress change ($\Delta\gamma$) which would not be detected by any of these techniques operating separately. In a separate study, the same group described the simultaneous change in electrode potential, surface mass and specific surface energy during the oxidation of formic acid on Pt electrode. The change in specific surface energy was calculated from the Kösters laser interferometer signal. Results allowed determining the rate of chemisorbtion vs. oxidation; again, this would not be possible by the sole application of EQCM. Microgravimetry/laser interferometry technique has also been applied to studies of Au films exposed to an aqueous K_2SO_4 electrolyte,[105] and an aqueous HCl electrolyte as well as to study the underpotential deposition (UPD) of Pb, Tl and Zn on Au electrodes.[106] EQCM has also been combined with ellipsometry yielding valuable data. Rishpon and co-workers reported use of EQCM/ellipsometry in studies of electrodeposition of PANI films **(**authors collected ellipsometer readings simultaneously with the EQCM ones, effectively monitoring films' mass (gravimetric signal) as well as its' thickness and optical absorbance (optical signal). Results presented included an in-situ, real time measured, mass/thickness plots. Such a feat is usually only achieved by the use of electrochemical AFM or scanning electrochemical microscope (SECM) with both techniques being expensive and invasive as opposed to affordable and non-invasive set-up used.[107] Different deposition patterns and density for potentiostatic and galvanostatic depositions were recorded. Authors rightly emphasized that the simultaneous use of multiple probes effectively removes the artefacts and verifies the individual signals. Lower average density was obtained for potentiostatically grown films and gradual density decrease was observed prior to the formation of dense base

layer covered by less compact external layer. This observation is in good agreement with work of Rahindramahazaka et al who postulated the existence of 'compact' and 'open' zones in the potentiostatically deposited CP films.[11] Rishpon's work has been later followed by Shimazu and co-workers who reported novel combination of Fourier transformation infra red (FTIR) spectroscopy combined with EQCM (FTIR/EQCM) in studies of 11-ferrocenyl 1 undecanethiol ($FcC_{11}SH$) monolayers. Since FTIR is a structural probe its application offers excellent opportunity to compensate for quartz oscillator inherent lack of selectivity. Therefore, the FTIR/EQCM was able to offer a unique insight into the monolayer structural changes upon oxidation and reduction, namely the movement of the monolayer alkyl chains. The magnitude of these structural changes was reported to be closely correlated with water ingress/egress, this postulation was based on the gravimetric signal.[108]

Recently, Berkes and co-workers reported a comprehensive study of electrogravimetry combined with visible spectroscopy.[109] This particular experimental set-up (EQCM/UV-Vis) has been reported before but not in such detailed way. Authors derived an equation correlating the frequency response to the concentration of absorbers while rightly concluding that in any electrochemical process this concentration is potential dependent (as the species are continuously converted into molecules with different structure). This method presents potentially a very useful tool in studies of CP or metal monolayer electrodeposition. Apart from spectroscopy, EQCM has also been combined with hydrodynamic methods (notably rotating disc and wall jet electrode[95]) as well as mass spectroscopy.[110] This particular area of research seems to be very promising as the authors proved that real-time analysis of the deposition – dissolution products is possible for both solid phase (probed by EQCM) and gaseous phase (probed by mass spectrometer). This provides non-specific information about mass change as well as specific information about the amount and identity of the gaseous species absorbed/desorbed from the electrode.

1.3.3 Probe Beam Deflection (PBD)

1.3.3.1 Introduction

Classical electrochemical techniques like cyclic voltammetry concentrated on the measurements of the electron flux at the electrode/electrolyte interface.

Unfortunately, purely electrochemical techniques have significant limitations restricting the range of the information available. While extending it has been achieved through the use of different perturbation techniques and/or variations of the electrolyte properties (T, pH) it has long become obvious that solely electrochemical techniques are able only to provide limited information about the ionic fluxes in solution. Since then, a plethora of spectroscopic techniques has been developed to study the electrode/electrolyte interfacial processes.

Gravimetric techniques (EQCM) are able to precisely determine the surface population changes but are unable to yield any specific information about the origin of the species (i.e. by using EQCM alone, one cannot distinguish whether the increase in mass is attributable to small population of heavy species or large population of light species). The electrode population changes originate from fluxes (which can be thermally, chemically or electrochemically induced) in the electrolyte. Any ion flux forms a concentration gradient which may be detected by a variety of methods. One of them is the interferometry.[2,111] However, its popularity is marginal due to the lack of sensitivity and rather complex experimental set–up. Other techniques applied to study this process utilized radioactive tracing, pH changes, fluorescence, absorption, diffraction and perhaps the most advanced of all of these methods, scanning electrochemical microscopy.[111]

While these techniques have provided a very valuable insight into the mechanistic of the electrode fluxes in the electrode vicinity, they suffer from either sensitivity issues (interferometry) or economical barriers (scanning microscopy) obstructing their widespread applications. Thus, the need remained for the affordable, simple way to measure the concentration gradients.

A breakthrough occurred during the development of a related spectroscopic technique, namely Photothermal Deflection Spectroscopy (PDS) when some rather unexpected phenomenon was noted. PDS is based on the application of the laser beam to observe the thermal gradients. Direct observation is usually impossible but it is a widely known fact[112] that the solute concentration is temperature dependant and this implies that the refractive index (determined by the concentration) would also be temperature dependant. In PDS the thermal gradients are therefore detected as the refractive index gradient causes the laser beam to deflect from its original course. It was noted during the early experiments that the beam suffered from a significant deviation in the absence of any temperature gradients. It was thus elucidated that the

electrochemically (or chemically) induced concentration gradients resulted in a formation of the refractive index gradients deflecting the laser beam. This conclusion led to the creation of an entirely new technique, termed Probe Beam Deflection (PBD). Other, less frequently used names are Optical Beam Deflection or 'Mirage effect'.[2]

Initial applications were hampered by the technical and economic barriers (lack of affordable lasers and position sensing detectors (PSD)), however the eventual development of reliable, inexpensive equipment resulted in this technique being applied to study various processes with PBD deployed on its own or in a combination with other techniques like EQCM.[113]

1.3.3.2 Basic principles

The basic principles are as follows: flux of species in an electrolyte forms a concentration gradient and since its relationship with refractive index is constant for a given species, the flux formation results in a refractive index gradient. The laser beam propagating through the region of the refractive index gradient (i.e. in a close proximity of the working electrode) can be described as a wave and this wave speed is:

$$v = \frac{c}{n} \qquad \textbf{[9]}$$

Where: *v* is the speed of light in the given electrolyte, *c* is the speed of light in vacuum and *n* is the electrolyte refractive index. Therefore any change in refractive index will affect light speed deflecting the laser beam from its original course. Through the use of a simple geometric approximation (small angle approximation) the resulting angle of deflection can be expressed as:

$$\theta_{(x,t)} = \left(\frac{l}{n}\right)\left(\frac{\delta n}{\delta C}\right)\left(\frac{\delta C_{(x,t)}}{\delta x}\right) \qquad \textbf{[10]}$$

Where: *l* is the interaction pathway, *n* is the electrolyte refractive index, *C* is the analysed species concentration and *x* is the electrode/beam distance. The possible variations of PBD are limited solely by the variations of electrochemical experiments as the principles of the technique can be applied contemporaneously with cyclic voltammetry, chronoammperometry, coloumetry etc. Regardless of the application, the

working principles of the technique remain unchanged. Any given electrochemical system could be envisaged as a flat, square electrode immersed in an effectively infinite bathing electrolyte solution. The electrode width is defined as *w*. The diffusion layer forms at the electrode/electrolyte interface with a thickness several orders of magnitude smaller than *w*. This eliminates any possible 'border effects'. If the laser beam is now passed parallel to the electrode it can be assumed that *w=l* with *l* being the length of the beam passing in the electrode vicinity. Electrochemical reactions occur at the electrode surface (where distance *x = 0*), hence the diffusional (viscosity dependent) delay is an important factor in PBD analysis since beam is inevitably located (see figure 17) at distance *x > 0* from the electrode's surface.

The entire process is quantified using a following equation:

$$\delta^2 C/\delta x^2 = \frac{1}{D}\frac{\delta C}{\delta t} \qquad \textbf{[11]}$$

Where: *x* is the beam/electrode distance and *t* is the diffusion time. Equation 11 emphasises the importance of the 'right' electrode/beam distance obligatory for a successful PBD analysis. If the distance is too small this will result in a total obstruction of the beam, if it is too large, the diffusional delay will distort the signal to the extent of it no longer representing the surface processes. Thus, as a rule of thumb the PBD signal is deemed acceptable if the recorded deflection signal resembles the current signal recorded at the electrode as the entire electrode electrochemistry is either a result of, or results in, a flux in the electrode's vicinity. The diffusion of species from the electrode to the beam is depicted in the left panel of the figure 17. The physical separation of the analysed process located at the working electrode and the analytical tool of the laser probe results in a temporal barrier between the electrochemical and optical signals. The origins of the barrier lie in the diffusional delay. This represents a significant problem in the analysis of the PBD data. Since the delay arises from the beam location being at a finite distance from the source of the concentration perturbations (WE) the detection of the refractive index (concentration) gradient is inevitably procrastinated. This delay depends on the electrode-beam distance, species diffusion coefficient and the rate at which the electrochemical processes are conducted. A graphic representation of the diffusional barrier is shown in the right panel of the figure 17.

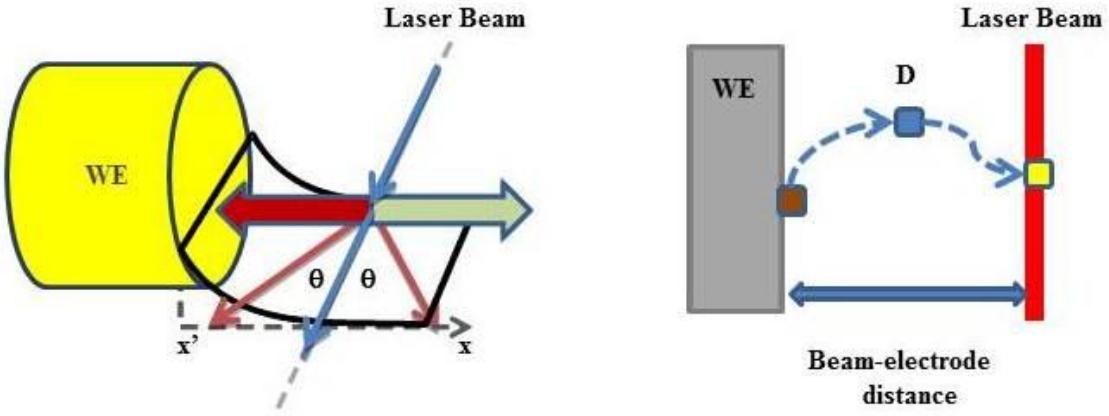

Figure 17. Left panel: Schematic representation of the laser beam passing in front of the working electrode. Formation of the concentration gradient (negative – red arrow, positive – green arrow) results in the laser beam being deflected in the x or x' direction by an angle θ. Right panel: Schematic representation of the diffusion of species from the electrode surface into the optical deflection zone. Brown, blue and yellow squares represent species attached to the electrode, in transit and in the optical path respectively.

As it was stated before, the intrinsic delay between the electrochemical reaction at the electrode's surface and its detection by the probe beam has an effect on the shape of the deflectogram. In chronodeflectometry, the effect is visible as a temporal delay, while in cyclic experiments it is a potential shift. Furthermore, the distortion of the optical signal increases if the beam is located further away from the electrode's surface. Accurate, quantitative analysis of the PBD data necessitates the removal of the diffusional delay. This is usually conducted either by digital numeric simulation or convolution of the experimental optical signal. In the first approach a variety of mathematical approaches are used to calculate the ion fluxes at the electrode using the PBD experimental data as well as species diffusion coefficients (these are obtained from respective individual ionic contributions). Numerical convolution is the most popular approach used to quantify the PBD data. It was initially proposed by Vieil and co-workers[114] and it is based on a concept of calculation of the electrochemical flux at the *x* distance followed by direct comparison of the calculated signal with the experimental optical signal. The advantage of the convolution approach lies in the fact that both diffusion coefficients and beam-electrode distance values can be estimated from x/x_0

plots. These are obtained in an uncomplicated way from chronodeflectometric experiments conducted at variable *x* distance. This is allowing for the analysis of systems for which $\delta n/\delta C$ data does not exist in the available literature.

High sensitivity of the technique coupled with the unique ability to reveal the intimate knowledge of the electrode/electrolyte interface fluxes resulted in PBD (either alone or in combination with other techniques such as EQCM) applied to study a variety of processes. A particularly interesting combination is the PBD-EQCM technique as these two techniques complement each other very well. A simultaneous monitoring of electrochemistry, microgravimetry and the concentration gradient presents a unique opportunity to probe both the electrode and its immediate vicinity. The whole concept is presented in the figure 15. EQCM/PBD combination has been applied to study Ag deposition/dissolution**,**[113] Poly(o-toluidine)[115] and PEDOT films redox chemistry in both molecular and deep eutectics solvents as well as silver and tin redox chemistry in DES**.**[116]

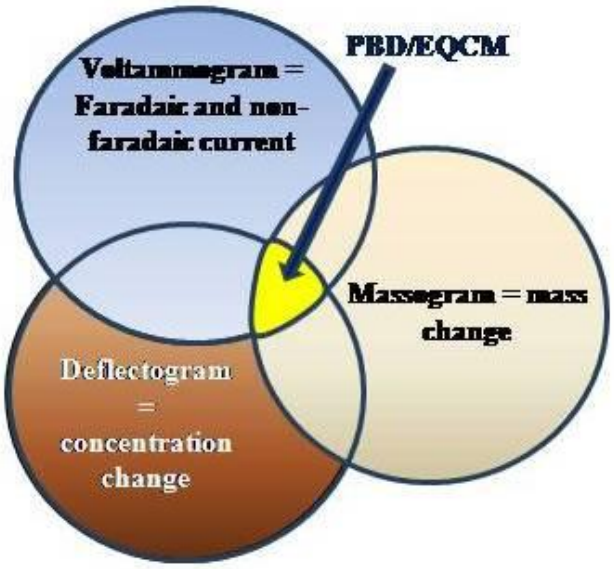

Figure 18. Graphic representation of the PBD/EQCM concept and the benefits this technique affords. Voltammetric signal allows for current measurements, gravimetric signal for mass measurements and optical signal for the measurements of the concentration change. PBD-EQCM allows for the collection of all three signals and their comparison, it also allows for the removal of artefacts.

1.3.3.3 PBD studies in molecular electrolytes

The conducting polymer which chemistry was undoubtedly most scrutinized by the PBD analytical tool is Polyaniline (PANI) and its various derivatives.[117,118,119,120] Majority of these studies were restricted to the parent polymer redox cycled in aqueous acidic ($HClO_4$, H_2SO_4, HCl) and molecular organic ($LiClO_4/CH_3CN$) electrolytes. In all of the above, anions were confirmed as a main dopant with expulsion of cations directly preceding the anion ingress into the polymer film. Heteropolyanions influence on redox chemistry of the conducting polymers was also studied using the PBD. $H_4SiW_{12}O_{40}$ in aqueous solutions of H_2SO_4 as well as in HCl were tested as bathing electrolytes for a conducting polymer films.[2] These particular studies have confirmed the expectations of the heteropolyanions being unable to dope the bulk of the polymer film.

Contrasting behaviour was observed in a PANI film doped with heteropolyacids like phosphotungstic acid. In this case, anion immobilization leaves balancing the electroneutrality to protons.[2] Poly(o–toluidine) (POT) films redox ion exchange in aqueous solutions of perchloric acids was a subject of a detailed PBD – EQCM study. It revealed a significant cation (H^+) contribution to the ion exchange. This result's significance is emphasized by the fact that the EQCM alone is unable to detect cation of such a small mass.[115]

As for PANI derivatives, poly(N-methyl)aniline optical deflection analysis confirmed anions as the exclusive dopants. This is reasoned to be a result of the methyl group induced, steric hindrance which makes the imino group deprotonating impossible.[2]

Cyclic voltadeflectometry studies were also conducted for films of poly(o–ethyl)aniline, [121]poly(3-methylthiophene),[122] polynaphtothiols[123] and polypyrrole.[2] In the latter case, observations drawn allowed for the direct correlation of the ion exchange process to the anion size. Barbero and co-workers reported[2] that the use of small anions like Cl^- resulted in anion ingress upon PPy oxidation:

$$PPy^0 \rightarrow e^- + Cl^- = (PPy^+)\,(Cl^-)$$

However, in the case of an electrolyte which contained only big anions the pattern was reversed and cation egress occurred instead:

$$PPy^0 \rightarrow e^- - Na^+ = (PPy^+)\,(TsO^-)$$

This behaviour was further confirmed by Hillman and co-authors to occur upon oxidation of PEDOT films in $LiClO_4/CH_3CN$.[49] In this process however the anion ingress dominated:

$$PEDOT^0 \rightarrow e^- + ClO_4^- = (PEDOT^+)\,(Cl^-)$$

While in Ethaline cation egress dominated:

$$PEDOT^0 \rightarrow e^- - Ch^+ = (PEDOT^+)\,((EG)_2Cl^-)$$

PBD was also used to study redox chemistry of noble metals, UPD processes and the electrochemistry of carbon based electrodes.[2] It was also used in the studies of nanostructured electrodes with rather promising results.[124] Application of both cyclic deflectometry and chronodeflectometry allowed for the determination of faradaic processes and potential of zero charge (pzc). Planes and co-workers reported study of aerogel electrodes in NaF/H_2O and $LiClO_4/CH_3CN$ based electrolytes.[125] Large active area of nanostructures resulted in a prominent electrochemical flux and therefore strong optical deflection signal.

Gas evolution can have a detrimental impact on many electrochemical processes (e.g. in fuel cells charge/discharge cycle). PBD was used extensively to study gas evolution on metal electrodes. The technique is particularly useful for this purpose as for liquids: $\delta n/\delta C > 0$, while for gases $\delta n/\delta C < 0$. PBD ability to detect gaseous fluxes allowed to quantify the effects of CO electro-oxidation as resulting in the formation of CO_2 and H_3O^+. Barbero et al investigated CO_2 formation on mesoporous Pt electrode. Obtained deflectogram revealed a multiflux of CO_2 and H_3O^+ (in opposite directions). This result could not have been obtained by most of the other techniques.

Layer-by-layer (LbL) multilayers are a class of materials which are formed through sequential deposition of different polyelectrolytes onto the solid surface. During redox processes, these films are doped and undoped by a mixture of dopants. Depending on the system, intrinsic or extrinsic processes as well as a mixture of these two processes can maintain the electroneutrality. In the first case negative charge is balanced by the positive charges on the adjacent polymer chain, in the second one an ingress of

an external dopant from the bathing solution balances the charge on the polymer chain. As LbL materials have great scope in applications such as permselective gas membranes, noncentrosymmetric films for non-linear optics and selective area patterning they were a subject of optical deflection studies.[126] Results allowed estimating the fluxes of individual dopants and the fractions of redox charge compensated by them as well as determining the extent of intrinsic and extrinsic doping.

1.3.3.4 PBD studies in ionic liquids and deep eutectic solvents

Since PBD relies on the presence of the concentration gradient for the analysis to proceed, it works favourably in diluted electrolytes. High ionic concentration obviously associated with ionic liquids and eutectic solvents forms a significant barrier to successful optical analysis in this media. As ionic solvents have generally high viscosity, which contributes significantly to longer diffusion times, the diffusional delay (i.e temporal delay between the electrochemical reaction and species reaching the laser beam) presents an additional obstacle. Hence, reports on the optical studies conducted in ionic solvents are very limited. So far, only Hillman and co-workers have reported the optical deflection studies of PEDOT/DES[49] as well as silver and tin redox chemistry in Ethaline.[116]

1.3.4 Atomic Force Microscopy (AFM)

Investigation of both conductive and insulating materials on an atomic scale has long been considered to be of great scientific importance. Over the years, various techniques have been developed and applied to study surface morphology on the atomic scale. While electron microscope has some unquestionable advantages (magnification of > 100000) it can only provide 2 D images, hence the attention was centred on probe microscopes that would allow obtaining 3 D images.[127] Jones et al. investigated the use of electrostatic field to measure inter atomic displacement. Using devices with variable capacitance the resolution of up to 10^{-4} Å could be measured. Superconducting quantum interference devices (based on Josephson effect and currently used in gravity gradiometers) were also investigated with the accuracy reaching 10^{-6} Å. Similar results were achieved using an x-ray interferometry. Using this approach Deslattes and co-workers achieved spatial resolution of 10^{-6} Å.[127]

A long awaited breakthrough occurred in 1981 when Binnig and Rohrer invented a scanning tunnelling microscope (STM), which had earned them 1986 Nobel Prize.[128] As the name implies, this method relies on the quantum tunnelling effect to create the image reflecting the sample surface morphology. STM deploys a sharp tip (similar to the one used in stylus profilometer) which traverses the sample surface at a 10 – 20 Å distance. Simple application of potential (the whole analysis is conducted in a vacuum chamber to exclude air dielectric effects) results in an electron flow. Magnitude of the flow is restricted by the tip – surface distance and is used to form a 3 D image.

Despite the obvious success of achieving atomic scale resolution on both the lateral and spatial scales and the unprecedented ability to create 3 D atomic scale images this technique suffered from serious limitations as it could only be applied to conductive surfaces. Situation changed in 1985 when Binning, Quate and Gerber reported the invention of a new instrument called atomic force microscope (AFM).[127] Their approach was based on the use of a very small mass cantilever attached to a modified STM-type stylus. Since the mass of the cantilever was very small its operational force is also minute having a magnitude of ~ 10^{-18} N. Cantilever is being oscillated on a spring attached to one of its ends (with spring being the crucial part of the instrument). The other end of the cantilever houses a sharp ended tip (usually fabricated from silicon nitride) facing the samples surface. AFM measurements are obtained through the measurement of the forces acting on the tip/cantilever assembly due to the samples' proximity.

The complete experimental set-up is as follows: the cantilever is attached to a piezoelectric element (modulating piezo) which serves as a generator of the cantilever resonant frequency. The modulating piezo is attached to a three-dimensional (operating in the x, y and z axis) piezoelectric drive which uses feedback loop to keep the force expressed on the stylus at the constant level. Noise reduction (which usually originates from building vibrations that commonly are at circa 100 Hz level) is generally achieved by setting the whole instrument on an air – table and also by using high resonant frequency (5.8 kHz). During the analysis, stylus moves over the sample in a raster mode creating a 3 D image of the surface morphology.[127] Working principles of the atomic force microscope are shown in the figure 15.

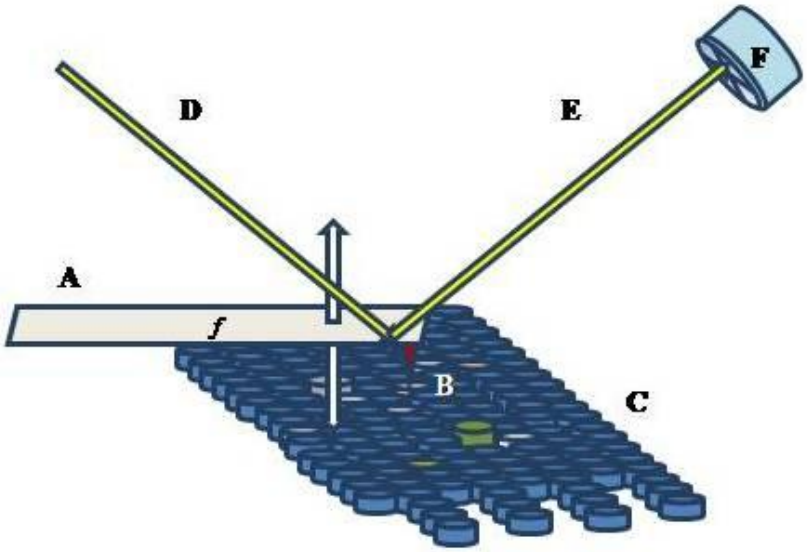

Figure 19. Graphic representation of the AFM experimental set-up. A- cantilever (oscillating at the constant frequency *f*), B – tip, C – analysed sample, D incident laser beam, E – reflected laser beam, F – position sensing detector.

The change in resonant frequency is calculated using the following equation:

$$f_0 = (1/2\pi)(k/m_0)^{1/2} \quad \textbf{[12]}$$

Where k is the spring constant (typically 50 N/m) and m_0 is the spring loading mass (hence mass of one atom is the AFM practical limitation). Force acting on the stylus results in changes of the resonant frequency and this data is used to form a graphic image. Depending on the actual design and progress in micro fabrication, inventors estimated the practical limits of the spring loading to be as little as 10^{-18} N.[129] To put this into perspective, the inter-atomic forces range from 10^{-11} (van der Walls forces) to 10^{-7} for ionic bonds therefore well above the AFM theoretical lower limits of detection. As comparing to STM, AFM not only is capable of analysing the non-conductive samples but it also does not require vacuum to operate making it suitable for biological applications.[130]

Since its invention, AFM have been successfully applied to analyse the morphology of ceramics, composites, conductive and non-conductive polymers, metals and semiconductors. Over the years, several operating modes of the AFM were developed with the main ones being contact and tapping (non-contact) modes.[131] The

first one relies on the physical contact between the cantilever tip and the sample. Hence, it is only suitable for hard samples due to the risk of indentation. Tapping mode AFM (TM-AFM) has been developed to prevent the indentation risk allowing for the analysis of soft samples.

During the TM-AFM analysis two types of signals are collected.[132] Firstly, oscillation of the cantilever above the sample's surface leads to a change in the oscillation amplitude. These changes are collected and displayed as a *topography image.* Secondly, the oscillation phase difference between the cantilever operating end (i.e. one which houses the tip) and the mounting end (i.e. one connected to a modulating piezoelectric element) is also collected and used to create phase images. The origin of the phase shift is the power dissipated by the cantilever during its physical contact with the sample and therefore it reflects the viscoelastic properties of the sample. Quantitative analysis of the TM-AFM signal requires the accurate determination of amplitude and phase signals as a function of the cantilever/sample distance and application of this data to obtain the image that is an accurate reflection of the samples' morphology. This allows for the quantitative analysis of heterogeneous solid/elastic samples like copolymers. A complete analytical approach based on TM-AFM analysis of poly(styrene-block-butadiene-block-styrene) has been thoroughly described by Knoll and co-workers.[132] An electrochemical application (where stylus serves as a WE) has also been created and successfully applied to study a variety of processes. Application of this particular technique allows monitoring thickness change of elastic electroactive materials and in-situ observation of formation and decomposition of redox products on the electrode's surface.[133] Multi-frequency force microscopy is a further development of the AFM. In conventional force microscopy all information about the sample's morphology that originates from deflection at frequencies different than the cantilever operating frequency cannot be collected. Use of two or more frequencies allows overcoming this problem and might possibly even allow for in-situ observation of sub-surface processes such as sub-surface ion diffusion in batteries.[130]

1.3.5 Viscometry

One of the most important physical properties of a solvent is viscosity. It is often described as liquid's internal resistance to flow and is commonly attributed to the

internal mechanistic of a fluid under tensile and shear stress.[134] Viscosity is also defined as a ratio of shear stress to shear rate using the following equation:

$$\eta = \frac{\tau}{\gamma} = \frac{{}^{F}/_{A}}{{}^{du}/_{dy}} \quad \textbf{[13]}$$

Where: η is viscosity, *du/dy* is the local shear velocity, *F* is the force applied and *A* is the stress area. It is also defined as the rate at which momentum is transferred through the liquid. Yet another description of viscosity is the rate of energy dissipation through the liquid.[95] Viscosity of a liquid determines its conductivity and diffusion coefficient (among other properties) hence it impacts the reaction rate in a given solvent. Viscosity of organic and aqueous solvents has been a subject of numerous studies[135,136] starting with the work of Hagen and Poiseuille in the mid 19th century. In these works, movement of the molecules in the solvent had been described as a continual state of soft, slow collisions which results in changes between internal and translational energy of the molecules. The analytical method concerned with measurements of viscosity is called viscometry. In viscometry of liquids, probably the most popular analytical tool is a rotating cylinder viscometer. In the usual experimental setup a polytetrafluoroethylene (PTFE) cylinder probe is immersed and rotated in the liquid at a set speed. The torque necessary to rotate the probe is recorded and used to calculate the viscosity by conversion of the following equation:

$$\eta = \frac{M}{4\pi h\Omega}\left[\frac{1}{R_p^2} - \frac{1}{R_c^2}\right] \quad \textbf{[14]}$$

Where: *h* is the probe height, *M* is the torque, Ω is the angular velocity and R_p and R_c are the diameters of the probe and the container respectively. Varying the probe types (small surface area probes are used for high viscosity liquids and large surface area probes are used for liquids of low viscosity) and the temperature allows to measure the viscosity/temperature dependence. If the solvent displays Arrhenius behaviour, activation energy can also be calculated.[136]

Development of ambient temperature ionic liquids followed by DES has called for a new theory that could explain their unusually high viscosity. In order to explain this phenomena Abbott and co-workers have developed Hole theory which describes the

ionic motion in these fully ionic environment as a movement of ions from one (irregularly spaced) void to another. In simplistic terms, Hole theory relates viscosity of a liquid to its free volume and surface tension Hole theory explains why ionic liquids and DES do not obey the equation derived by Bockris[137] for high temperature molten salts:

$$E_n = 3.74\, RT_m \qquad \textbf{[15]}$$

Where E_n is the viscous flow activation energy, R is a gas constant and Tm is the melting point. Instead for DES this equation has been reported to be:

$$E_n = 23.0\, RT_m \qquad \textbf{[16]}$$

This notable increase in the proportionality factor has been assigned to the large ion/void size gap. This holds true especially for complex anions whose existence has been postulated in many ChCl based type III DES.[48] Rotational viscometry has been successfully applied to study the viscosity of DES with results displaying clear Arrhenius-type viscosity/temperature correlation.[39,45,138]

1.4 Objectives

The overarching aim of the work described in this thesis was the application of optical deflection technique to study the electrochemistry of Deep Eutectic Solvents. For reasons of clarity the whole study has been separated into three parts.

First part was concerned with the performance of the DES as the electrolytes in PEDOT based charge storage systems. The objective of this study was to evaluate which of the DES tested would be potentially the most suitable electrolyte for a secondary charge storage device as well as for an electrochemical actuator. To achieve this, gravimetric and electrochemical techniques were employed.

Second part was the detailed study of the redox behaviour of PEDOT in eutectic solvents selected in the first part. The objective was to apply the EQCM/PBD technique to study the local population changes of dopants. This was considered to be of particular importance due to its influence on charge/discharge cycles in secondary charge storage

devices. This was achieved using electrochemical, gravimetric, optical and imagining techniques.

Third part of the study was the application of the EQCM/PBD technique in studies of metal electrodeposition conducted in DES. The objective of this part was to study the redox chemistry of this process with particular focus on the changes to oxidation states of the metals of interest, as well as the DES influence on the produced deposits. To achieve this, electrochemical, gravimetric, optical and imagining techniques were employed.

1.5 References

[1] D. A. MacInnes, *The Principles of Electrochemistry*, New York, 1939

[2] G. G. Lang, C. A. Barbero, *Laser Techniques for the Study of Electrode Processes*, Berlin, 2012.

[3] T. A. Skotheim, J.R. Reynolds (Ed.): *Handbook of Conducting polymers*, New York, 2007.

[4] A. F. Diazet al., *Handbook of conducting polymers 2*, New York, 1986.

[5] R. Corradi, S.P. Armes, *Synthetic Metals* 1997, **84**, 453-454

[6] T. Holstein, *Annals of Physics*, 1959, Vol**8**, 3, 8-325

[7] A .J. Epstein, Conducting polymers: electrical conductivity. In*: Physical properties of polymers handbook,* ed. J.E. Mark. Berlin: Springer-Verlap, chap. 46.

[8] R. S. Kohlman, J. Joo, Y. Z. Wang, J.P Pouget, H. Kaneko, T. Ishiguro and A. J. Epstein, *Physical Review Letters*, **74**, 5, 773-776.

[9] A.R. Hillman, K.S. Ryder, C.J. Zaleski, C. Fullarton and E. L. Smith, *Z. Phys. Chem.* 2012, **226**, 1049-1068.

[10] A. R. Hillman, S. J. Daisley, S. Bruckenstein, *ElectrochimicaActa*, 2008, **53**, 3763-3771.

[11] H. Randriamahazaka, C. Plesse, D. Teyssié, C. Chevrot, *Electrochemistry Communications*, 2003, **5**, 613-617.

[12] M. J. Brown, A. R. Hillman, S. J. Martin, R. W. Cernosek and H. L. Bandey, *Journal of Materials Chemistry*, 2000, **10**, 115-126

[13] H. Grande, T.F. Otero, *Journal of Physical Chemistry B*, **1998**, 102, 7535-7540.

[14] G. Zotti, *Synthetic Metals*, 1998, **97**, 267-272

[15] G.A. Snook, P. Kao, A.S. Best, *Journal of Power Sources*, 2011, **196**, 1-12

[16] R. Bhattacharya, M.M. de Kok, J. Zhou, *Applied Physics Letters*, 2009, **95**, 223305-1-2233305-3

[17] Y. Xu, Y. Wang, J. Liang, Y. Huang, Y. Ma, X. Wan and Y. Chen, 2009, *Nano Research*, 2009, **3**, 343-348

[18] D. DeLongchamp, P. T. Hammond, *Advanced Materials*, 2001, **13**, 1455-1459

[19] M.A.G. Namboothiry, T. Zimmerman, F. M. Coldren, J. Liu, K. Kim, D. L. Carroll, *Synthetic Metals*, 2007, **157**, 580-584

[20] T. Christen, M. W. Carlen, *Journal of Power Sources*, 2000, **91**, 210-216

[21] E. Frąckowiak, V. Khomenko, K. Jurewicz, K. Lota, F. Béguin, *Journal of Power Sources*, 2006, **153**, 413-418

[22] K. S. Ryu, Y. Lee, Y. Hong, Y. J. Park, X. Wu, K. M. Kim, M. G. Kang, N.Park, S. H. Chang, *ElectrochimicaActa*, 2004, **50**, 843-847.

[23] M. Ocypa, M. Ptasinska, A. Michalska, K. Maksymiuk, E.A.H. Hall, *Journal of Electroanalytical Chemistry*, 2006, **596**, 157-168.

[24] T.Y. Kim, M. Suh, S. J. Kwon, T. H.Lee, J. E. Kim, Y. J. Lee, J. H. Kim, M. P. Hong and K. S. Suh, *Macromolecular Rapid Communications*, 2009, **30**, 1477

[25] M. Döbbelin, R. Marcilla, M. Salsamendi, C. Pozo-Gonzalo, P. M. Carrasco, J. A. Pomposo and D. Mecerreyes, *Chemistry Materials*, 2007,**19**, 2147-2149.

[26] M. Döbbelin, R. Marcilla, C. Pozo-Gonzalo and D. Mecerreyes, *Journal of Materials Chemistry*, 2010,**20**, 7613-7622.

[27] J. L. Segura, R. Gomez, R. Blanco, E. Reinold, P. Bäuerle, *Chemical Materials*, 2006, **18**, 2834-2847

[28] O. Inganäs, in *Handbook of Organic Conductive Molecules and Polymers*, 1997, **vol 3**, ch 15, ed. H. S. Nalwa, John Wiley & Sons Ltd.

[29] M. Döbbelin, , C. Pozo-Gonzalo, R. Marcilla R. Blanco, J. L. Segura, J. A. Pomposo, D. Mecerreyes, *Journal of Polymer Science, Part A: Polymer Chemistry*, 2009, **47**, 3010-3021.

[30] T.Y. Kim, T. H. Lee, J. E. Kim, R. M. Kasi, C. S. P. Sung and K. S. Suh, *Journal of Polymer Science, Part A: Polymer Chemistry*, 2008, **46**, 6872 - 6879.

[31] W. Lu, A. G. Fadeev, B. Qi, E. Smela, B. R. Mattes, J. Ding, G. M. Spinks, J. Mazurkiewicz, D. Zhou, G. G. Wallace, D. R. MacFarlane, S. A. Forsyth and M. A. Forsyth, *Science*, 2002, **297**, 983-987.

[32] F. Vidal, C. Plesse, D. Teyssié and C. Chevrot, *Synthetic Metals*, 2004, **142**, 287-291.

[33] Y. Shibata, T. Kato, T. Kado, R. Shiratuchi, W. Takashima. K. Kaneto and S. Hayase, *Chemical Communications*, 2003, 2730-2731.

[34] J. M. Pringle, V. Armel, M. Forsyth and D. R. MacFarlane, *Australian Journal of Chemistry*, 2009, **62**, 348-352.

[35] J. P. Hallett, T. Welton, *Chemical Reviews*, 2011, **111**, 3508–3576.

[36] Q. Zhang, K. D. O.Vigier, S. Royer and F. Jérôme, *Chemical Society Reviews*, 2012, **41**, 7108-7146.

[37] A. P. Abbott, G. Capper, D. L. Davies, R. K. Rasheed and V. Tambyrajah, *Chemical Communications*, 2003, 70-71

[38] M. Francisco, A. van den Bruinhorst and M. C. Kroon, *AngewandteMinireviews: Green Solvents*, 2013, **52**, 3074-3085.

[39] A. P. Abbott, J. C. Barron, K. S. Ryder, and D. Wilson, 2007, **13**, 6495-6501.

[40] A. P. Abbott, R. C. Harris, K. S. Ryder, C. D'Agostino, L. F. Gladden and M. D. Mantle, *Green Chemistry*, 2011, **13**, 82-90.

[41] A. D. Ballantyne, C. J. Zaleski, R. C. Harris, D. Price and K. S. Ryder,*The Journal of the Institute of Circuit Technology*, Vol. **7**, No 2, 6-10.

[42] M. H. Chakrabarti, F. S. Mjalli, I. M. Al Nashef, M. A. Hashim, M. A. Hussain, L. Bahadori, C. T. J. Low, *Renewable and Sustainable Energy Reviews*, 2014, **30**, 254-270.

[43] P. Martis, V. S. Dilimon, J. Delhalle, Z. Mekhalif, *ElectrochimicaActa*, 2010, **55**, 5407-5410.

[44] A. P. Abbott, G. Frisch, J. Hartley and K. S. Ryder, *Green Chemistry*, 2011, **13**, 471-481.

[45] A. P. Abbott, G. Frisch, S. J. Gurman, A. R. Hillman, J. Hartley, F. Holyoak and K. S. Ryder, *Chemistry Communications*, 2011, **47**, 10031-10033.

[46] A. P. Abbott, J. Collins, I. Dalrymple, R. C. Harris, R. Mistry, F. Qiu, J. Scheirer and W. R. Wise, *Australian Journal of Chemistry*, 2009, **62**, 341-347.

[47] A. P. Abbott, D. Boothby, G. Capper, D. L. Davies and R. K. Rasheed,*Journal of American Chemical Society*, 2004, **126**, 9142-9147.

[48] C. D'Agostino, R. C. Harris, A. P. Abbott, L. F. Gladden and M. D. Mantle, *Physical ChemistryChemical Physics*, 2011,**13**, 21383-21391.

[49] A. R. Hillman, K. S. Ryder, V. C. Ferreira, C.J. Zaleski, E.Vieil, *ElectrochimicaActa*, 2013, **110**, 418-427.

[50] A. P. Abbott, G. Capper and S. Gray, *Physical ChemistryChemicalPhysics*, 2006,**7**, 803-806.

[51] D. Lloyd, T. Vainikka, M. Ronkainen, K. Kontturi, *ElectrochimicaActa*, 2013, **109**, 843-851.

[52] F. Golgovici, A. Cojocaru, M. Nedelcu, T. Visan, *Chalcogenide Letters*, 2009, **6**, 323-333.

[53] S. Salomé, N. M. Pereira, E. S. Ferreira, C. M. Pereira, A. F. Silva, *Journal of Electroanalytical Chemistry*, 2013, **703**, 80-87.

[54] Y. Matsuda, K. Tanaka, M. Okada, Y. Takasu, M. Morita, T. A. Matsumura-Inoue, *Journal of Applied Electrochemistry*, 1988, **18**, 909-914.

[55] M. R. Palacin, *Chemical Society Reviews*, 2009, **38**, 2565-2575.

[56] A. P. Abbott, G. Capper, D. L. Davies, K. J. McKenzie and S. U. Obi, *Journal of Chemical and Engineering data*, 2006, **51**, 1280-1282.

[57] A. P. Abbott, G. Capper, K. J. McKenzie, K. S. Ryder, *Journal of Electroanalytical Chemistry*, 2007, **599**, 288-294.

[58] A. P. Abbott, K. El Ttaib, G. Frisch, K. S. Ryder and D. Weston, *Physical ChemistryChemical Physics*, 2012,**14**, 2443-2449.

[59] A. P. Abbott, K. El Ttaib, G. Frisch, K. J. McKenzie and K. S. Ryder, *Physical Chemistry Chemical Physics*, 2009, **11**, 4269-4277.

[60] E. Gómez, P. Cojocaru, L. Magagnin, E. Valles, *Journal of Electroanalytical Chemistry*, 2011,**658**, 18-24.

[61] D. D. Shivagan, P. J. Dale, A. P. Samantilleke and L. M. Peter, *Thin Solid Films*, 2007, **515**, 5899-5903.

[62] P. J. Dale, A. P. Samantilleke, D. D. Shivagan, and L. M. Peter, *Thin Solid Films*, 2007, **515**, 5751-5754.

[63] A. P. Abbott, G. Capper, D. L. Davies and R. K. Rasheed, *Chemistry- European Journal*, 2004, **10**, 3769-3774.

[64] A. Bakkar and V. Neubert, *Electrochemical Communications*, 2007, 9, 2428-2435.

[65] P. Martis, V. S. Dilimon, J. Delhalle and Z. Mekhalif, *ElectrochimicaActa*, 2010, **55**, 5407-5410.

[66] M. A. Skopek, M. A. Mohamoud, K. S. Ryder and A. R. Hillman, *Chemical Communications*, 2009, 935-937.

[67] A. P. Abbott, S. Nandhra, S. Postlethwaite, E. L. Smith and K. S. Ryder,*Physical Chemistry Chemical Physics*, 2007, **9**, 3735-3743.

[68] C. D. Gu, X. J. Xu and J. P. Tu, *Journal of Physical Chemistry C*, 2010, **114**, 13614-13619.

[69] A.P. Abbott, G. Capper, B.G. Swain, D.A. Wheeler, *Transactions of the IMF*, 2005, **83**, 51-53.

[70] A. P. Abbott, P. M. Cullis, M. J. Gibson, R. C. Harris and E. Raven, *Green Chemistry*, 2007, **9**, 868-872.

[71] M .Hayyan, F. S. Mjalli, M. A. Hashim and I. M. Al Nashef,*Fuel Processing Technology*, 2010, **91**, 116-120.

[72] K. Shahbaz, F. S. Mjalli, M. A. Hashim and I. M. Al Nashef,*Energy Fuels*, 2011, **25**, 2671-2678.

[73] X. Li, M. Hou, B. Han, X. Wang and L. Zou, *Journal of Chemical & Engineering Data*, 2008, **53**, 548-550.

[74] W. C. Su, D. S. H. Wong and M. H. Li, *Journal of Chemical &Engineering Data*, 2009, **54**, 1951-1955.

[75] H. G. Morrison, C. C. Sun and S. Neervannan, *International Journal of Pharmaceutics*, 2009, **378**, 136-139.

[76] F. Ilgen, D. Ott, D. Karlish, C. Reil, A. Palmeberger and B. König, *Green Chemistry*, 2009, **11**, 1948-1954.

[77] S. Hu, Z. Zhang, Y. Zhou, J. Song, B. Han, H. Fan, W. Li, J. Song and Y. Xie, *Green Chemistry*, 2008, **10**, 1280-1283.

[78] A. P. Abbott, G. Capper, D. L. Davies, R. K. Rasheed and V. Tambyrajah, *Green Chemistry*, 2002,**4**, 24-26.

[79] J. D. Mota-Morales, M. C. Gutiérriez, I. C. Sanchez, G. Luna-Barcenas and F. del Monte, *Chemistry Communications*, 2011, **47**, 5328-5330.

[80] S. B. Phadtare, G. S. Shankarling, *Green Chemistry*, 2010, **12**, 458-462.

[81] Y. A. Sonawane, S. B. Phadtare, B. N. Borse, A. R. Jagtap and G. S. Shankarling, *Organic Letters*, 2010, **12**, 1456-1459.

[82] O. Coulembier, V. Lemaur, T. Josse, A. Minoia, J. Cornil and P. Dubois, *Chemical Sciences*, 2012, **3**, 723-726.

[83] G. Imperato, R. Vasold and B. König, *Green Chemistry*, 2006, **8**, 1051-1055.

[84] F. Ilgen, B. König, *Green Chemistry*, 2009, **11**, 848-854.

[85] J. T. Gorke, F. Srienc and R. J. Kazlauskas, *Chemical Communications*, 2008, 1235-1237.

[86] N. Azizi, E. Batebi, S. Bagherpour and H. Gharufi, *RSC Advances*, 2012, **2**, 2289-2293.

[87] S. Gore, S. Baskaran, B. König, *Green Chemistry*, 2011, **13**, 1009-1013.

[88] A. P. Abbott, A. D. Ballantyne, J. P. Conde, K. S. Ryder and W. R. Wise, *Green Chemistry*, 2012, **14**,1302-1307.

[89] E. R. Copper, C. D. Andrews, P. S. Wheatley, P. B. Webb, P. Wormald and R. E. Morris, *Nature*, 2004, **430**, 1012-1016.

[90] E. A. Drylie, D. S. Wragg, E. R. Parnham, P. S. Wheatley,*AngewandteChemie International Edition*, 2007, **46**, 7839-7843.

[91] J. H. Liao, P. C. Wu and Y. H. Bai, *Inorganic Chemical Communications*, 2005, **8**, 390-392.

[92] P. Jhang, N. Chuang and S. Wang, *AngewandteChemie International Edition*, 2010, **49**, 4200-4204.

[93] R. G. Compton, C. E. Banks, *Understanding Voltammetry*, Singapore, 2007.

[94] *Autolab Application Note EC08*, MetrohmAutolab B.V. 2011.

[95] A. R. Hillman, *Journal of Solid State Electrochemistry*, 2011, **15**,1647–1660.

[96] Z. Jusys, H. Massong, H. Baltruschat, 1999, *Journal of the Electrochemical Society*, **146**, 1093–1098.

[97] A. P. M .Glassford, *Journal of Vacuum Science & Technology*,1978, **15**, 1836-1843.

[98] S. Bruckenstein, M. Shay, 1985, *ElectrochimicaActa*, **30**, 1295–1300

[99] Sauerbrey G, *ZeitschriftPhysikalishe*,1959,**155**, 202–222.

[100] K. K. Kanazawa, J. G. Gordon, *Analytical ChimicaActa*, 1985, **175**, 99–105

[101] K. K. Kanazawa, *Faraday Discussions*, 1997, **107**, 77-90.

[102] S.Bruckenstein , A.Fensore , Z. Li , A. R. Hillman, *Journal of Electroanalytical Chemistry*,1994, **370**, 189–195.

[103] T. Nomura, M. Ilima, *AnalyticaChimicaActa*, 1981, **131**, 97-102.

[104] G.G. Láng: *Kösters laser interferometer*. In: *Electrochemical dictionary*, A. J. Bard G. Inzelt, F. Scholz (eds). 2008, Springer, Berlin.

[105] G.G. Láng, K.E. Heusler, 1995, Elektrohiymia, **31**, 826-835.

[106] L. Jaeckel, G.G. Láng, K. Heusler, 1994, *ElectrochimicaActa*, **39**, 1031–1038

[107] J. Rishpon, A. Redondo, C. Derouin and S. Gotttesfeld, *Journal of Electroanalytical Chemistry*, 1990, **294**, 73-85.

[108] K. Shimazu, S. Ye, Y. Sato, K. Uosaki, *Journal of Electroanalytical Chemistry*, 1994, **375**, 409-413.

[109] B. B. Berkes, S. Vesztergom, G. Inzelt, *Journal of Electroanalytical Chemistry*, 2014, **719**, 41-46.

[110] Z. Jusys, H. Massong, H. Baltruschat, *Journal of Electrochemical Society*, **146**, 1093-1098.

[111] C. A. Barbero, *Physical Chemistry Chemical Physics*, 2005, **7**, 1885-1899.

[112] C. A. Barbero, M. C. Miras, R. Kötz, O. Haas, *Solid State Ionics*, 1993, **60**, 167-172.

[113] M. J. Henderson, A. R. Hillman, E. Vieil, C. Lopez, *Journal of Electroanalytical Chemistry*, 1998, **458**, 214-248.

[114] E. Vieil, *Journal of Electroanalytical Chemistry*, 1994, **264**, 9-15.

[115] M. J. Henderson, A. R. Hillman, E. Vieil, *Journal of Electroanalytical Chemistry*, 1998, **454**, 1-8.

[116] A. R. Hillman, K. S. Ryder, C. J. Zaleski, V. Ferreira, C. A. Beasley, E. Vieil, *ElectrochimicaActa*, 2014, accepted manuscript.

[117] C. A Barbero, M. C. Miras, *The Journal of the Argentine Chemical Society*, 2003, **91**, 1-40.

[118] C. A. Barbero, M. C. Miras, O. Haas and R. Kötz, *Synthetic Metals*, 1993, **55**, 1539-1544.

[119] T. Matencio, E. Vieil, *Synthetic Metals*, 1991, **44**, 349-356.

[120] K. Kozieł, M. Łapkowski, E. Vieil, *Synthetic Metals*, 1997, **84**, 91.

[121] G. A. Planes, M. C. Miras, C. A. Barbero, *Polymers International*, 2002, **51**, 429-433.

[122] O. Haas, *Faraday Discussions Chemical Society*, 1989, **88**, 123-131.

[123] M. C. Pham, J. Molish, C. A. Barbero, O. Haas, *Journal of the Electroanalytical Chemistry*, 1991, **316**, 143-149.

[124] G. Gracia, M. M. Bruno, G. A. Planes, J. L. Rodriguez, C. A. Barbero and E. Pastor, *Physical Chemistry Chemical Physics*, 2008, **10**, 6677-6685.

[125] G. A. Planes, M. C. Miras, C. A. Barbero, *Double layer properties of carbon aerogel electrodes measured by probe beam deflection and AC impedance techniques.*In: Advanced batteries and supercapacitors, PV-2001. The Electrochemical Society, Penninigton, 2002.

[126] J. B. Schlenoff, H. Ly, M .Li, *Journal of the American Chemical Society*, 1998, **120**, 7626-7634.

[127] G. Binnig, C. F. Quate and Ch. Gerber, *Physical Review Letters*, 1986, **56**, 930-933.

[128] G. Binnig and H. Rohrer, *Scientific American*, 1985, **253**, 50.

[129] K. E. Peterson, *Proceedings of the IEEE*, 1982, **70**, 420-457.

[130] R. Garcia, E. T. Herruzo, *Nature Nanotechnology*, 2012, **7**, 217-226.

[131] S. N. Magonov, V. Eilngs, M. H. Whangbo, *Surface Science Letters*, 1997, **375**, 385-391.

[132] A. Knoll, R. Magerle, G. Krausch, *Macromolecules*, 2001, **34**, 4159-4165.

[133] R. Wen, H. R. Byon, *Chemical Communications*, 2014, **50**, 2628-2631.

[134] J. H. Hildebrand, *Science*, 1971, **174**, 490-492.

[135] M. SoudersJr, *Journal of the American Chemical Society*, 1938, **60**, 154-158.

[136] P. Atkins, J. De Paula, *Atkins' Physical Chemistry*, Oxford University Press, 2006.

[137] J. O'M. Bockris, A. K. N. Reddy, *Modern Electrochemistry*, Vol 1. Plenum Press, Ney York, 1970, Ch. 6.

[138] A. P. Abbott, G. Capper, D. L. Davies and R. K. Rasheed, *Chemistry – European Journal, 2004*, **10**, 3769-3774.

Chapter II

General experimental and data analysis procedures

2.1 Introduction

This chapter contains the description of the materials, general analytical, data analysis and sample preparation techniques as well as the equipment used. Due to the complexity of the analytical approach, gravimetric and optical-gravimetric methods have been described in separate sub-chapters. The mathematical approach used for convolution of the optical and gravimetric data has been presented. Diversity of systems studied in this thesis resulted in more specific details like electrodeposition of conducting polymer films or metal deposits to be covered more extensively in the relevant results chapters.

2.2 Materials

Table 1 contains the list of chemicals used in this project. Potassium ferrocyanide trihydrate, choline chloride, urea, ethylene glycol, propylene glycol, maleic acid, acetic acid, glycerol, acetonitrile, dichloromethane, choline iodide, lithium perchlorate, ethyl ammonium bromide, 3, 4 ethylene(dioxy)thiophene, silver nitrate, silver chloride, copper(II)chloride, tin(II)chloride, bismuth(III)chloride, sodium chloride and perchloric acid were all supplied by Sigma Aldrich and used as received.

Compound	MW g mol^{-1}	Chemical formula	Application
Sodium chloride	58.44	NaCl	Reference electrode calibrant
Potassium Ferrocyanidetrihydrate	422.39	$K_4Fe(CN)_6 \times H_2O$	Reference electrode calibrant

Lithium perchlorate	106.39	$LiClO_4$	Supporting electrolyte
Tetraethyl ammonium bromide	210.16	$C_8H_{20}NBr$	Supporting electrolyte
3, 4 Ethylenedioxythiophene	142.18	$C_6H_6O_2S$	CP monomer
Acetonitrile	41.05	CH_3CN	Molecular solvent
Dichloromethane	84.93	CH_2Cl_2	Molecular solvent
Choline Chloride	139.62	$C_5H_{14}ClNO$	Quaternary ammonium salt
Ethylene Glycol	62.07	$C_2H_6O_2$	Hydrogen bond donor
Propylene Glycol	76.09	$C_3H_8O_2$	Hydrogen bond donor
Acetic Acid (glacial)	60.05	CH_3COOH	Hydrogen bond donor
Malonic Acid	104.06	$C_3H_4O_4$	Hydrogen bond donor
Glycerol	92.09	$C_3H_8O_3$	Hydrogen bond donor
Urea	60.06	CH_4N_2O	Hydrogen bond donor
Perchloric acid (70% aq)	100.46	$HClO_4$ aq	Supporting electrolyte
Silver nitrate	169.87	$AgNO_3$	Metal salt
Silver chloride	143.32	AgCl	Metal salt
Copper chloride	134.45	$CuCl_2$	Metal salt
Tin chloride	189.62	$SnCl_2$	Metal salt
Bismuth chloride	315.34	$BiCl_3$	Metal salt

Table 1. List of chemical compounds used in the course of this project.

2.3 Procedures

2.3.1 Preparation of reference electrode calibrating solution.

The procedures used for the preparation of RE calibrating solutions were as follows:

Preparation of saturated NaCl solution

Sodium chloride was added to 100 ml de-ionised H_2O with continuous heating (60 ºC) and stirring (using hotplate equipped with magnetic stirrer) until the salt no longer dissolved.

Preparation of an aqueous $K_4Fe(CN)_6$ solution

0.211 g of $K_4Fe(CN)_6$ was added to 100 ml of de-ionised H_2O. Mixture was then sonicated until complete dissolution of solids (2 minutes). Prepared electrolyte was stored at 5 ˚C in the dark conditions.

Preparation of a $K_4Fe(CN)_6$/Ethaline 200 solution

0.211 g of $K_4Fe(CN)_6$ was added to 100 ml of Ethaline 200. Mixture was then heated at 50 ˚C with continuous stirring (on a magnetic hotplate) until a homogeneous, colourless liquid was formed. Solution was then cooled and stored at 40 ˚C.

Preparation of an aqueous $K_4Fe(CN)_6$/Propaline 200 solution

0.211 g of $K_4Fe(CN)_6$ was added to 100 ml of Propaline 200. Mixture was then heated at 50 ˚C with continuous stirring (on a magnetic hotplate) until a homogeneous, colourless liquid was formed. Solution was then cooled and stored at 40 ˚C.

2.3.2 Preparation of the electrolytes used in the conducting polymer experiments.

The procedures used for the formation of systems described in Chapters III and IV was as follows:

Preparation of EDOT/lithium perchlorate/acetonitrile solution

To 20 ml of CH_3CN 1.076 g of $LiClO_4$ was added followed by 0.710 g of 3, 4 ethylene(dioxy) thiophene. Resulting mixture was toped up with CH_3CN up to 100 ml mark in a volumetric flask and sonicated until complete dissolution of solids (2 minutes). Prepared electrolyte was stored at 5 ˚C in the dark conditions.

Preparation of lithium perchlorate/acetonitrile solution

1.076 g of $LiClO_4$ was topped with CH_3CN up to 100 ml mark in a volumetric flask and sonicated until complete dissolution of solids (2 minutes). Prepared electrolyte was stored at 5 ˚C in the dark conditions.

Preparation of tetraethyl ammonium bromide/dichloromethane system

2.102 g of $C_8H_{20}NBr$ was topped with CH_2Cl_2 up to 100 ml mark in a volumetric flask and sonicated until complete dissolution of solids (2 minutes). Prepared electrolyte was stored at 5 ˚C in the dark conditions.

Preparation of the Ethaline 200 DES

Choline chloride and ethylene glycol were mixed in a 1:2 molar proportions. Mixture was subsequently heated with continuous stirring (on a magnetic hotplate) until a homogeneous, colourless liquid was formed. Solvent was subsequently cooled and stored at 40 ˚C.

Preparation of the Propaline 200 DES

Choline chloride and propylene glycol were mixed in a 1:2 molar proportions. Mixture was subsequently heated with continuous stirring (on a magnetic hotplate) until a homogeneous, colourless liquid was formed. Solvent was subsequently cooled and stored at 40 ˚C.

Preparation of the Acetaline 200 DES

Choline chloride and glacial acetic acid were mixed in a 1:2 molar proportions. Mixture was subsequently heated with continuous stirring (on a magnetic hotplate) until a homogeneous, colourless liquid was formed. Solvent was subsequently cooled and stored at 40 ˚C.

Preparation of the Maline 200 DES

Choline chloride and malonic acid were mixed in a 1:2 molar proportions. Mixture was subsequently heated with continuous stirring (on a magnetic hotplate) until a homogeneous, colourless liquid was formed. Solvent was subsequently cooled and stored at 40 ˚C.

Preparation of the Glyceline 200 DES

Choline chloride and glycerol were mixed in a 1:2 molar proportions. Mixture was subsequently heated with continuous stirring (on a magnetic hotplate) until a homogeneous, colourless liquid was formed. Solvent was subsequently cooled and stored at 40 ˚C.

Preparation of the Reline 200 DES

Choline chloride and urea were mixed in a 1:2 molar proportions. Mixture was subsequently heated with continuous stirring (on a magnetic hotplate) until a homogeneous, colourless liquid was formed. Solvent was subsequently cooled and stored at 40 ˚C.

2.3.3 Preparation of the electrolyte for the metal deposition/dissolution experiments.

The procedures used for the formation of systems described in Chapter V were as follows:

Preparation of silver nitrate/perchloric acid electroplating solution.

2.174 ml of perchloric acid (70 % aqueous) was mixed with 50 ml of de-ionised H_2O and then 0.017 g of silver nitrate was added. The mixture was then topped up with de-ionised H_2O up to 100 ml in a volumetric flask and sonicated until complete dissolution (2 minutes). Prepared electrolyte was stored at 5 ˚C in dark conditions.

Preparation of silver chloride/Ethaline 200 electroplating solution.

0.143 g of silver chloride was added to 100 ml of Ethaline 200. Mixture was then heated at 50 ˚C with continuous stirring (on a magnetic hotplate) until a homogeneous, colourless liquid was formed. Solution was then subsequently and stored at 40 ˚C.

Preparation of copper chloride/Ethaline 200 electroplating solution.

0.134 g of copper(II)chloride was added to 100 ml of Ethaline 200. Mixture was then heated at 50 ˚C with continuous stirring (on a magnetic hotplate) until a homogeneous, colourless liquid was formed. Solution was subsequently cooled and stored at 40 ˚C.

Preparation of tin chloride/Ethaline 200 electroplating solution.

0.190 g of tin(II)chloride was added to 100 ml of Ethaline 200. Mixture was then heated at 50 ˚C with continuous stirring (on a magnetic hotplate) until a homogeneous, colourless liquid was formed. Solution was subsequently cooled and stored at 40 ˚C.

Preparation of bismuth chloride/Ethaline 200 electroplating solution.

0.315 g of bismuth(III)chloride was added to 100 ml of Ethaline 200. Mixture was then heated at 50 ˚C with continuous stirring (on a magnetic hotplate) until a homogeneous, colourless liquid was formed. Solution was subsequently cooled and stored at 40 ˚C.

Preparation of bi-metal (silver/copper)/Ethaline 200 electroplating solution.

0.0717 g of silver chloride and 0.067 g of copper(II)chloride was added to 100 ml of Ethaline 200. Mixture was then heated at 50 ˚C with continuous stirring (on a magnetic hotplate) until a homogeneous, colourless liquid was formed. Solution was subsequently cooled and stored at 40 ˚C.

2.4 Instrumental

2.4.1 EQCM instrumentation

Cyclic voltammetry and chronoammperometry were conducted using a potentiostat (μAUTOLAB III) coupled to frequency analyser (Hewlett Packard 8751 A Network Analyser). Cyclic voltammetry experiments were carried out at 2, 5, 10, 20, 50, 100 and 200 mv/s scan rate. Quartz crystal impedance spectra were recorded in a reflectance mode. The acoustic impedance readings were acquired every 4 seconds on average. Current, charge and the voltage were recorded using the frequency analyser data storage facility.

2.4.2 Electrodes

EQCM working electrode (WE)

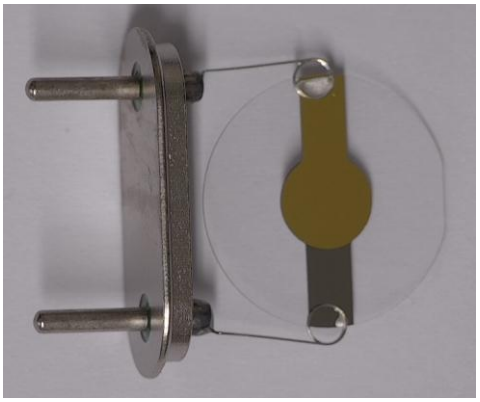

Figure 1. The working electrode (WE) used in EQCM experiments. 10 MHz, AT-cut polished, thickness shear mode quartz resonator (ICM Manufacturing, Oklahoma City, USA). Cr electrodes are located on both faces of the resonator. Electrodes were Au coated (by means of Physical Vapour Deposition). Piezoelectric and electrochemically active areas are 0.21 cm^2 and 0.23 cm^2 respectively.

Counter electrode (CE)

Electrochemical processes involve change of electroactive and non-electroactive species concentration. The source of the concentration gradient is the working

electrode.[1] Theoretically, any pair of electrodes could be used, however, in practice if both WE and CE are of similar sizes they will significantly influence each other electrochemical responses.[1] The counter electrode was an IrO_2 coated Ti mesh (DeNora) with 2 cm^2 electroactive area. The size of CE was deliberately increased in order to provide surplus electroactive area in the event of CE partial blockage.[1] The electrode was formed in a L shape (1:3 length ratio) to provide maximum proximity of WE and the lower part of the CE during the electrochemical experiments.

Reference electrode (RE)

An Ag/AgCl wire exposed to the chloride media was used as a reference electrode; this has been shown to provide a stable reference potential in choline chloride based eutectics.[2] To provide a link to other data, ferri-/ferrocyanide couple was used as a calibrant. The E_0 of this couple (approximated as the mean of the anodic and cathodic peak potentials in slow scan voltammetry) was found to be 0.220 V in an aqueous solution, 0.227 V in Ethaline 200 and 0.185 V in Propaline 200.

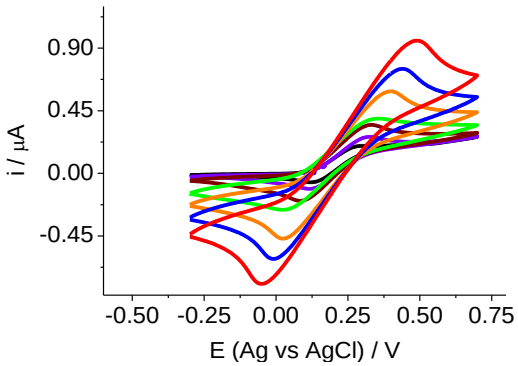

Figure 2. Voltammograms of Au plated quartz crystal resonator redox cycled from - 0.3 V → 0.7 V → - 0.3 V in an aqueous 0.005 M $K_4Fe(CN)_6$. Black line 2 mV s^{-1}, violet 5 mV s^{-1}, wine 10 mV s^{-1}, green 20 mV s^{-1}, orange 50 mV s^{-1}, blue 100 mV s^{-1}, red 200 mV s^{-1} respectively.

ChCl based DES like Ethaline and Propaline have inherent high chlorine concentration (5.4 and 4.6 M respectively). In order to replicate the conditions of Ag/AgCl boundary (formed in these media upon the immersion of bare silver wire) in an aqueous solution, Ag wire was initially coated with AgCl layer. This was achieved through chronoammperometric (0.8 V, 120 s) deposition from an aqueous saturated

solution of NaCl. This AgCl coated Ag wire was used as RE in an aqueous 0.005 M $K_4Fe(CN)_6$ solution.Figures 3 and 4 show the current increase in the oxidation stage, this is due to the Au (i.e. the electrode surface) oxidation potential being lower in DES than it is in an aqueous solution.

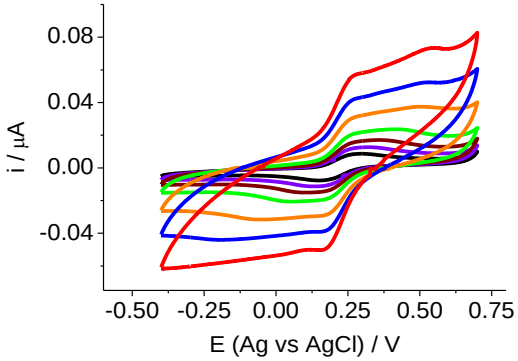

Figure 3. Voltammograms of Au plated quartz crystal resonator redox cycled from - 0.3 V → 0.7 V → - 0.3 V in 0.005 M $K_4Fe(CN)_6$/ Ethaline 200. Black line 2 mV s^{-1}, violet 5 mV s^{-1}, wine 10 mV s^{-1}, green 20 mV s^{-1}, orange 50 mV s^{-1}, blue 100 mV s^{-1}, red 200 mV s^{-1} respectively.

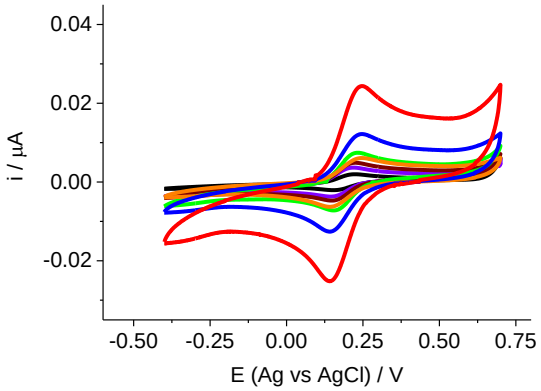

Figure 4. Voltammograms of Au plated quartz crystal resonator redox cycled from - 0.3 V → 0.7 V → - 0.3 V in 0.005 M $K_4Fe(CN)_6$/Propaline 200. Black line 2 mV s^{-1}, violet 5 mV s^{-1}, wine 10 mV s^{-1}, green 20 mV s^{-1}, orange 50 mV s^{-1}, blue 100 mV s^{-1}, red 200 mV s^{-1} respectively.

2.4.3 EQCM electrochemical cell

Electrochemical cell used during the gravimetric experiments in this study is presented in figure below.

Gravimetric electrochemical cell

Figure 5. PTFE in-house made electrochemical cell. External dimensions h = 49 mm, diameter = 35 mm, maximum electrolyte volume = 20 ml, electrolyte volume used = 10 ml. The same CE and RE were used for the gravimetric and optical-gravimetric experiments. EQCM crystal was mounted in a PTFE cell in such a way that one of its sides was exposed to the electrolyte and the other one to the air. The electrolyte facing side formed the working electrode, while the other side of the quartz crystal provided the reference resonant frequency.

2.4.4 PBD-EQCM instrumentation

EQCM – PBD experiments were carried out using a Gamry potentiostat/galvanostat/EQCM instrument (Gamry 600) coupled to in – house made probe beam deflection instrument. The entire experimental set–up consisted of a potentiostat/galvanostat unit and a separate eqcm analyser (these elements compromised the EQCM system) and 632.8 nm wavelength Ne–He laser (Uniphase model 1122, 4 mV power output), position sensing detector (dual silicon based photodiode – Optilas model 1243 bi-cell, 2.5 ×2.5 mm active area, 127 μm gap between the active surfaces), differential amplifier, oscilloscope and voltmeter (these were used to monitor the DC current produced by a PSD) and *x*, *y*, *z* axis motorised electrochemical cell stage. Set – up of the complete EQCM – PBD instrument can be seen in the figure 6.

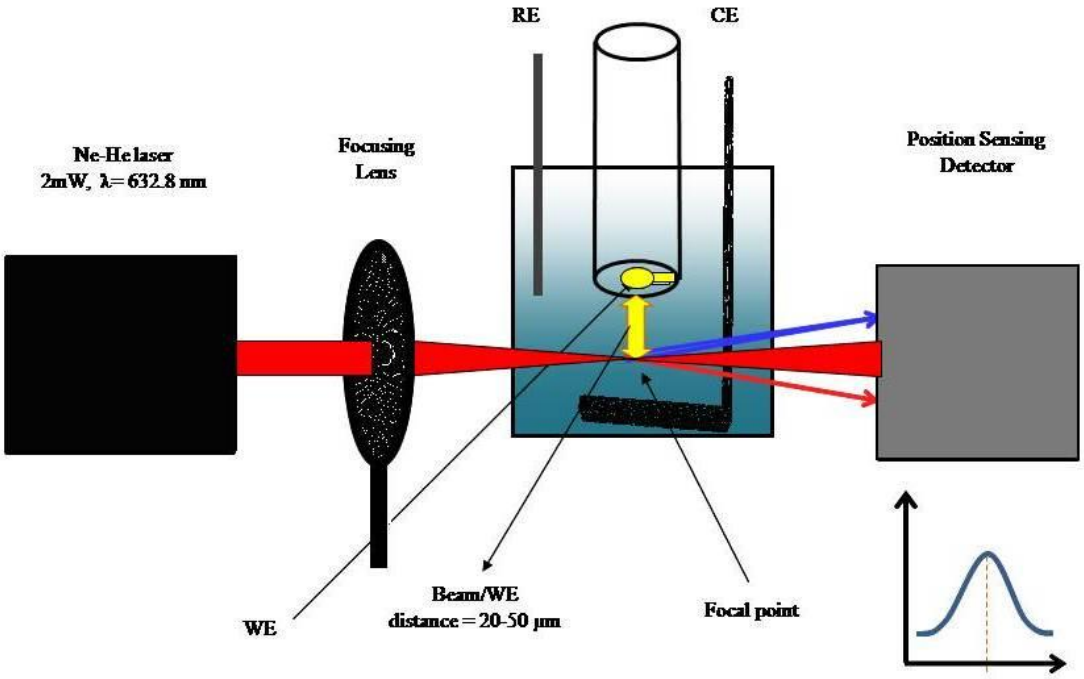

Figure 6. Schematic representation of the PBD-EQCM instrument. Stage was remotely controlled via Unidex 12 control unit, (these elements compromised the PBD). The electrochemical cell stage comprised an aluminium cradle mounted on a translation table allowing for vertical (*x*), transverse (*y*) and rotational (*z*) motion with 0.1 μm (*x*, *y*) and 0.025 arc min (*y*) resolutions. These functions allowed for the adjustment of the alignment, distance and parallelism between the laser beam and surface of the working electrode. The Gaussian graph (visible in the bottom right corner of figure 6) represents the intensity of the laser beam with the peak representing the maximum light intensity (i.e present it the centre of the laser beam). All components of the instrument were installed on a steel breadboard. The entire instrument was connected to a personal computer and operated through the Gamry software.

2.4.5 Electrodes

EQCM-PBD working electrode (WE)

These electrodes were made in-house. WE assembly procedure and final product are presented below in figure 7:

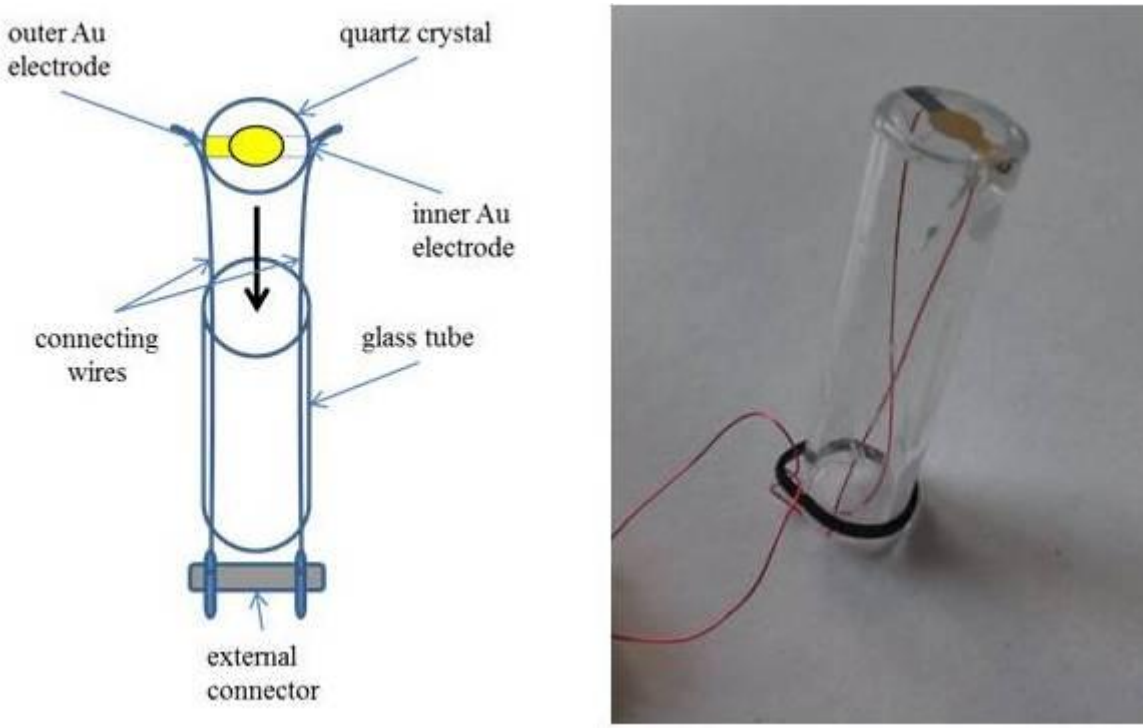

A *B*

Figure 7. Panel A: assembling procedure of the EQCM-PBD working electrode. Connecting wires were attached to the quartz (10 MHz AT-cut polished, thickness shear mode) resonator. Piezoelectric and electrochemically active areas were 0.21 cm^2 and 0.23 cm^2 respectively) with silver conducting glue (Electrolube Ltd) and soldered to the external connector. Inner face of the quartz crystal was glued to the glass tube (l. 55mm, Ø 13mm) with RS 692-542 silicon adhesive sealant. Panel B: assembled working electrode used in PBD - EQCM experiments.

2.4.6 Electrochemical cell

Optical-gravimetric electrochemical cell

The electrochemical cell used for the EQCM – PBD experiments was a glass quartz cuvette (Helma Inc). It had an external size of 42mm×42mm×30mm (height/breadth/width respectively). The cell was equipped with a Teflon ™ lid into which the electrodes were set. The PBD electrochemical cell and its arrangement of electrodes are shown in figure 8.

Optical - gravimetric electrochemical cell

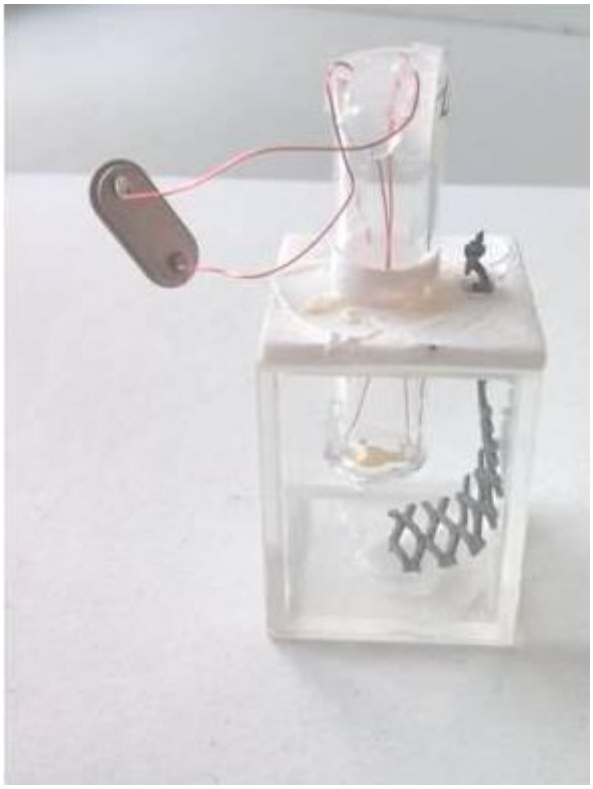

Figure 8. Electrochemical cell used for the optical-gravimetric experiments. WE and CE installed.

CE was made of IrO_2 coated titanium mesh with 2.0 cm^2 active surface, RE - reference electrode (not shown) was silver wire used for all of the experiments in both aqueous and molecular solvents as well as in DES. The WE was custom made as described above.

2.5 Experimental and data analysis procedures.

2.5.1 Experimental procedures

EQCM Experimental procedures

Electrode cleaning, polymer films electrodeposition and characterisation procedures were universal for both EQCM and EQCM-PBD experiments.

Electrode cleaning procedures

CE were cleaned through rinsing with de-ionised H_2O, acetone and dried in the oven (set to 60 ˚C) for 5 min. RE were cleaned using emerald sandpaper then washed with distilled H_2O, acetone and dried in the oven (set to 60 ˚C) for the same period of time. WE were cleaned by the removal of the material deposited during the experiments using cotton swabs soaked in 1:1 H_2O/HNO_3 solution followed by rinsing with de-ionised H_2O, acetone and subsequent drying with compressed air. All EQCM experiments were conducted at room temperature. EQCM crystal was placed at the bottom of the cell, sandwiched between two-silicone rubber o–rings (providing an air tight seal) in such a way that one of the crystal sides was exposed to the solution and the other one faced the air. The side of the crystal exposed to the solution formed the WE – see figure 1.

Electrodeposition of the polymer films

Polymer films used in the gravimetric experiments were electrodeposited and characterized in a PTFE 3 – electrode electrochemical cell. The same counter and reference electrodes were used as for the optical-gravimetric experiments. Electrolyte amount was 10 ml for all of the gravimetric experiments. All films were grown using chronoamperommetry (potential of 1.2 V applied for 30 s) from the solution of 0.05 M EDOT in 0.1 M $LiClO_4/CH_3CN$. The resulting polymer films had a $Q_{dep} = 70 \pm 15$ mC cm^{-2}.

Characterization of the polymer films

To avoid the so called ‘history effect’ influence on the results of the analysis all the polymer films were soaked and cycled 3 times in an electrolyte (at 200 mV s^{-1} scan rate) prior to the experiment. Potentiodynamic (cyclic voltammetry) and potentiostatic (chronoammperometric) experiments were conducted immediately afterwards. In order to achieve the stability of Δm and I signals, experiments were repeated 3 times with the 3^{rd} data set used for the analysis.

EQCM-PBD experimental procedures

Prior to the EQCM – PBD experiments the electrochemical cell was washed with de-ionised H_2O, acetone, dried and washed with filtered electrolyte. All solutions used were filtered through nylon 0.45 μm pore size filters (Cronus) prior to use in the electrochemical experiments. In order to overcome their high viscosity at room temperature all DES were filtered at ºC 60.

Electrodeposition of metal deposits

Metal deposits studied in Chapter V were electrodeposited potentiodynamically. 3 cyclic voltammetry experiments were conducted for each scan rate studied, with the 3rd data set used for the analysis.

Beam-electrode adjustment

The direct measurement of the laser beam deflection in real time was not possible in the current experimental set-up. Thus, the adjustment of the beam/electrode distance was achieved through a series of chronodeflectometry (CD) experiments conducted with the same conditions except a variable *x* (beam-electrode distance) with simultaneous monitoring of the optical signal.

X values that were too low (i.e. the WE was obscuring majority of the laser beam) resulted in a reduced optical signal intensity. Too large *x* values (i.e. WE was too far from the laser beam) resulted in a loss of the optical signal sensitivity (due to the "diffusion barrier" effects). A trial and error approach used, allowed for the creation of a range of *x* values. This range was subsequently used to locate an optimum distance of approach value, at which the optical signal bore a closest possible resemblance to the electrical signal (this distance was be denoted x_0). Upon establishing the optimum distance the chronodeflectometric experiments were conducted again at several increasing (+ 10, + 20, + 30 μm) and decreasing (-10, - 20, - 30 μm) distances. These results then formed a range of *x* values which when plotted versus $x/\sqrt{D}$ parameter (obtained from the convolution software) formed a linear plot. The gradient of this plot is equal to the diffusion coefficient of the electroactive species. Its value was used as an accuracy indicator of the convolution protocol (i.e. the values of the diffusion

coefficient quoted in the literature and the values obtained from the Cottrell plots were compared to the values obtained by optical deflection). When a close agreement was found for the *x/(x/D)* linearity, its values were subsequently extrapolated to reveal the -x_0 which was then treated as the actual physical (i.e absolute) beam/electrode distance.

Calculation of the laser beam diameter at the focal point

The major objective was achieving minimal possible distance of approach, as the main experimental objective was the observation of a very small concentration gradients present during electrochemical processes conducted in an ionic media.

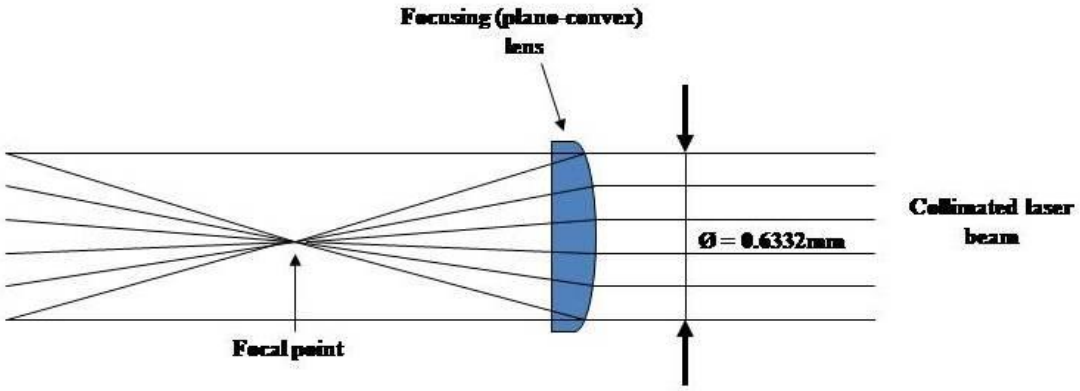

Figure 9. Schematic representation of the laser beam passage prior to, at, and after the focal point.

The beam diameter was calculated using the following equation:

$$r = 1.27\frac{f}{\emptyset}\lambda \qquad \textbf{[1]}$$

Where *f is* the distance between the focusing lens and the focal point (i.e. the focal length of the focusing lens used), λ is the laser wavelength and Ø is the beam diameter. Using the focal point diameter obtained (79.83μm) the laser beam radius at the focal point was calculated to be 39.92μm. This value is similar to the values used in other PBD experiments.[3,4,5]

Calculation of the beam divergence angle.

According to the manufacturer specifications, the diameter of the laser beam at the point of cavity exit was 0.63 mm. However, this value is only valid for the laser beam at the point of exit from the cavity. Upon leaving the cavity the beam diverges due to the interactions between photons and air.

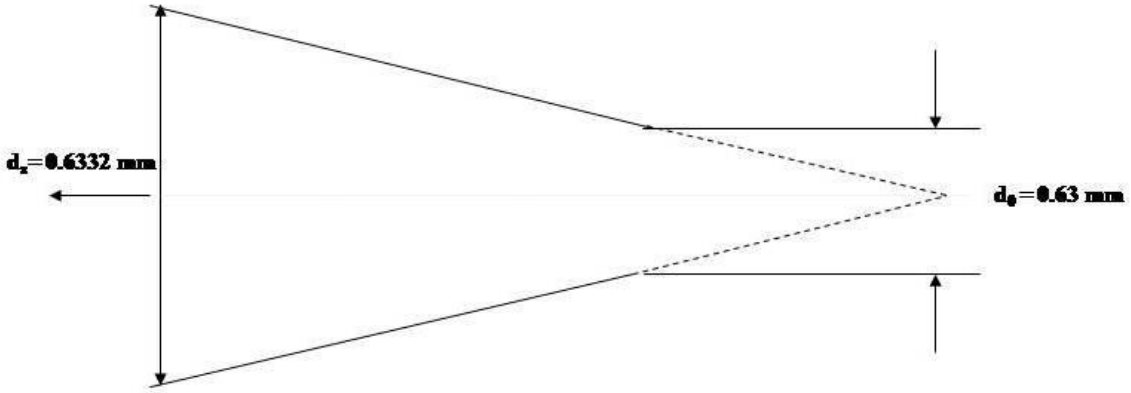

Figure 10. Schematic representation of the beam divergence upon its exit from the laser cavity. d_0 is the laser beam diameter upon its exit from the laser cavity and d_z is the laser beam diameter at the focusing lens.

Beam divergence angle was calculated using the following equation:

$$\Theta = \frac{4}{\pi}\frac{\lambda}{d_0} \quad \textbf{[2]}$$

Where d_0 is the initial laser beam diameter. The calculated beam divergence angle was 1.279×10^{-3} rad. This result was further confirmed using the equation 3, which relates the beam diameter at the cavity exit (d_0) to the one at focal point (d_z):

$$(d_z)^2 = (d_0)^2 = \left[1 + \left(\frac{(\Theta \times Z)}{d_0}\right)^2\right] \quad \textbf{[3]}$$

Where Z is the distance between the laser and the focusing lens (50 mm), d_z is the beam diameter at the focal lens and Θ is the beam divergence angle.

Calculation of the distance of minimum approach

This value determines how close to the electrode the focal point can be located. The following equation was used to determine this value:

$$\chi_{min} = \frac{S}{4}\frac{d_z}{f} \quad \textbf{[4]}$$

Where S is the laser beam interaction length (i.e the external diameter of the working electrode). Set-up used allowed for the decrease of the minimum approach distance to 32.72 μm (measured from the centre of the focal point). Since the focal point diameter is 79.83 μm, at the minimum distance of approach the WE would obscure ~ 41 % of the beam. This is within the values reported in the literature as values of up to 70 % were previously reported.[4]

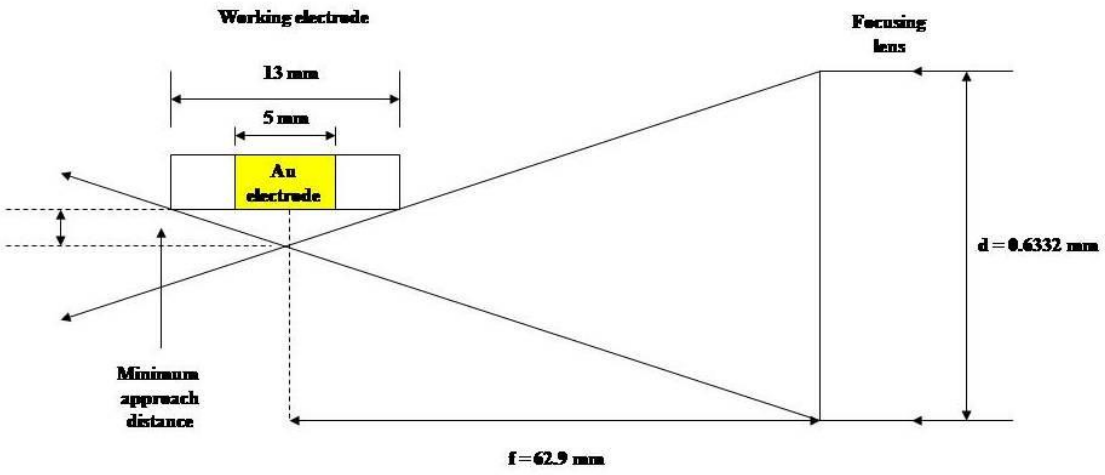

Figure 11. Schematic representation of the distance of minimum approach.

Calculation of the maximum permissible deviation angle

Calculation of this value is necessary for the determination of the range of deflections that can be recorded experimentally. Schematic representation of this is shown in figure 12.

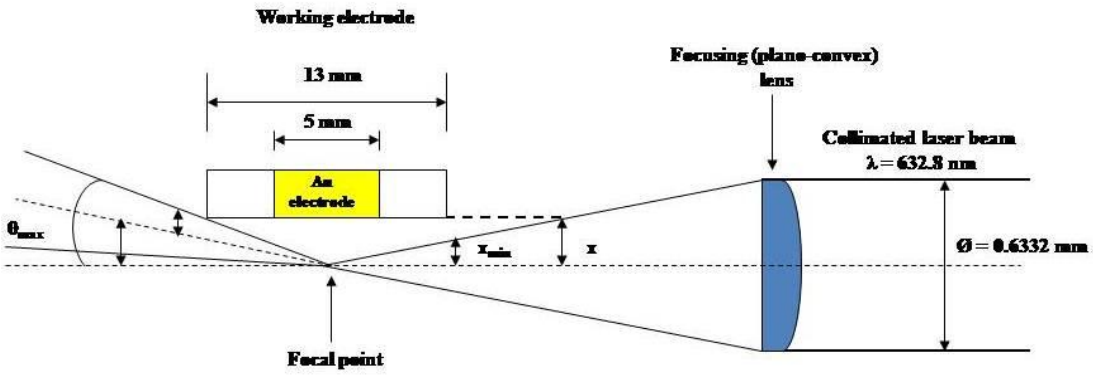

Figure 12. Schematic representation of the laser beam maximum permissible deviation angle.

Laser beam deflections exceeding this value will have a very low (or zero) intensity due to the laser beam being obscured by WE and thus being unable to reach the PSD (or give values below the detector lower limit of detection (LOD)).

From the calculations presented in the previous step the minimum distance of approach was determined as x_{min}= 32.72 μm. The following relationship was used to determine the maximum angle of deflection:

$$\theta_{max} \approx tan(\theta_{max}) = \frac{ds/2}{s/2} \quad \textbf{[5]}$$

$$\text{Thus} \quad X_{min} \approx X - ds/2 \quad \textbf{[6]}$$

$$\text{Therefore} \quad ds/2 \approx x - \left(\frac{s}{4}\frac{d}{f}\right) \quad \textbf{[7]}$$

Assuming that the electrode's surface is located 25 μm away from the focal point and the $d_{s/2}$ = 7.72 μm, then, by inference from equations 5, 6 and 7:

$$\theta_{max} = \frac{ds/2}{s/2} \quad \textbf{[8]}$$

Therefore, when the laser beam is positioned 25 μm from the WE, the maximum permissible angle of deflection is 1.19 mrad. At the θ_{max}. values exceeding this limit, the intensity of the optical signal will decrease beyond experimentally useful values.

Calculation of the laser spot diameter at the detector

The diameter of the laser beam at the detector must not be larger than the optically active surface as this would inevitably result in a very low sensitivity of the detector to the displacement of the spot (i.e point with the maximum light intensity). At the same time it must be significantly larger than the gap (127μm) between the photodiodes to avoid signal loss. Therefore, the detector was placed at a sufficient distance with the light spot covering circa 45% of the PSD surface, but at the same time close enough for the beam divergence effects still being negligible. The graphic representation of the laser spot diameter measurement is shown in the figure 13.

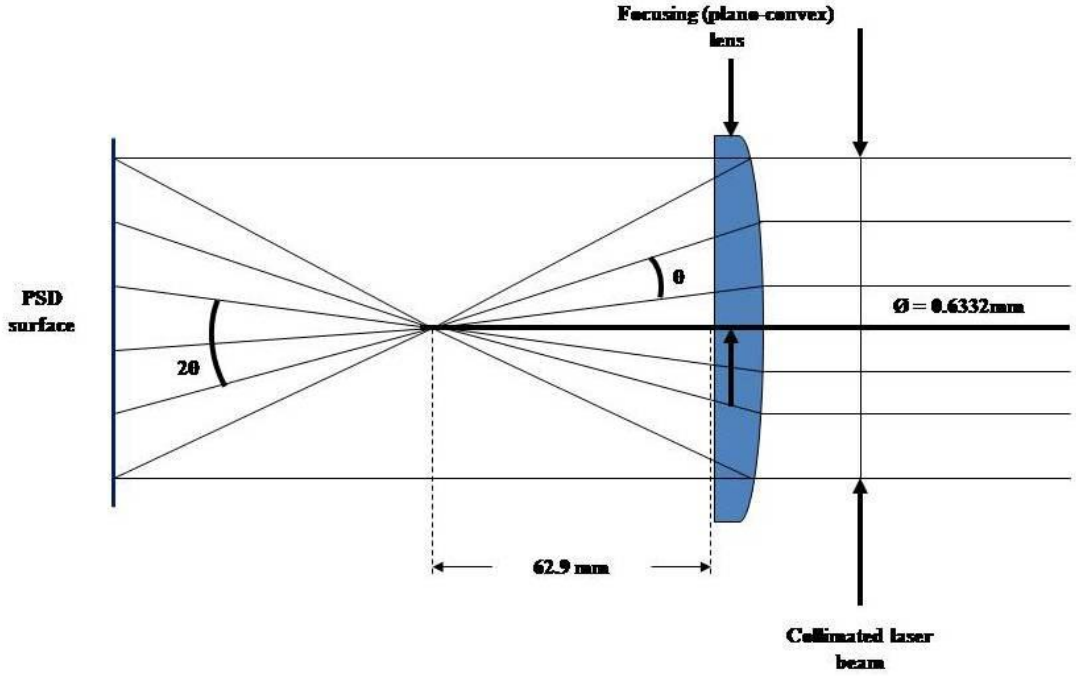

Figure 13. Schematic representation of the laser spot diameter formation at the PSD surface.

The area of the laser spot was calculated in the following way:

$$tan\,\theta = \frac{opposite}{adjacent} \quad \textbf{[9]}$$

$$tan\,\theta = \frac{d_0}{f} \quad \textbf{[10]}$$

Obtained value of 2 θ = 0.01006 rad represents the beam divergence angle prior to and after the focal point. Laser spot diameter on the PSD is equal to the laser beam diameter at that point. Equation 3 was used to calculate the laser spot diameter

The obtained spot radius value of 1.882 mm allowed calculating the spot area as 2.78 mm^2. The PSD optically active area is a square having 6.25 mm^2 area. The distance between the focal point and the detector was used as a regulating factor to ensure that the laser spot is placed on the PSD throughout the experiments even at the maximum recorded laser beam displacements (see next section).

Calculation of the laser beam displacement and the measurement of the PSD sensitivity

In the current set-up, if the displacement of the beam (Δd) is 1μm, then the deflection angle is 5.348 μrad. This relation was calculated the following way:

$$\theta \approx tan\theta = \frac{opposite}{adjacent} = \frac{1\mu m}{187\mu m} \approx 5.348\ \mu rad \qquad \textbf{[11]}$$

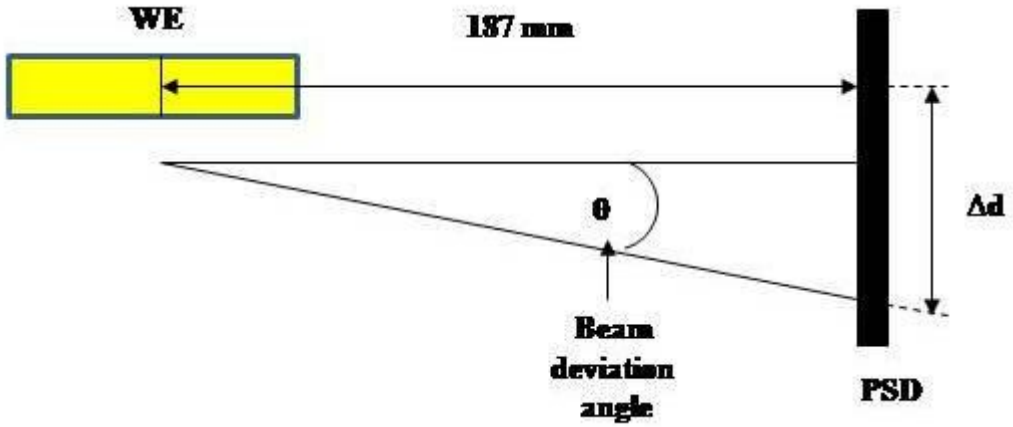

Figure 14. Schematic representation of laser beam displacement on the PSD surface.

Hence, the maximum permissible angle of deviation is 1.19 mrad, this corresponds to a displacement of 222.5 μm.

PSD size is 2500 μm × 2500 μm, therefore assuming that the laser spot is located at the detector centre prior to the analysis, even the significant change in the

refractive index resulting in maximum angle of deflection would not place the laser spot out of the detector optically active area.

During the optical experiments conducted in the course of this project, typical angular deflections were contained between the following limits:

$$\theta = 0.01\ mrad\ \rightarrow 1.87\ \mu m \quad \textbf{[12]}$$

$$\theta = 1\ mrad\ \rightarrow 187\ \mu m \quad \textbf{[13]}$$

Upon the laser spot displacement PSD produces variable DC potential. The experimental set-up used in this experiment resulted in the PSD sensitivity of 12.23 mV/μm, thus $\Delta d = 82\ \Delta E$, therefore:

$$\theta = \frac{82\Delta E}{187} = 0.439\ \mu rad/mV \quad \textbf{[14]}$$

The above ratio was used to translate the variable potential generated by PSD into the beam deviation angle.

Translation of beam deviation into the concentration gradient.

The deflection of the laser beam was detected by the PSD and translated into a direct current. The voltage of the PSD was then amplified and measured using a voltmeter while the potential stability was monitored on an oscilloscope. This allowed for beam stability measurements prior to any electrochemical experiments. The stability readings were collected for 15 min before any experiment and the signal was considered stable if the beam did not vary more than 1 – 2 mV (deemed acceptable due to the laser beam passing through the air). Before each experiment the voltmeter was regulated so that the DC current resulting from the laser beam passing through the electrochemical cell was 0.5 V and any positive deflection of the beam (i. e. towards the WE) would yield positive signal (i.e. > 0.5 V) while negative deflection (outwards from WE) would yield negative signal (i.e. < 0.5 V).

2.5.2 Data Analysis procedures.

EQCM data analysis procedures

Acquisition of the data was conducted using software based on Agilent Virtual Engineering Environment (VEE v. 7.52). Upon acquisition, the relevant impedance spectra were fitted into the theoretical model (based on Sauerbrey equation and therefore assuming full rigidity of the deposited material) and this file was used as a matrix for the processing of the relevant batches of spectra. Fitting of the acquired spectra into the theoretical model was conducted using the in - house developed software (KSR 200) based on Visual Basic (Microsoft Office Professional 2003). Each batch of data comprised 10 – 4000 csv files. Batch processing was conducted using in – house software (Macro files - Microsoft Excel Professional 2003).

Translation of the frequency changes into mass variations was conducted with the use of the Sauerbrey equation incorporated into the Excel spreadsheet (Microsoft Excel Professional 2003). Upon completion of the calculations, data contained in Excel spreadsheets was used to create graphs (Origin Pro 8 software) which were used for the visual presentation of the data. Mass changes were calculated from frequency changes using Sauerbrey equation:[6]

$$\Delta f = \left(\frac{-2 f_0^2}{A\sqrt{p_q \mu_q}}\right) \Delta m \qquad \textbf{[15]}$$

The thus obtained mass change (Δm) was plotted versus the electrical charge passed during the experiment in order to calculate the molar mass of species exchanged (i.e – the charged and non-charged species exchanged):

$$M = zF\left(\frac{dm}{dQ}\right) \qquad \textbf{[16]}$$

Where M is the molar mass, z is the number of electrons exchanged and ΔQ/dm value was obtained from the gradient of the ΔQ/dm graph by a previously described method.[7] Mass obtained from gravimetric signal was plotted versus charge passed (obtained from voltammetric signal). Calculated values were then used to calculate average mass of exchanged species. Presence of hysteresis was assumed to result from

the heterogeneous mass exchange. Average mass exchanged was calculated using the following equation:

$$M_{Av} = \frac{(m/F)}{1000000} \quad \textbf{[17]}$$

Therefore the final equation that was used to calculate the mass exchanged was:

$$M = M_{ion} + nM_{neutral} \quad \textbf{[18]}$$

Where M_{ion} is the mass of the ion, n is the number of solvent molecules exchanged per one ion and M_{neutral} is the molecular mass of the neutral species. Since the above method was originally intended for molecular solvents it was adapted for ionic liquids and deep eutectic solvents electrochemistry (i.e fully ionic environments) in the following way:

$$M = M_{cation} + nM_{anion} \quad \textbf{[19]}$$

Or

$$M = M_{anion} + nM_{cation} \quad \textbf{[20]}$$

Depending on whether the process was cation or anion dominated mass exchange. Further modification was necessary to measure the individual metals molar ratios upon metal co-deposition. For the system studied in section 5.5.7 (simultaneous deposition and dissolution of copper and silver), the following method was used to obtain the molar fraction:

$$Cu^{2+} + 2e \rightarrow Cu^{0} \quad \textbf{[21]}$$

$$Ag^{+} + e \rightarrow Ag^{0} \quad \textbf{[22]}$$

$$\chi_{Cu} + \chi_{Ag} = 1 \quad \textbf{[23]}$$

Therefore:

$$\chi_{Cu} = 1 - \chi_{Ag} \quad \textbf{[24]}$$

$$Mass\ (\Delta m) = \chi_{Cu} RMM_{Cu} + \chi_{Ag} RMM_{Ag} \quad \textbf{[25]}$$

$$Charge\ (Q) = \chi_{Cu}\, 2F + \chi_{Ag} F \quad \textbf{[26]}$$

Therefore:

$$Q = \chi_{Cu} 2F + (1 - \chi_{Cu})F \quad \textbf{[27]}$$

$$Q = F(\chi_{Cu} + 1) \quad \textbf{[28]}$$

Thus:

$$\frac{\Delta m}{Q} = \frac{\chi_{Cu} RMM_{Cu} + (1 - \chi_{Cu}) RMM_{Ag}}{F(\chi_{Cu} + 1)} \quad \textbf{[29]}$$

And:

$$\chi_{Cu} = \frac{(RMM_{Ag} - \frac{\Delta m}{Q} F)}{(\frac{\Delta m}{Q} F - RMM_{Cu} + RMM_{Ag}} \quad \textbf{[30]}$$

The calculated values were then plotted (Δm/Q vs. molar fraction). Obtained numbers indicated the molar fraction of individual metals in the deposited layer.

EQCM-PBD data analysis procedures.

Application of the convolution protocol.

Numerical convolution approach to process the electrochemical data is a well-known technique.[8] It enables the calculation of the concentration gradients at a finite distance from the working electrode by taking into account the diffusional effects. This is a necessity in processing (or simulation) of the optical deflection data).

Translation of the beam deviation into the concentration gradient

Processing of the experimental beam deflection data by convolution was initially proposed by Vieil.[9] In this approach the experimental optical beam deviation (inevitably recorded *at a distance* from the electrode's surface) is used to calculate the ionic flux *at the* electrode's *surface*. Thus obtained ionic flux is directly compared with the flux of electrons (i.e. electrochemical current) and these two signals are related using Fick's law. Potential window of the optical deflection signal is smaller than voltammetric one (due to the diffusional gap), therefore observation of the electrode processes at the extreme potentials might not be achievable.

Convolution of current

The purpose of this operation is to derive the dopant ion flux (in conducting polymers redox chemistry) or metal cation flux (in metals redox chemistry) from the ionic flux (optical deflection signal). Recorded beam deflection (expressed in μrad) and electrochemically determined current (expressed in μA) are the input values for the convolution software. Using the following set of assumptions:

1) Electron flux *originates in* or *results from* ionic flux
2) Electrode processes result in simultaneous ion and electron exchange
3) Analysed process is instantaneous (i.e. electrode ion exchange is rapid in comparison to diffusional delay).

The mathematical treatment is as follows. The total ionic flux f_{PBD} is a sum of fluxes towards and outwards the electrode:

$$f_{PBD} = \frac{\theta^{+}}{\theta^{-}+\theta^{+}} \qquad \textbf{[31]}$$

Projection of current and mass signals from the electrode surface into the electrolyte requires fulfilment of several assumptions. Firstly, the electroacitve deposit on the electrode has to act as an ideal transducer between the electrical input and the ionic output. Secondly, the species propagation delay has to be negligent.

Based on these assumptions, the measured current $\mathbf{i_{(t)}}$ can be treated as being proportional to the total flux of charged species and is described by the equation:

$$i_{(t)} = FA\Sigma\,(z_k J_k)_{(0,t)} \quad \textbf{[32]}$$

Where $\mathbf{k}$ = C^+ or A^- and $J_{(0,t)}$ represents the species flux at the film electrode interface (where the distance is zero). The convolution analysis is based on the extrapolation of the flux measurements from the electrode surface (distance = 0) into a focal point (distance = x, this it is the actual physical distance between the electrode and the laser beam). In this place the optical deflection measurements (i.e. refractive index changes) are collected. The convolution analysis is based on the following equation:

$$J_{C^+A^-(x,t)} = F_{(x,t)} \times J_{C^+A^-(0,t)} \quad \textbf{[33]}$$

Where $F_{(x,\,t)}$ is the convolution factor. This factor is based on the assumption of mass transfer being semi-infinite diffusion in the dimension perpendicular to the electrode surface. Then, the application of Fick's 1st law allows to relate the flux of the species to the concentration gradient:

$$J_{(x,t)} = -D\left(\frac{\delta c_{(x\,t)}}{\delta x}\right) \quad \textbf{[34]}$$

Combination of equations **[32], [33]** and **[34]** reveals the convolution factor as a function of diffusion:

$$F_{(x,t)} = \left(\frac{x}{2\sqrt{\pi D t^3}}\right) e^{\frac{-x^2}{4Dt}} \quad \textbf{[35]}$$

Where D is the diffusivity of the transferred species, t is the propagation delay and x is the propagation distance. The relationship between the optical deflection and concentration gradient then becomes:

$$\theta = -\frac{l}{n}\,\frac{\delta n}{\delta c}\,\frac{1}{D}\,J_{(x,t)} \quad \textbf{[36]}$$

Equation 36, when expressed as a function of the electrode current develops into the equation 37. This equation directly relates the species flux with optical deflection:

$$\theta_{(x,t)} = -\frac{h_k L}{z_k F A} F_{(x,t)} \times i_{(t)} \quad \textbf{[37]}$$

Where $h_k = ((1/n) \times (\delta n/\delta c) \times (1/D))$ and it is a constant for a given electrolyte. This approach eliminates the need for measurement of δn/δc (which would otherwise had to be conducted prior to the experiment). The convolution software thus removes the propagation delay effectively extrapolating the optical deflection signal from distance x_0 to the electrode surface and compares it to the experimental electrical signal. Using the x/√D parameter the best possible fit of the experimental and convolved signal was obtained and compared with the diffusion coefficient values calculated from Randles-Sevcik equation. The result was the convolved current (i.e. current measured at the the focal point). This value and the value of x/√D were recorded and stored for further calculations.

Convolution of mass

The purpose of this operation was to derive mass flux of the individual species from the experimental optical deflection. Recorded beam deflection and gravimetrically determined mass changes are the input values for the convolution software. The following set of assumptions is being used:

1) Ionic flux is accompanied by a solvent (or neutral species) flux
2) Ionic flux does and solvent flux does not result in formation of a concentration gradient
3) Mass flux is instantaneous

Optical deflection and current densities are related to each other and to the mass flux via Faraday's Law. The mathematical treatment is a follows:

Current density: $$\frac{i}{AF} = z_{C^+} J_{C^+}(x,t) + z_{A^-} J_{A^-}(x,t) \quad \textbf{[38]}$$

Optical deflection: $$\theta_{(x,t)} = L\left(-h_{C^+} J_{C^+}(x,t) - h_{A^-} J_{A^-}(x,t)\right) \quad \textbf{[39]}$$

Mass flux: $$\frac{dM(x,t)}{dt} = m_{C^+} J_{C^+}(x,t) + m_{A^-} J_{A^-}(x,t) + m_N J_N(x,t) \quad \textbf{[40]}$$

The above approach allows for the determination of individual contributions of cations, anions and solvent molecules to the overall dynamics of the analysed system. In order to apply the convolution protocol gravimetric mass signal was converted to charge and then to current. The obtained mass-derived-current was then the input value for the convolution software. The same x/√D factor which was used for the current convolution was applied. The resulting convolved current and the convolved mass were used for the subsequent ion and/or solvent flux calculations. As it can be seen above, this step required gravimetrically and electrochemically derived assumptions about the dopant ion identity. Identity of ions was deduced from the gravimetric and voltammetric signals (i.e. mass increase of PEDOT film upon oxidation in $LiClO_4$/ACN infers ClO_4^- as a dopant, Ag deposition/dissolution from AgCl/Ethaline infers Ag^+ as the charge balancing cation).

Calculation of the qualitative ionic and solvent (neutral species) contributions.

Prior to the separation of the cation, anion and solvent individual contributions, the following assumptions were formed:

1. Experimental deflection signal represents the total flux of electroactive as well as non-electroactive species.
2. Convolved current represents exclusively the dopant ion flux.
3. Convolved mass represents the total mass flux of dopants as well as the counter ions
4. Any part of the experimental optical signal which does not represents anion or cation flux represents the solvent flux.

The generic protocol (for a solvent based, anion doped) system is presented below:

$$\theta - \left(\frac{i_{(x,t)}hL}{zFA}\right) = C^+ \quad \textbf{[41]}$$

$$\left(\frac{i_{(x,t)}hL}{zFA}\right) = A^- \quad \textbf{[42]}$$

$$\left(\frac{dM_{(x,t)}}{dt}\right)\left(\frac{zFAhL}{RMM}\right) - \left(\frac{i_{(x,t)}hL}{zFA}\right) = (C^+ + N) \quad \textbf{[43]}$$

$$\left(\left(\frac{dM_{(x,t)}}{dt}\right)\left(\frac{zFAhL}{RMM}\right)-\left(\frac{i_{(x,t)}hL}{zFA}\right)\right)-\left(\theta-\left(\frac{i_{(x,t)}hL}{zFA}\right)\right)=N \qquad \textbf{[44]}$$

Where θ is the experimental optical deflection, $\left(\frac{i_{(x,t)}hL}{zFA}\right)$ is projected current, $\left(\frac{dM_{(x,t)}}{dt}\right)\left(\frac{zFAhL}{RMM}\right)$ is projected mass flux and *RMM* is the dopant ion molar mass. C^+, $A^-$and N are contributions of cation, anion and neutral species (i.e. solvent molecules) respectively. Convolution methodology returns solvent (synonymous with 'net neutral') flux contribution. In DES case, this contribution is assumed to be composed of equal amounts of anions and cations. Thus, solvent flux is partitioned into anion and cation transfers. These in turn are added to (determined separately) ion fluxes (obtained using the convolution software). Therefore, N contribution is not present in convolution products of DES experimental data.

Calculation of the quantitative ionic and solvent contributions

Integration of the differential responses obtained in the previous stage returns the quantitative results of the anion, cation and solvent fluxes. The mathematical treatment is as follows:

$$\frac{\theta}{h}\times dt\times\left(\frac{RMM}{F}\right)=\theta_{quant} \qquad \textbf{[45]}$$

$$\frac{\left(\left(\frac{i_{(x,t)}hL}{zFA}\right)\right)}{h}\times dt\times\left(\frac{RMM}{F}\right)=\left(\frac{i_{(x,t)}hL}{zFA}\right)_{quant} \qquad \textbf{[46]}$$

$$\left(\frac{\left(\left(\frac{dM_{(x,t)}}{dt}\right)\left(\frac{zFAhL}{RMM}\right)\right)}{h}\right)\times dt\times\left(\frac{RMM}{F}\right)=\left(\frac{dM_{(x,t)}}{dt}\right)\left(\frac{zFAhL}{RMM}\right)_{quant} \qquad \textbf{[47]}$$

Where $_{quant}$ adjective designates the quantitative level of response. The obtained signals are individual fluxes of each species expressed as concentration gradients (n mol^{-1} cm^{-2}).

2.6 Atomic force microscopy

2.6.1 Instrumentation.

The morphologies of the deposits were observed by Atomic Force Microscopy (AFM) using Digital Instruments, Dimension™ 3100 microscope. Microscope was coupled to Nanoscope® Dimension™ 3100 Controller and Nanoscope® Scanning Probe Microscope Controller. The entire instrument was controlled through Nanoscope® software.

2.6.2 Experimental procedures

Measurements were made *ex situ* in tapping mode. Silicon nitride (Si_3N_4) tips were used. Materials analysed were deposited on Au-plated quartz slides (1.75 cm^2 EA, total area 3 cm^2). PEDOT films were electrodeposited by potentiostatic method from 0.05 M EDOT dissolved in 0.1 M $LiClO_4/CH_3CN$ (30s CA, 1.2 V), average Q_{dep}= 75 mC cm^{-2}. Metal deposits were formed through potentiodynamic deposition (υ = 0.03125 mV s^{-1} → 2.5 mV s^{-1}).

2.7 Viscosity measurements

2.7.1 Instrumentation

Viscosity of all electrolytes was measured using a Brookfield DV-E viscometer equipped with a thermostatically controlled water jacket. The temperature control was achieved by the means of a water bath (Techne RB-5) coupled to a temperature controller (Techne Temp unit TU16D) capable of providing a variable temperature continuous flow. Depending on the liquid type (i.e molecular or ionic) different spindles were used.

2.7.2 Experimental procedures

The viscosity values were calculated from the torque necessary to revolve the spindle in the liquid at set values of rpm. All values were collected at the ambient temperature (20 ˚C) after 30 minutes equilibration period.

2.8 References

1 R. G. Compton, C. E. Banks, *Understanding Voltammetry*, 2nd Edition, 2011, Imperial College Press.

2 A.R. Hillman, K.S. Ryder, C.J. Zaleski, C. Fullarton and E. L. Smith, *Z. Phys. Chem.* 2012, **226**, 1049-1068.

3 M. J. Henderson, A. R. Hillman, E. Vieil, C. Lopez, *Journal of Electroanalytical Chemistry*, 1998, **458**, 214-248.

4 C. A Barbero, M. C. Miras, *The Journal of the Argentine Chemical Society*, 2003, **91**, 1-40.

5 C. A Barbero, M. C. Miras and R. Kötz, *ElectrochimicaActa*, 1992, **37**, 429-437.

6 Sauerbrey G, *ZeitschriftPhysikalishe*, 1959, **155**, 202–222.

7 A. Bund, S. Neudeck, *Journal of Physical Chemistry B*, 2004, **108**, 17845-17850.

8 G. G. Lang, C. A. Barbero, *Laser Techniques for the Study of Electrode Processes*, Berlin, 2012.

9 E. Vieil, *Journal of Electroanalytical Chemistry*, 1994, **264**, 9-15.

Chapter III

Electrolytes survey - comparison of mass exchange characteristics of PEDOT films redox cycled in molecular solvents and Deep Eutectic Solvents

3.1 Introduction

3.1.1 Conducting polymers

Polythiophene (PTh) and its derivatives belong to the polyheterocyclic family of conducting polymers (CP).[1] One of its most prominent members is the poly(3,4 ethylenedioxythiophene - PEDOT). In this polymer, the presence of ether groups on positions 3 and 4 of the thiophene ring not only prevents α–β cross–linking during the electropolymerization (improving the film homogeneity) but also stabilizes the whole molecule as it prevents the degradation processes occurring through the attack at the positions 3 and 4.[1]

It is widely acknowledged that the substitution of the conjugated ring allows for modification of the CP electronic properties in general and lowering of the band gap in particular.[1] PEDOT, where this effect is exploited to its full capability, is one of the very few CP that can be p and n doped (i.e. oxidised and reduced).[1,2] Also, the appendage of ether substituents significantly lowers PEDOT oxidation (p-doping) potential as compared to the parent (PTh) molecule.[1] These favourable characteristics make it a widely studied and applied material. PEDOT attracts great interest as it's potential applications span many technologies. These are electrical energy production (photovoltaic cells)[3] and storage (batteries and capacitors),[4] sensor manufacture (electrochromic devices as well as all-solid-state ion sensors),[5] thermochromic devices, conducting textiles, corrosion control (multilayer films with each layer containing different dopants),[6] antistatic coatings and biochemical applications (electrochemical actuators for artificial muscles).[7] So far its main limitations are conductivity, longevity (i.e. electrochemical stability) and capacitance.[8] PEDOT films can be formulated

through oxidative polymerization either chemically or electrochemically (through electrodepostion from monomer solution in the presence of supporting electrolyte). Both of these processes results in the formation of highly conductive (c.a. 500 S cm $^{-1}$), p–doped polymeric layer.[2]

Performance of any electrochemical device (e.g. battery charge/discharge rate or actuator speed of response) is governed by ion transport dynamics. Ion movement is the key feature of the polymer films electrochemical switching between the doped and undoped states. Oxidation results in positive charges being formed on the polymer backbone. The electroneutrality force compensates these charges by injection of anions into, or expulsion of cations from, the polymer film (processes colloquially known as doping). This ion movement is usually accompanied by a solvent transfer. Electrolyte (commonly a salt dissolved in a molecular solvent) acts as an ion source/sink. Doping in PEDOT films was previously reported to be orders of magnitude faster than in any other polymer film hitherto studied.[1] The character (size and structure) of the dopant ions (both those incorporated during the polymer film deposition as well as those present during the redox switching) are known to have remarkable influence on the dynamics of the film's redox processes.[8,9] For example, redox cycling of PPy in tetrabutylammonium trifluoromethane sulfonate/propylene carbonate solution resulted in a mixed - ion transfer[10], however if sodium sulphate salt dissolved in an aqueous solvent was deployed instead, cation transfer became dominant.[11] Anion exchange dominated mass transfer was reported for PPy films redox cycled in lithium perchlorate and sodium perchlorate aqueous electrolytes.[11] Complex, non-monotonic mass transfer was also reported for PPy films redox cycled in sodium tosylate solutions.[12] Additionally, dopant ions were reported to have a profound effect on the polymer structure, stability and conductivity.[1]

3.1.2 Deep eutectic solvents

Deep eutectic solvents (DES) are one of the results of ionic liquids (IL) development.[13] Similarly to IL these solvents offer a fully ionic environment albeit the chemistry through which this is achieved is different. They comprise two constituents, a quaternary ammonium salt (QAS) and a hydrogen bond donor (HBD). Upon the solvent formation, the latter acts as the complexing agent for the former. The DES

number indicates the molar ratio, for example, Ethaline 200 is composed of one mole of choline chloride and two moles of ethylene glycol. One of the greatest advantages of the DES is their wide electrochemical window allowing reaching previously inaccessible potentials. This, combined with their substantial electrochemical stability as well low toxicity, lack of sensitivity to air and water and ease of formation makes them a feasible alternative for currently existing technologies.[13] For the purpose of this study, the only QAS used was choline chloride. This salt has previously been used as a most common precursor for the DES.[13,14] Being a commodity bulk chemical, it is a viable economical option for industrial applications.

3.1.3 Ion mobility

Conducting polymer films can be described as a 'mesh' from which, during redox cycling, ions repeatedly ingress and egress. The 'mesh' is an elastic network of polymer strands, which repeatedly expand and contract during the redox cycle.[4]

The overwhelming majority of the CP based systems studied so far concentrated on molecular solvent based electrolytes. The redox induced mass exchange in these systems is usually dominated by an anion exchange although the cation-dominated processes were also reported.[4] These exceptional cases occur only when the anion is rendered immobilised due to its size, structure (highly branched) or entanglement due to the cross linking. Study by Williams et al [15] reported a polymer film expansion and contraction (resulting from ion ingress and egress) as directly proportional to measured current. Thus, the question arose about the nature of these processes in DES.

The overarching goal of this chapter was to identify the mass transfer processes occurring at the interface of the PEDOT film while redox cycled in DES media. The linear relationship between the supporting electrolyte (SE) concentration and the current response occurring in the case of diffusional control had been discussed elsewhere.[4] One might therefore expect that in DES where the number of potential charge carriers vastly exceeds the one usually encountered in the 'classic' electrolytes, the current response could be the orders of magnitude higher than in SE electrolytes (usually ~ 0.1 M). This is known not to be the case with DES due to their considerable viscosity (circa 40 ~ 22000 cP) as well as their fully ionic nature.[16] Charge transport is governed by ions mobility. Mobility is in turn (to a large extend) affected by the medium viscosity. The

large ion/void size ratio in DES (comparable to IL) decreases the probability of ions finding a suitable neighbouring void to move into, thus hampering the ions transfer. This effect was previously extensively researched by Abbott et al and quantified using the 'hole theory'. Their conclusion was that it is not the number but the mobility of the charge carriers that determines the conductivity in the DES. [17]

Furthermore, in terms of the gravimetric analysis, the presence of such a viscous electrolyte can be viewed as an additional layer on the deposited polymer film. Gravimetric analysis was used as a main analytical tool in order to create conditions one might encounter in a practical application (for example a secondary battery), thus ring disc electrodes or wall jet electrodes techniques were deemed not suitable for the purpose of this study.

3.2 Objectives

The objectives of this chapter were: first, considering DES high viscosity and known technical limits of the EQCM is was necessary to establish whether the PEDOT film responses while immersed in DES could still be interpreted gravimetrically. Second, it was sought necessary to explore how the different DES formulations affect the electrode/electrolyte charge storage capability of the PEDOT modified electrodes. The third objective was selection of those DES, which proved to possess advantageous electrochemical stability and charge storage capability over the molecular solvents as subjects for further studies. The fourth objective was the elucidation of the ions maintaining the electro neutrality. The fifth and final objective was the verification of the long term stability of the selected DES versus 'classic' electrolytes.

3.3 Results and discussion

3.3.1 Gravimetric versus viscoelastic behaviour

For a range of chemically or electrochemically deposited polymer films the effects of viscoelasticity were already studied in detail.[18] The deviation from a 'rigid' (i.e. acoustically thin) behaviour into a non–rigid (i.e. viscoelastic) one, transpires as a

result of the phase shift between the deposited layer and the resonator. The degree of the viscoelasticity is parameterized in terms of shear moduli, which requires different calculation approach than the gravimetric analysis. Such deviation might occur for a thin film of a very soft material as well as for a thicker film of a more rigid material. The graphic differences in the quartz resonator (also called Thickness Shear Mode (TSM) resonator) motions are presented in Figure 1.

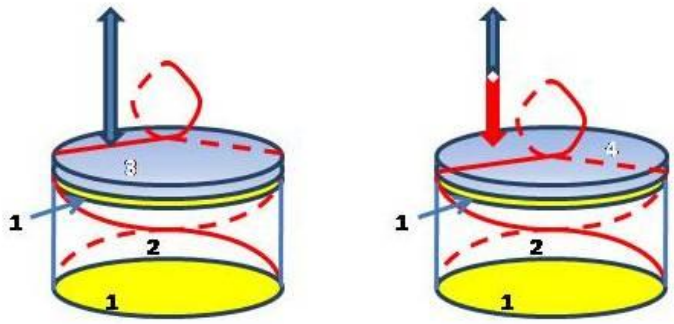

Figure 1. Cartoon representation of TSM resonator motions, immersed in liquid under rigidly coupled mass (left panel) and immersed in liquid under viscoelastic mass (right panel). 1 – Au covered faces of the quartz crystal, 2 – quartz crystal, 3 – rigidly coupled mass, 4 – viscoelastic film.

The validity of the Sauerbrey equation (used to convert frequency into mass) is limited by the admittance changes

$$\Delta f = -\left(\frac{2}{\rho_q v_q}\right) f_0^2 \Delta M = -S\Delta M \qquad \textbf{[1]}$$

Where ρ_q is the quartz density, ν_q is the acoustic wave velocity in quartz and f_0 is the fundamental frequency. For the deposit to be classified as rigid, the relative frequency change (Δm) upon the deposition must not exceed circa 2 % of the fundamental frequency. Figure 2 depicts the admittance and frequency changes upon the electrodeposition of the PEDOT film and it reveals the frequency change as being only circa 1.2 %. However, it can be noted from this figure that the decrease in the resonant admittance is a significant circa 60%. Thus, it may be possible that these films are not fully rigid but at least partially viscoelastic in their nature. The importance of detecting the presence (or otherwise) of any possible viscoelastic effects arises from the fact that this study uses thicker than usual polymer films.[4] It has also been proven that even the thin polymer films cannot always be classified as a thin, rigid layers.[18]

Additional difficulties arise when electrolyte becomes trapped within the polymer film itself (process known as 'coupling of fluid').[19] In such a case solvent trapping might present another level of complication. Significant surface unevenness further complicates the matter, particularly if it has the same order of magnitude as the shear wave penetration depth in the electrolyte. However, it was previously proven that from a practical point of view this does not represent a problem because liquid trapped within the morphological features is unable to move in lateral directions.[19] Therefore, it behaves as a rigid layer (despite not being such). Besides, acoustic delay length is proportional to viscosity, so in DES it is orders of magnitude smaller than in aqueous or organic solvents (circa 100 to 200 nm in the molecular solvents, circa 10 nm in DES). When redox cycled in the bathing electrolyte, solvent molecules permeate the polymer film acting as plasticizers. The extent of this process depends on solvent polarity, density, viscosity and the polymer structure and oxidation state as well as (as confirmed by Rahrindramahazaka et al.[20]) relative proportions of the 'open' and 'compact' structures within the polymer film. For comparison purposes, the measurements were initially conducted in the molecular solvent.

0.1 M $LiClO_4$ / CH_3CN	0.1M $(C_2H_5)_4NBr$ / DCM	Ethaline	Propaline	Maline	Acetaline	Glyceline	Reline
0.8 cP	0.85 cP	40 cP	80 cP	850 cP	50 cP	250 cP	700 cP

Table 1. Viscosity (η) of the electrolytes measured at 298 K. Literature values were used for the molecular solvents. DES data were obtained using Brookfield rotating cylinder viscometer.

The admittance responses in figure 3 are typical for molecular solvents; the immersion of the crystal in the solvent results in circa fourfold drop in admittance, deposition of the polymer film reduces the admittance by a further 50%. As the main purpose of this study is gravimetric response in DES, faced with these consideration the main interests was the admittance response in DES. Figures 4 and 5 depict the admittance responses of the respectively bare crystals resonating in the air, in solvent and polymer film coated crystal resonating in the solvent. Comparison of the immersed and emerged crystals displays large admittance drop, however (unlike in the molecular

solvents) the presence of the polymer films does not have a significant impact as most of the dissipation energy results from the ionic solvent high viscosity. Thus, the polymer films can be treated as acoustically rigid and interpreted gravimetrically.

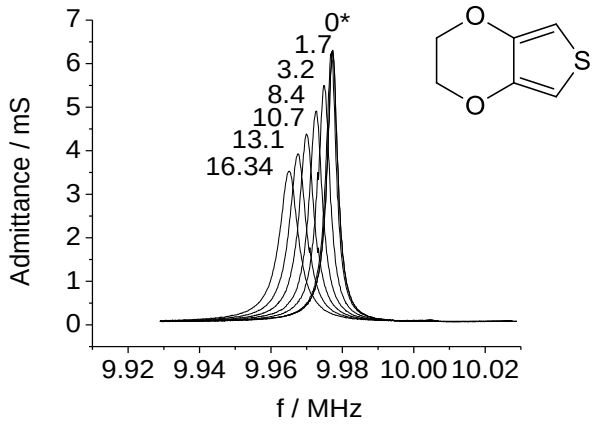

Figure 2. Admittance spectra collected during the deposition of a PEDOT film [Q_{dep} = 71.04 mC cm^{-2}] potentiostatically deposited from 0.05 M EDOT in 0.01 M $LiClO_4$/MeCN solution. Numbers indicate charge [mC = 0.23 cm^{-2}] passed during the electrodeposition process. Initial frequency (prior to the deposition) is marked with a star.

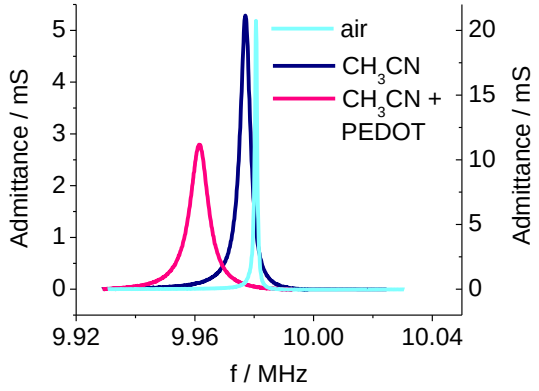

Figure 3. Admittance versus frequency for a bare EQCM crystal resonating in the air (cyan line – right scale), CH_3CN (blue line – left scale) and EQCM crystal with polymer film [Q_{dep}= 71.04 mC cm^{-2}] deposited on it resonating in CH_3CN (red line – left scale). The admittance decrease between the bare and PEDOT modified electrode (both immersed in the solvent) equals to 47.3 %.

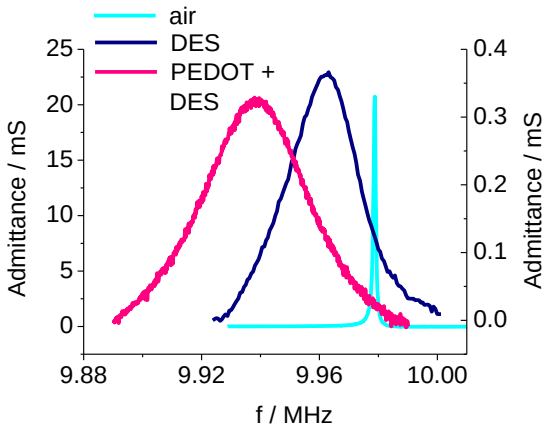

Figure 4. Admittance versus frequency for a bare EQCM crystal resonating in the air (cyan line – right scale), Ethaline 200 (blue line – left scale) and EQCM crystal with polymer film [Q_{dep} = 71.04 mC cm^{-2}] deposited on it, resonating in Ethaline 200 (red line – left scale).The admittance decrease between the bare and PEDOT modified electrode (both immersed in the solvent) equals to 11.7 %.

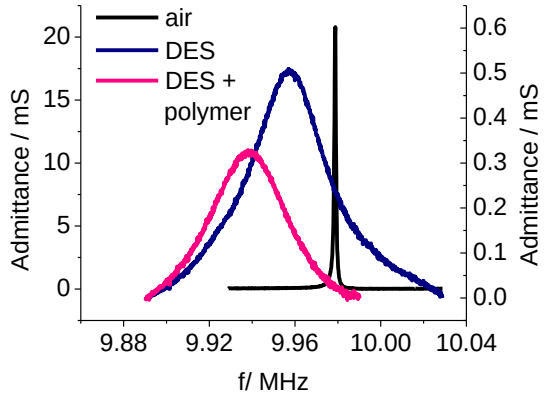

Figure 5. Admittance versus frequency for a bare EQCM crystal resonating in the air, (cyan line – right scale), Propaline 200 (blue line – left scale) and EQCM crystal with polymer film [Q_{dep} = 71.04 mC cm^{-2}] deposited on it resonating in Propaline 200 (red line – left scale). The admittance decrease between the bare and PEDOT modified electrode (both immersed in the solvent) equals to 33.5 %.

3.3.2 AFM analysis of electrodeposited PEDOT films.

AFM images (figures 6 - 10) complete the picture depicting the typical cauliflower – like morphology of the deposited films.

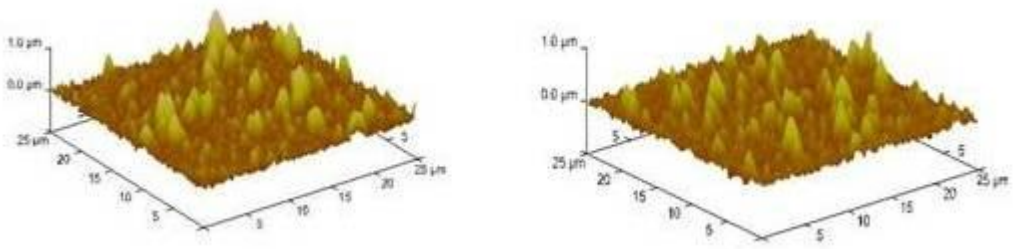

Figure 6. Left panel: ex–situ, dry PEDOT film electrodeposited from 0.05 M EDOT dissolved in 0.1 M $LiClO_4/CH_3CN$ (30s chronoammperometry conducted at 1.2 V), [Q_{dep}=70.9 mC cm^{-2}] on a Au coated glass slide (EA = 1.75 cm^2). Right panel: film presented in the left panel after redox cycling in CH_3CN/ 0.1 M $LiClO_4$, from - 0.3 V $\rightarrow$ 1.0 V $\rightarrow$ - 0.3 V. ν = 5 mVs^{-1}.

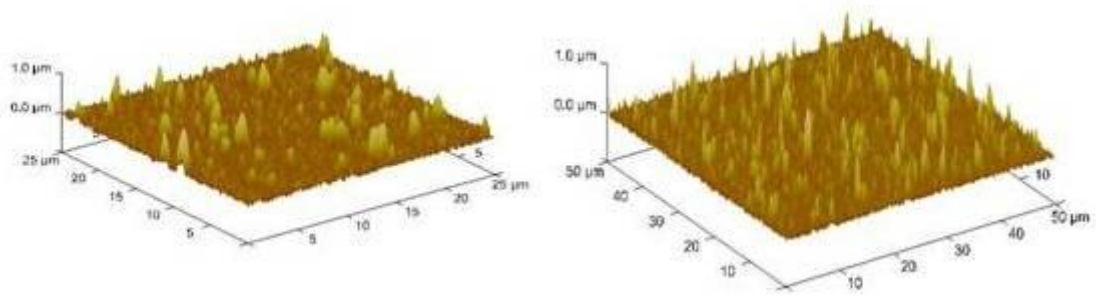

Figure 7. Left panel: Film from figure 6 (right panel) redox cycled in Ethaline 200 from - 0.3 V $\rightarrow$ 1.0 V $\rightarrow$ - 0.3 V. ν = 5 mVs^{-1}. Right panel: film presented in the left panel after redox cycling in Propaline 200, from - 0.3 V $\rightarrow$ 1.0 V $\rightarrow$ - 0.3 V. ν = 5 mV s^{-1}.

Analysis presented in figures 6 – 8, revealed the surface features being within 100 – 200 nm range. The AFM images were used to measure the thickness of the dry (emerged) films and revealed that the removal of solvent did not result in film collapse but instead allowed to form a structure with an average void volume fraction of ca 0.5. (see calculations below) The average thickness of the dry polymer films [Q_{dep} = 79.9

mC cm^{-2}] was measured as h_f = 0.8 µm. Ignoring the uncertainty which obviously arises while averaging over such a rough surface (with individual surface features reaching 0.2 µm) the polymer film was treated as a cylinder with height of 0.8 µm.

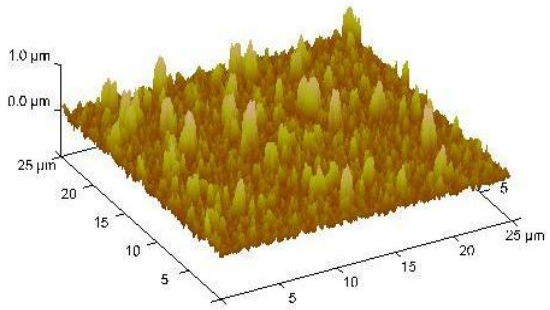

Figure 8. Film from the figure 7 (right panel) redox cycled in 0.1 M $LiClO_4/CH_3CN$ from - 0.3 V → 1.0 V → - 0.3 V. ν = 5 mV s^{-1}.

Based on the deposition charge of 79.9 mC cm^{-2} and an assumption of the fully efficient deposition and doping level of 0.3^4 the polymer film coverage (Γ) when expressed as a number of EDOT monomer units per area is equal to 361 nmol cm^{-2}. Hypothetical assumption that all solid matter in the polymer film collapses to form a dense layer and use of the EDOT molar volume V^0 = 106.8 cm^3 mol^{-1} allows to calculate the theoretical thickness of such deposit as h_f^0 = 0.34 µm. Deduction of this value from the measured real thickness allows calculating the relative ratio of voids to solids present in the polymer films. The resulting void fraction value of ca. 0.425, although slightly different from the literature reported [21] value of 0.4 indicates that the polymer does contain a sufficient amount of dopants and counter ions without the need to restore to the bathing electrolyte during the redox process. Thicker than usually reported films were used in this study to create conditions one might approach while constructing a practical device (e.g. lightweight battery).

3.3.3 Gravimetric observation of redox–driven ion transfers in PEDOT films

Methodology

Quantification of the data revealed molar mass changes (defined by the gradient of the Δm/Q plot) (equation 2):

$$M_{app} = zF\left(\frac{\Delta m}{\Delta Q}\right) \quad \textbf{[2]}$$

Where z is the charge of the anion and F is the Faraday's constant. Thus, with z and F being constant the M_{app} value equals to δm/δQ which is the Δm/ΔQ plot gradient. Any eventual discrepancy between the calculated molar mass and the mass of the perchlorate ion is due to the flux of solvent and/or co and counter ions (in opposite direction). The calculated value is a sum signal representing the number of molecules expulsed from and injected into the polymer film (eq 3):

$$M_{app} = M_{ion} + \alpha M_{solvent} \quad \textbf{[3]}$$

.

Molecular solvents

Prior to conducting any DES studies it was deemed appropriate to investigate the electrodeposited film behaviour in the molecular electrolyte. To exclude any effects of film 'memory' of the prior electrolyte, all polymer films studied were redox cycled to exchange the residual species into the effectively infinite reservoir of the bathing electrolyte.

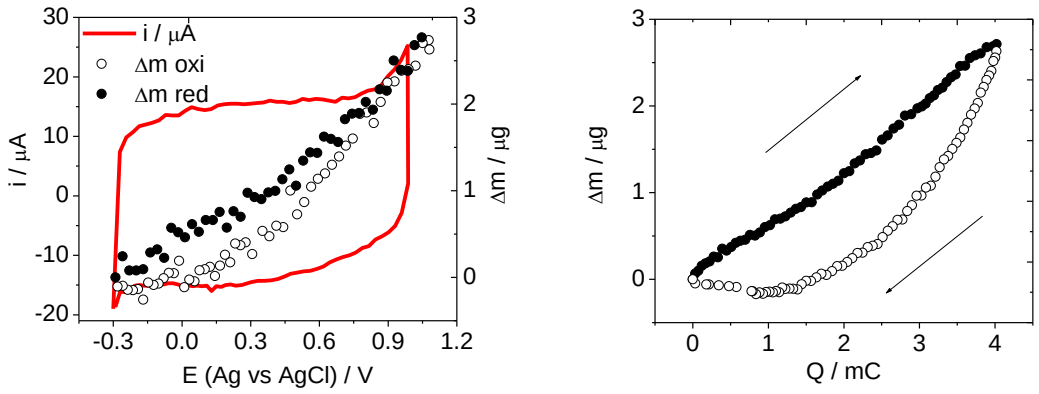

Figure 9. Left panel: Massogram (Δm vs. E plot) overlaid on a voltammogram of a PEDOT 0.8 µm [± 0.1 µm] film (Q_{dep}= 85. 43 mC cm^{-2}) redox cycled from - 0.3 V → 1.0 V → - 0.3 V, ν = 5 mVs^{-1}in 0.1 M $LiClO_4/CH_3CN$. Increase in film mass upon oxidation indicates anion incorporation. Right panel: Δm as a function of injected Q. Arrows indicate the direction of the potential scan. Full circles represent oxidation and empty circles represent reduction.

Ion exchange of CP films redox chemistry in the molecular solvents is a complex but generally well researched process. A thorough study by Hillman et al on the subject of PEDOT films p – doping in $LiClO_4/CH_3CN$ was used as a basic standard.[22] Supporting electrolyte $Li^+ClO_4^-$ was dissolved in CH_3CN and PEDOT films gravimetric behaviour in this solution was observed. Perchlorate ions ingress into the polymer film upon oxidation of CP in molecular solvents is a known behaviour.[23] The left panel in figure 9 above (massogram of PEDOT in 0.1 M $LiClO_4/CH_3CN$) displays the anticipated anion exchange dominated ion transfer, usually occurring in molecular solvents. It can be noted that (at least on the timescale employed here) the mass values return to the original values. This means that there are no noticeable effects of the polymer evolution or degradation within the timescale of the experiment. Data from this molecular solvent experiment, serve as a link to the existing literature and is in agreement with previous work by Hillman[22] and Bund.[23] The calculated value of 0.97 molecules of acetonitrile being ejected for every perchlorate anion injected is in good agreement with values reported in Bund's study. Thus, this calculation was used as a validation test for the entire study. The results are confirmed by hysteresis present (see the right panel of figure 9: $\Delta m/Q$ plot – hysteresis visible as a disparity between the oxidation and reduction signal) which is attributed to the movement of the solvent molecules in the opposite direction to the dopant ion. Presence of hysteresis in a gravimetric signal is also a plausible indicator of presence of slow–polymer based processes (relaxation) however not necessarily resulting in the permanent alteration of the polymer film characteristics.[4] To further investigate redox induced mass exchange of PEDOT films in the molecular solvents, supporting electrolyte $(C_2H_5)_4N^+Br^-$ was dissolved in dichloromethane (DCM) and PEDOT films gravimetric behaviour in this solution was observed. Despite the differences in anion size as expected on the basis of the previous work [23] results (CV and massogram in the left panel and $\Delta m/Q$ plot in the right panel of figure 10) indicate the anticipated mass film increase upon oxidation (p–doping). Qualitative explanation of this phenomenon in this case can be simplified as an ingress of bromide anions into the polymer film upon oxidation. The exchanged molar mass is only circa 45% of the bromide anion mass but this has been attributed to the high molecular mass of the solvent deployed. Thus, for every anion entering the polymer film there is 0.39 molecules of DCM expelled. This value is significantly lower than for the $LiClO_4/CH_3CN$, however there is a significant difference between the

molecules sizes. The distortion of the gravimetric signal (i.e. poor signal to noise ratio) might be attributed to the DCM high density (1.33 g cm^{-3}).

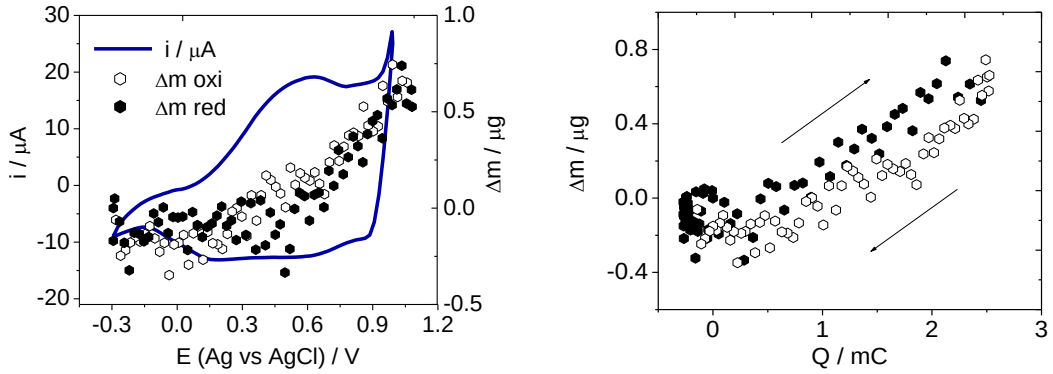

Figure 10. Left panel: Massogram (Δm/E) overlaid on a voltammogram of a PEDOT 0.8 μm [± 0.1 μm] film (Q_{dep}= 85.43 mC cm^{-2}) redox cycled from - 0.3 V → 1.0 V → - 0.3 V, ν = 5 mVs^{-1} in 0.1 M $(C_2H_5)_4NBr$/DCM. Increase in film mass upon oxidation indicates anion incorporation. Right panel: Δm as a function of injected Q. Arrows indicate the direction of the potential scan. Full hexagons represent oxidation and empty hexagons represent reduction.

Deep Eutectic Solvents

The revolutionary EQCM design originally described by Bruckenstein and Shay[24] although perfectly suited for its original application had to be combined with network analyzer (NA) to allow for operation in such a viscous media (40 – 1000 cP in case of the DES tested). The NA advantage lies in providing more energy for the resonator allowing it to overcome significant viscous dissipation of energy (colloquially termed as damping) inevitably present in such liquids.

Solvation of PEDOT films immersed in Ethaline and Propaline has been a subject of recent study and revealed a completely different pattern to the one observed in 'classic' electrolytes.[4] Historically, solvent is one of the key players in Marcus theory and its role in outer sphere electron transfer is an unquestionable dogma.[25] Here (i.e. in DES) the physical properties are not dominated by the presence of neutral molecules, ionic strength is extremely high and viscosity is orders of magnitude higher than in the molecular solvents.

Ethaline 200 (a solvent composed of choline chloride and ethylene glycol in a 1:2 molar ratio) was used as an electrolyte and PEDOT films gravimetric behaviour in this solution was observed. Previous work on the subject is rather limited but a prior study of PPy redox cycled in Ethaline 200 forecasted a radically different behaviour then the one observed in molecular electrolytes.[26]

Data in figure 11 confirms that the gravimetric signal is indeed radically different than the one observed in presence of perchlorate and bromide anions. In Ethaline 200, mass of the polymer film decreases upon PEDOT film oxidation. On the qualitative level, this can be considered as a simple replacement of the perchlorate anion by a choline cation reported to be present in this liquid. The qualitative result is in agreement with the work of Skopek and co-workers, however as the anion in Ethaline 200 has already been confirmed to be a complex anion not the Cl^- as previously thought, it is not only the ion size that shapes the gravimetric response.[27]

The general effects of the dopant character in ion exchange have been widely acknowledged.[23, 26] These effects are particularly visible if a rather radical change occurs like a swap of a small perchlorate anion with the diameter of 0.45 nm (used during the electropolymerization of the PEDOT film) for large complex anions present in the DES (Ch^+ diameter is 0.65 nm).

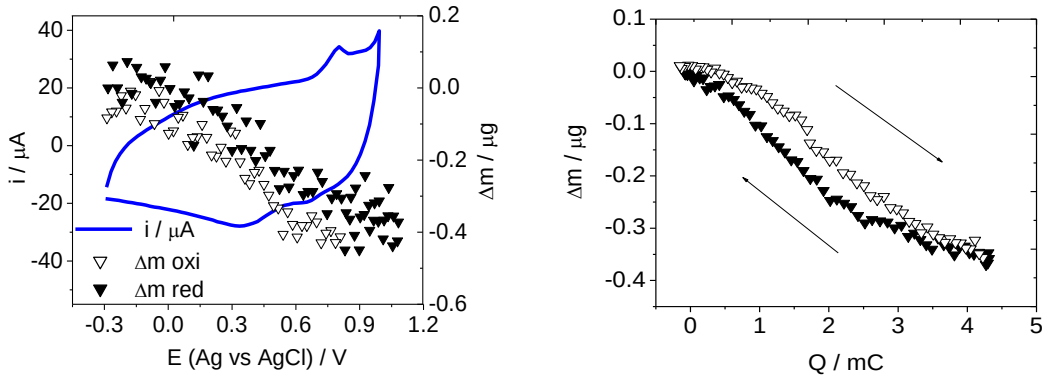

Figure 11. Left panel: Massogram (Δm/E) overlaid on a voltammogram of a PEDOT 0.8 µm [± 0.1 µm] film (Q_{dep} = 85.43 mC cm^{-2}) redox cycled from - 0.3 V → 1.0 V → - 0.3 V, ν = 5 mV s^{-1} in Ethaline 200. Decrease in film mass upon oxidation indicates cation expulsion. Right panel: Δm as a function of injected Q. Arrows indicate the direction of the potential scan. Full triangles represent oxidation and the empty ones reduction.

The behaviour of the same PEDOT film immersed in DES is not readily attributable only to the ion size or the effective lack of the solvent. By inference from the molecular solvent data it can be classified as a cation egress upon oxidation. The lack of solvent is confirmed by a much smaller hysteresis than in any of the molecular solvents (i.e. see right panel of figure 11 where $\Delta m/Q$ gravimetric reduction almost retraces the oxidation one). The molar mass change upon oxidation equals 74.4 g mol^{-1}, significantly less than the choline cation mass of 104.6 g mol^{-1}. This can be only explained as mixed anion ingress – cation egress transfer. The prerequisite for the cation expulsion is presence of the sufficient number of cations in the polymer film at the onset of the oxidation cycle. Since nothing is known about PEDOT films being permselective towards DES it is right to assume that an equivalent amount of anions and cations are present in the $PEDOT^0$ film. Using the previously calculated (see point 3.3.2) value of a void fraction of 0.425 and under the assumption of the maximum doping level, the ratio of DES ions to polymer positive charge sites has been estimated as circa 1.9. Therefore, it becomes obvious that there is more than sufficient reservoir of cations in the polymer film to last for the entire redox cycle. It is also worth mentioning that the charge passed (Q_{pas}= 4.27 mC cm^{-2}) upon redox cycling of the polymer films in Ethaline surpassed that of any other electrolyte tested in this study signalling its excellent potential as a battery electrolyte.

In Propaline (solvent composed of choline chloride and propylene glycol in a 1:2 molar ratio) increase of the anion size (from EG_2Cl^- to PG_2Cl^-) results in a 'V' shape gravimetric signal (see figure 12). Decrease of the mass during the first half of the redox cycle is followed by an increase in the second half. There are previous accounts of films prepared with sulfonate monovalent anions which displayed both cation and anion being involved in charge compensation during redox cycling,[10] however no such process in a fully ionic environment had previously been reported. Obviously, electroneutrality requirement in Propaline are met by a much more complicated mechanism than in Ethaline. It comprises two stages, during the former mass decreases and during the latter mass increases are recorded.

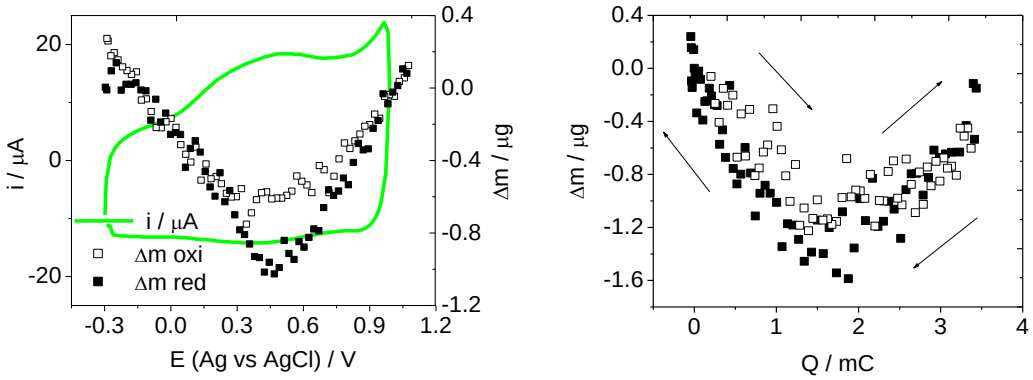

Figure 12. Left panel: Massogram (Δm/E) overlaid on a voltammogram of a PEDOT 0.8 µm [± 0.1 µm] film ($Q_{de\ p}$= 85.43 mC cm^{-2}) redox cycled from - 0.3 V → 1.0 V → - 0.3 V, ν = 5 mV s^{-1} in Propaline 200. Decrease in film mass upon oxidation indicates cation expulsion. Increase in the film mass upon oxidation indicates anion incorporation. Right panel: Δm as a function of injected Q. Arrows indicate the direction of the potential scan. Full squares represent oxidation and the empty ones reduction.

The exchanged molar mass of the first stage is lower than that of choline cation (and very close to the value reported for Ethaline – see table 2). Since the molar mass in the anion ingress regime part equals to circa 0.4 of the PG_2Cl^- molecular mass, this implies mixed transfer in both cases. In the molecular solvent this disparity could be allocated to the neutral solvent molecules. In the case of DES, it is assumed to be an equal flux of anions and cations, effectively forming a flux of a neutral salt. Q_{pas} (charge passed during the oxidation and reduction part of the scan – see tables 5 and 6) of the PEDOT redox cycling in Propyline did not reach the Ethaline values; this has been attributed to the former solvent higher viscosity diminishing the diffusion rate. The rather interesting mechanism of mass exchange of PEDOT films redox cycled in Propaline 200 is further explored in section 3.3.5 of this chapter.

It is noteworthy that simple start-to-end measurements of the mass changes would not have allowed revealing any of these effects. Further explorations of the HBD (which effectively is the main factor controlling the anion identity) variations on the gravimetric signal concentrated on carboxylic acid based DES. Maline 200 (a solvent composed of choline chloride and malonic acid in a 1:2 molar ratio) rather unexpectedly displayed mass increase at the application of the positive potential (oxidation) thus

implying anion incorporation. This particular DES has been previously reported to display different relative motions of the anions and cations than Ethaline.[27]

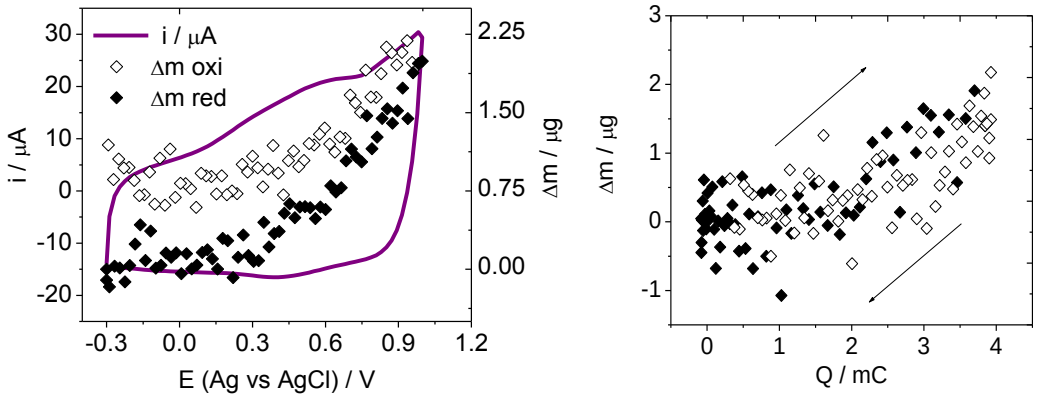

Figure 13. Left panel: Massogram (Δm/E) overlaid on a voltammogram of a PEDOT 0.8 μm [± 0.1 μm] film (Q_{dep} = 85.43 mC cm^{-2}) redox cycled from - 0.3 V → 1.0 V → - 0.3 V, ν = 5 mV s^{-1} in Maline 200. Increase in film mass upon oxidation indicates anion incorporation. Right panel: Δm as a function of injected Q. Arrows indicate the direction of the potential scan. Full diamonds represent oxidation and empty diamonds represent reduction.

This interesting trend can be attributed to pairing between malonic acid molecules and choline cations. D'Agostino and co-workers have previously reported low molecular mobility (and thus low self-diffusion rates) in Maline.[27] According to the authors, there are two most plausible explanations for this fact, both of them attributable to the presence of dicarboxylic acid in the electrolyte. First possibility is the presence of malonic acid in its disassociated form. Resulting carboxylate anion would be prone to interact with choline cation forming large neutral specie. Second possibility is the formation of malonic acid dimers. The dimerization phenomena could then propagate to form chains which would restrict the diffusivity of both cationic and anionic species in Maline. Since malonic acid and choline chloride are in 2:1 ratio, even (purely theoretical) complexation of all choline cations would still leave half of the malonic acid molecules to form complex anions (Mal_2Cl^- or $MalCl^-$). These, having greater mobility than effectively immobilized cations would then serve as dopant ions during the redox cycling process. Maline dominant mode of anion ingress has been quantified by the calculation of the apparent molar mass as 37.2 g mol^{-1} (data from Δm/Q graph – right panel of figure 13). This is significantly less than the molar mass of

even the smaller anion ($MalCl^-$ MW = 139 g mol^{-1}) but the result is with all probability distorted by a mixed origin counter transfer.

Acetaline (solvent composed of choline chloride and acetic acid in a 1:2 molar ratio) is a novel DES formulated specifically for the purpose of this study, thus no previous description of its ion transfer characteristics exist. Acetaline preparation was based on DES formulation rules set by Abbott et al.[13] The gravimetric outcome of PEDOT films redox cycle (figure 14) conducted in this solvent shows a rather interesting 'V' shape. Similarly to the one observed in Propaline it indicates mass decrease followed by, mass increase although here the 'switch' process is not so dramatic with prominent hysteresis distorting the picture. This effect is attributed (like in Propaline) to the relative speed of the ions transfer occurring in this process (see Propaline extended study in section 3.3.5). Evidently, the 'V' effect is HBD related as it can be observed with the same QAS complexed to two radically different HBD, propylene glycol in Propaline and acetic acid in Acetaline.

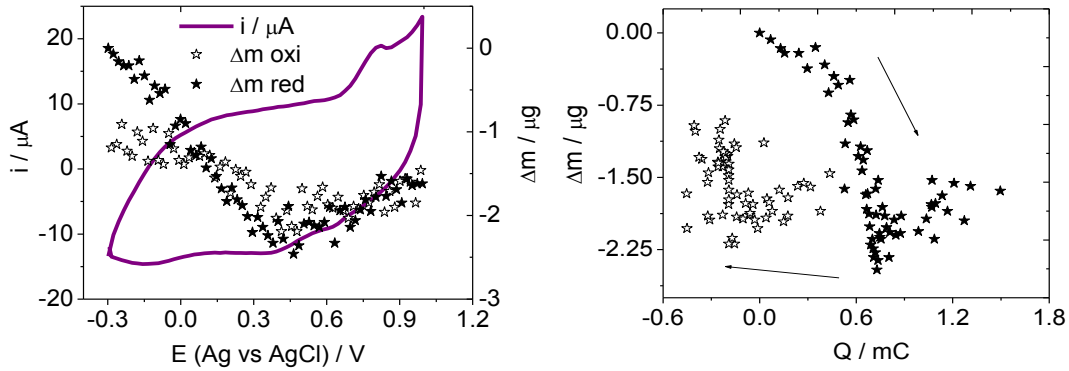

Figure 14. Left panel: Massogram (Δm/E) overlaid on a voltammogram of a PEDOT 0.8 µm [± 0.1 µm] film (Q_{dep}= 85.43 mC cm^{-2}) redox cycled from - 0.3 V → 1.0 V → - 0.3 V, ν = 5 mV s^{-1} in Acetaline 200. Decrease in film mass upon oxidation indicates cation expulsion. Increase in the film mass upon oxidation indicates anion incorporation. Right panel: Δm as a function of injected Q. Arrows indicate the direction of the potential scan. Full stars represent oxidation and empty stars represent reduction.

It is worth noting that in both carboxylic acids based DES the final mass values do not return to the initial ones. This hints at rather limited rate of mass transport, possibly also at low stability of the PEDOT films in these solvents – confirmed later in

this chapter (see stability testing), and may result from the corrosive nature of the acetic acid. In case of Maline it can also be the effect of this solvent considerable viscosity. (See table 1)

The gravimetric response in urea based DES – Reline (a solvent composed of choline chloride and urea in a 1:2 molar ratio) shows strikingly low current values as compared to the other DES. This can be attributed to the more extensive network of hydrogen bonds, probably lowering the mobility of the dopants. The hydrogen bonding between choline cation and the HBD has been proven to be the most extensive in both Reline and Glyceline as suggested by Mantle et al. Since both of the hydrogen bond donors (Urea and Glycerol) are branched molecules, the degree of HBD–Ch^+ branching may severely restrict the ion movement necessary to maintain the electroneutrality. This results in a diminished current response as compared to glycols and carboxylic acids based DES (see table 5).

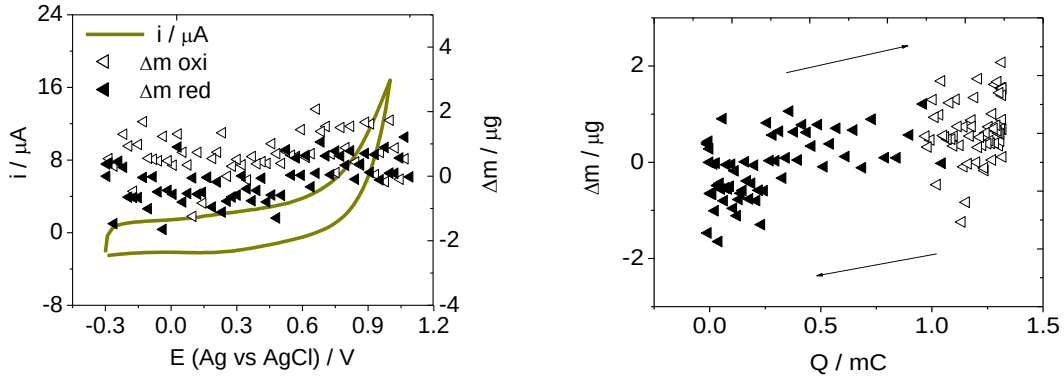

Figure 15. Left panel: Massogram (Δm/E) overlaid on a voltammogram of a PEDOT 0.8 µm [± 0.1 µm] film (Q_{dep}= 85.43 mC cm^{-2}) redox cycled from - 0.3 V → 1.0 V → - 0.3 V, ν = 5 mV s^{-1} in Reline 200. Decrease in film mass upon oxidation indicates cation expulsion. Increase in the film mass upon oxidation indicates anion incorporation. Right panel: Δm as a function of injected Q. Arrows indicate the direction of the potential scan. Full triangles represent oxidation and the empty ones reduction.

In Reline, the gravimetric mass transfer indicates transfer of approximately equal masses in exactly opposite directions. This result is consistent with the work of Abbott et al on ionic species in Reline 200.[14] Their FAB–MS study reported a mixture of [Ur_2Cl^-] and [$UrCl^-$] anionic species and a Ch^+ cation. Since nothing is known about the

relative ratio of these species, a simple calculation assuming a eqiumolar ratio of both types of anions results with mean anion molar mass of 115.8 g mol^{-1}. This being slightly higher than the cation molar mass (104.6 g mol^{-1}) would explain the upwards slope of the Δm/Q plot in the right panel of figure 15. Failure of the charge value to return to their initial values can be assigned to the considerable viscosity of this particular solvent which is the highest of all DES tested (see table 1). Upon closer analysis of the Reline gravimetric mass transfer, one cannot exclude the possibility that the overall signal is composed of a four different diffusions processes (analysed in detail in section 3.3.5) previously encountered in Propaline and Acetaline with the 'real' signal being masked by this solvent high viscosity slowing the rate of the ionic transfer.

Figure 16 depicts the volammetric (left panel) and gravimetric (right panel) responses of Glyceline 200 (Ch^+Cl^- + 2 ($C_3H_8O_3$)) where HDB is a highly branched glycerol molecule. Mass decrease upon oxidation indicates cation expulsion. This leads to an explanation that on the qualitative level the $((C_3H_8O_3)_2Cl)^-$ anion and possibly $((C_3H_8O_3)Cl)^-$ anion and Ch^+ cation are the ionic species in this electrolyte with the smaller, thus more mobile Ch^+ species dominating the gravimetric mass transfer.

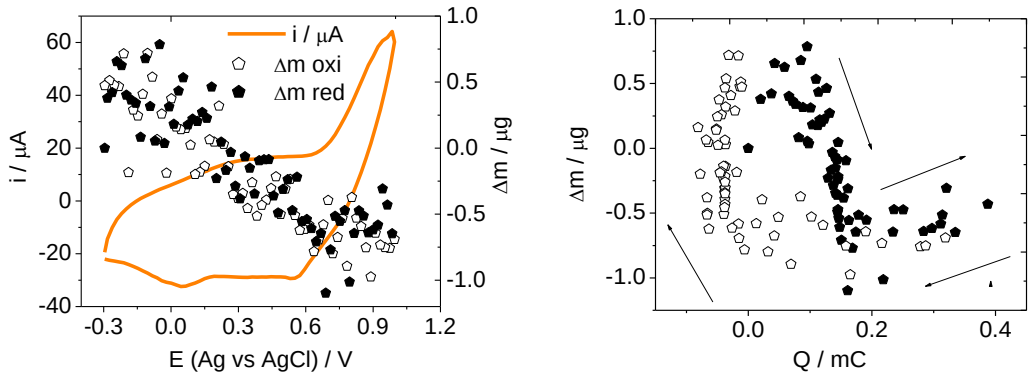

Figure 16. Left panel: Massogram (Δm/E) overlaid on a voltammogram of a PEDOT 0.8 µm [± 0.1 µm] film (Q_{dep} = 85.43 mC cm^{-2}) redox cycled from - 0.3 V → 1.0 V → - 0.3 V, ν = 5 mV s^{-1} in Glyceline 200. Decrease in film mass upon oxidation indicates cation expulsion. Increase in the film mass upon oxidation indicates anion incorporation. Right panel: Δm as a function of injected Q. Arrows indicate the direction of the potential scan. Full pentagons represent oxidation and the empty ones represent reduction.

Glyceline Δm/Q plot (right panel of figure 16) indicates rapid mass loss followed in the later stages of the redox cycle by an exchange of species of almost equivalent molar masses (plateau visible in the low Q regime in the right panel of figure 16). Significant hysteresis is observed in the initial stage. Conclusions gained from the analysis of other DES allow classifying this process as a cation expulsion; however, the mass change in the initial (high Q regime) is so rapid that the calculated exchanged molar mass is much larger than the glycerol molar mass. This hints at concurrent cation and salt expulsion from the polymer film with the majority of species being neutral (i.e. salt molecules). The exchanged molar mass stands at 730 g mol^{-1} whereas the proposed anionic specie $((C_3H_8O_3)_2Cl)^-$ has a mass of 219.6 g mol^{-1}. Thus, simple calculation reveals that there is an approximately 1.3 molecule of salt for every cation exchanged in the high Q regime.

Electrolyte	Molar mass exchanged upon oxidation (g mol^{-1})		Molar mass exchanged upon reduction (g mol^{-1})	
	Low Q regime	High Q regime	Low Q regime	High Q regime
$CH_3CN/LiClO_4$	64.8 ± 0.01	n/a	65.5 ± 0.04	n/a
DCM / $(C_2H_5)_4NBr$	26.7± 0.02	n/a	29.1 ± 0.02	n/a
Ethaline 200	-74 ± 0.01	n/a	90.6 ± 0.01	n/a
Propyline 200	-77 ± 0.06	55 ± 0.06	69.8 ± 0.07	23.6 ± 0.05
Maline 200	37.2 ± 0.05	n/a	33.8 ± 0.05	n/a
Acetaline 200	- 316.5 ± 0.3	37.1 ± 0.2	- 19 ± 0.4	18 ± 0.2
Glyceline 200	- 732 ± 1	17 ± 1	-57 ± 0.4	286 ± 3
Reline 200	115.8 ± 0.3	n/a	109 ± 0.7	n/a

Table 2. Molar mass exchanged upon the oxidation and reduction part of the redox cycle of a PEDOT 0.8 µm [± 0.1 µm] film (Q_{dep} = 85.43 mC cm^{-2}) redox cycled from - 0.3 V → 1.0 V → - 0.3 V at ν = 5 mV s^{-1}.

	CH_3CN/ $LiClO_4$	DCM/ $(C_2H_5)_4$ NBr	Ethaline 200	Propaline 200	Maline 200	Acetaline 200	Glyceline 200	Reline 200
Q_{pas}	4.024	2.525	**4.27**	3.43	3.85	1.496	0.388	1.319

Table 3. Charge passed (mC cm^{-2}) as a function of scan rate during the redox cycling of a PEDOT 0.8 µm [± 0.1 µm] film (Q_{dep}= 85.43 mC cm^{-2}) redox cycled from - 0.3 V $\rightarrow$ 1.0 V $\rightarrow$ - 0.3 V.

Electrolyte	Cation	Anion	Process
CH_3CN / $LiClO_4$	Li^+	ClO_4^-	Anion incorporation
DCM / $(C_2H_5)_4NBr$	$(C_2H_5)_4N^+$	Br^-	Anion incorporation
Ethaline 200	Ch^+	EG_2Cl^-/$EGCl^-$	Cation expulsion
Propyline 200	Ch^+	PG_2Cl^-/$PGCl^-$	Anion incorporation/ cation expulsion
Maline 200	Ch^+	$[CH_2(COOH)_2]_2Cl^-$/ $CH_2(COOH)_2\,Cl^-$	Anion incorporation
Acetaline 200	Ch^+	$[CH_3COOH]_2Cl^-$/ $CH_3COOHCl^-$	Anion incorporation/ cation expulsion
Glyceline 200	Ch^+	$[C_3H_8O_3]_2Cl^-$/ $C_3H_8O_3Cl^-$	Anion incorporation/ cation expulsion
Reline 200	Ch^+	$[(NH_2)_2CO]_2Cl^-$ / $(NH_2)_2COCl^-$	Anion incorporation/ cation expulsion

Table 4. Dominant ion transfer during redox cycling.

3.3.4 Selection of electrolytes for further study

Calculation of the charge passed as well as the initial observations of the polymer film stability allowed selecting the most favourable electrolytes. Ethaline was selected on the basis of charge passed (promising in terms of future charge storage applications) while Propaline was deemed an interesting object to study due to the shape of the gravimetric mass transfer (recorded upon redox cycling of the polymer films in this particular solvent) which may allow for a creation of a versatile actuator.

Excellent stability of PEDOT films while redox cycled in these two DES was considered to be an additional bonus. Both carboxylic acid based DES were deemed unsuitable due to the solvent degradation (Maline) and solvent inherent corrosiveness (Acetaline). The properties of Acetaline were a particular subject of concern during the bracketed experiments (see Experimental section). Polymer films which were redox cycled in Acetaline proved to have their voltammetric and gravimetric performance irreversibly and detrimentally modified. The morphology of these degraded films was not analysed; however, it can be reasonably assumed that the recorded current output and mass exchange changes occurred because of structural as well as morphological conversions. Reline and Glyceline charge storage performance did not match that of Ethaline, thus they were also omitted from further study. Acetonitrile was selected as a representative molecular solvent on the basis of significant literature available.

3.3.5 Electrolytes of choice – extended study. Voltammetric analysis of the selected electrolytes.

The performance of any electrochemical device is most commonly denoted in terms of i/E output (i.e. cyclic votlammogram). Figure 17 shows voltammetric responses of PEDOT films redox cycled in CH_3CN, Ethaline and Propaline at lowest and highest values of the potential scan rate investigated.

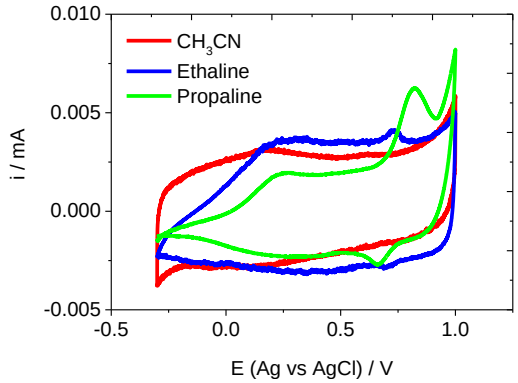

Figure 17. Voltammograms of a 0.8 µm [+/-0.1 µm] PEDOT film (Q_{dep} = 79.7 mC cm^{-2}) redox cycled from - 0.3 V → 1.0 V → - 0.3 V in 0.1 M $LiClO_4/CH_3CN$, Ethaline 200 and Propaline 200 (in chronological order). Film was washed between the consecutive experiments to avoid the history effect. ν = 2 mV s^{-1}. Blue line represents Ethaline 200, green line Propaline 200, red line $LiClO_4$.

Major differences between the voltammograms of PEDOT films redox cycled in each electrolyte are clearly visible. The analysis of the data in table 5 reveals that the charge passed does not scale linearly with the scan rate. The obvious conclusion is that in a film of such thickness at ν ≥ 10 mVs^{-1} full redox conversion of the entire polymer film is not achievable in any of the three selected solvents.

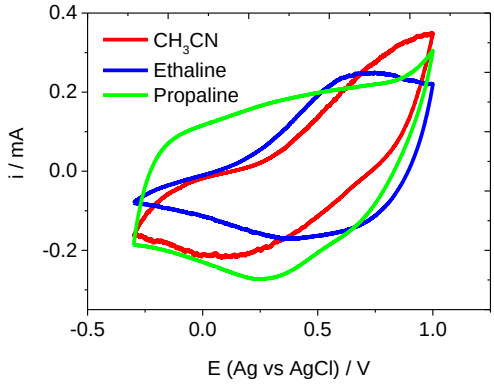

Figure 18. Voltammograms of a 0.8µm [+/-0.1 µm] PEDOT film (Q_{dep}= 79.7 mC cm^{-2}) redox cycled from - 0.3 V → 1.0 V → - 0.3 V in 0.1 M $LiClO_4$ /MeCN, Ethaline 200 and Propaline 200 (in chronological order). Film was washed between the consecutive experiments to avoid the history effect. ν = 200 mV s^{-1}. Blue line represents Ethaline 200, green line Propaline 200, red line $LiClO_4$.

ν [mV s^{-1}]	0.1 M $LiClO_4$ Q (mC)	Ethaline 200 Q (mC)	Propaline 200 Q (mC)
2	0.87	3.95	1.43
5	1.91	2.15	0.97
10	1.77	1.52	0.83
20	1.63	1.30	0.73
50	2.35	1.04	0.58
100	1.76	0.92	0.43
200	1.44	0.79	0.27

Table 5. Charge passed as a function of scan rate during the oxidation phase of the PEDOT 0.8 μm [+/-0.1 μm] polymer film redox cycled from - 0.3 V → 1.0 V → - 0.3 V, in 0.1 M $LiClO_4$, Ethaline 200 and Propaline 200.

It was already proposed by Hillman[8] and Randriamahazaka[20] that the electrodeposited polymer films are far from homogeneous but instead consist of a bottom, rigid zone (compact layer) with long and highly conjugated chains overlaid by a top, flexible, so called 'open' zone (elastic layer) composed of short, less conjugated chains.

ν [mV s^{-1}]	0.1 M $LiClO_4$ Q (mC)	Ethaline 200 Q (mC)	Propyline 200 Q (mC)
2	0.69	3.43	1.22
5	1.75	2.05	0.91
10	1.69	1.49	0.81
20	1.59	1.27	0.72
50	2.10	1.04	0.58
100	1.63	0.92	0.43
200	1.36	0.79	0.27

Table 6. Charge passed as a function of scan rate during the reduction phase of the PEDOT 0.8 μm [+/-0.1 μm] polymer film redox cycled from - 0.3 V → 1.0 V → - 0.3 V, in 0.1 M $LiClO_4$, Ethaline 200 and Propaline 200.

Increase in the scan rate shortens the time window available for the dopants preventing them from reaching the compact zone, this results in a lower charge recorded. As anticipated, there is a progressive decrease in a charge passed while using

the CH_3CN at the lowest scan rate. However, such low scan rate experiments are reputed to be the most susceptible to any kind of drift.[28] It can be reasoned that there are no kinetic effects and diffusional limitations as such obstacles would result in a smaller current at high ν values which is exactly opposite to the results presented in table 6.

Considering the theoretical complete redox conversion charge (0.3 e per EDOT unit, deposition conversion 2.3 e^- per EDOT monomer and Q_{dep} = 18.34 mC cm^{-2}) the maximum charge value that can theoretically be reached upon redox cycling of this particular polymer film is Q_{max} = 2.39 mC cm^{-2}. Applying this value to the measured values the responses for CH_3CN do not display a linear correlation to scan rate and are reaching circa 40 – 45 % of the Q_{max}. In Ethaline, most promising for charge storage applications, low scan (2 mV s^{-1}) values approach the Q_{max}. In Propaline, probably due mainly to the viscosity of this electrolyte even the low ν values reaches only approximately 35 % of the theoretical maximum. To simplify the analysis of the dynamic forces that control the amount of charge passed (Q_{pas}) charge values were plotted as a function of the scan rate. The logarithmic format allows spreading the data for more clarity but also enables searching for a possible power law dependency.

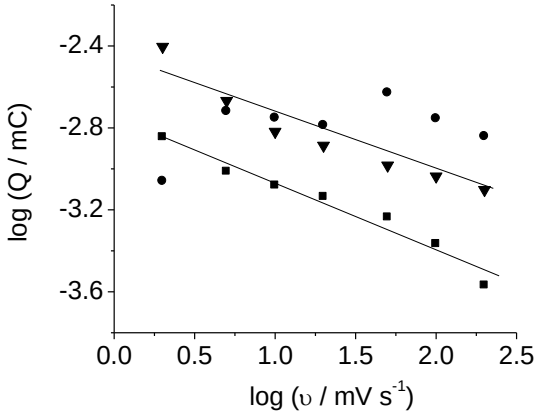

Figure 19. Charge passed as a function of the scan rate during the oxidation phase of the PEDOT 0.8 µm [+/-0.1 µm] polymer film (Q_{dep} = 79.7 mC cm^{-2}) redox cycled from - 0.3 V → 1.0 V → - 0.3 V. Circles represent 0.1 M $LiClO_4/CH_3CN$, triangles Ethaline 200, squares Propaline 200. No linear fit could be obtained for 0.1 M $LiClO_4/CH_3CN$. The gradient of the linear fit for Ethaline is - 0.3 (± 0.1), for Propaline it is also - 0.3 (± 0.1).

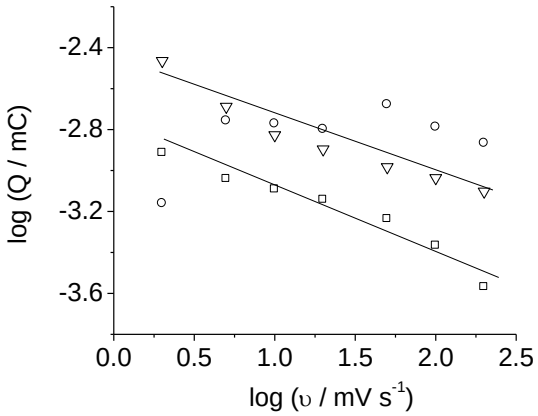

Figure 20. Charge passed as a function of the scan rate during the reduction phase of the PEDOT 0.8 µm [+/-0.1 µm] polymer film (Q_{dep} = 79.7 mC cm^{-2}) redox cycled from - 0.3 V → 1.0 V → - 0.3 V. Circles represent 0.1 M $LiClO_4/CH_3CN$, triangles Ethaline 200, squares Propaline 200. No linear fit could be obtained for 0.1 M $LiClO_4$/ H_3CN. The gradient of the linear fit for Ethaline is - 0.3 (± 0.1), for Propaline it is also - 0.3 (± 0.1).

Gradient of the log Q/log ν is commonly applied to reveal the controlling factors (be it kinetic or diffusional) in electrochemical systems. While $LiClO_4/CH_3CN$ electrolyte did not display any kind of linearity (and is of limited interest here anyway) only the values for both DES have been calculated. For both Ethaline and Propaline this value is approximately – 0.3 in both the oxidation and reduction part. Although these values are rather distant from – 0.5 which signals full diffusional control they are closer to it than to 0 which is the value that indicates full kinetic control (i.e diffusion independent process).[4] This data provides a brief overview of the charge transport occurring upon redox cycling of PEDOT films immersed in these selected DES. The unusual redox switch mechanism in Propaline was deemed of great interest for potential actuator applications and is scrutinized in more detail below.

3.3.6 Propaline gravimetric switch – extended study

Profile of the Propyline gravimetric response indicates a cation–based mechanism during the first part of the redox cycle, followed by an anion-based mechanism in the second part. This mixed cation/anion regime signal almost reaches the initial mass values at the intermediate scan values (5 mV s^{-1} – see figure 16). This

means that the overall mass change between the fully neutral (at - 0.3 V) and fully oxidized (at 1.0 V) polymer film is close to zero. Then the entire process is reversed and anion expulsion is followed by cation incorporation. In the undoping half cycle the transition is not so prominent but the undoping gravimetric signal generally traces the doping gravimetric response. This rather interesting mass 'switch' prompts questions about its possible origins. It has been already discussed above that there are more DES ions present in the neutral state polymer film than the amount egressed in the cation regime of the cycle. This rule out the possibility of simple exhaustion of the cation reserves necessitating the switch to the anion reserves. Another important factor is the relative diffusivity of the relatively small cation (Ch^+) and large anion (PG_2Cl^-) depending on the scan rate. At the lowest scan rate (ν = 2 mV s^{-1}) in the cation regime cation (anion) transport numbers are 0.79 (0.21). Fivefold increase in the scan rate (ν = 10 mV s^{-1}) results in the transport numbers for cation (anion) rising up to 0.89 (0.11). At even faster scan rates the observed molar mass exceeds that of choline cation. This implies transport of uncharged species (in this case, due to the lack of solvent as such, uncharged species are equivalent numbers of cations and anions – usually termed salt in the vernacular of the molecular electrolytes and solvent in the one of ionic liquids'). Anion-based regime also shows increase of cation transport number with the scan rate but it is a rather modest one from 0.29 (0.71) at 2 mV s^{-1} to 0.44 (0.56) at 10 mV s^{-1}. Thermodynamically controlled mechanisms are known to occur independently of the time scale applied (which in this case is the cyclic voltammetry scanning rate).[4] This is clearly not the situation observed here. The data in table 8 and figure 21 unambiguously prove that as the scan rate is increased the mass switch gravimetric profile progresses towards more anodic potentials distorting the regular V shape observed at 5 mV s^{-1}. Although this trend is not very strong, it can be noted that the cation/anion competition is less symmetrical at the lowest scan rate and comparatively most equal and of regular shape at 5 mV s^{-1}.

On the basis of the experimental evidence, a plausible explanation seems to be related to the ions relative transfer rates. Propaline gravimetric signal can be separated into four different ion transfer processes. Egress of the cation (process one) with simultaneous, however limited in scale ingress of anion (process two), followed by ingress of the anion (process three) with simultaneous, however minor egress of the cation (process four). Since nothing is known about permselectivity of the polymer film

it can be assumed that the slowest moving ion would be the largest one, the complex anion [PG_2Cl^-]. Thus, anion injection into the film would be the slowest of the four processes in the complete redox cycle. This initial assumption is reinforced by a recurrent observation that ingress of any species into the network of internal voids of the polymer film (i.e. confined space) is a much slower process than the egress of these species from the same voids into the effectively unlimited bathing electrolyte solution.[4]

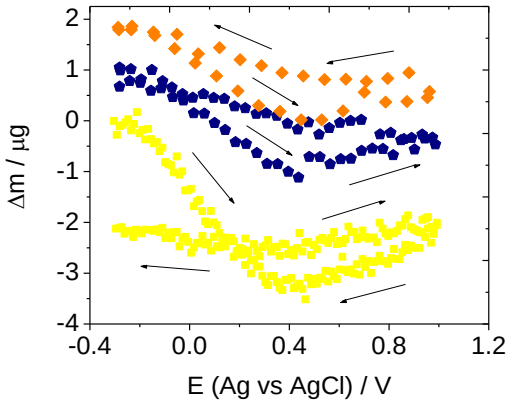

Figure 21. Δm as a function of the applied potential. PEDOT 0.8 μm [+/-0.1 μm] film (Q_{dep}= 79.7 mC cm^{-2}) redox cycled in Propaline 200 from - 0.3 V → 1.0 V → - 0.3 V. ν = 2 mV s^{-1} (yellow line), 10 mV s^{-1} (blue line) and 20 mV s^{-1} (red line).

ν [mV s^{-1}]	E_{switch} [V] oxidation	E_{switch} [V] reduction	Q_{pas} at E_{switch} oxidation	Q_{pas} at E_{switch} reduction	Q_{pas} oxidation	Q_{pas} reduction
2	0.38	0.19	0.37	1.214	2.97	0.038
5	0.42	0.3	1.3	1.61	3.31	0.082
10	0.46	0.53	0.76	1.26	1.83	0.074
20	0.57	0.67	1.00	1.32	1.75	0.05

Table 8. Q_{pas} recorded during successive parts of the redox cycle. PEDOT 0.8 μm [+/-0.1 μm] film (Q_{dep} = 79.7mC cm^{-2}) redox cycled from - 0.3 V → 1.0 V → - 0.3 V in Propaline 200.

As it was explained above it can be reasoned that due to its size anion ingress into the polymer film would be the slowest of all processes in the complete redox cycle. Since egress is generally faster than ingress then cations (smaller, more mobile ions) egress would be the fastest process. This elimination allows us to establish that the third in the rapidity order is anion egress (fast process, slow anion) and second is cation ingress (fast ion, slow process). This model is graphically presented below in figure 22:

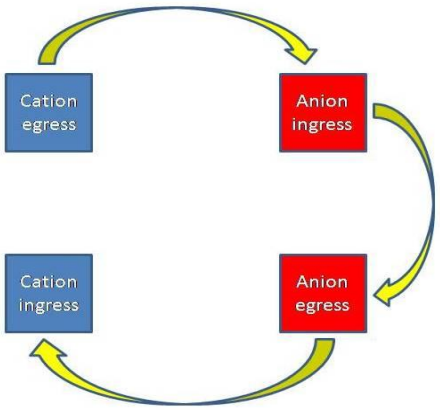

Figure 22. Graphical representation of the 'mass switch' occurring upon redox cycling of PEDOT films in Propaline and Acetaline.

This model is supported by the data in table 9 (below) and figure 21, from which it can be noted, that faster processes display greater variation with timescale changes, while slower processes do not display much of such incongruity.

ν [mV s^{-1}]	Δm (g mol^{-1}) 0.1 M $LiClO_4$/MeCN	Δm (g mol^{-1}) Ethaline 200	Δm (g mol^{-1}) Propaline 200 Cation expulsion	Δm (g mol^{-1}) Propaline 200 Anion incorporation
2	48	123	690	43
5	58	74	77	55
10	60	72	269	35
20	63	68	199	52

Table 9. Molar mass changes ($\frac{\Delta mF}{Q}$) for the oxidation half cycle of PEDOT films redox cycled in CH_3CN, Ethaline and Propaline. Data obtained from the experiments presented in figures 12 and 21.

3.3.7 PEDOT film stability in Ethaline, Propaline and Acetonitrile/lithium perchlorate electrolytes.

Commercial applications of CP in charge storage devices are so far not widespread. It was proved in the early 1990's that polyaniline (PANI) can serve as a cathode in a polyaniline – lithium battery (Bridgestone Corp. Japan).[29] However, since this device encountered significant problems with cyclability as well as the capability to deliver constant charge, its' further developments were hampered. Though some progress has been achieved in this field since then, CP based electrodes still fall short in terms of long term stability, particularly when compared with Li_xCoO_2 and Li_xMPO_4 olivines.[29] It is indisputable that CP have significant advantages (apart from the obvious economical ones) over the widespread Li – ion technology, namely their flexibility (for use in flexible, textile woven photovoltaic and photochromic materials) and their fully organic nature (all–plastic, radar invisible, lightweight military applications). As for the fully ionic electrolytes, Lewandowski and co-workers reported that the same type of carbon capacitor filled with ionic liquid has energy density order of magnitude higher than the same device operating while filled with the aqueous electrolyte.[30]

It can be noted from comparison of figures 23, 24 and 25 that the oxidised/neutralized PEDOT films in DES display greater stability than the PEDOT films redox cycled in the molecular solvent (Acetonitrile). This effect cannot be simply attributed to the latter volatility and thus salt concentration change; it can however at least partially originate from the absence of 'conformational memory' in CP films redox cycled in ionic liquids and Deep Eutectic Solvents. Similar observations regarding polymer films stability have previously been reported by Randiramahazaka and co-authors.[20]

A recent work by Levy et al. determined that, regardless of their nature, CP's cycling ability (when redox cycled in molecular solvents) still remains an issue to be addressed.[29] Similar conclusion was reached by Kiefer and co – workers in their study of PEDOT based actuators cyclability in $TBACF_3SO_3$/PC during which they noted a gradual degradation of the polymer film when large potential window was applied.[31] Thus, it was deemed appropriate to compare the long term stability of PEDOT film redox cycled in Ethaline and Propaline versus CH_3CN.

The long term failure of the CP/molecular electrolyte systems is widely attributed to the polymer films ageing. Since this does not seem (at least on a timescale of these experiments) to occur in the experimental data presented here it is interesting to dwell on the origin of the degradation absence in the ionic environment.

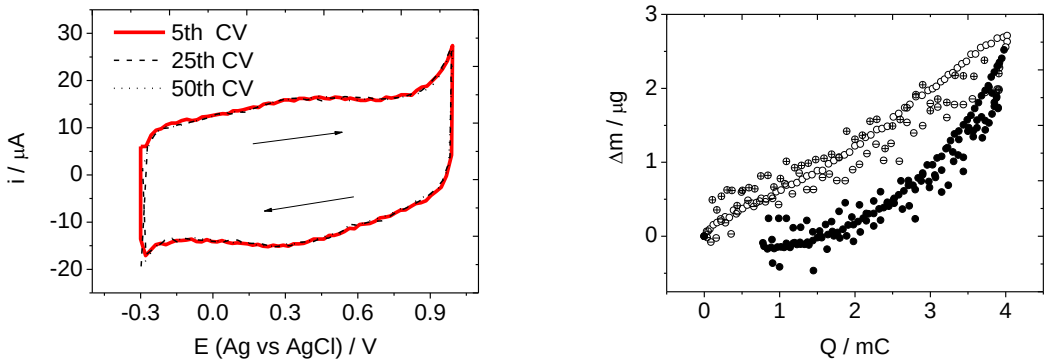

Figure 23. Left panel: Voltammograms of a 0.8 µm [+/-0.1 µm] PEDOT film redox cycled - 0.3 V → 1.0 V → - 0.3 V in 0.1 M $LiClO_4/CH_3CN$. ν = 5 mV s^{-1}. Solid red line represents 5th scan, dashed black line 25th scan, and dotted black line 50th scan. Right panel: change of mass as a function of charge passed. Full circles represent oxidation and empty circles represent reduction. Circles represent 5th scan, circles with line across represent 25th scan and circles with a cross represent 50th scan.

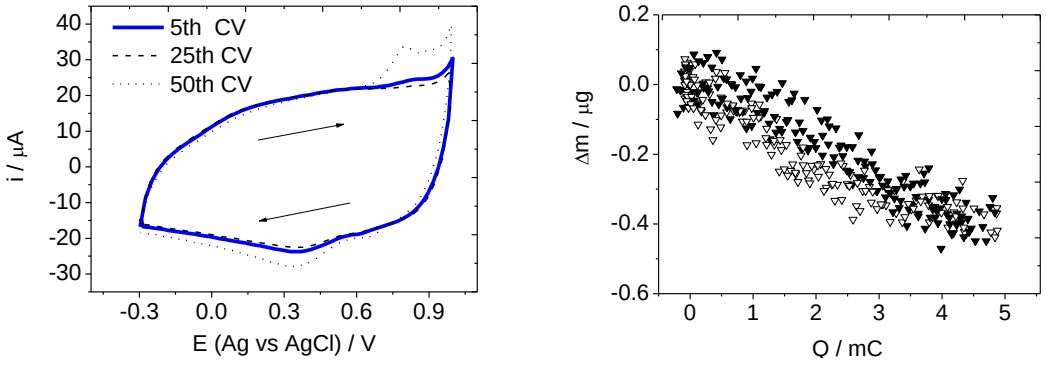

Figure 24. Left panel: Voltammograms of a 0.8 µm [+/-0.1 µm] PEDOT film redox cycled - 0.3 V → 1.0 V → - 0.3 V in Ethaline 200. ν = 5 mV s^{-1}. Solid blue line represents 5th scan, dashed black line 25th scan, and dotted black line 50th scan. Right panel: change of mass as a function of charge passed. Full triangles represent oxidation and empty triangles represent reduction.

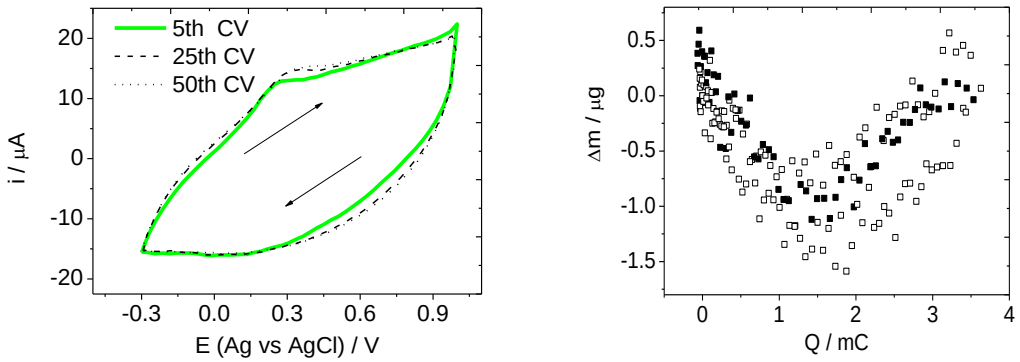

Figure 25. Left panel: Voltammograms of a 0.8 µm [+/-0.1 µm] PEDOT film redox cycled - 0.3 V → 1.0 V → - 0.3 V in Propaline 200. ν = 5 mV s^{-1}. Solid green line represents 5th scan, dashed black line 25th scan, and dotted black line 50th scan. Right panel: change of mass as a function of charge passed. Full squares represent oxidation and empty squares represent reduction.

CP film ageing is alleged to originate from a gradual decrease of the amount of itinerant solvent present in the polymer film. Diminished amount of solvent may result in a lower number of available dopants partaking in a redox cycle (excluding evaporation effect, which, in a sealed electrochemical system, is a reasonable assumption). The lower number of dopants results in the lesser charge passed. The decrease of the solvent volume is in turn generated by the CP voids (free volume) being gradually obstructed by 'solid' conformations of the macromolecules formed during the repetitive redox cycling. An early indication of a polymer film ageing is a change in gravimetric signal without significant change in the *i*/E response (see figure 23, right panel). PEDOT films redox cycled in DES similarly to the ones cycled in CH_3CN do not display significant changes of the *i* – E trace. A higher oxidation current visible in the 50th CV of the PEDOT/Ethaline stability test is attributed to the oxidation of the underlying Au current connector (EQCM crystal) and is irrelevant to the polymer film/electrolyte system overall stability. Comparison of the data contained in the right panels of figures 23 (Δm vs Q – CH_3CN), 24 (Δm vs Q – Ethaline) and 25 (Δm vs Q – Propaline) unequivocally shows that the Δm / Q signal for the molecular solvent clearly displays onset of film ageing in the CH_3CN based system but is not present to any noticeable extent in both DES tested.

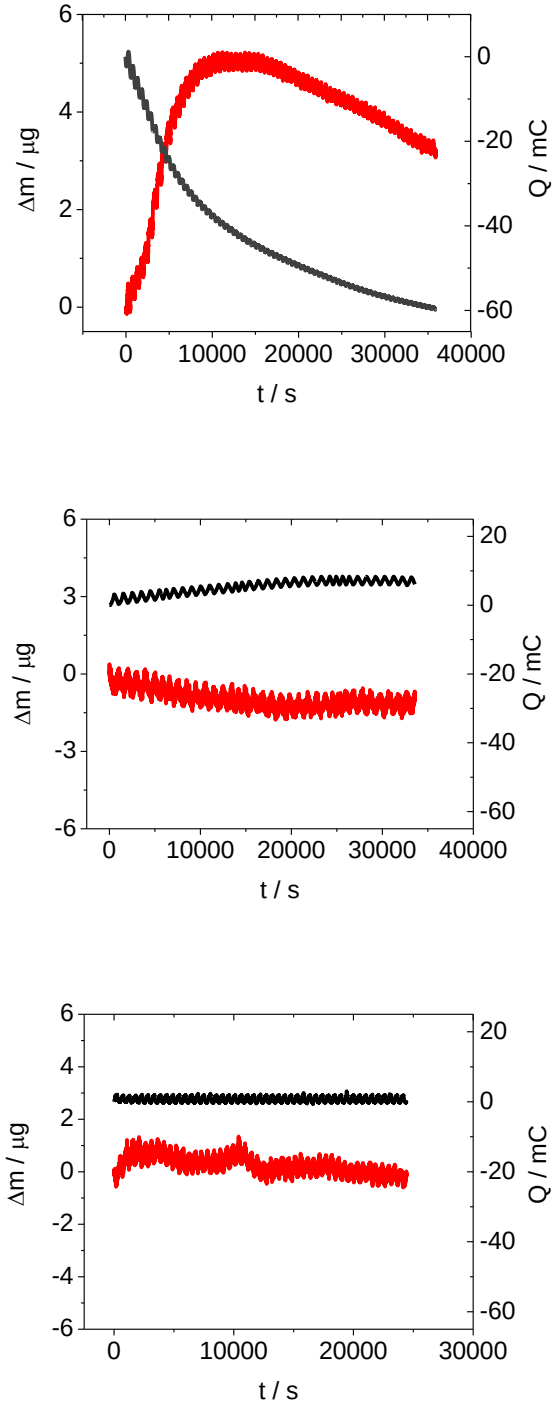

Figure 26. Mass (red line) and charge (black line) changes of a 0.8 µm [+/-0.1 µm] PEDOT films expressed as a function of time. All films redox cycled - 0.3 V → 1.0 V → - 0.3 V at ν = 5 mV s^{-1}. Top panel: Film redox cycled in 0.1 M $LiClO_4$ /CH_3CN. Middle panel: Film redox cycled in Ethaline 200**.** Film redox cycled in Propaline 200.

As the lack of solvent *per se* seems to radically improve the stability of exactly the same polymer film the most logical answer seems to lie in the liquid's fully ionic

nature. Stability of the electrochemical systems was further explored in terms of the total mass and charge changes over time. These are depicted in figure 26 (top panel (CH_3CN), middle panel (Ethaline) and bottom panel (Propaline)).

Thus, the proposed explanation of CP films superior stability in DES is as follows. Relatively large (and branched) cations and even larger (and more branched) anions present in large amounts in the polymer film throughout the entire redox cycle prevent formation of the 'frozen' conformations inhibiting any shape changes and additionally acting as plasticizers increasing films' elasticity. This deduction is supported by the data in the bottom panel of the figure 26 (below) where it can be noted that the PEDOT/Propaline system (largest anion) displays stability surpassing the one of Ethaline.

These large ions keep the total void volume at effectively constant level providing charge stability vastly surpassing the one recorded in molecular solvents. This observation combined with DES non–flammability and insignificant volatility makes them very promising electrolytes for rechargeable storage applications (both batteries and redox flow cells).

It can be noted that the results obtained from redox cycling of PEDOT films in molecular solvent confirmed the instability reported by Levy et al.[29] Conversely to the acetonitrile based experiment in Ethaline and in Propaline, both mass and charge signals seem to stabilize with time. Although the experiments conducted here are not as extensive (in terms of timescale) as the industry standards, where ~ 10^4 charge/discharge cycles are frequently employed they give a good indication of long term CP-DES based battery performance.

3.4 Conclusions

The main objective of this study (validity of the gravimetric measurements) was successfully fulfilled. It was proven that despite the film possible partially viscoelastic nature, the DES viscosity had a dominant effect with the polymer film presence (or the lack of it) being insignificant in the terms of dissipating energy levels.

As anticipated, the mass transfer dynamics originating during the potential

driven CP redox switching in deep eutectic liquids is of a very different character as compared to that observed in 'classic' molecular solvent based electrolytes. Ion movement dynamics are controlled by ionic liquid composition as well as by the experimental timescale. Both 'classic' electrolytes tested (0.1 M $LiClO_4/CH_3CN$ and 0.1 M $(C_2H_5)_4NBr/DCM$) displayed (as expected) anion incorporation dominated gravimetric signal. With DES, things are clearly more complicated as, depending on the type of the hydrogen bond donor used to prepare the eutectic solvent, similar PEDOT polymer films redox cycled in these electrolytes displayed cation exclusion, anion injection and (most strikingly), a mixture of both these processes. This information might form a basis for the development of the sensor selective only for specified ions as well as electrochemical actuators.

If, as previously suggested by Skopek et al. chloride ion was the anionic species in the choline chloride based DES (which is already dubious as no Cl_2 evaporation has ever been observed from these liquids during redox cycling of CP films) then this small, spherical, highly mobile anion would undoubtedly dominate the gravimetric signal. This is clearly not the case. Instead, in Ethaline [EG_2Cl^- anion] and Glyceline [$[C_3H_8O_3]_2Cl^-$ anion] it is the choline cation that dominates the mass transfer. Mass changes observed during the redox cycling of PEDOT films in all of the DES analysed in this study indicated that the ingress/egress of ions is far from homogeneous. This is noticeable due to the presence of hysteresis (more prominent in Glyceline, smaller, albeit still noticeable in Ethaline) as well as the fact that the normalized molar mass of the mobile species varies from Ch^+. Ion flux heterogeneity arises from movements of 'salt' (equal amounts of cations and anions travelling together and having an effective zero net charge) in addition to minor anion counter flux. Acetaline and Propaline displayed rather unusual cation egress/anion ingress process with Propaline being a particularly prominent example. For all of the systems tested it was proven that the free volume available in the polymer film (voids) (i.e. the volume which can be assumed to be filled with electrolyte prior to the redox commencement) vastly exceeds the volume of cation expelled in the first stage of the redox cycle. Thus, a simple possibility of the mass 'switch' being a result of a simple exhaustion of the film based supply of cations was eliminated. Conversely, the amount of DES present in $PEDOT^0$ was confirmed to be more than adequate to supply the cations for the entire redox cycle. The possibility of thermodynamic control was eliminated as the process observed in Propaline displayed strong dependence on the scan rate applied. Based on these observations, the

mechanism based on relative speed of four different ion fluxes was elucidated. The proposed mechanism was further confirmed as a time–dependence of faster process was confirmed as being larger than for the slower processes. Due to Acetaline corrosiveness, most of the 'switch' mechanism detailed study was conducted in Propaline as the stability and longevity of PEDOT films in both carboxylic acid based DES was proved to be unsatisfactory. This instability is also related to Maline inherent instability and the possible decomposition of malonic acid over time. The rather unexpected anion transfer domination in Maline/PEDOT systems is probably a result of pairing between malonic acid molecules and choline cations, effectively immobilizing the cations. Since, in this DES, malonic acid and choline chloride are in a 2:1 molar ratio, even (theoretical) full complexation of all choline cations would still leave sufficient number of complex anions ($((CH_2(COOH)_2)_2Cl^-$ and/or $CH_2(COOH)_2\ Cl^-$) to serve as dopants in the redox cycle. Reline gravimetric analysis was distorted by this solvent's very high viscosity. However, previous assumptions made by Abbott and co-workers regarding the identity of the ionic species, were tentatively confirmed.[27]

Important conclusions that can be drawn from this chapter indicate that CP film composition is determined by ion–film interactions, but it is only ion relative mobility that determines the redox reaction dynamics. The experimental results are in a good agreement with previous work by Ryu et al.[32] indicating that the PEDOT film has a significant diffusional pseudo-capacitance originating from the incorporated electrolyte. Furthermore, work conducted by Bobacka et al on molecular solvents (where authors concluded that the polymer film contains an amount of the electrolyte more than suitable for the entire redox cycle) was extended here to embrace DES with similar results.

Stability study revealed profound advantages of the DES as compared to molecular solvents. The effects of the polymer film ageing were not observed on these experiments timescale (although it must be indicated that industrial cyclability testing is usually conducted on a much longer time scale – here not possible due to the equipment limitations). Additionally, over time the mass and charge of PEDOT films cycled in Ethaline and Propaline seemed to stabilize over time (unlike in CH_3CN). Mattes and co-workers[33] have previously confirmed the superior stability of several CP electrochemically cycled in IL. This study sheds light on CP/DES systems electrochemistry yielding similar conclusions with DES having the additional environmental and economic advantages over ionic liquids. Work contained in this

chapter confirms and expands work conducted so far on CP/DES gravimetric mass transfers. The absence of film ageing is in agreement with previous work by Randriamahazaka and co-workers regarding CP stability in IL (PEDOT films redox cycled in EMITFSI).[34]

This behaviour proves superior electrochemical stability of these liquids when compared to the molecular solvents thus expanding the currently work by Dőbbelin et al [35] and Marchesi and co-workers[36] about our knowledge of CP redox chemistry in a fully ionic environment.

3.5 References

1 T. A. Skotheim, J.R. Reynolds (Ed.): *Handbook of Conducting polymers*, New York, 2007.

2 M. Skompska, J. Mieczkowski, R. Holze and J. Heinze, *Journal of Electroanalytical Chemistry*, 2005, **577**, 9-17.

3 Y. Hsiao, W. Whang, C. Chen and Y. Chen, *Journal of Materials Chemistry*, 2008, **18**, 5948-5955.

4 A.R. Hillman, K.S. Ryder, C.J. Zaleski, C. Fullarton and E. L. Smith, *Z. Phys. Chem.* 2012, **226**, 1049-1068.

5 T. Chen, T. Tsai, S. Chen and K. Lin, *Int. J. Electrochem. Sci*. 2011, **6**, 2043-2057.

6 M. Döbbelin, R. Marcilla, C. Pozo-Gonzalo and D. Mecerreyes, *J. Mater. Chem*, 2010,**20**, 7613-7622.

7 C. Zhou, Z. Liu, X. Du and S.P. Ringer, *Synthetic Metals*, 2010, **160**, 1636-1641.

8 A. R. Hillman, S. J. Daisley, S. Bruckenstein, *ElectrochimicaActa*, 2008, **53**, 3763-3771.

9 G. Casalbore-Miceli, M.J. Yang, N. Camaioni, C.M. Mari, Y. Li, H. Sun and M. Ling, *Solid State Ionics*,2000, **131**, 311-321.

10 R. Kiefer, S.Y. Chu, P. A. Kilmartin, G. A. Bowmaker, R. P. Cooney and J. Travas-Sejdic, *ElectrochimicaActa*, 2007, **52**, 2386-2391.

[11] S. Bruckenstein, J. Chen, I. Jureviciute and A. R. Hillman, ,*ElectrochimicaActa*, 2009, **54**, 3516-3525.

[12] S. Bruckenstein, K. Brzezinska, A. R. Hillman, *ElectrochimicaActa*, 2000, **45**, 3801-3811.

[13] A. P. Abbott, D. Boothby, G. Capper, D. L. Davies and R. K. Rasheed, *Journal of the American Chemical Society*, 2004, **126**, 9142-9147.

[14] A. P. Abbott, G. Capper, D. L. Davies, R. K. Rasheed and V. Tambyrajah, *Chemical Communications*, 2003,70-71

[15] C. Laslau, D. E. Williams, B. E. Wright and J. Travas-Sejdic, *Journal of the American Chemical Society*, 2011, **133**, 5748-5751.

[16] D. Carriazo, M. C. Serrano, M. C. Gutierrez, M.L. Ferrer and F. del Monte, *Chemical Society Reviews*, 2012, **41**, 4996-5014

[17] A. P. Abbott, G. Capper and S. Gray, *Physical ChemistryChemical Physics*, 2006, **7**, 803-806.

[18] M. J. Brown, A. R. Hillman, S. J. Martin, R. W. Cernosek and H. L. Bandey, *Journal of Materials Chemistry*, 2000, **10**, 115-126.

[19] A. R. Hillman, *Journal of Solid State Electrochemistry*, 2011, **15**, 1647-1660

[20] H. Randriamahazaka, C. Plesse, D. Teyssié, C. Chevrot, *Electrochemistry Communications*, 2003, **5**, 613-617.

[21] P. Chandrasekhar: *Conducting Polymers, Fundamentals and Applications.A practical Approach*, Kulwer Academic Publishers, Boston, 1999.

[22] A. R. Hillman, S. J. Daisley, S. Bruckenstein, *Electrochemistry Communications*, 2007, **9**, 1316-1322.

[23] A. Bund, S. Neudeck, *Journal of Physical Chemistry B*, 2004, **108**, 17845-17850.

[24] S. Bruckenstein, M. Shay, *ElectrochimicaActa*, 1985, **30**, 1295-1300.

[25] R. A. Marcus, *The Journal of Physical Chemistry*, 1968, Volume **73**, Number 3, 891-899.

[26] M. A. Skopek, M. A. Mohamoud, K. S. Ryder and A. R. Hillman, *Chemical Communications*, 2009,935-937.

[27] C. D'Agostino, R. C. Harris, A. P. Abbott, L. F. Gladden and M. D. Mantle, *Physical ChemistryChemical Physics*, 2011,**13**, 21383-21391.

[28] A. R. Hillman, K. S. Ryder, V. C. Ferreira, C.J. Zaleski, E.Vieil, *Electrochimica Acta*, 2013, **110**, 418-427.

[29] N. Levy, M. D. Levi, D. Aurbach, R. Demadrille and A. Pron, *Journal of Physical Chemistry C*, 2010, **114**, 16823-16831.

[30] A. Lewandowski, A. Olejniczak, M. Galinski, I. Stepniak, *Journal of Power Sources*, 2010, **195**, 5814-5819.

[31] R. Keifer, G. A. Bowmaker, R. P. Cooney, P. A. Kilmartin, J. Travas-Sejdic, *Electrochimica Acta*, 2008, **53**, 2593-2599.

[32] K. S. Ryu, Y. Lee, Y. Hong, Y. J. Park, X. Wu, K. M. Kim, M. G. Kang, N.Park, S. H. Chang, *ElectrochimicaActa*, 2004, **50**, 843-847.

[33] W. Lu, A. G. Fadeev, B. Qi, E. Smela, B, R. Mattes, J. Ding, G. M. Spinks, J. Mazurkiewicz, D. Zhou, G. G. Wallace, D. R. MacFarlane, S. A. Forsyth, M. Forsyth, *Science*, 2002, **297**, 983-987.

[34] H. Randriamahazaka, T. Bonnotte, V. Nöel, P. Martin, J. Ghilane, K. Asaka and J-C Lacroix, *Journal of Physical Chemistry B*, 2011, 11**5**, 205-216.

[35] M. Döbbelin, R. Marcilla, M. Salsamendi, C. Pozo-Gonzalo, P. M. Carrasco, J. A. Pomposo and D. Mecerreyes, *Chemistry Materials*, 2007,**19**, 2147-2149.

[36] L. F. Q. P. Marchesi, F. R. Simões, L. A. Pocrifka and E. C. Pereira, *The Journal of Physical Chemistry B*, 2011, **115**, 9570-9575.

Chapter IV

Application of the combined PBD – EQCM technique to the analysis of PEDOT/DES redox processes

4.1 Introduction

4.1.1 Aims and scope

The aim of the work described in this chapter was to analyze (by a combined optical and gravimetric technique) the ionic fluxes present during the redox cycling of PEDOT modified electrodes in two deep eutectic solvents. Ethaline 200, which is a mixture of one mole choline chloride and two moles of ethylene glycol and Propaline 200 which is a mixture of one mole choline chloride and two moles of propylene glycol. A thorough understanding of ionic fluxes is crucial in terms of the modification of the electrode properties. These parameters in turn are of paramount importance in the final design of any electrochemical device whether it is a battery, an electrochemical actuator or any other appliance.[1,2,3,4,5]

4.1.2 Poly (3, 4 ethylenedioxy) thiophene

The possibility offered by a combination of the electrical conductivity of metals with elasticity of polymers make conducting polymers very attractive material, for a variety of electrochemical applications.[6] The structural feature, which enables CP to act as electronic conductors, is the conjugated π electron system that acts as the charge source/sink.

Complete substitution of the thiophene ring (with ether substitutions at 3 and 4 positions of the ring, respectively) equips PEDOT with unique electrochemical stability and longevity under redox cycling. Additionally, PEDOT films are hydrophobic, their chemical

structure is relatively well defined and their oxidation potential is comparatively low.

Because of this, PEDOT and its analogues have been a subject of exceptionally detailed electrochemical studies.[7,8,9,10,11] Majority of these concentrated on applications of either pure polymer or of polyanionic blends of PEDOT in a variety of electrochemical and chemical applications.[12,13] These applications have already been reviewed in Chapter I.

4.1.3 Classical electrolyte - Acetonitrile with Lithium Perchlorate as a supporting electrolyte.

The mechanistic studies of redox induced doping/dedoping processes in CP films have so far concentrated mostly on molecular solvents. Perhaps the best understood and possibly the most frequently analysed of those 'classical' electrolytes is a solution of Lithium Perchlorate in Acetonitrile.

Extensive work on p and n-doping of PEDOT in $LiClO_4/CH_3CN$ conducted by Hillman et al[1] and Bund et al[14] among others resulted in this system being frequently regarded as a basic standard for other mechanistic studies. Rahindramahazaka et al[15] and Levy et al[16] have also used this system to elucidate (by inference) the mechanisms of doping in ionic solvents.

4.1.4 Ethaline.

Ethaline belongs to a family of solvents classified as Deep Eutectic Solvents (DES). The DES chemistry and (resulting from it) significant depression of the freezing point (as compared to the starting material) have already been discussed in Chapters I and III. In Ethaline 200, the denomination indicates the molar ratio of 1: 2 of the quaternary ammonium salt (QAS) which is choline chloride and the hydrogen bond donor (HBD) here, ethylene glycol. Upon the solvent formation the HBD complexes the anion forming an eqiumolar mix (salt in the IL vernacular) of Ch^+ cations and EG_2Cl^- complex anions.

This complexation pattern is supported by the negative excess molar volume (V^E) calculated for Ethaline by Leron and co-workers.[17] Negative V^E indicates increase in density as compared to the ideal solution. Similar effects were observed for many ionic liquids. Additionally, a recent NMR study by Abbott et al, of molecular self-diffusion in

DES has indicated that the ionic identities in Ethaline are indeed choline cation and ethylene glycol-chloride complex anion.[18] Ethaline has rather low viscosity of 40 cP while IL viscosities are usually reported to be in the 10 – 20000 cP range.

All DES have the capacity to remove metal oxides (through the oxidation of the metal surface). Au oxidation potential in both Ethaline and Propaline occurs at ca. 0.8 V. Therefore, conducting the cyclic voltammetry experiments in the - 0.3 V $\rightarrow$ 1.0 V electrochemical window (applied in the gravimetric experiments) could result in a dissolution of the Au layer, rendering the electrode inoperable. Hence, due to the complex design of the electrodes used for the electrochemical/optical/gravimetric experiments described in this chapter, potential windows were limited to - 0.3 V $\rightarrow$ 0.7 V range. Potential was measured with respect to the Ag/AgCl reference electrode described in Chapter II.

4.1.5 Propaline

Propaline is a further extension of a diol based DES concept. In the formulation of this liquid, use of 1, 2 propylene diol (PG) as a HBD has resulted in a solvent with rather different properties from those of Ethaline. Two fold increase in viscosity (40 cP $\rightarrow$ 80 cP) has been assigned to the higher viscosity of PG comparing to the EG, while the decrease of density (see table 1) is related to the fact that 1, 2 propylene diol is a branched molecule, therefore its application results in a formation of branched complex anion of lower molecular density. By inference from Ethaline, the ionic species in Propaline are assumed to be a mixture of Ch^+ cations and PG_2Cl^- complex anions. Until now, the only two studies of electrochemical ion transfer mechanism in Propaline are by Hillman and co-workers.[1,19,20]

4.1.6 Mechanism and kinetics of PEDOT electrochemical p-doping.

Movement of ions during the redox reactions is achieved by the electroneutrality principle, which requires balancing of charges on both the cathode and the anode. Considering the electroactive film redox behaviour as a surface confined process, the

charge compensation may be conducted in three different ways. Positive charges formed upon oxidation can be compensated by one of the following processes:

influx of anions: $[P^0, C^+, A^-] + \mathbf{A}^- \rightarrow [P^+, C^+, \mathbf{2A}^-]$

outflux of cations: $[P^0, C^+, A^-] \rightarrow [P^+, A^-] + \mathbf{C}^+$

and (or) a mixture of

both processes : $n[P^0, C^+, A^-] \rightarrow n_1[P^+, A^-] + \mathbf{C}^+ + n_2[P^+, C^+, \mathbf{2A}^-]$

where $n = n_1 + n_2$ and n represents total dopants number, P represents the host electroactive film, A represents the anion and C represents the cation.

The redox switching of the conducting polymer films has been previously described using a 'moving front' concept. The CP film can be envisaged as an interpenetrating network of polymer chains and voids. Such structural arrangement has been previously proposed by Skompska,[21] Hillman[22] and Rahrindramahazaka[10, 23] to be composed of open and compact zones. The open zone (facing the film/electrolyte interface) is thought to be composed of short polymer chains with a low degree of conjugation. The compact zone comprises long, highly conjugated polymer chains forming more rigid polymer structure. This spatial arrangement result in a significant difference in solvation levels between open zone (high level) and the compact zone (low level). As the electrolyte is incorporated into the polymer film, during the redox processes ions present in the electrolyte become dopants. The CP film selection of the dopant is not related to its availability in the bathing solution but instead it depends on the interaction between ions and the charged sites within the polymer film.

Since electrodeposited CP films are disordered at the molecular scale and homogeneous at the macroscopic scale, this leads to the conclusion that depending on their internal structure, dynamic processes within the film will have a different duration and time scales. Additionally, the potentiostatically deposited films used here were reported to have less homogeneous structure (i.e. more prominent 'zones effect') than potentiodynamically deposited films. [24]

The rate of charge transport is primarily dependant on the flux of electrons, ions and solvent molecules (if present). However, it is also dependent on the rate of conductive zones formation inside the polymer film.[25] Additionally, the response of the polymer film to changes in solvation associated with redox cycling is accompanied by structural as well as conformational changes, with the latter resulting in polymer film volume changes. The correlation between CP film expansion during net ion ingress and contraction during net ion egress has been confirmed by a recent SICM (Scanning Ion Conductance Microscopy) study[26] as well as work of Kim and co-workers[27] who conducted the electrochemical Atomic Force Microscopy (EC-AFM) study of PPy films.

Many researchers agree that the electric field driven motion of ions is the most accurate description of ion transport during the redox switching of conducting polymers. Monte Carlo simulations also supported these findings.[28] ESCR (electrochemically stimulated conformational relaxation) is a model proposed by Otero and co-workers.[29] According to this model, kinetics of a redox switching depend on two processes. First is the electrochemically induced electronic and ionic transport while the second is the change of polymer conformation (colloquially termed as 'relaxation'). This leads to the conclusion that the actual charge/discharge process is retarded by the relaxation rate of the polymer film. This rate in turn is profoundly influenced by the electrolyte properties. Another factor (which importance in the solvation process was stressed out by Hillman and co-workers in their study of PHT films[17]) is the effect of non-idealites (repulsive or attractive interactions between the polymer redox sites and the electrolyte). The validity of the ESRC model has been confirmed through polypyrrole[30] and polyaniline studies.[31]

In many of the practical applications, CP modified electrodes spend a dominant portion of their lifetime in an intermediate (i. e. neither fully oxidised nor fully reduced) state.[1] Rechargeable charge storage devices are a particularly good example here. Thus, understanding of the doping/charge relationship is critical in the future designs of the secondary charge storage devices.

4.1.7 Probe Beam Deflection – Electrochemical Quartz Crystal Microbalance.

Classic electrochemical techniques concentrated on the measurements of the electron flux at the electrode/electrolyte interface. PBD collects the concentrations profiles

in the electrode vicinity while EQCM provides the information about the local population changes. Therefore, the combination of these two techniques through conductance of simultaneous gravimetric and optical data provides a unique insight into the electrochemical processes. Optical and acoustic techniques complement each other. PBD is not sensitive to the solvent transfer, which is a significant hindrance in elucidation of mobile species transfers using EQCM alone.[32] As the refractive index gradient is related to the type of the specie and not only its mass, PBD is able to detect fluxes of protons and hydronium ions as well as gases. This technique is also particularly well suited to the analysis of the gaseous fluxes because gas phase refractive index is of opposite sign to the liquid phase refractive index, thus, the presence of gas phase within a liquid phase results in a prominent deflection signal. Such observations usually lie beyond the quartz crystal resonator analytical capacity. Additionally, optical deflection is not affected by a viscoelastic phenomena so often present in microgravimetry. Thus, gravimetric, optical, and electric signals provide complimentary set of quantitative data.[1]

Temporal convolution of the PBD-EQCM data allows for the quantitative analysis of the separate species concentration gradients. This enables 'assumption free' analysis of the entire spectra of mobile species population fluxes. Henderson et al. have previously reported the quantitative evaluation of the three measurements (θ, i and Δm) for a conductive polymer films.[33] This chapter contains the description of this technique extension into the PEDOT/DES environment.

4.2 Objectives

The overarching goal of this chapter was the optical analysis of the redox-induced ion exchange of PEDOT in two Deep Eutectic Solvents (DES), Ethaline and Propaline.

This main objective induced a pre-requisite objective; here termed an objective one, which was the optical analysis of ionic fluxes during redox cycling of PEDOT films in $LiClO_4/CH_3CN$. This was conducted in order to create a standard analytical model used for comparisons with DES as these solvents (or any other IL's) have hitherto not been subjects of any kind of the optical analysis. Molecular solvent selection was based on the extensive literature available on this particular system [1,10,14,16,20] and former analysis (see Chapter III)

of the doping/undoping mechanism of PEDOT films in this electrolyte.

Fulfilment of the first objective was a leading step towards the second objective, which was the optical analysis of the fluxes during redox cycling of PEDOT films in Ethaline and Propaline.

Diffusion induced time delay is known to be an important factor in a beam deflection analysis. Since diffusion can be generalized as being inversely proportional to viscosity and DES have viscosity orders of magnitude higher[34] than most of the molecular solvents, the third objective was the estimation of the viscosity effect on the feasibility of optical analysis in DES.

Fourth objective was the determination of possible optical signal dependence on sweep rate. This was conducted to confirm the previously noted (Chapter III) partial diffusion control in PEDOT/DES electroacitve systems.

Process of electrodeposition is one of the most important factors determining performance and longevity of the CP modified electrodes. Thence, fifth and final objective of this chapter was the investigation of the PEDOT films electrodeposition using combined PBD-EQCM approach.

4.3 Results and discussion

4.3.1 Overview of the population changes and fluxes of PEDOT films redox cycled in $LiClO_4/CH_3CN$.

It is a widely accepted fact that during the oxidation part of PEDOT films redox cycling in this electrolyte, electroneutrality is maintained by a perchlorate anion.[1,9] This study is therefore used a methodology test to form a 'baseline' for optical studies in ionic liquids.

4.3.1.1 Cyclic deflectometry of PEDOT in $LiClO_4/CH_3CN$.

Representative profiles of the current, gravimetric and optical deflection responses of PEDOT films exposed to 0.1 M $LiClO_4/CH_3CN$ solution recorded at variable sweep rates ($2 \rightarrow 200$ mV s^{-1}) are presented in figures 1 and 2.

The purpose of the PBD experiment is to monitor the electrode's surface processes. Thus, the deflection signal is expected to trace the electrode current as Fick's law relates these two processes (current and concentration gradient) to each other.[35] A close resemblance of the optical and electric signals is therefore considered a diagnostic indicator of a successful PBD experiment.

On the qualitative level, data presented confirm the results of CH_3CN/PEDOT study described in Chapter III – see figure 1. The massogram (see figure 2 – left panel) indicates the film mass increase. This is in a good agreement with the previous work[1], also indicating mass increase as a consequence of PEDOT films oxidation in these media. Mass increase is accompanied by a negative deflection of the laser beam (i.e. away from the electrode) visible in the right panel of the figure 1. This negative deflection is a result of ClO_4^- concentration decrease in the electrode vicinity. The perchlorate concentration decrease is a direct result of the anion ingress into the polymer film.

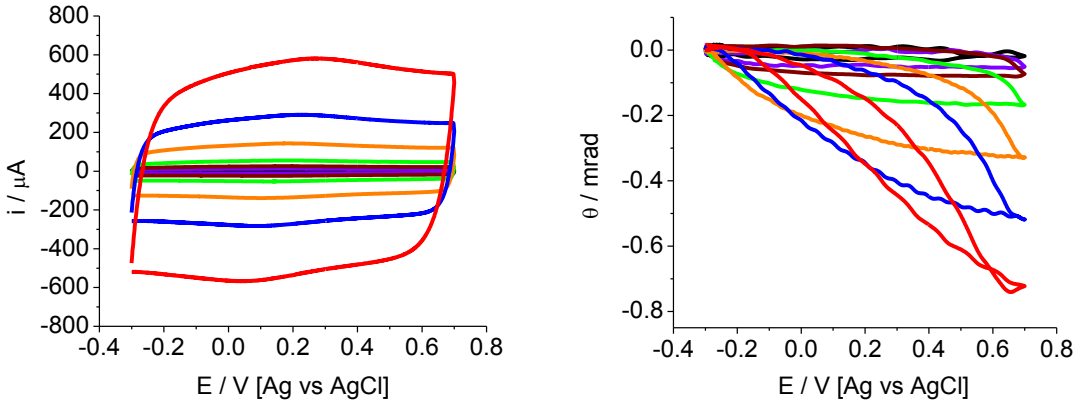

Figure 1. Left panel: voltammograms of a 0.8 µm [+/- 0.1 µm] PEDOT film (Q_{dep} = 75.2 mC cm^{-2}) redox cycled from - 0.3 V → 0.7 V → - 0.3 V in 0.1 M $LiClO_4/CH_3CN$. Black line 2 mV s^{-1}, violet 5 mV s^{-1}, wine 10 mV s^{-1}, green 20 mV s^{-1}, orange 50 mV s^{-1}, blue 100 mV s^{-1}, red 200 mV s^{-1} respectively. Right panel: experimental optical deflection profiles, colours as above.

Since the optical deflection is originating from changes in concentration, one would expect its magnitude to scale linearly with the current magnitude. However, the comparison of the figures in the left and right panel of figure 1 indicates that this is not the case, although the regular pattern of change in θ at different υ is clearly visible. At slow sweep

rates (2 → 10 mV s^{-1}), the θ signal is diminished. This is expected since it originates from low current values. Poor signal-to-noise ratio is evident, as the noise level remains constant throughout while the flux (hence the magnitude of θ) at low ν is small.

At intermediate sweep rate (20 mV s^{-1}) the deflection signal follows the current rather closely. This correlation then deteriorates at faster sweep rates (50 → 200 mV s^{-1}). This forms the evidence that at 20 mV s^{-1} the flux detected as the beam deflection in the focal point can be treated as a reliable representation of the electrode processes (i.e. the temporal delay between the surface processes and the observed optical deflection is not significant).

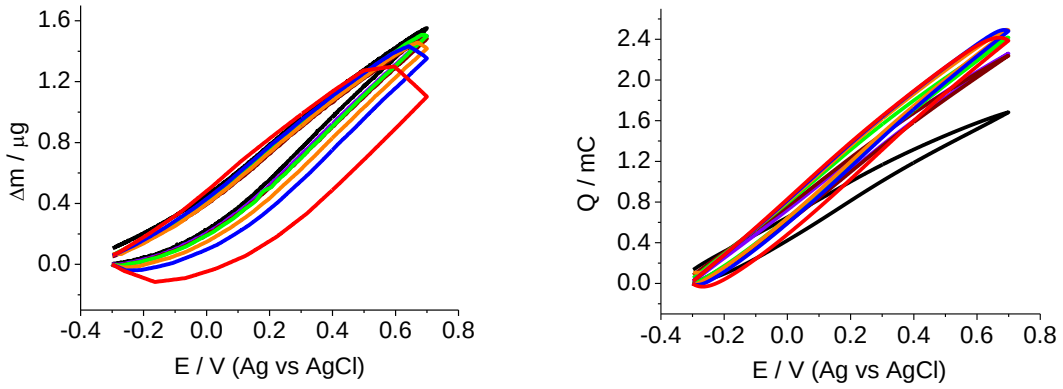

Figure 2. Left panel: massograms of a 0.8 μm [+/- 0.1 μm] PEDOT film (Q_{dep} = 75.2 mC cm^{-2}) redox cycled from - 0.3 V → 0.7 V → - 0.3 V in 0.1 M $LiClO_4/CH_3CN$. Black line 2 mV s^{-1}, violet 5 mV s^{-1}, wine 10 mV s^{-1}, green 20 mV s^{-1}, orange 50 mV s^{-1}, blue 100 mV s^{-1}, red 200 mV s^{-1} respectively. Right panel: Q_{pas} upon redox cycling, colours as above.

At lower ν the signal to noise ratio deteriorates and at higher ν the diffusional barrier delays the θ signal until it becomes a less accurate description of the electrode current (due to the electrode processes occurring on a much shorter timescale than changes in the concentration gradient). A similar effect has been previously reported for poly (*o*-toluidine) films redox cycled in an aqueous solution of $HClO_4$.[27] Analysis of the gravimetric and optical signals, whether as a function of ν or Q indicated significant hysteresis. In the context of these experiments hysteresis is defined as a divergence of the experimental signal from a straight line. Figure 3 shows the magnitude of the signal and hysteresis

present in the gravimetric signal as a function of ν and √ν.

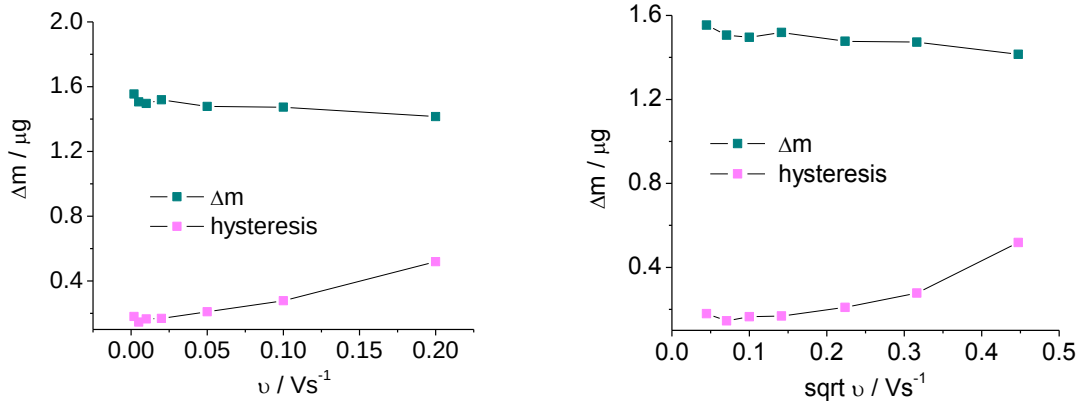

Figure 3. Left panel: magnitude (grey line) and hysteresis (blue line) in Δm as a function of ν. Right panel: magnitude (grey line) and hysteresis (blue line) in Δm as a function of √ν.

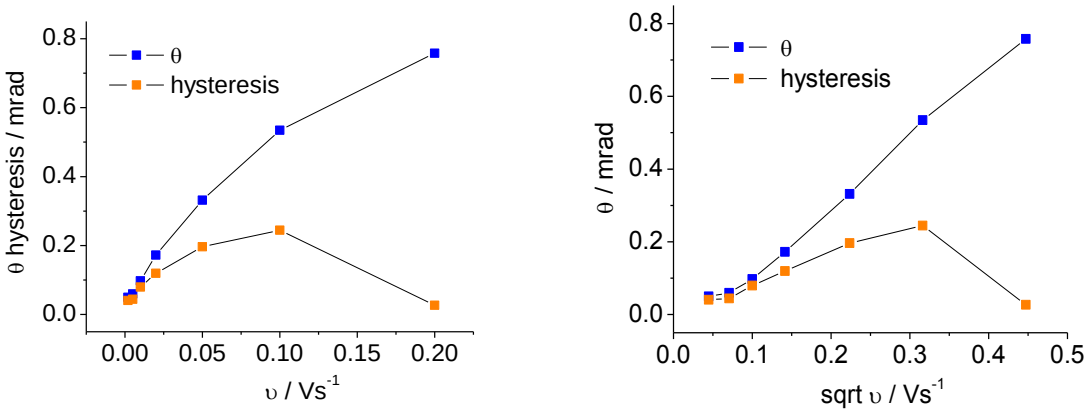

Figure 4. Left panel: magnitude (grey line) and hysteresis (red line) in θ as a function of ν. Right panel: magnitude (grey line) and hysteresis (red line) in θ as a function of √ν.

Relatively stable maximum mass signal (see right panel of the figure 3) indicates that the redox conversion of PEDOT films is close to complete in this shortened potential window (as opposed to the results for elongated potential window analysed in Chapter III). The almost linear relationship between the magnitude of the optical deflection signal (see figure 4) and ν as well as √ν indicates that optical deflection is very responsive to the sweep rate but the presence of variable level of hysteresis is probably an outcome of the diffusion

barrier. Presence of hysteresis in the Δm/Q signal (see below – figure 5) suggests that the number of species transformed must be more than one (i. e. anion and at least one solvent molecule with possible small cation counter flux present). Its presence in the Δm/Q plots confirms the predominant diffusion control present in these systems. This result confirms the heterogenic nature of the flux present with perchlorate anions and acetonitrile molecules forming the majority of the moving species.

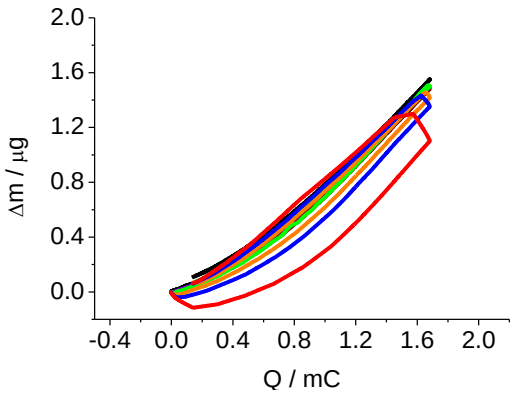

Figure 5. Δm/Q plot of a 0.8 μm [+/- 0.1 μm] PEDOT film (Q_{dep} = 75.2 mC cm^{-2}) redox cycled from - 0.3 V → 0.7 V → - 0.3 V in 0.1 M $LiClO_4/CH_3CN$. Black line 2 mV s^{-1}, violet 5 mV s^{-1}, wine 10 mV s^{-1}, green 20 mV s^{-1}, orange 50 mV s^{-1}, blue 100 mV s^{-1}, red 200 mV s^{-1} respectively.

Influence of the beam electrode distance on the quality of the optical signal.

Failure of the optical deflection signal to return to its original values has previously been attributed to an excessive electrode-beam distance.[27,36] Figure 6 shows the deterioration of the optical signal at the increase of distance. It can be noted in the figure 6 that the deflectogram resembles current signal most closely at a distance of 51.8 μm (close match of the red and blue lines in figure 6). If the beam is positioned closer, the reflection of the light affects the signal intensity (see Figure 6 black line; note the elevated baseline of this signal). At larger distances, the diffusion barrier effects become prominent (see smaller magnitude of 61.6 μm and 71.9 μm signals). It has to be noted that both anodic and cathodic fluxes analysed in this study are of heterogeneous nature.

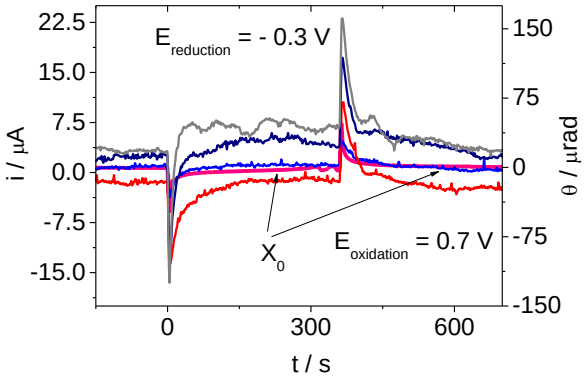

Figure 6. Comparison of the electrode's current and the experimental optical signal (expressed as a function of the relative electrode-beam distance). Data obtained from the chronoammperogram and chronodeflectogram of a 0.8 µm [+/- 0.1 µm] PEDOT film (Q_{dep} = 55.1 mC cm^{-2}). Potential has been stepped from 0.7 V → - 0.3 V in 0.1 M $LiClO_4/CH_3CN$. Duration of each step = 120 s. Red line represents electrode's current. Blue, green, orange and gray lines represent optical deflection signal recorded at 41.8 µm, 51.8 µm, 61.6 µm and 71.9 µm respectively. x_0 denotes the deflectogram recorded at 51.8 µm.

In the case of mixed direction fluxes (i.e opposing fluxes of co and counter ions) the total deflection (abbreviated as f_{pbd}) recorded becomes:

$$f_{pbd} = \frac{\theta^-}{\theta^- + \theta^+} \quad \textbf{[1]}$$

Where θ^- and θ^+ are the deflections originating from fluxes towards (negative sign) and outwards (positive sign) the electrode.

Convolution analysis - methodology.

The general purpose of the convolution process is to remove the temporal delay, which exist between the electrode's surface and the point of focus. The magnitude of this temporal delay depends on the diffusion coefficient of targeted species. Projection of current and mass signals from the PEDOT modified electrode surface into it's environment

requires fulfilment of two assumptions. Firstly, the PEDOT film has to act as an ideal transducer between the electrical input and the ionic output. Secondly, the species propagation delay has to be negligible.

Based on these assumptions, the measured current $\mathbf{i_{(t)}}$ can be treated as being proportional to the total flux of charged species and is described by the equation:

$$i_{(t)} = FA\Sigma(z_k J_k)_{(0,t)} \quad \textbf{[2]}$$

where k = Li^+ or ClO_4^- and $J_{(0,t)}$ represents the species flux at the film electrode interface (where the distance is zero).

The convolution analysis is based on the extrapolation of the flux measurements from the electrode surface (where distance is 0) into a focal point (where the distance is x – this is the distance between the electrode and the laser beam). This is where the optical deflection measurements are collected. The convolution analysis is based on the following equation:

$$J_{Li^+ClO_4^-(x,t)} = F_{(x,t)} \times J_{Li^+ClO_4^-(0,t)} \quad \textbf{[3]}$$

Where $F_{(x,t)}$ is the convolution factor. This factor is based on the assumption of a mass transfer being a semi-infinite diffusion in the dimension perpendicular to the electrode surface. Then, application of Fick's 1st law allows for relating the flux of species to the concentration gradient:

$$J_{(x,t)} = -D\left(\frac{\delta c_{(x\,t)}}{\delta x}\right) \quad \textbf{[4]}$$

Combination of equations **[3]** and **[4]** yields the convolution factor as a function of diffusion :

$$F_{(x,t)} = \left(\frac{x}{2\sqrt{\pi D t^3}}\right) e^{\frac{-x^2}{4Dt}} \quad \textbf{[5]}$$

Where D is the diffusion coefficient of the transferred species and x is the

propagation distance. By inference from the equation 2 the relationship between the optical deflection and concentration gradient becomes:

$$\theta = -\frac{l}{n}\frac{\delta n}{\delta c}\frac{1}{D}J_{(x,t)} \quad \textbf{[6]}$$

Which expressed as a function of the electrode current develops into the equation 7. This equation subsequently directly relates the species flux with optical deflection:

$$\theta_{(x,t)} = -\frac{h_k L}{z_k F A}F_{(x,t)} \times i_{(x,t)} \quad \textbf{[7]}$$

Where $h_k = ((1/n) \times (\delta n/\delta c) \times (1/D))$ and it is a constant for a given electrolyte. This is because the value of l (electrode width and therefore laser interaction path) and n (electrolyte refractive index) remain constant throughout the process. The same applies to δn/δc value (describing the refractive index/concentration ratio) and the species diffusion coefficient. Hence, the whole equation can be expresses as one constant value. This approach eliminates the need for measurement of δn/δc (which would otherwise had to be conducted prior to the experiment).

Convolution analysis – application in PEDOT/$LiClO_4$ system.

Representative profiles of the current, optical deflection (left panel) and gravimetric (right panel) responses of PEDOT film exposed to 0.1 M $LiClO_4/CH_3CN$ solution recorded at sweep rate of 20 mV s^{-1} are presented in figure 7.

The qualitative data for the experiments conducted in $LiClO_4/CH_3CN$ solution are entirely consistent with the widely recognized fact that PEDOT oxidation in this medium is dominated by perchlorate anion ingress/egress as well as solvent egress. The convolution analysis (assuming k = ClO_4^-) was applied to the recorded electric, gravimetric and optical signals.

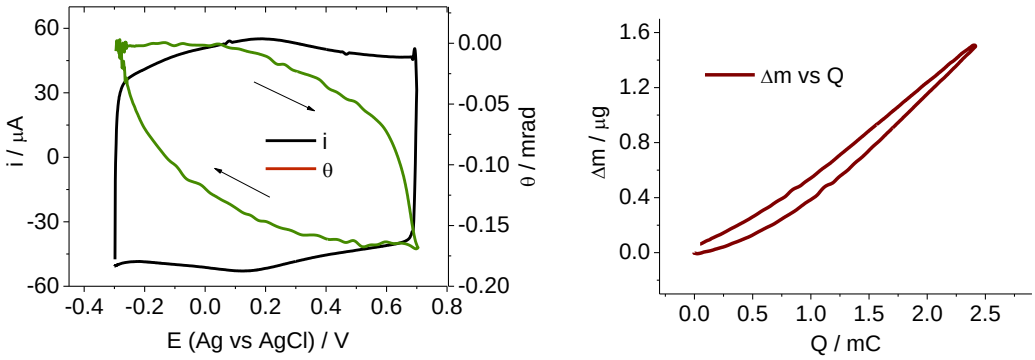

Figure 7. Left panel: cyclic voltammogram (black line) and cyclic deflectogram of a 0.8 µm [+/- 0.1 µm] PEDOT film (Q_{dep} = 75.2 mC cm^{-2}) redox cycled from - 0.3 V → 0.7 V → - 0.3 V in 0.1 M $LiClO_4/CH_3CN$. ν = 20 mV s^{-1}. The experimental optical signal has been recorded at 51.8 µm. Right panel: corresponding mass change (Δm) versus charge (Q) plot. Gradient of the graph allows estimating the exchanged molar mass $\left(F\frac{dm}{dQ}\right)$ at circa 50 g mol^{-1}.

Proceeding now to the qualitative analysis, left panel of the figure 8 contains the electrode recorded current plotted together with convolved current and mass which represents mass and electron fluxes present in the focal point (here = 51.8 µm from the electrode surface). It has been previously reported by Randriamahazaka et al that PEDOT cycling in CH_3CN is accompanied by a significant change in solvation state of the polymer film.[10] Application of the EQCM-PBD allows for further exploration of this EQCM based theory with its confirmation visible as a significant solvent flux (Figure 8; right panel). The overall result of PEDOT/CH_3CN cyclic deflectometry can be summarized as a confirmation of the mixed species transfer. The flux heterogeneity is evident from the data in figure 8 (left panel). Firstly, the convolved current does not superimpose onto the optical signal during the oxidation stage. This suggests at least minor Li^+ co-transfer in this potential region. During reduction stage, the convolved current superimposes the optical signal almost completely. This suggests exclusive perchlorate ion transfer as history effects (i.e. permanent conformational changes in the structure of the polymer film induced by dopants and solvents used prior to the experiment) were excluded from these experiments through the careful choice of the experimental conditions. Secondly, the convolved mass flux does

not superimpose the optical signal except for the high potential range (0.4 V → 0.7 V). This suggests significant solvent co-transfer.

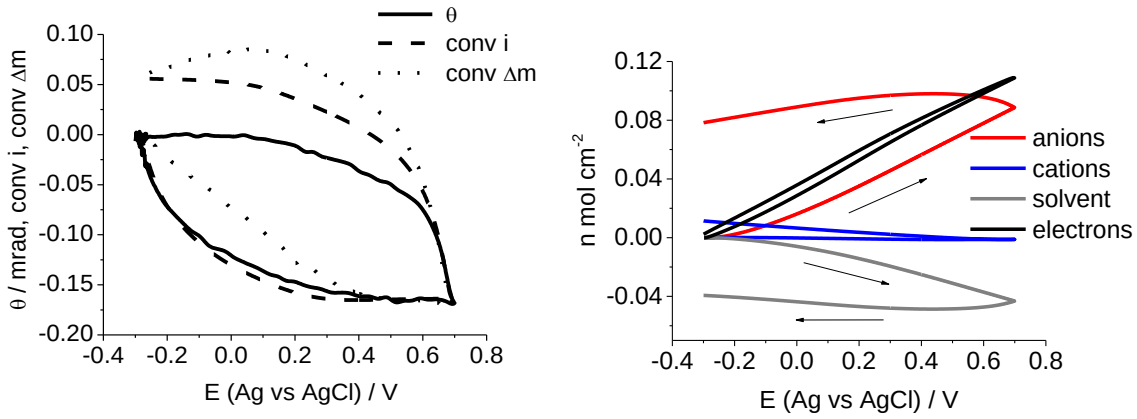

Figure 8. Left panel: solid line - experimental beam deflection (θ), dashed line - convolved current ($i_{(x,t)}hL/zFA$) and dotted line - convolved mass variation ($(dM_{(x,t)}/dt)zFAhl/m_{ClO4^-}$. Right panel: Comparison of the convolved signal integrals. Data derived from the same experiment as shown in figure 7.

The graphic representation of mobile species concentration changes is presented in figure 9.

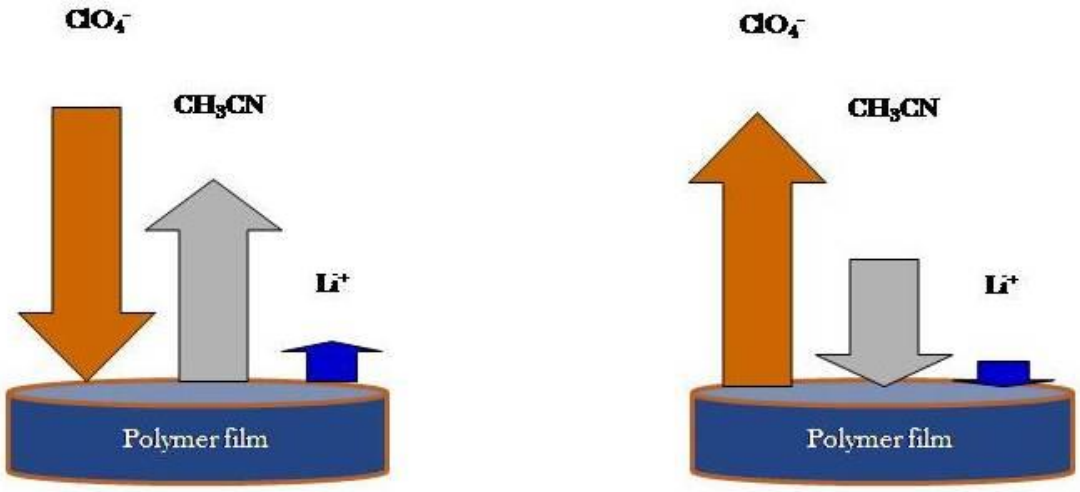

Figure 9. Cartoon representation of species flux during the potentiodynamic cycle of PEDOT in $LiClO_4/CH_3CN$. Left panel: oxidation, right panel: reduction.

Time scale effects of PEDOT in $LiClO_4/CH_3CN$.

Practical CP based devices (such as a secondary battery) might encounter variable charge/discharge rates during use. Therefore, the question arises of how these conditions would affect the mobile species fluxes (and thus the device performance).

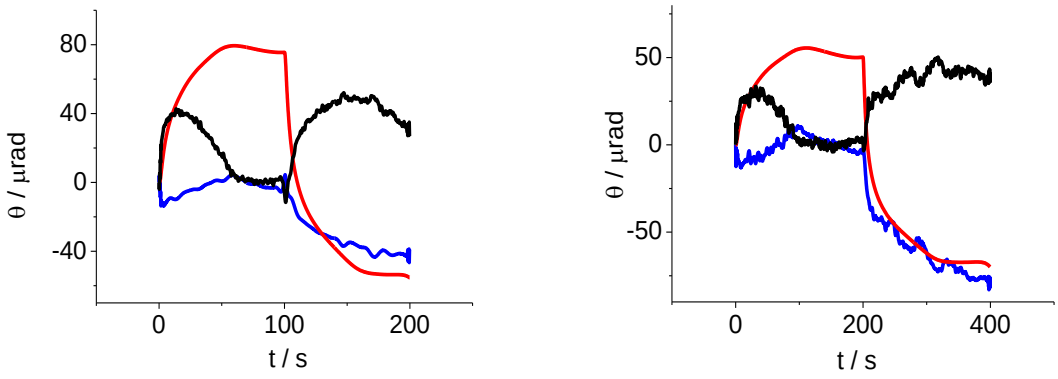

Figure 10. Left panel: Comparison of the anion (red line), cation (blue line) and solvent (black line) contributions as a function of time. Optical signal recorded at a distance of 51.8 µm. υ = 5 mV s^{-1} Right panel: as above at υ = 10 mV s^{-1}. Data derived from the same experiment as shown in figure 1.

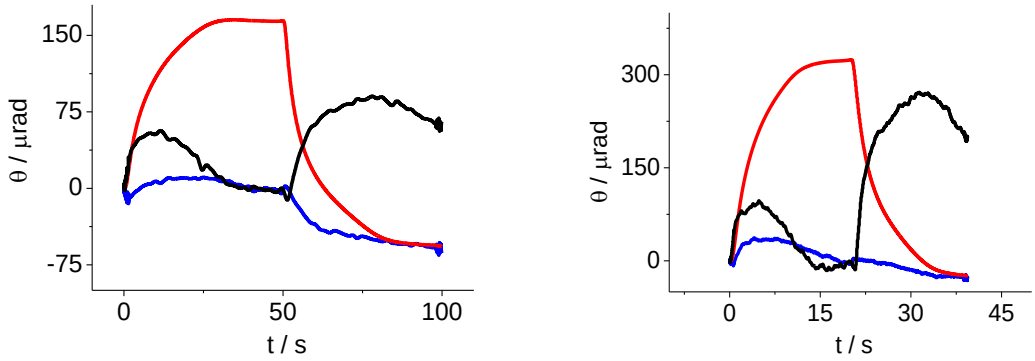

Figure 11. Left panel: Comparison of the anion (red line), cation (blue line) and solvent (black line) contributions as a function of time. Optical signal recorded at a distance of 51.8 µm. υ = 20 mV s^{-1} Right panel: as above at υ = 50 mV s^{-1}. Data derived from the same experiment as shown in figure 1.

The question of relative magnitudes of the Li^+, ClO_4^- and CH_3CN transfers was answered by a variation of the experimental time scale. The resolved contributions are visible in figures 10 – 12. Henderson et al have previously reported an increase of perchlorate flux at fast sweep rates in a similar system (poly(*o*-toluidine) in 1 M $HClO_4$ aq electrolyte)[27], here this effect is also clearly visible.

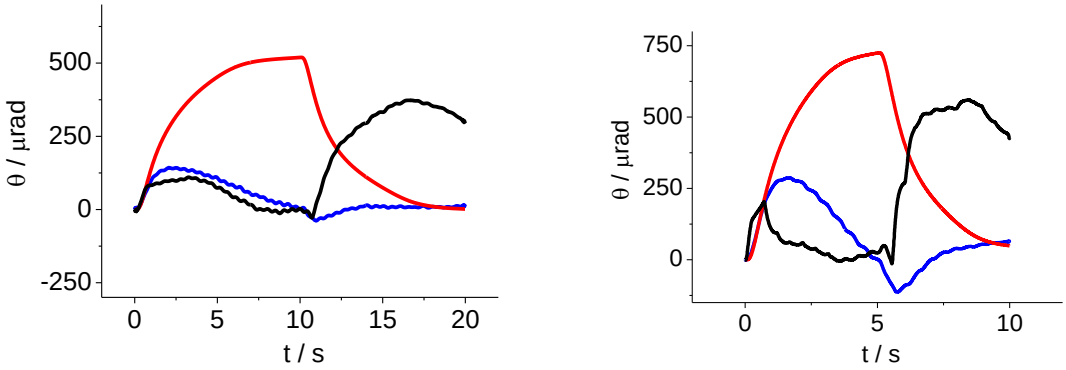

Figure 12. Left panel: Comparison of the anion (red line), cation (blue line) and solvent (black line) contributions as a function of time. Optical signal recorded at a distance of 51.8 μm. υ = 100 mV s^{-1} Right panel: as above at υ = 200 mV s^{-1}. Data derived from the same experiment as shown in figure 1.

In all of the cases, solvent movement is of a larger magnitude (see figures 10 – 12) than cations movement. It also appears to be more closely associated with anions flux than with cations. While the magnitudes of both solvent and perchlorate ion fluxes increase with rising sweep rate the relative magnitudes change in favour of the perchlorate anion. This observation is consistent with the proposed relaxation-dependent variable volume constraints.

Henderson et al. [27] and Bruckenstein et al [37]previously postulated kinetic separation of the mobile species. Similar effects are observed here, with the dominant perchlorate ion flux and relatively diminishing cation and solvent fluxes. Although the timescale where the exclusive anion transfer would be observed has not been reached, it appears to be a reasonable limiting scenario. Thus, at the fastest practically applicable sweep rate the process would be limited only by the film permselectivity to ClO_4^-.

4.3.1.2 Potential step experiments of PEDOT in $LiClO_4/CH_3CN$.

The optical deflection analysis of a continuous processes (like chronoamperometry or chronocoluometry) was previously described to be less complicated than that of the discontinuous processes (like cyclic voltammetry).[38] The chronocoulogram for the reduction and oxidation of the PEDOT film in acetonitrile based medium is shown in figure 13. The polymer film was initially reduced at - 0.3 V, then oxidised at 0.7 V and finally neutralized again at - 0.3 V. The duration of each potential step was set up in order to compensate for impaired diffusion in even the most viscous DES tested which was Propaline. Temporally extended steps allowed for the species to travel the distance from the electrode's surface to the optical deflection zone. The difference in conducting polymer film/electrolyte systems responses to potentiodynamic and potentiostatic experiments has been previously reported by Rahrindramahazaka and co-workers.[10,19] This group had described the 'open' and 'compact' film zones behaving as two RC-circuits (resistor-capacitor) with two different time constants. Such an assumption treats the PEDOT film as composed of two zones with different thermodynamic and kinetic characteristics. A rapid application of a relatively large (1.0 V) potential step may, therefore, significantly change the polymer structure as well as its morphology.

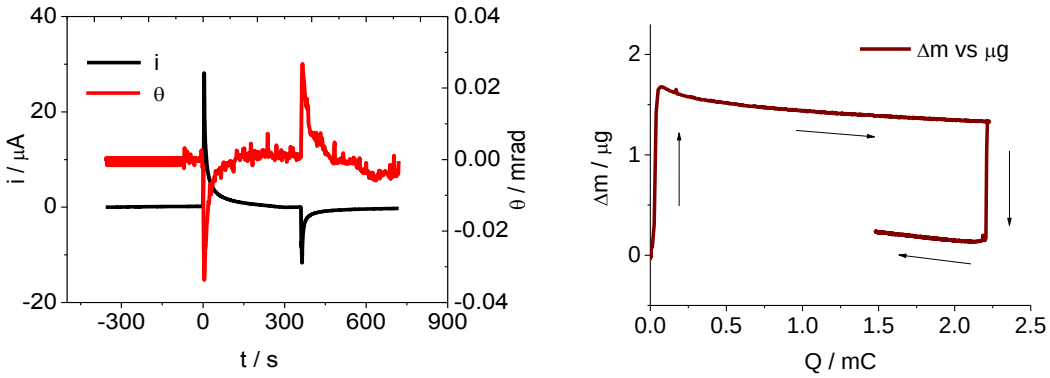

Figure 13. Left panel: chronoammperogram (black line) and chronodeflectogram (red line) of a 0.8 μm [+/- 0.1 μm] PEDOT film (Q_{dep} = 55.1 mC cm^{-2}) potential stepped from - 0.3 V → 0.7 V → - 0.3 V in 0.1 M $LiClO_4/CH_3CN$. Duration of each step = 360 s. Right panel: corresponding mass change (Δm) versus charge (Q) plot.

On a more specific level, such changes may lead to a change in a film solvation properties and even more importantly to alteration of the 'open' and 'compact' zones proportions which would directly influence the polymer film permselectivity and indirectly, its charge storage properties. It can be noted in figure 13 that PEDOT film oxidation in acetonitrile solution is accompanied by a negative optical deflection (see left panel) and a mass decrease (see right panel). This is the reverse of the gravimetric signal recorded during the CV of this system, here assigned to be a result of Li^+ expulsion. This certainly rather unusual observation has been assigned to the polymer film structural changes induced by a large amplitude potential step. Such structure change would result in a fraction of the previously inactive 'compact' zone become more accessible (through the disentanglement of the 'frozen' conformations), and release of the lithium cations trapped there during the deposition process. This process explains the mass decrease upon film oxidation shown in the figure 13 (left panel). This hypothesis is supported by the fact that the recorded current (*i*) and thus charge passed (Q_{pas}) in the potential step experiment are significantly higher than for a comparable PEDOT film during potentiodynamic experiment.

Vorotyntsev et al. have reported that an abrupt change in the electrode polarization may significantly affect the optical signal origins.[39] This occurs due to the voltage-induced redistribution of background ions. Since PBD detects refractive index difference between the bulk of the electrolyte and the focal point, significant re-arrangement of the bulk species may lead to incorrect conclusions about the direction of ions transfer. Here, this effect is proposed as an explanation of the observed (see figure 14, left panel) beam deflection away from the electrode which in a potentiostatic experiment indicates loss of Li^+ and not a gain of ClO_4^- as in potentiodynamic experiments.

Loss of the optical signal beyond the minimum approach distance (x_0) has been observed in all of the experiments (regardless of the electrolyte and technique used). Therefore, values of x_0 which were very similar, to cyclic deflectometry derived values of x_0 were considered optimal. Mobile species identity is explored in more detail in the figure 15 (below).

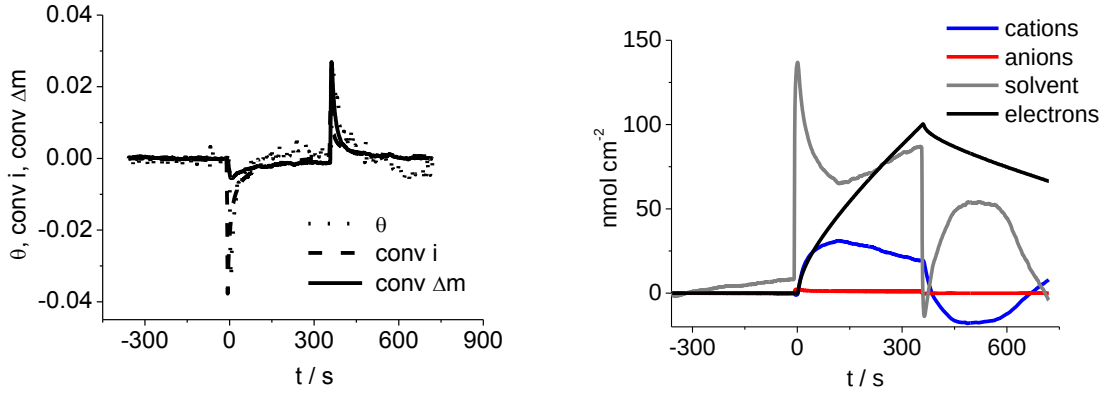

Figure 14. Left panel: experimental beam deflection (θ), convolved current ($i_{(x,t)}$hL/zFA) and convolved mass variation (($dM_{(x,t)}$/dt)zFAhl/m_{ClO4}^-. Right panel: comparison of the convolved signal integrals.

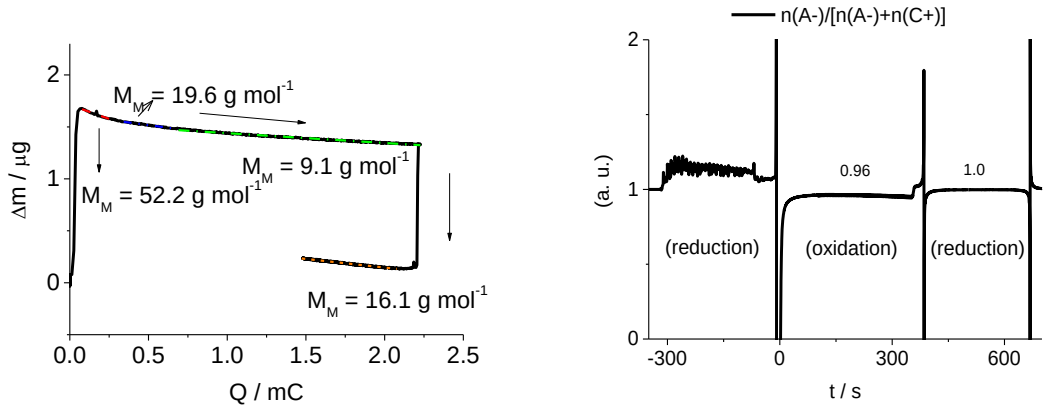

Figure 15. Left panel: Molar masses of the mobile species present during the potential step experiments of a 0.8 μm [+/- 0.1 μm] PEDOT film (Q_{dep} = 55.1 mC cm^{-2}) potential stepped from - 0.3 V → 0.7 V → - 0.3 V in Ethaline 200, each step duration = 360s. Right panel: respective transport numbers.

On the commencement of the oxidation phase, mobile species mass (henceforth abbreviated as MS_M) 52.2 g mol^{-1} was recorded. This is significantly larger than the cation mass (2 g mol^{-1}) and therefore probably originates from the simultaneous entry of solvent. In the high charge region, the MS_M decreases to 19.6 g mol^{-1}. This is a possible evidence of the concurrent anion flux. Reduction phase starts with a rapid loss of mass. This is followed (in the reduction later phase) of the decrease to 16.1 g mol^{-1} indicating rather significant solvent transfer. The transport numbers (figure 15; left panel) further supports this data. The

oxidation phase overall transport number for the cation is 0.96 (hence 0.04 for the anion) and for the reduction phase 1 (0 for the anion). This is in good agreement with the quantitative data (figure 14; right panel) where both the oxidation and reduction phases are dominated by the cation flux.

$x/\sqrt{D}$ plots were derived from convolution of identical electro/optical transients. Each transient was conducted at different *x* distance thus providing data set for the plot. The obtained linearity was then extrapolated to obtain the real electrode-beam distance.

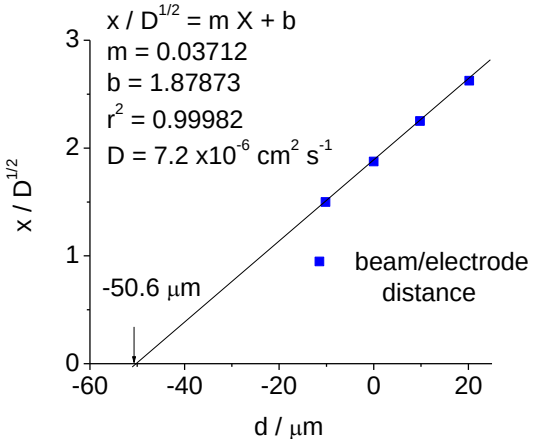

Figure 16. Plot of the convolution parameter ($x/\sqrt{D}$) expressed as a function of the relative beam/electrode distance. Arrow indicates the extrapolation of the linearity which reveals real beam electrode distance (here 50.6 μm).

Figure 16 shows the values of the convolution factor $x\sqrt{D}$ calculated for the different electrode/beam distances. Linear regression equation derived from this plot and used to estimate the diffusion coefficient of mobile species in this system is shown in the upper left corner of the figure 16.

The overall result of the PEDOT/CH_3CN potential step deflectometry is cation flux dominance in the electro neutrality maintenance. The graphic representation of mobile species concentration changes is presented in figure 17.

A net motion of ions *away* from the electrode accompanies the oxidation step. Considering the sign of the gravimetric signal this must be Li^+ expulsion. A net motion of ions *towards* the electrode, which, again considering the gravimetric and electric signals are proposed to be lithium cations, accompanies the reduction step.

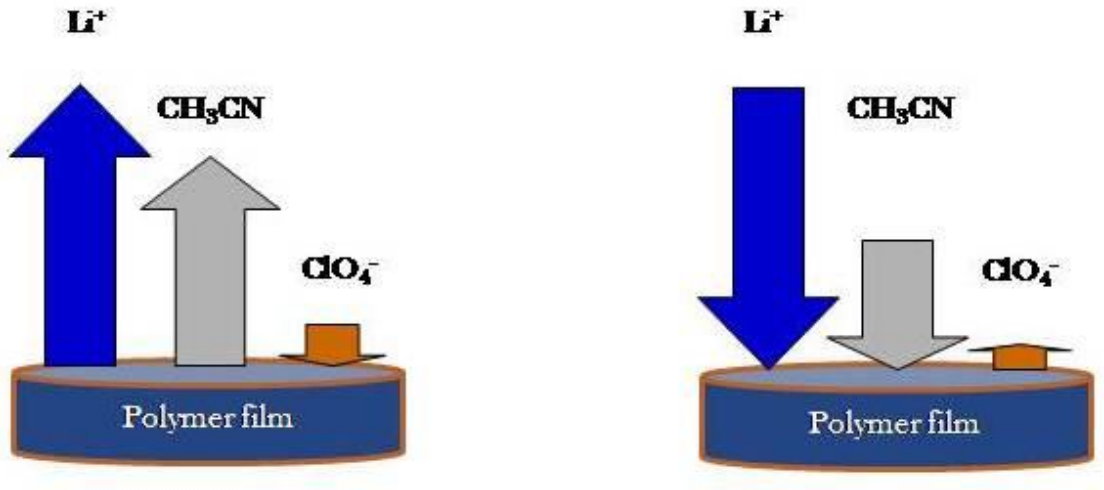

Figure 17. Cartoon representation of species flux during the potentiostatic cycle of PEDOT in $LiClO_4/CH_3CN$. Left panel: oxidation, right panel: reduction.

4.3.2 Overview of the population changes and fluxes of PEDOT films redox cycled in Ethaline 200.

Ethaline is the less viscous of the two DES tested. Skopek[40] as well as Hillman and co-workers[1] have previously conducted a detailed study of the PEDOT/Ethaline gravimetric signal upon redox cycling. Study described in the following sub-chapter is an optical – gravimetric extension of the previous work.

4.3.2.1 Cyclic deflectometry of PEDOT in Ethaline 200.

Completely different solvation properties and radical increase in viscosity (fifty fold in the case of CH_3CN/Ethaline transition and hundred fold in the case of CH_3CN/Propaline transition) have a profound effect on the electrochemical performance of PEDOT films immersed in DES. The only available work that attempts to describe the possible difficulties of conducting optical experiments in concentrated solutions is a theoretical study by Voronytsev et al.[39] This research did not concern ionic liquids, however it did describe the situation of a large excess of supporting electrolyte being present (as opposed

to a case of diluted binary electrolytes like the acetonitrile solution used in the earlier part of this study). Since DES are widely acknowledged to comprise exclusively of charged species, the variation of the bulk concentration may only be compensated by a flux of co- or counter-ions but not by neutral solvent molecules. This further signifies the importance of the type of convolution protocol applied here, as classic δn/δc measurements would not return correct results (any significant change in cation/anion ratio would result in a profound change in viscosity, density, conductivity and solvation properties).

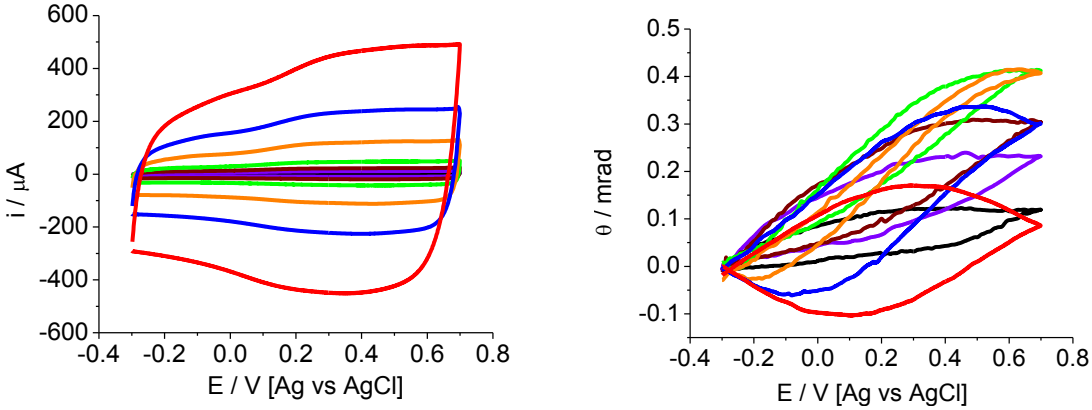

Figure 18. Left panel: voltammograms of a 0.8 µm [+/- 0.1 µm] PEDOT film (Q_{dep} = 74.2 mC cm^{-2}) redox cycled from - 0.3 V → 0.7 V → - 0.3 V in Ethaline 200. Black line 2 mV s^{-1}, violet 5 mV s^{-1}, wine 10 mV s^{-1}, green 20 mV s^{-1}, orange 50 mV s^{-1}, blue 100 mV s^{-1}, red 200 mV s^{-1} respectively. Right panel: experimental deflection profiles, colours as above.

During the discontinuous experiments conducted in Ethaline, (i.e. cyclic voltammetry/deflectometry) experiment (figure 18 – left panel) simultaneously recorded optical deflection was positive (see figure 18 – right panel). Upon the oxidation, mass decrease was recorded (see below: figure 19 – left panel). This is in agreement with our initial study (see Chapter III) of cation expulsion during the PEDOT film oxidation in Ethaline. The results shown above in figures 18 and 19 indicate the beam deflection towards the electrode and are consistent with $Ch^+/(EG)_2Cl^-$ concentration gradient changing in favour of the choline cation (the cationic specie has higher refractive index than anionic) being expelled from the polymer film into the bathing electrolyte.

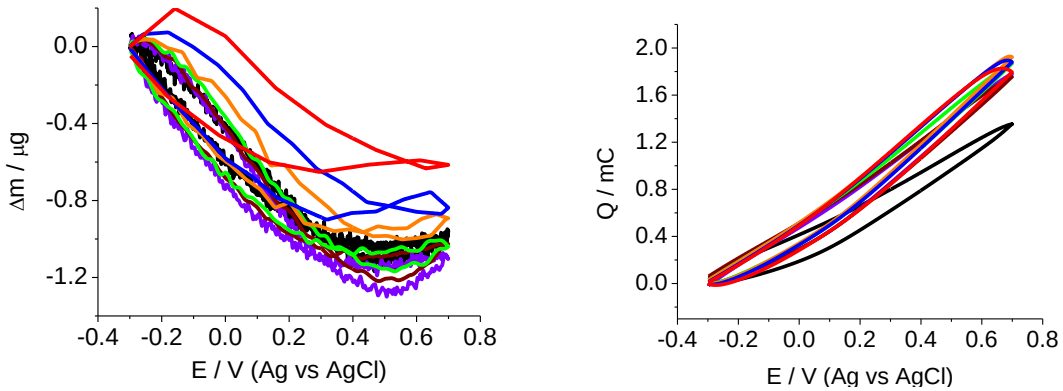

Figure 19. Left panel: massograms of a 0.8 μm [+/- 0.1 μm] PEDOT film (Q_{dep} = 74.2 mC cm^{-2}) redox cycled from - 0.3 V → 0.7 V → - 0.3 V in Ethaline 200. Black line 2 mV s^{-1}, violet 5 mV s^{-1}, wine 10 mV s^{-1}, green 20 mV s^{-1}, orange 50 mV s^{-1}, blue 100 mV s^{-1}, red 200 mV s^{-1} respectively. Right panel: Q_{pas} upon redox cycling, colours as above.

It must be mentioned here, that the δn/δc factor for the electrolytes depends on the refractive indexes of the components (i.e choline cation and ethylene glycol/chloride anion in this case) and these have not yet been studied. Analysis of the i/E plot (figure18, left panel) indicates that in Ethaline, (notwithstanding the experimental scatter) the current/sweep rate ratio is linear. This indicates that (within the experimental time scale used here) the PEDOT film redox conversion in Ethaline is complete. The electric and gravimetric data are in agreement with the previous results; however, analysis of the optical signal is much more complicated. In view of the fact that a Fick's law directly relates current and concentration gradient, one would expect the good correlation to occur for the beam deflection, unfortunately, this is not the case. While the electrochemically induced concentration gradient irrefutably occurs, the detection of it in high viscosity medium (Ethaline viscosity is 40 cP as opposed to 0.8 cP for acetonitrile) is somewhat questionable during the potentiodynamic experiments. Scrutiny of the deflection profiles (figure 18, right panel) recorded at variable ν (2 → 200 mV s^{-1}) reveals significant distortion of the shapes with none of the deflectograms resembling the shape of the cyclic voltammograms. The magnitudes of the optical, gravimetric and electric signals were determined as a function of a scan rate with results visible in figures 20 (Δm) and 21 (θ).

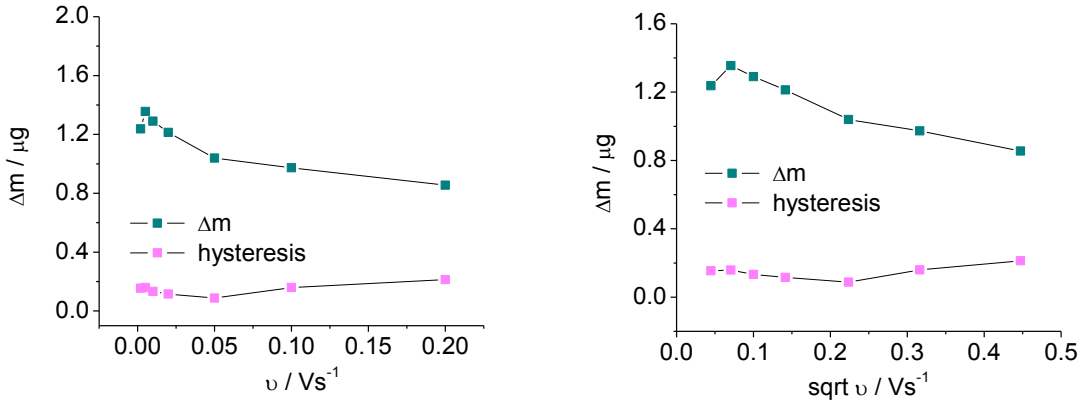

Figure 20. Left panel: magnitude (grey line) and hysteresis in Δm as a function of ν. Right panel: magnitude (i.e. absolute values - grey line) and hysteresis (i.e. divergence of the signal from the straight line) in Δm as a function of √ν.

The magnitude of the optical deflection in Ethaline initially increases to then decrease (in the 100 → 200 mV s^{-1} range). This observation is attributed to the large diffusional delay effect, which is this viscous media resulted with the deflectograms recorded at the fast sweep rates (100 → 200 mV s^{-1}) no longer representing the electrode processes.

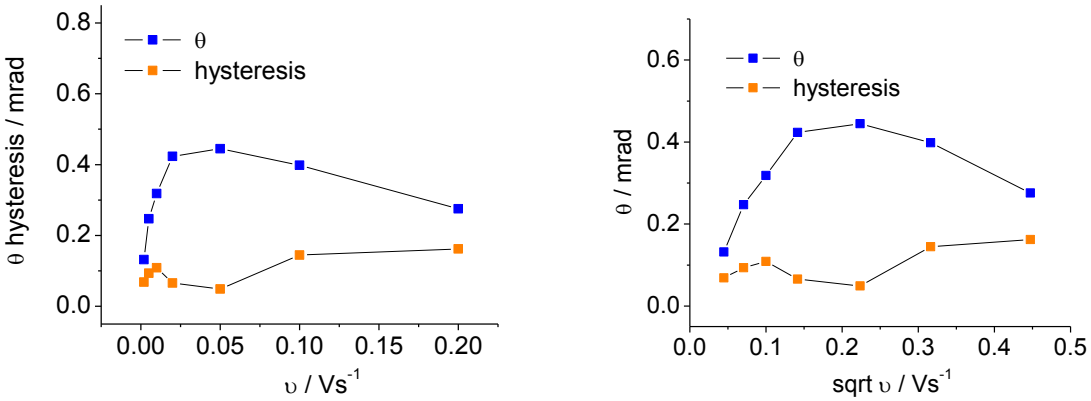

Figure 21. Left panel: magnitude (grey line) and hysteresis in θ as a function of ν. Right panel: magnitude (i.e. absolute values - grey line) and hysteresis (i.e. divergence of the signal from the straight line) in θ as a function of √ν.

Decrease of the maximum redox mass exchanged is noticeable at higher scan rates (figure 19) and has been previously (Chapter III) assigned to DES high viscosity and hence low diffusion rates. Unlike in acetonitrile, in Ethaline the magnitude of the optical deflection signal does not display any correlation with the electric signal (see figure 18).

Heterogeneous nature of the mass transfer at every scan rate is confirmed by hysteresis present in m/Q plot (figure 22 below). Hysteresis is relatively (compared to the signal magnitude which is almost constant) larger at fast scan rates indicating increase of the anion content in the overall mass flux.

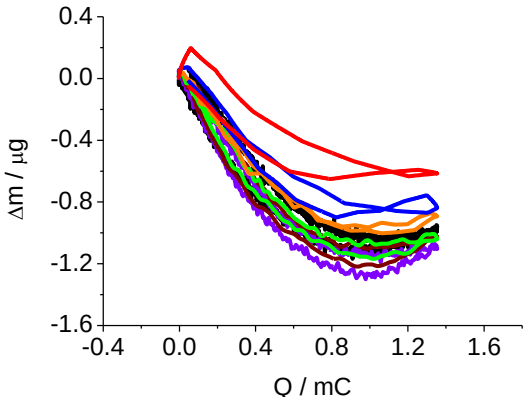

Figure 22. Δm/Q plot of a 0.8 μm [+/- 0.1 μm] PEDOT film (Q_{dep} = 75.2 mC cm^{-2}) redox cycled from - 0.3 V → 0.7 V → - 0.3 V in Ethaline 200. Black line 2 mV s^{-1}, violet 5 mV s^{-1}, wine 10 mV s^{-1}, green 20 mV s^{-1}, orange 50 mV s^{-1}, blue 100 mV s^{-1}, red 200 mV s^{-1} respectively.

As described earlier, in order to derive useful quantitative data from the convolution of the optical and mass signals into the component fluxes a fundamental requirement is that the measured current and optical responses should resemble each other in form i.e. they should be synchronous. Given that this is not the case here (because of slow diffusion) then no useful data can be extracted from the convolution process. Successful convolution analysis of the CV/CD experiments in acetonitrile is a confirmation of this experimental approach being valid. This indicates that the obstacles of repeating this process in Ethaline are not related to the technique applied (cyclic deflectometry) or the electrode used. As for the polymer film its surface roughness has been previously (see Chapter III) reported as being approximately within the 100 – 200 nm range, therefore significantly smaller than the

beam – electrode distance. Thus, one must consider factors present in Ethaline itself – namely: refractive index, viscosity, and ion transport properties.

	0.1 M $LiClO_4/CH_3CN$	Ethaline 200	Propaline 200
Density (η)	1.344	1.467	1.475
Viscosity (μ)	0.8	40	80
Refractive index (ρ)	0.798	1.113	1.106

Table 1. Refractive indexes, densities and viscosities of the electrolytes used. All values measured at 25˚.

Measurements of the refractive index of the electrolytes used (see table 1) revealed that although the DES's refractive index are rather high, successful PBD experiments were previously reported in electrolytes of even higher refractive indexes.[32] Significant optical profile changes which were recorded in Ethaline and excellent signal to noise as well as stability of the signal upon repeated redox cycling supported the idea that the optical deflection analysis is possible in a fully ionic environment. To overcome the difficulties solution transport properties and related to it liquid viscosity were considered next.

'Hole theory' is currently (2015) formally recognized as a most accurate description of the ionic motion in a fully ionic environment.[41] As it relates the ion mobility to the molten salt viscosity, this provides a plausible explanation of the encountered optical analysis limitations when current – deflection relationship breaks down. The exact diffusion coefficients of Ch^+ and $(EG)_2Cl^-$ are not known, however application of the Hole theory derived equation, used for the probability of finding a hole of a suitable radius *r* (suitable for an ion to move into) is presented below:

$$P_{dr} = \frac{16}{15\sqrt{\pi}} a^{7/2} r^6 e^{-ar^2} dr \qquad \textbf{[8]}$$

This equation has previously been applied to liquids with high surface tension like choline chloride based DES.[35] Simple calculations reveal that high viscosity and surface tension result in severely impaired ion mobility. This is further supported by an application of the Walden rule which relates viscosity of the liquid with its diffusion coefficient.[42] This

formula was originally intended to consider dilute aqueous solutions therefore; it is used only as an indicator here. Nevertheless, even this approximate approach (previously applied by Abbott and co-authors[43]) yielded an estimate diffusion coefficient in Ethaline as 1.4×10^{-7} cm^2 s^{-1}. It is significantly smaller than in majority of molecular and aqueous solutions and it results (assuming an average electrode/beam distance of ca. 50 μm and $x = \sqrt{\pi D_0 t}$) in a time lag of approximately 50 s between the electrode surface processes and the maximum concentration gradient reaching the focal point.

Clearly, in all but the slowest sweep rate experiments (which inevitably suffer from poor signal to noise ratio as well as considerable experimental drift) the potential sweep would have already switched the directions before any detectable amounts of the species have entered (or left) the optical deflection zone. This is a vindication of a radical difference between the shapes of cyclic voltammograms and cyclic deflectograms recorded in Ethaline. Thus, the optical experimental signal could not be interpreted using a convolution analysis.

4.3.2.2 Potential step experiments of PEDOT in Ethaline 200.

Figure 23 shows the electrical (i), gravimetric (Δm/μg) and optical (θ) responses of a PEDOT modified electrode immersed in Ethaline. Significant lag of the optical deflection signal can be noted despite the extended equilibration time after potential step. This discrepancy between electric, gravimetric and optical signal is a consequence of the slow diffusion in this medium.

At the second switching point (0.7 V $\rightarrow$ - 0.3 V) the concentration gradient is still present (i.e electric and gravimetric signals have returned to zero values but the beam deflection has not). This observation further explains the inability to conduct successful cyclic deflectometry in DES as potentiodynamic experiments were conducted on a much shorter experimental timescale. On a qualitative level of the analysis, the film mass decreases upon oxidation in Ethaline. This is in agreement with the previous work on the subject (see Chapter III) but in contrast to the effects of potentiostatic experiment in $LiClO_4/CH_3CN$ medium.

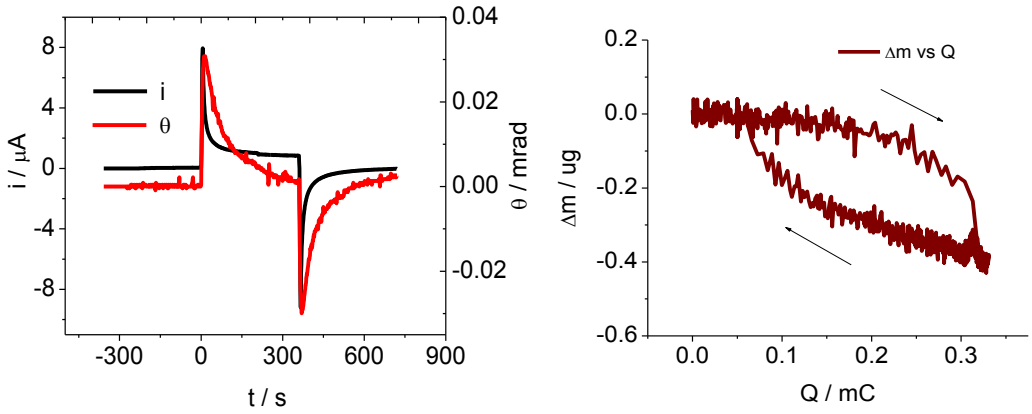

Figure 23. Left panel: chronoammperogram (black line) and chronodeflectogram (red line) of a 0.8 μm [+/- 0.1 μm] PEDOT film (Q_{dep} = 55.1 mC cm^{-2}) potential stepped from - 0.3 V → 0.7 V → - 0.3 V in Ethaline 200. Duration of each step = 360 s. Right panel: corresponding mass change (Δm) versus charge (Q) plot.

Contrary to the effects observed in acetonitrile lack of memory effects or any significant ageing as well as better overall stability for PEDOT films redox cycled in DES (see Chapter IV) and IL's has already been reported.[19] It therefore seems reasonable to extend Rahrindramahazaka and co-workers theory (based on PEDOT/1-ethyl-3-methylimidazolium bis((trifluoromethyl)sulfonyl)amide system)[19] to the current observations. Although in their study a 'classic' EMITFSI ionic liquid was used, this solvent bears resemblance to Ethaline in terms of both of them being composed entirely of ions (the underlying formulation chemistry is not considered relevant here). This leads to an initial conclusion that the different solvation properties of the ionic liquids result in stable relative ratio of the open and compact zones of PEDOT films exposed to DES (and IL's) regardless of whether the potentiostatic or potentiodynamic technique was applied. This is in contrast with the behaviour of PEDOT in $LiClO_4/CH_3CN$ where the mechanism of charge neutralization is ClO_4^- based (during a potential sweep) and Li^+ based (during a potential step) and therefore dependent on the potential application rate (gradual in CV and rapid in CA). This explains the gravimetric and optical signal of PEDOT/DES system being consistent in both dynamic and static experiments (i. e. regardless of the induction method oxidation of PEDOT results in Ch^+ expulsion). In other words, stability of the PEDOT films in DES prevents the polymer film from undergoing any kind of conformational

changes even if a large potential step is applied. This inherent stability has already been assigned (see Chapter III) to the presence of bulky ions preventing the film internal voids from collapsing.[11]

The quantitative analysis of the PEDOT/Ethaline ion fluxes (figure 24; right panel) displays (unlike in acetonitrile) no solvent trace. The underlying reason is that although the (originally intended for 'classical' electrolytes) convolution software returns 'net neutral' flux, here in a fully ionic environment it was partitioned into a cation and anion fluxes and summed with the (separately determined) Ch^+ and $(EG)_2Cl^-$ fluxes.

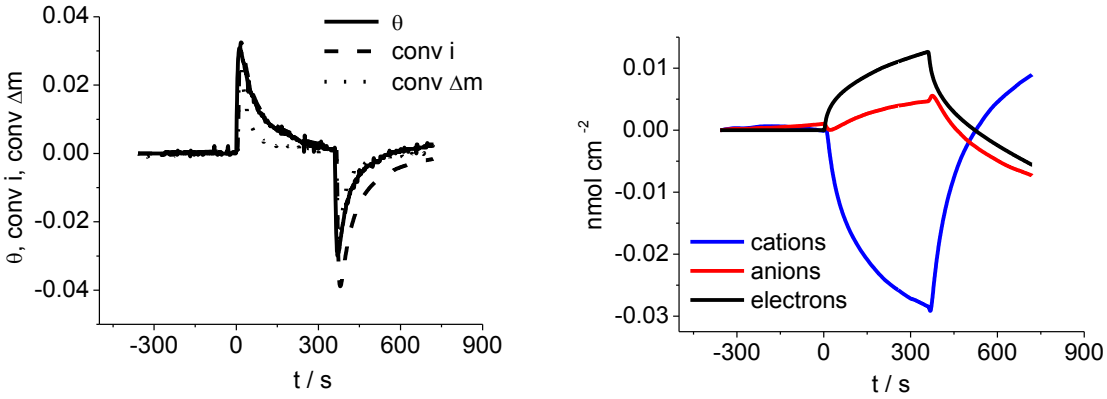

Figure 24. Left panel: experimental beam deflection (θ), convolved current ($i_{(x,t)}hL/zFA$) and convolved mass variation ($(dM_{(x,t)}/dt)zFAhl/m_{ClO_4^-}$. Right panel comparison of the convolved signal integrals.

Opposite directions of the cation (figure 24, right panel, blue line) and electron (as above, black line) fluxes confirm the EQCM based hypothesis (see Chapter III) of the cation expulsion maintaining the electroneutrality of PEDOT films upon oxidation in Ethaline. The magnitude of the anion counter transfer (figure 24, left panel, red line) is approximately 5 times smaller than that of cation. This result complies with the results of potentiodynamic experiments. The almost exclusive choline cation transfer in the oxidation phase is followed by a more heterogeneous flux in the reduction phase where the opposing fluxes of cation and anion are of almost equal magnitude. This is evident in the deviation of the convolved current, which in the reduction phase no longer superimposes onto the experimental optical signal. The convolved mass signal does not superimpose on the optical

signal during the oxidation phase. This suggests the flux of net neutral species (here; equimolar Ch^+ and $(EG)_2Cl^-$. Absence of any deviation (i.e. full overlay of the deflection and convolved mass signals) in the reduction phase may indicate that during this phase less mobile anions may be temporally impeded in the polymer films. Mobile species identity is explored in more detail in the figure 25 (below). On the commencement of the oxidation phase, mobile species mass of - 159.1 g mol $^{-1}$ was recorded. This is significantly larger than the cation mass (104.6 g mol $^{-1}$) and therefore probably originates from simultaneous exit of salt (the only 'neutral' specie available in this kind of environment).

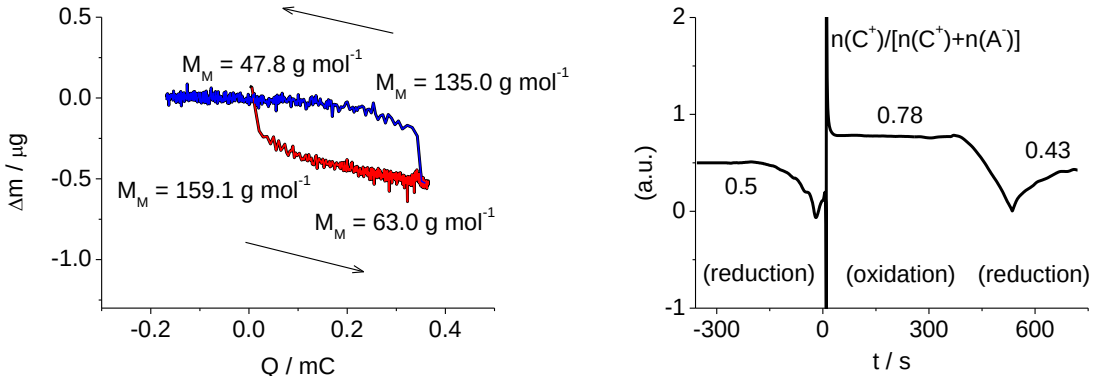

Figure 25. Left panel: Molar masses of the mobile species present during the potential step experiments of a 0.8 μm [+/- 0.1 μm] PEDOT film (Q_{dep} = 55.1 mC cm^{-2}) potential stepped from - 0.3 V → 0.7 V → - 0.3 V in Ethaline 200. Duration of each step = 360 s. Right panel: respective transport numbers.

In the high charge region, the MS_M decreases to - 63 g mol $^{-1}$. This (in this fully ionic environment) is a possible evidence of the concurrent anion flux. Reduction phase starts with an exit of 135 g mol $^{-1}$ (cation + 'salt'). This is followed (in the reduction later phase) by the decrease to 47.8 g mol $^{-1}$ indicating rather significant anion counter transfer. The transport numbers (figure 24; left panel) further supports this data. During the oxidation phase overall transport number for the cation is 0.78 (hence 0.22 for the anion) and for the reduction phase 0.43 (0.57). This is in good agreement with the quantitative PBD data (figure 23; right panel) where the oxidation is dominated by the cation flux while during reduction cation and anion fluxes are almost equal in magnitude.

Based on the work of Barbero, it was expected that the application of the optical deflection technique in ionic media would result in a small optical signal magnitude.[44] Larger beam deflections are observed in the dilute electrolytes, as the electrode-electrolyte concentration gradient is relatively large. As the electrolyte concentration is increased, the magnitude of the concentration gradient diminishes. In such conditions, the effective optical deflection analysis requires the alignment of the electrode as close as physically possible to the laser beam. Therefore, much smaller distance of approach (see figure 26) had to be used in Ethaline than in acetonitrile. The only limiting factor was the diameter of the focal point (see the experimental procedures – Chapter II).

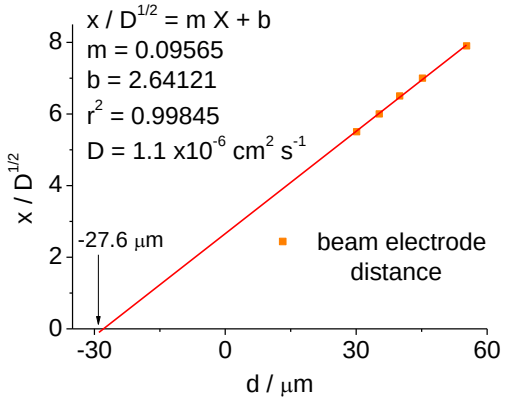

Figure 26. Plot of the convolution parameter ($x/\sqrt{D}$) expressed as a function of the relative beam/electrode distance. Extrapolation of the linearity reveals real beam electrode distance (here 27.6 µm).

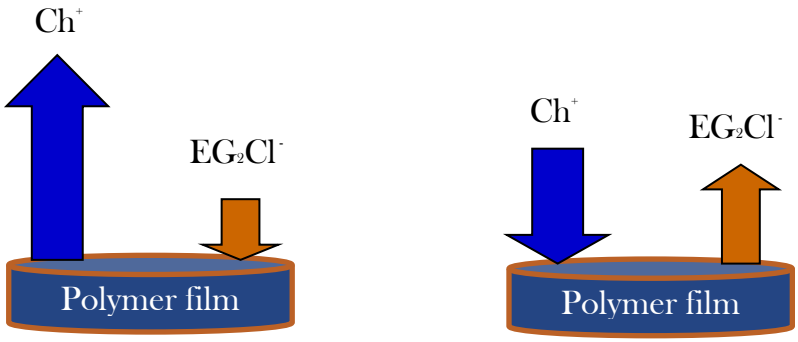

Figure 27. Cartoon representation of species flux during the potentistatic cycle of PEDOT in Ethaline 200. Left panel: oxidation, right panel: reduction.

The overall result of PEDOT/Ethaline chronodeflectometry can be summarized as a cation flux dominance in the electro neutrality maintenance. Oxidation proceeds with cation flux as the dominant mobile specie. In the reduction phase, the cation and anion fluxes are approximately equal in size. The graphic representation of the mobile species concentration changes is shown in figure 27.

4.3.3 Overview of the population changes and fluxes of PEDOT films redox cycled in Propaline 200.

Propaline is the most viscous and therefore (from the optical analysis point of view), most challenging electrolyte used in this study. Its gravimetric response during PEDOT redox cycle has an interesting 'V' shape, which is a result of four separate ionic fluxes with distinctively different reaction rates. Therefore, PEDOT/Propaline system was considered to be interesting object for a combined optical-gravimetric study.

4.3.3.1 Cyclic deflectometry of PEDOT in Propaline 200

Derivative of Ethaline, branched glycol based DES Propaline 200 (number denotes the molar composition; 1 mole of ChCl and 2 moles of 1, 2 propylene glycol) was a subject of this study. This solvent displays the viscosity twice that of the mother solvent (Propaline viscosity is 80 cP, as opposed to 40 cP, measured for Ethaline). The non-monotonic gravimetric signal has been previously observed for PEDOT films redox cycled in Propaline. Thus, it has been reasoned that the heterogeneous mass transfer in Propaline will manifest itself in a heterogeneous optical signal.

Analysis of the data in the right panel of the figure 28 indicates that this indeed is the case but only at low sweep rates. Proceeding now to the magnitude of the signals at increasing sweep rates (figure 28; left panel) the electrical response in Propaline were found to be consistent with that of Ethaline (i .e. linear) while the optical signal does not display any kind of correlation with the scan rate change (figure 28; right panel). The gravimetric signal in Propaline displayed excellent stability over time and little variation with the scan rate applied. By inference from Ethaline results, this has been ascribed to full redox conversion of the polymer films within the experimental timescale applied. The

discrepancy of this result with the preliminary study (see Chapter III) is considered to be a result of a different potential windows used (-0.3 V → 1.0 V used in the experiments described in Chapter III as opposed to -0.3 → 0.7 V used in the experiments described in this chapter).

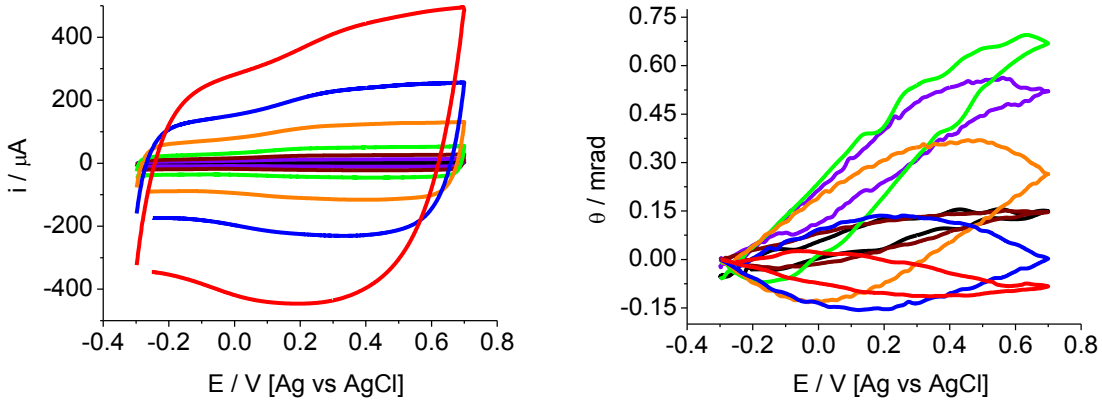

Figure 28. Left panel: voltammograms of a 0.8 µm [+/- 0.1 µm] PEDOT film (Q_{dep} = 75.2 mC cm^{-2}) redox cycled from - 0.3 V → 0.7 V → - 0.3 V in Propaline 200. Black line 2 mV s^{-1}, violet 5 mV s^{-1}, wine 10 mV s^{-1}, green 20 mV s^{-1}, orange 50 mV s^{-1}, blue 100 mV s^{-1}, red 200 mV s^{-1} respectively. Right panel: experimental deflection profiles, colours as above.

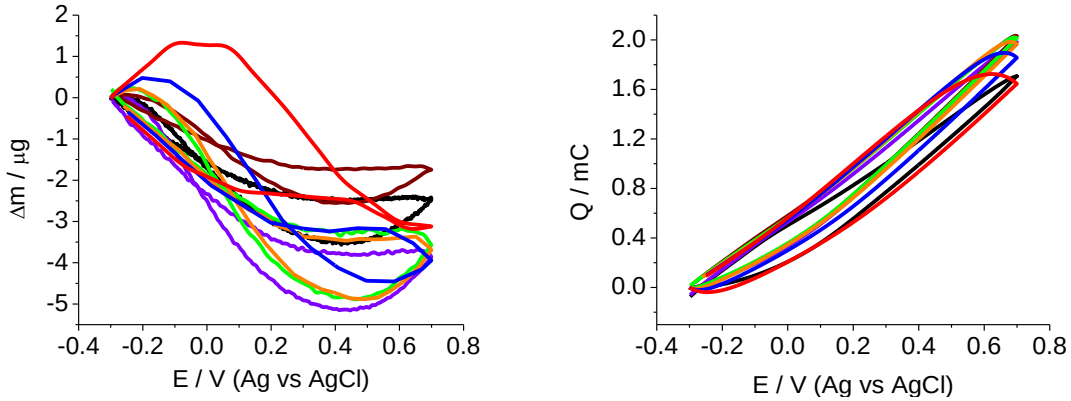

Figure 29. Left panel: massograms of a 0.8 µm [+/- 0.1 µm] PEDOT film (Q_{dep} = 74.2 mC cm^{-2}) redox cycled from - 0.3 V → 0.7 V → - 0.3 V in Propaline 200. Black line 2 mV s^{-1}, violet 5 mV s^{-1}, wine 10 mV s^{-1}, green 20 mV s^{-1}, orange 50 mV s^{-1}, blue 100 mV s^{-1}, red 200 mV s^{-1} respectively. Right panel: Q_{pas} upon redox cycling, colours as above.

In a more specific terms, the shortened potential window applied here does not allow the symmetrical 'V' shaped mass exchange to occur. The non-monotonic gravimetric signal has previously been observed in cyclic massograms of PEDOT films redox cycled in Propaline. In the gravimetric data presented here (see figure 29; left panel) the previously reported 'V' shape is not as prominent as the cycle end potential has been alerted (for reasons already mentioned).

Nevertheless, the heterogeneous gravimetric signal presented in figure 29, should theoretically return a similar in pattern optical deflection signal. This has been deducted by inference from Ethaline where almost entirely homogeneous process of cation transfer resulted in a homogeneous optical signal.

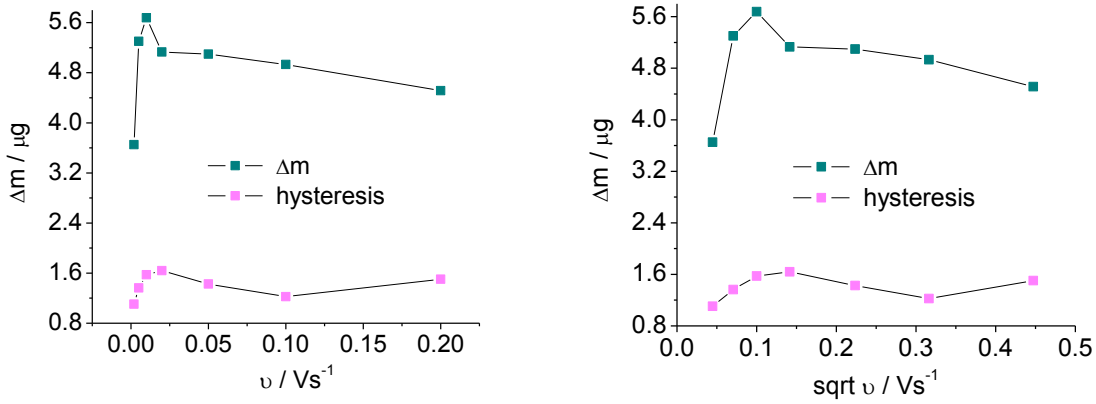

Figure 30. Left panel: magnitude (grey line) and hysteresis in Δm as a function of ν. Right panel: magnitude (grey line) and hysteresis in Δm as a function of √ν.

The magnitudes of the optical, gravimetric and electric signals were determined as a function of a scan rate with results visible in figures 30 (Δm) and 31 (θ). These signals in Propaline display even more prominent hysteresis than in Ethaline. This is expected due to the increase in viscosity.

This effect (i.e distortion of the optical signal at higher scan rates) undoubtedly originates from Propaline higher viscosity. Diffusion coefficient in Propaline (which determines mass transport and, in DES its value can be approximated to be inversely proportional to viscosity – this treatment was inferred from CH_3CN and Ethaline analyses)

was estimated to be 0.7×10^{-7} cm^2 s^{-1} using a Walden rule approximation. This is half of the value recorded in Ethaline and it provides explanation of even more distorted cyclic deflectograms shapes recorded in this solvent.

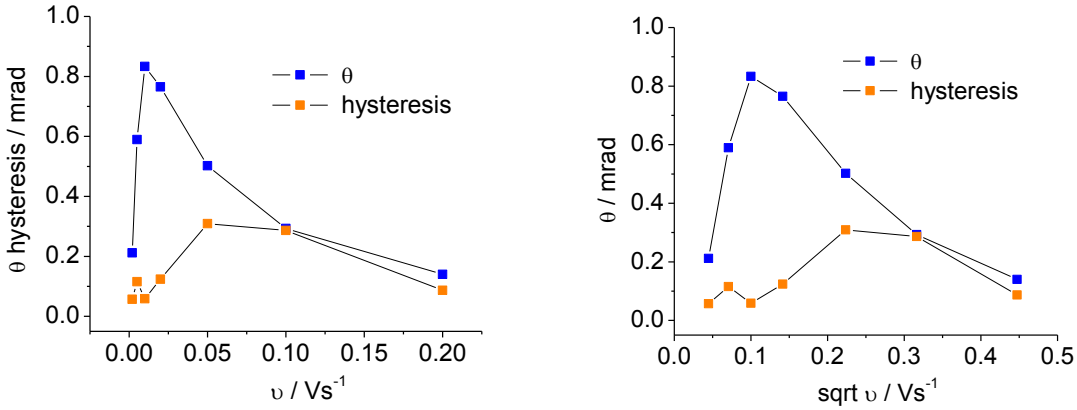

Figure 31. Left panel: magnitude (grey line) and hysteresis in θ as a function of ν. Right panel: magnitude (grey line) and hysteresis in θ as a function of √ν.

Δm/Q plot for PEDOT/Propaline system (figure 32) indicates presence of a very prominent hysteresis; this is excepted due to the highly heterogeneous nature of the mass transfer.

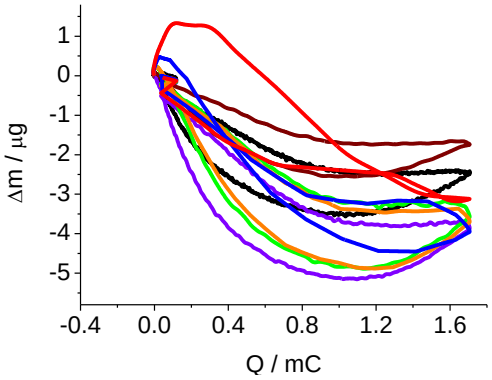

Figure 32. Δm/Q plot of a 0.8 μm [+/- 0.1 μm] PEDOT film (Q_{dep} = 75.2 mC cm^{-2}) redox cycled from - 0.3 V → 0.7 V → - 0.3 V in Propaline 200. Black line 2 mV s^{-1}, violet 5 mV s^{-1}, wine 10 mV s^{-1}, green 20 mV s^{-1}, orange 50 mV s^{-1}, blue 100 mV s^{-1}, red 200 mV s^{-1} respectively.

The convolution analysis of cyclic deflectograms from Propaline experiments was considered impossible for exactly the same reasons as in Ethaline (i. e. the beam deflection not being representative of the electrically induced concentration gradient due to the extended diffusion induced temporal delay). Distortion of the optical signal shapes in Propaline was even more prominent than in Ethaline, which proves that the viscosity of the solvent, not a high refractive index, is the main barrier in conducting cyclic optical deflection experiments.

4.3.3.2 Potential step experiments of PEDOT in Propaline 200.

Figures 32 and 33 show the electrical and optical responses of the PEDOT films immersed in Propaline and subjected to potential steps. As expected (based on twofold increase in viscosity), the diffusional delay is more prominent than in Ethaline.

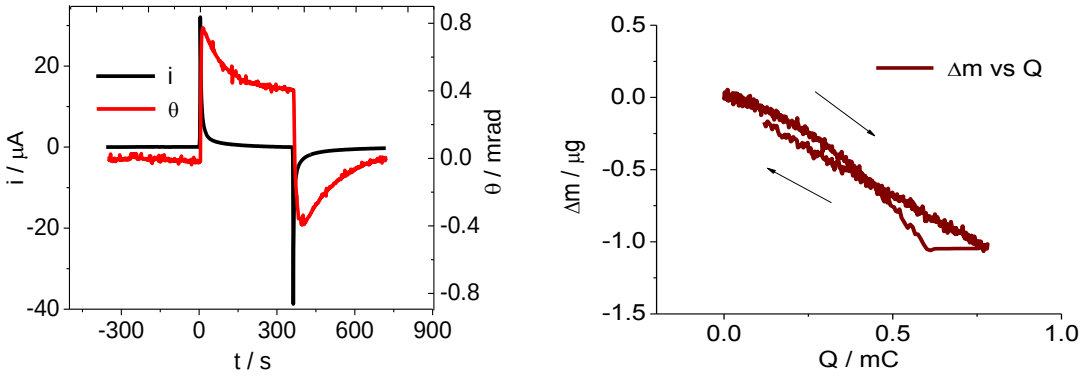

Figure 33. Left panel: chronoammperogram (black line) and chronodeflectogram (red line) of a 0.8 μm [+/- 0.1 μm] PEDOT film (Q_{dep} = 55.1 mC cm^{-2}) potential stepped from - 0.3 V → 0.7 V → - 0.3 V in Propaline 200. Duration of each step = 360 s. Right panel: respective Δm/Q plot.

Higher stability of the optical signal (visible in the improved signal/noise ratio) is consistent with the previous observation (see Chapter IV) of the good overall stability of PEDOT/Propaline systems. The gravimetric analysis of potentiodynamic experiments conducted in Propaline revealed a very interesting 'V' shape (see Chapter IV). As the direct observation of this process by the optical deflection method proved impossible, the

potentiostatic experiment was deployed instead.

The influence of the potential application method (i. e. dynamic or static) on the film/electrolyte mass exchange has already been described in the earlier part of this chapter (see paragraph 4.3.1 and 4.3.2). Here this theory is extended to include the observations of polymer film relaxation/contraction in Propaline. By inference from CH_3CN and Ethaline experimental observations, it can be reasoned that the application of the large potential step will result in major conformational changes of the polymer film. This will result in relaxation process enabling the solvent trapped in the 'compact' zone of the polymer film to partake in the electrochemistry. As Ch^+ is a smaller, thus more mobile specie, it leaves the inherent (now temporally relaxed) 'compact' zone much faster than the bulky $(PG)_2Cl^-$ anion. This process of cation egress is coupled with anion ingress (visible as hysteresis in the $\Delta m/Q$ plot – figure 33; left panel). It also overlaps both spatially and temporally with the cation egress visible in the first part of the cyclic electrogravimetry experiments (see Chapter IV) thus masking the anion ingress influence on the overall shape of the massogram. The gravimetric signal recoreded during the potential step experiments (Figure 33; left panel) displayed monotonous mass decrease without any resemblance to the 'V' shape encountered in the cyclic experiments. Figure 34 (left panel) contains the results of the application of the convolution protocol (the procedure used was the same as for $CH_3CN/LiClO_4$ and Ethaline).

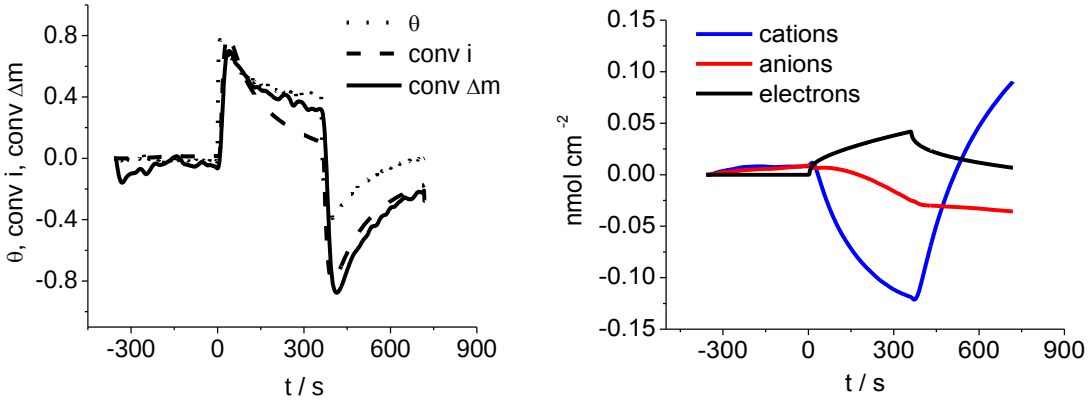

Figure 34. Left panel: experimental beam deflection (θ), convolved current ($i_{(x,t)}hL/zFA$) and convolved mass variation ($(dM_{(x,t)}/dt)zFAhl/m_{ClO_4^-}$. Right panel: Comparison of the convolved signal integrals.

As in Ethaline, the PEDOT/Propaline quantitative analysis of the ionic fluxes (figure 34, right panel) does not contain any solvent trace. Opposite directions of cation (egress) and electron (ingress) fluxes, support the theory of cation egress being the main process providing the electroneutrality. Heterogenic nature of mass flux in Propaline is more evident than in Ethaline. This is visible in the significant departures of both the convolved current and convolved mass from the experimental optical signal.

Firstly, the convolved current does not superimpose onto the optical signal in the latter part of the oxidation. This suggests anion co-transfer and is consistent with the EQCM observations (see below). During reduction, the optical deflection signal and convolved current are more closely related (see figure 33; left panel) but lack of complete superimposition suggests minor anion counter transfer. Secondly, the convolved mass does not superimpose onto the optical deflection signal during most of the oxidation (although the deviation is small) to then deviate from it significantly in the reduction phase. This is an unequivocal evidence of salt transfer (i.e neutral species) being present.

Detailed analysis of the PEDOT/Propaline system redox mass transfer is visible in figure 35. At the onset of the oxidation, the MS_M value of - 191 g mol $^{-1}$ has been obtained. This vastly exceeds the cation molar mass and is an unequivocal evidence of heterogeneous flux. Here it is assigned to the 'salt' exit occurring concurrently with the cations exit. Latter part of the oxidation phase returns the MS_M value of - 80.7 g mol $^{-1}$, this suggests cation egress with simultaneous anion ingress. At the start of the reduction phase MS_M reaches value of 196.4 g mol $^{-1}$, this again is an evidence of coupled cation and 'salt' ingress. MS_M then decreases to 65.2 in the later stage of the reduction (cation flux with anion counter flux). Final part of the reduction phase reveals the mass value of just suggesting anion and cation fluxes almost equal in magnitude but in opposite directions. Respective transport numbers (figure 35, right panel) indicate almost equal transfer of cations and anions (0.5), which upon oxidation changes in favour of the cation (0.76) to then, in the final reduction phase decrease to 0.29 hence suggesting anion transfer dominance.

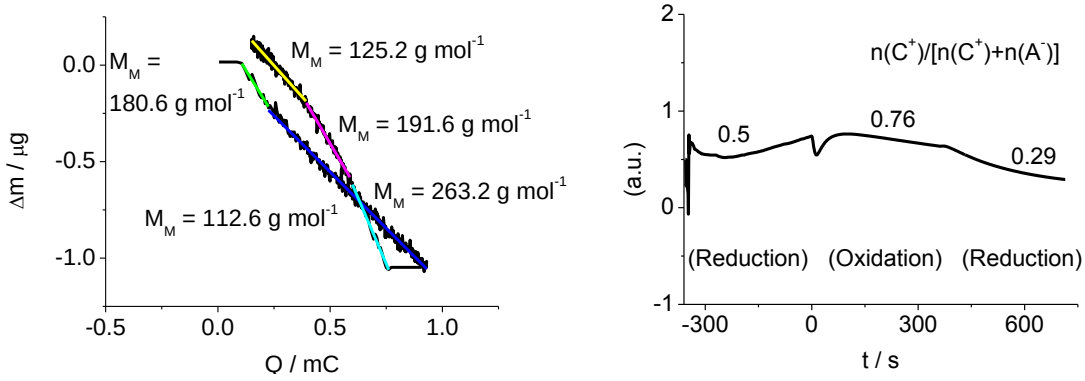

Figure 35. Left panel: Molar masses of the mobile species present during the potential step experiments of a 0.8 µm [+/- 0.1 µm] PEDOT film (Q_{dep} = 55.1 mC cm^{-2}) potential stepped from - 0.3 V → 0.7 V → - 0.3 V in Ethaline 200. Duration of each step = 360 s. Right panel: respective transport numbers.

Optical signal originates from the concentration gradient formed at the electrode/electrolyte interface. Because the probe beam samples the concentration changes at some distance from the electrode's surface, there inevitably is a delay before maximum concentration gradient arrives in a focal point.

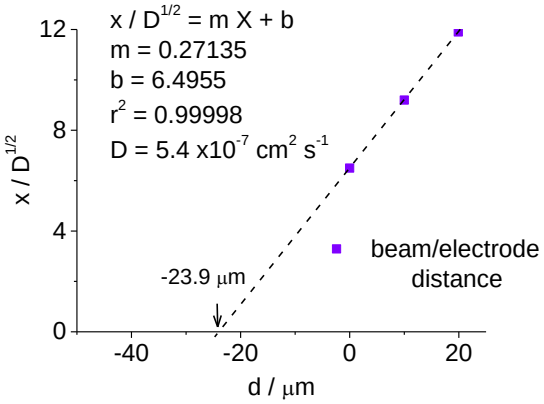

Figure 36. Plot of the convolution parameter ($x/\sqrt{D}$) expressed as a function of the relative beam/electrode distance. Extrapolation of the linearity reveals real beam electrode distance (here = 23.9 µm).

This delay is diffusion controlled and DES diffusion is related to viscosity. Since Propaline is the most viscous solvent used in this study (η = 80 cP), the distance of

approach was reduced even further in order to obtain optimum results. Electrode/beam distance was obtained using $x/\sqrt{D}$ plot (see figure 36). $x/\sqrt{D}$ plots also allowed for a more precise determination of the diffusion coefficient (previously estimated using the Walden rule). The diffusion coefficient in Propaline obtained from $x/\sqrt{D}$ plots was 1.7×10^{-7} cm^2 s^{-1}, which although higher than the Walden rule estimate is still substantially below the value obtained for the $LiClO_4/CH_3CN$ electrolyte. Comparison of this result with the diffusion coefficient estimated for Ethaline indicates that indeed in DES diffusion is inversely related to viscosity (Ethaline 40 cP, D = 5.4 cm^2 s^{-1}, Propaline 80 cP, D = 1.7 cm^2 s^{-1}).

	0.1 M $LiClO_4/CH_3CN$	Ethaline 200	Propaline 200
$D_{calculated}$ cm^2 s^{-1}	1.2×10^{-6}	1.4×10^{-7}	0.7×10^{-7}
$D_{experimental}$ cm^2 s^{-1}	7.2×10^{-6}	1.1×10^{-6}	5.4×10^{-7}

Table 2. Comparison calculated (based on Walden's rule) and measured (obtained from $x/\sqrt{D}$ plots) diffusion coefficients.

The overall result of PEDOT/Propaline system chronodeflectometry can be described as being more heterogenic in nature than the Ethaline one. The graphic representation of this process is shown in figure 37.

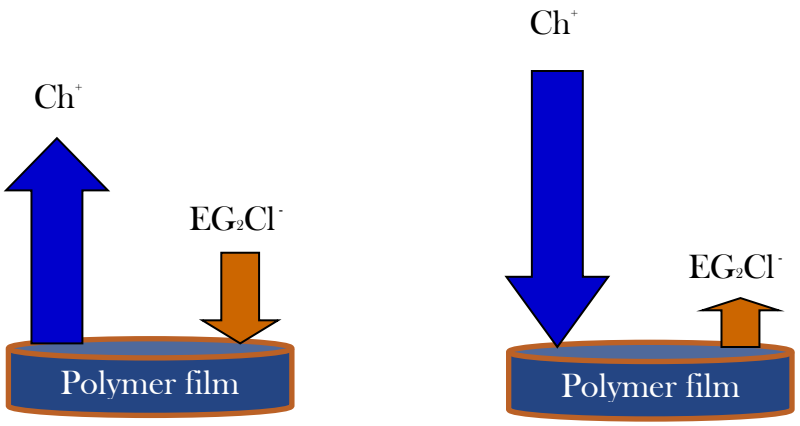

Figure 37. Cartoon representation of species fluxes during the potentistatic cycle of PEDOT in Propaline 200. Left panel: oxidation, right panel: reduction.

Cation flux is still the main process satisfying the electroneutrality but the anion flux (partially visible as a part of 'salt' flux) forms much more significant portion of the total flux than during the redox cycling of PEDOT films in Ethaline.

4.3.4 Optical analysis of the PEDOT films electrodeposition.

The process of electrodepostion of conducting polymer films has a profound influence on the film properties. It has previously been shown that the type of electrodepostion (i.e. potentiodynamic, potentiostatic, or galvanostatic) results in a formation of CP films with markedly different permselectivity and charge storage properties.[10,18,45]

Hence, a significant effort has been placed on the elucidation of the electrodepostion process.[46],[47] Apart from the classic electrochemical and gravimetric techniques, ellipsometry as well as beam deflection methods have been applied to study this process. A thorough analysis of the electrodeposition process requires information on the fluxes present in front of the electrode. While the electrode surface population changes are well addressed by the gravimetric analysis, PBD is ideally suited to study ion flow processes. Optical deflection has previously been applied in studies of P(3 MeTh)[39] and PPy,[18] here, first optical study of PEDOT electrodepostion is presented.

Potentiostatic deposition of PEDOT is widely accepted to proceed through deposition of oligomers of given length to the electrode surface.[48] The overall electroneutrality of the thus formed polymer film is maintained through anion incorporation. It must be mentioned that the determined experimentally overall growth charge is consumed to form all of the oligomers. Only part of them then proceeds to form a polymer film. The formation of oligomers proceeds through oxidation of monomers to form radical cations as illustrated below:

$$EDOT \rightarrow EDOT^{+}$$

These in turn form the oligomers:

$$EDOT^{+} + nEDOT^{+} \rightarrow n[EDOT^{+}]$$

Since the monomers are suspended in the solvent with the presence of supporting electrolyte (here present in double the concentration of the monomer), the following fluxes must be considered in the analysis:

1. Flux of oligomers towards the electrode
2. Flux of cations (Li^+) away from the electrode
3. Flux of unconsumed oligomers away from the electrode
4. Flux of anions (ClO_4^-) towards the electrode
5. Flux of solvent away from the electrode

Each of these fluxes contributes to the total recorded flux. The respective individual contribution of these fluxes (denoted k_i) can be expressed as flux using the following equation:

$$J_{i(0,t)} = k_i \left(\frac{I_{(t)}}{FA}\right) \quad \textbf{[9]}$$

The experimental results of the optical analysis are visible in the left panel of figure 37. Current and beam deflection transients display good initial agreement followed by a fast decay in current (upon the physical end of the electrodepostion) accompanied by a slow decay of the optical signal. The shape of the optical profile is a result of flux non-consumed oligomers away from the electrode. Δm/Q plot (figure 37, right panel) indicates the mass of mobile specie of 115.3 g mol $^{-1}$ being deposited on the electrode. Since this is lower than the monomer molar mass (142.15 g mol $^{-1}$) a reasonable assumption can be made that the monomer influx is countered by solvent flux away from the electrodes' surface. Simple calculation reveals that for every monomer transferred to the electrode's surface 1.6 solvent molecules are forced from it.

The heterogeneous nature of this process (as compared to for example, electrodepostion of metals) brings further complications in the application of the convolution protocol. Transfer of soluble oligomers towards the electrode is delayed due to the non-consumed oligomers counter flux. Additionally, once the polymer film forms, the anion flux starts towards the electrode competing with the oligomers flux. Thus, two time delays, henceforth called T_{Dolig} and T_{Danion} were introduced.

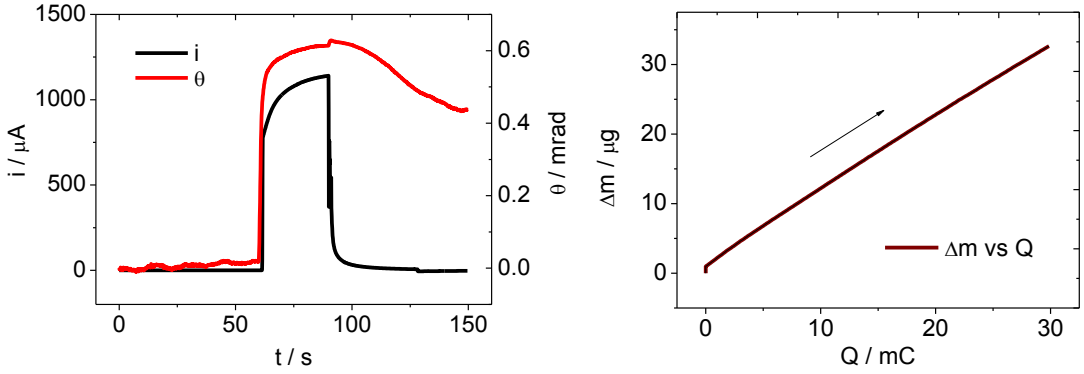

Figure 38. Left panel: potential step ammperogram (black line) and chronodefletcogram of a PEDOT film [Q_{dep} = 30.0 mC cm^{-2}] potentiostatically deposited from 0.05 M EDOT in 0.01 M $LiClO_4/CH_3CN$ solution. Right panel: corresponding mass change (Δm) versus charge (Q) plot.

The convolution protocol was applied using the following assumptions:

1. Partition of oligomers occurs (i.e. not all formed oligomers are deposited on the electrode but part of them diffuses away). Thus the flux of monomers towards the electrode can be described as:

$$J_{i(0,t)} = \alpha J_{i\ deposited(0,t)} + (1 - \alpha) J_{i\ soluble\ (0,t)} \quad \textbf{[10]}$$

and in relation to the electrode's current:

$$J_{i(0,t)} = K_i \left(\frac{I_{(t)}}{FA}\right) \quad \textbf{[11]}$$

2. Upon formation, the polymer film exists in an oxidised state hence anion flux forms and its magnitude is related to the increase in film thickness.
3. The total amount of all individual fluxes recorded can exceed the total flux value derived from the experimental beam deflection signal.[18]

Contributions of the different species to the laser beam net deviation, here expressed as an integral form of the convolved signals are shown in the right panel of figure 39. The magnitude of the anion signal (red line) explains the lack of superimposition of the convolved current (figure 39, left panel) onto the experimental optical signal. The value of the convolved current was calculated assuming PEDOT oligomers flux towards the electrode to be the major contribution to the signal. The temporal delay (indicated by an arrow) of the anion flux is consistent with the expectations (i. e. significant anion flux cannot precede the initial polymer film growth stage).

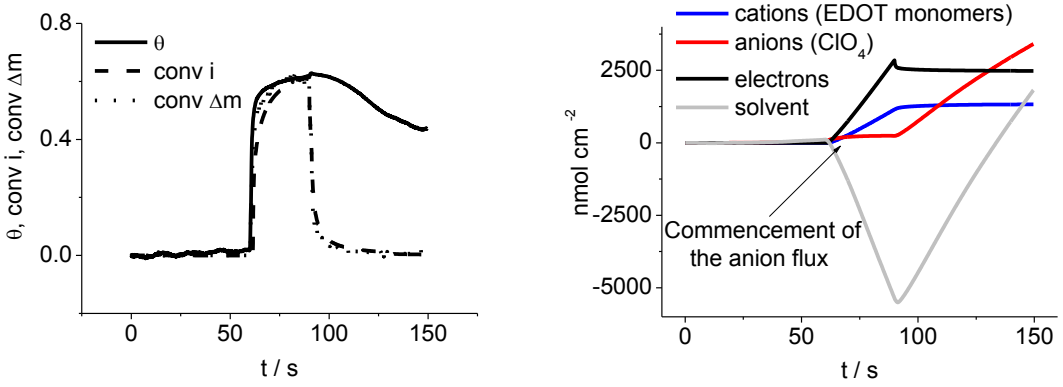

Figure 39. Left panel: experimental beam deflection (θ), convolved current ($i_{(x,t)}hL/zFA$) and convolved mass variation ($(dM_{(x,t)}/dt)zFAhl/m_{ClO_4^-}$. Right panel: Comparison of the convolved signal integrals.

Upon the commencement of the deposition, the solvent molecules move away from the electrode. Once the polymer film forms, solvent flux changes direction to solvate the film. The temporal delay of the anion flux has been quantified as 27 s. In practical terms, it means that a deposition of film with 0.38 μm thickness results in an onset of oxidative anion flux being recorded by a measurable laser beam deflection.

$x/\sqrt{D}$ plot (figure 40), allowed for the determination of the diffusion coefficient for EDOT monomers as 3.5×10^{-6} cm^2 s^{-1}. Value of the diffusion coefficient presented in figure 40 is lower than for perchlorate anions as it was expected due to size difference between the perchorate anions and EDOT monomers. Correia et al, reported a diffusion coefficient of 3.97×10^{-5} cm^2 s^{-1} for 3-MeTh monomers in the same electrolyte, however their convolution protocol was markedly different as it was based on multiflux convolution as

opposed to monoflux convolution used throughout this thesis .[39]

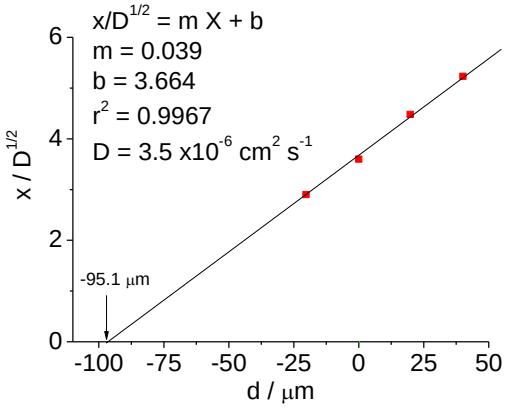

Figure 40. Plot of the convolution parameter ($x/\sqrt{D}$) expressed as a function of the relative beam deflection. Extrapolation of the linearity reveals real beam electrode distance (here x_0 = 95.1 µm).

The graphic representation of the fluxes present during the electrodeposition of PEDOT films from 0.05 M EDOT in 0.01 M $LiClO_4/CH_3CN$ solution is shown in figure 41.

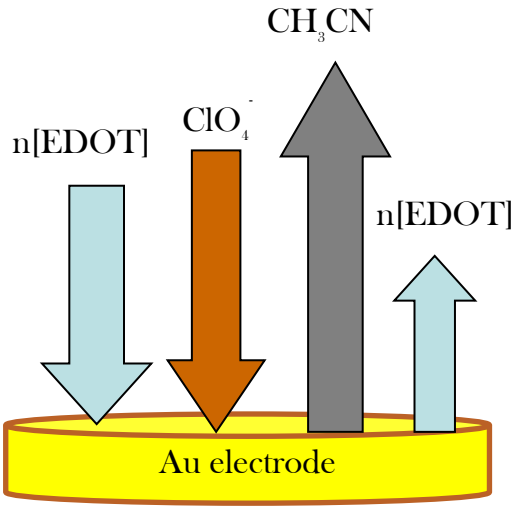

Figure 41. Cartoon representation of species flux during the potentiostatic electrodepostion of PEDOT films from from 0.05 M EDOT dissolved in 0.1 M $LiClO_4$ / CH_3CN (30s CA, 1.2 V).

This study shows the possibility of studying PEDOT electrodepostion by coupling the electrochemical (chronoammperometry), gravimetric (quartz resonator) and optical (beam deflection) techniques. This is a novel approach and an expansion of the previous work on the subject as the previous studies of the CP films electrodepostion were limited to PBD only without the complimentary EQCM. PBD-EQCM, supplemented by a convolution protocol proved to be a powerful tool for the analysis of CP films electropolymerization.

4.4 Conclusions

The overarching goal of this chapter was the optical analysis of the ionic fluxes present during the PEDOT redox cycle in two DES, Ethaline and Propaline. The combined EQCM – PBD analytical technique used, provided information about the *electron flux* through electrochemical response, *surface population changes* through the quartz crystal acoustic response and the *concentration gradient* through the optical signal (deflection of the laser beam). Application of the convolution protocol allows for the compilation of these data yielding valuable insight into the polymer/electrode interface exchange and identity of the species ingressing/egressing to/from the polymer film. The linearity observed in the i/ν plots for all both DES tested indicated full redox conversion of the polymer films and the diffusion control present in the system. The magnitude of the gravimetric signal confirms that the film conversion is essentially ν independent. The optical deflection signal recorded during cyclic experiments varied markedly between the acetonitrile and both DES mediums. Acetonitrile optical signal displayed clear θ/ν correlation, however the discontinuous experiments conducted in both Ethaline and Propaline showed no correlation between cyclic deflectograms and cyclic voltammograms. Instead, the magnitude of the optical signal initially increased to then decrease (rapidly so in Propaline), with significant variation in deflectogram shape.

The pre-requisite for successful application of the convolution protocol is the resemblance between the experimental optical deflection and the electrode current. The logic behind that is all electrode processes originate from or result in concentration gradients (which forms refractive index gradients – detectable through optical beam

deflection). Only the acetonitrile experimental data proved to be fully compatible with this requirement allowing for the successful correlation of the optical, electric, and gravimetric signals.

Convolution analysis results confirmed the conclusions of the gravimetric study (see Chapter III) of the anion dominating the electroneutrality balance. Anion transfer was coupled with significant solvent transfer and minor cation transfer. PEDOT films redox cycled in $LiClO_4/CH_3CN$ displayed clear effects of mobile species kinetic separation. Mostly the film relaxation processes, as opposed to field driven perchlorate anion flux, were proved to drive the cation and solvent fluxes. Due to the (diffusion dependent) temporal delay between the electrode surface processes and the concentration gradient, transfer of the representative concentration gradients to the optical detection zone was very slow. Because of this, the cyclic optical experiments in DES were unsuccessful. To overcome the problems of high viscosity and therefore slow mass transport in DES, potentiostatic experiments were conducted on all three electrolytes and these provided a valid, however rather unforeseen set of data. Good agreement was obtained between the experimental optical signal and the current and mass signals convolved on the base of it, with the prominent time lag visible in Propaline experimental data. In all of the electrolytes, the effect of the large potential step application was most startling in acetonitrile.

It is postulated that the rapid potential application results in the conformational changes of the polymer film. This alters the film solvation properties, namely it allows the 'compact' zone of the polymer film to partake in the electrochemical processes. This has a profound effect on the gravimetric signal as well as corresponding ion fluxes with the results catalogued below in table 3.

	CV	CA
0.1 M $LiClO_4/CH_3CN$	Anion incorporation	Cation expulsion
Ethaline	Cation expulsion	Cation expulsion
Propaline	Cation expulsion/Anion incorporation	Cation expulsion

Table 3. Electroneutrality compensation processes in PEDOT films subjected to potentiodynamic and potentiostatic conditions.

Observations made during the potentiostatic experiments conducted in acetonitrile are in a sharp contrast to the potentiodynamic experiments data and they emphasise the electrochemical technique influence on the CP film relaxation processes. This work confirms previous research by Rahrindramahazaka and co-workers on the importance of physical-chemical interactions between the electrolyte and CP films.[10.19] The theory of cation exchange maintaining the electroneutrality in all PEDOT films regardless of the electrolyte deployed is supported by increased *i* and Q_{pas} observed in the potentiostatic experiments. This improved electrochemical performance originated from the activity of the 'compact' zone (inactive in cyclic experiments). Such clear kinetic effects have previously been observed for polynaphtol films redox cycled in aqueous solution of hydrochloric and camphorsulphonic acids.[49] Pham and co-workers have studied poly(1-naphthol) electrodes redox cycled in acetonitrile and reported that during the fast sweep rates cycling anions were exchanged while at slow sweep rates it was the cations.[50] Kim et al has also described the effects of the potential dynamics on the dopants identity in a recent PPy study.[27]

Electrodepostion of PEDOT films has been studied using combined optical-gravimetric approach for the first time. The participations from anions, electrons, monomers, and solvent molecules have been successfully accounted for. The electron flux confirmed the doping ratio as 0.3 and the flux of solvent revealed the ratio of acetonitrile molecules leaving the electrode's surface in the wake of electrodepostion as 1.6 molecules of acetonitrile for every EDOT monomer partaking in the electrodepostion process. This forms a base that can be extended to studies of potentiostatic and galvanostatic CP films deposition.

Work described in this chapter is a novel application of the 'old' analytical tool. PBD has not been previously used in any observation of the ionic liquids electrochemistry (or ant other process). Ability to measure the concentration gradient of the variety of interfaces and processes which include but is not limited to liquid /solid or liquid/liquid interfacial processes, metal deposition and dissolution, is explored further in the following chapter. The PBD-EQCM ability to measure current, mass and concentration in a single experiment is an extremely powerful analytical tool, which should find wider application in the future research on ionic liquids and Deep Eutectic Solvents.

4.5 References

[1] A.R. Hillman, K.S. Ryder, C.J. Zaleski, C. Fullarton and E. L. Smith, *Z. Phys. Chem.* 2012, **226**, 1049-1068.

[2] D. Kumar, S.A. Hashmi, *Solid State Ionics*, 2010, **181**, 416-423.

[3] Q. Hao, W. Lei, X. Xia, Z. Yan, X. Yang, L. Lu, X. Wang, *Electrochimica Acta*, 2010, **55**, 632-640.

[4] J. M. Cooper, A. Glidle, A.R. Hillman, M. D. Ingram, C. Ryder and K. S. Ryder, *Physical Chemistry Chemical Physics*, 2004, **6**, 2403-2408.

[5] K. S. Jang, H. Lee, B. Moon, *Synthetic Metals*, 2004, **143**, 289-294.

[6] T. A. Skotheim, J.R. Reynolds (Ed.): *Handbook of Conducting polymers*, New York, 2007.

[7] A. Ispas, R. Peipmann, B. Adolphi, E. Efimov, A. Bund, Electrochmica Acta, 2011, **56**, 3500-3506.

[8] H. Randriamahazaka, G. Sini and F. Tran Van, *Journal of the Physical Chemistry C*, 2007, **111**, 4553-4560.

[9] J. Bobacka, A. Lewenstam, A. Ivaska, *Journal of Electroanalytical Chemistry*, 2000, **489**, 17-27.

[10] K. Wagner, J. M. Pringle, S. B. Hall, M. Forsyth, D. R. MacFarlane and D. L. Officer, *Synthetic Metals*, 2005, **153**, 257-260.

[11] B. Uglut, J. E. Grose, Y. Kiya, D. C. Ralph, H. D. Abruña, *Applied Surface Science*, 2009, **256**, 1304-1308.

[12] Y. Hsiao, W. Whang, C. Chen and Y. Chen, *Journal of Materials Chemistry*, 2008, **18**, 5948-5955.

[13] M. Döbbelin, R. Marcilla, C. Pozo-Gonzalo and D. Mecerreyes, *J. Mater. Chem*, 2010, **20**, 7613-7622.

[14] A. Bund, S. Neudeck, *Journal of Physical Chemistry B*, 2004, **108**, 17845-17850.

[15] H. Randriamahazaka, T. Bonnotte, V. Noël, P. Martin, J. Ghilane, K. Asaka and J-C Lacroix, *Journal of the Physical Chemistry B*, 2011, **115**, 205-216.

[16] N. Levy, M. D. Levi, D. Aurbach, R. Demadrille and A. Pron, *Journal of Physical Chemistry C*, 2010, **114**, 16823-16831.

[17] R. B. Leron, A. N. Soriano, M-H Li, *Journal of the Taiwan Institute of Chemical Engineeres*, 2012, **43**, 551-557.

[18] C. D'Agostino, R. C. Harris, A. P. Abbott, L. F. Gladden and M. D. Mantle, *Physical Chemistry Chemical Physics*, 2011, **13**, 21383-21391.

[19] A. R. Hillman, K. S. Ryder, V. C. Ferreira, C.J. Zaleski, E.Vieil, *Electrochimica Acta*, 2013, **110**, 418-427.

[20] A. R. Hillman, K. S. Ryder, C. J. Zaleski, V. Ferreira, C. A. Beasley, E. Vieil, *Electrochimica Acta,* 2014, accepted manuscript.

[21] M. Skompska, J. Mieczkowski, R. Holze and J. Heinze, *Journal of Electroanalytical Chemistry*, 2005, **577**, 9-17.

[22] M. J. Brown, A. R. Hillman, S. J. Martin, R. W. Cernosek and H. L. Bandey, *Journal of Materials Chemistry*, 2000, **10**, 115-126.

[23] V. Noël, H. Randriamahazaka, C. Chevrot. *Journal of Electroanalytical Chemistry*, 2003, **542**, 33-38.

[24] L. M. Abrantes, J. P. Correia, *Electrochimica Acta*, 1999, **44**, 1901-1910.

[25] H. Randriamahazaka, C. Plesse, D. Teyssié, C. Chevrot, *Electrochemistry Communications*, 2003, **5**, 613-617.

[26] C. Laslau, D. E. Williams, B. E. Wright and J. Travas-Sejdic, *Journal of the American Chemical Society,* 2011, **133**, 5748-5751.

[27] L. T. T. Kim, C. Gabrielli, A. Pailleret, H. Perrot, *Electrochmica Acta*, 2011, **56**, 3516-3525.

[28] F. Miomandre, M. N. Bussac, E. Vieil, L. Zuppiroli, *Chemical Physics*, 2000, **255**, 291.

[29] T. F. Otero, H. J. Grande and J. Rodriguez, *The Journal of Physical Chemistry B*, 1999, **44**, 1893.

[30] H. Grande, T.F. Otero, *Journal of Physical Chemistry B*, **1998**, 102, 7535-7540.

[31] A.R. Hillman, M. A. Mohamoud, *Electrochimica Acta*, 2006, **51**, 6018-6024.

[32] A. R. Hillman, *Journal of Solid State Electrochemistry*, 2011, **15**,1647–1660.

[33] M. J. Henderson, A. R. Hillman, E. Vieil, *Journal of Electroanalytical Chemistry*, 1998, **454**, 1-8.

[34] Q. Zhang, K. D. O. Vigier, S. Royer and F. Jérôme, *Chemical Society Reviews*, 2012, **41**, 7108-7146.

[35] G. G. Lang, C. A. Barbero, *Laser Techniques for the Study of Electrode Processes*, Berlin, 2012.

[36] M. J. Henderson, A. R. Hillman, E. Vieil, C. Lopez, *Journal of Electroanalytical Chemistry*, 1998, **458**, 214-248.

[37] S. Bruckenstein, K. Brzezinska, A. R. Hillman, *Electrochimica Acta*, 2000, **45**, 3801-3811.

[38] C. A Barbero, M. C. Miras, *The Journal of the Argentine Chemical Society*, 2003, **91**, 1-40.

[39] M. A. Voronytsev, C. Lopez and E. Vieil, *Journal of the Electroanalytical Chemistry*, 1994, **368**, 155-163.

[40] M. A. Skopek, M. A. Mohamoud, K. S. Ryder and A. R. Hillman, *Chemical Communications*, 2009, 935-937.

[41] A. P. Abbott, G. Capper and S. Gray, *Physical Chemistry Chemical Physics*, 2006, **7**, 803-806.

[42] A. P. Abbott, D. Boothby, G. Capper, D. L. Davies and R. K. Rasheed, *Journal of the American Chemical Society*, 2004, **126**, 9142-9147.

[43] A. P. Abbott, K. El Ttaib, G. Frisch, K. J. McKenzie and K. S. Ryder, *Physical Chemistry Chemical Physics*, 2009, **11**, 4269-4277.

[44] C. A. Barbero, *Physical Chemistry Chemical Physics*, 2005, **7**, 1885-1899.

[45] Y. P. Kayinamura, J. H. Roberts and J. F. Robinson, *Applied Materials and Interfaces*, 2012, **4**, 1601-1607.

[46] J. P. Correia, E. Vieil, L. M. Abrantes, *Journal of Electroanalytical Chemistry*, 2004, **573**, 299-306.

[47] A. J. Downard, D. Pletcher, *Journal of Electroanalytical Chemistry*, 1986, **206**, 139-145.

[48] T. A. Skotheim, J.R. Reynolds (Ed.): *Handbook of Conducting polymers*, New York, 2007.

[49] E. P. Cintra, R. M. Torresi, G. Louarn, S. I. Córdoba de Torresi, *Electrochimica Acta*, 2004, **49**, 1409-1415.

[50] M. C. Pham, J. Moslih, C, Barbero, O. Haas, *Journal of Electroanalytical Chemistry*, 1991, **316**, 143-154.

Chapter V

Metal deposition/dissolution in Deep Eutectic Solvents

5.1 Introduction

5.1.1 Aims and scope

The number and complexity of factors influencing the electrodeposition of metals remains a considerable challenge in this important industrial process. [1]

The main aim of this chapter is the investigation of the electrode/electrolyte interfacial kinetics during the metal deposition/dissolution processes performed in ionic fluids. This task has been achieved through a novel application of a combined optical-gravimetric technique. Accomplishing the first aim allow for fulfilment of the second one. The second aim is targeted at expanding our knowledge of behaviour displayed by metal ions in fully ionic environments. It is generally accepted that metal ions in aqueous solutions are stabilized through the formation of the solvation shell.[2] In ionic liquids and deep eutectic solvents (DES), metal ion is assumed to be 'naked' and its stability is reliant on its interactions with surrounding counter ions from the solvent. Third and final aim of this chapter was to investigate the individual metal ions speciations as well as the ionic fluxes present during co-deposition of metals in DES.

Optical deflection technique is not a structural probe and therefore this type of analysis provides circumstantial rather than factual evidence. Because of this the analysed metal/solvent systems were chosen on the basis of the previous work conducted using structural probes.

5.1.2 Electrodeposition of metals – historical development and industrial importance

Metal plating is an essential industrial process with a wide variety of applications. Among various methods of metal film deposition onto substrates such as

chemical vapour deposition (CVD), physical vapour deposition (PVD) and sputtering, the electrochemical methods (electrolytic and electroless) proved to be the most productive and adaptable to various conditions while being at the same time the least expensive ones.[3]

Historically, metal plating had been based on the use of aqueous solutions. A variety of organic and inorganic solvents has also been used for the electroplating of metals with various results (see Chapter I).[2] These media do posses some unquestionable advantages such as high solubility for supporting electrolytes and metal salts allowing for the formation of highly conductive plating solutions. In addition, due to their inherent low viscosity they have very high throwing power. This allows for efficient plating of complex shapes and confined internal surfaces. However, these solvents' applications are hampered by a variety of shortcomings, namely narrow potential windows, toxicity of ligands used, corrosiveness due to acidic and alkaline additives and in the case of molecular solvents like acetonitrile - volatility. Application of ionic liquids is of great interest to the metal plating industry as it can offer the route to improve the existing processes as well as enable the electrodeposition of very electronegative or water sensitive coatings like light (Aluminium) and refractory (Titanium) metals as well as elemental and alloyed semiconductors[4] and photovoltaic like Selenium. [5]

Electrodeposition of silver

Both electrolytic and electroless silver deposition processes are widely used in the plating industry. Superior electrical conductivity of silver and this metals' very good solderability makes this process particularly important in an electronics manufacture. [6] Commercial plating is usually conducted using aqueous solutions of $AgNO_3/HNO_3$ or AgSCN.[7] Environmental concerns arise from the use of this technology, these concerns combine with the technical difficulties in formation of thick Ag coatings (currently necessitating the use of Pd catalysts). Thus, there is an increasing need for the research into silver plating from ionic liquids and deep eutectic liquids.[8] Silver deposition from DES has been reported several times. All authors unambiguously agreed that the deposition from silver halides dissolved in chloride rich DES results in a formation of porous metallic silver films. Gu et al. concluded that this effect is a consequence of a

radically different environment encountered by silver ions resulting in a different metal ion speciation.[5]

Electrodeposition of copper

Copper plays a major role in modern metallurgy. Due to its very high electrical conductivity (surpassed only by silver), it is used on a major scale in the electronic industry.[9] Additionally, the ease of co-deposition and excellent corrosion resistance makes it a particularly suitable plating material for an automotive industry.[2] Copper is often applied as a preliminary layer for metals considered difficult to electroplate like, zinc alloys and magnesium alloys, prior to further plating.[10] It is also used for electrotypes in the printing industry, as a plumbing material, and for a variety of decorative purposes. Copper is also an important precursor for the production of selenium based semiconductors.[5] Electroplating from aqueous solutions of copper salts based on phosphates and cyanides are among the most common industrial electroplating techniques.[11]

Novel solvents, namely chloroaluminate ionic liquids (IL's) were deployed in the 1960's to improve copper plating as the aqueous solvent based solutions suffered from numerous drawbacks including low energy efficiency, toxic effluents and fumes. Unfortunately, their application was hampered by these solvents sensitivity to air and moisture. Subsequent introduction of [BF_4^-] and [Tf_2N^-] based, air and moisture insensitive IL improved the prospects of novel methods developments. More recently, the advent of Deep Eutectic Solvents (DES) presented first viable alternative for the currently dominating technologies. DES are a subclass of IL's reviewed elsewhere (see Chapter I). Although the underlying chemistry is different, the formed liquid consists entirely of charged species like a 'classic' IL. DES are biodegradable, inexpensive and straightforward to manufacture.[12] They display excellent solubility for metal oxides[13] as well as metal salts and thus are highly advantageous solvents for industrial electroplating of copper.

Electrodeposition of tin

Good corrosion resistance combined with excellent ductility and non-toxicity makes tin an important metallurgical substrate. Excellent solderability of this metal is of

prime importance for the electronics industry. Additional efforts are also placed on the application of tin plating to replace nickel and chrome plating, tin is also a promising alternative anode for lithium ion batteries.[14] Tin is a constituent of industrially important alloys like Zn-Sn alloy which display superior corrosion resistance even in marine environments.[15] Commercial tin plating usually relies on acid, base or cyanide-based aqueous plating solutions, sulphates, fluoborates and citrates are commonly employed.[16] Hence, the application of non-toxic, non-volatile media like DES presents a very attractive alternative. Deposition of tin[12] and zinc-alloys[13] from eutectic solvents as well as from RTIL[17] have already been reported. The metallic deposits formed were markedly different depending on the ionic liquid used. Both research groups concluded that tin ion speciation and (influenced by it) its diffusion coefficient, control the morphology and the growth rate of metallic deposits.

Electrodeposition of bismuth

Electrodeposition of bismuth is an important although *niche* industrial process. This semimetal has a variety of uses including, but not limited to, serving as a catalyst for electro-reduction of H_2O_2 and O_2,[18] being a component of electrochromic and piezoelectric devices, as well as being a part of bismuth telluride (Bi_2Te_3) which is a core part of thermoelectric materials.[19]

Mao et al.[6] reported electrodeposition of Bi from $BiCl_3$ dissolved in chloro and non-chloroaluminate IL as resulting in a formation of two radically different morphologies of the deposits. Agapescu and co-workers in two (EIS based) studies reported bismuth deposition from urea and oxalic acid based DES to be a diffusion controlled process that results in a continuous deposition of metallic layer.[20,21] Thus, ChCl based DES appear to be an attractive alternative for currently used acid and alkaline based plating solutions, which together with imidazolium IL, are presently employed for Bi plating.

Electrodeposition of bi-metal coatings

Co-deposition of metals is an important industrial process. In the electronics industry, silver is routinely applied to protect the copper tracks of printed circuit boards from oxidation.[3] In semiconductor manufacture, copper is a precursor for compound

semiconductors like $CuInSe_2$.[22] Abbott and co-workers have (by means of acoustic impedance) already investigated co-deposition of the Zn/Sn couple from ChCl-EG and ChCl-Urea deep eutectic solvents.[12] Due to the relative simplicity of this particular system (clear separate redox peaks), it was selected as a subject of proof of concept optical-gravimetric analysis. The underlying reason for the optical analysis was an attempt to observe different metal speciation kinetics and their effect on the deposits growth.

5.2 Metal ion complexation in solution

Research conducted so far indicates that metal ions form complex ions in ionic liquids. For example Te(IV) was reported to form $TeCl_6^{2-}$ anions in EMI-Cl-BF_4 ionic liquid, while Sb(III) was found to form $SbCl_4^-$ upon dissolution in Reline.[16] The electrochemical redox series of metals in Ethaline are shown in figure 1.

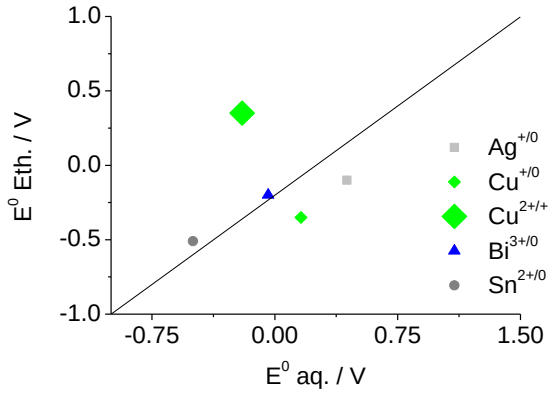

Figure 1. Formal electrode potentials of metals studied in this chapter. Comparison of metal speciation in Ethaline versus metal speciation in an aqueous solution. Data were corrected for the temperature and concentration. Potentials in an aqueous solution were measured versus saturated calomel electrode; potentials in Ethaline were measured versus Ag wire pseudoreference electrode. Line visible in the centre of the graph is the line of equivalence (i.e point at which potentials are the same in both aqueous and ionic solutions). Data used with permission from reference [23].

The line of equivalence determines the stability of the particular metal oxidation state in Ethaline. Oxidation states that are above the line are generally less stable than the ones below the line. Particularly striking is an example of copper, which in Ethaline

displays two clear Cu (I) and Cu(II) speciations which is in a stark contrast to Cu(I) disproportionation observed in aqueous solutions. Kekesi et al. investigated the deposition of copper from chlorinated aqueous solutions and reported that in an aqueous solution with high (> 1.0 M Cl^-) chloride concentrations (e.g. $CuCl_2$/HCl) copper forms stable chloro-complexes.[24] Authors reported the formation of very uneven cathodic deposits upon electrodeposition from this solution. This observation might be a direct evidence of metal ion speciation's influence on the deposit properties. This effect in DES is analysed further in this chapter.

5.3 Application of PBD-EQCM in metal electrodeposition studies

The majority of PBD-EQCM studies described in the literature have so far concentrated on the electroactive polymer films, with different fields like metal deposition not receiving suitable attention. Henderson, Hillman, and co-workers have conducted studies of silver[25] and lead[26] deposition from an aqueous solution, as well as studies of redox chemistry of nickel hydroxide in LiOH[27] while Abrantes et al studied oxidation of hypophosphite on a nickel electrode deposition of nickel.[28] Eriksson reported a comprehensive study of copper deposition from an aqueous solution noting that PBD can resolve concentration profiles down to 1 mM m^{-1}.[29]

Electrolytic (as well as electroless) deposition of metals from room temperature ionic liquids (RTIL) is a rapidly growing field.[2] However, to this date only one optical analysis of metal deposition from ionic liquids has been reported.[30] Fully ionic environments (like ionic liquids or their subclass Deep Eutectic Solvents) represent a significant challenge in terms of optical analysis. Optical deflection originates from electrochemically generated concentration gradients (resulting in the formation of refractive index gradients since these two are inexorably linked). Thus, in a highly concentrated medium the concentration of species in the electrode vicinity is not significantly different from that of a bulk electrolyte. Therefore, the resulting deflection is distinctively smaller than the one observed in dilute electrolytes. As already mentioned (see Chapter IV), rates of diffusion in DES are orders of magnitude lower than in aqueous or organic electrolytes.[31] The optical deflection signal is spatially (*circa* 50 μm) and therefore temporally separated from the electrodes' surface. This results in a

temporal separation of the signals as the diffusion of the species is subject to a (viscosity controlled) propagation delay. Thus, DES high viscosity is the main impediment of the quantitative PBD analysis in these ionic media.

DES chemistry relies on the hydrogen bonding which provides charge delocalization between the halide ion and the hydrogen bond donor. Elucidation of ionic species formed upon dissolution of metal salts is therefore a difficult task due to these bonds instability. The commonly deployed mass spectrometry often gives inconclusive results due to the species fragmentation during the ionization process.[32] Non-invasive, affordable technique of combined optical-gravimetric measurements provides an excellent tool to gain a unique insight into the DES based electroplating of metals. Coupling of these methodologies is thought to be especially advantageous as it exploits PBD sensitivity with the reliability of EQCM.[26]

5.4 Objectives

Deposition of metals in DES, has not been previously a subject of the optical analysis. Thus, the first objective of this chapter was overcoming of the viscosity obstruction in order to generate *qualitative* results of the electroplating process.

Successful achievement of the first objective formed then a base of objective two, which was the *quantitative* evaluation of the optical response.

Speciation of metals during electroplating is of profound importance in electroplating as the type (size, charge) of the species formed, affects the process thermodynamics. Each ion complexation has a different refractive index making the optical deflection a suitable tool for their analysis. Thus, PBD-EQCM can provide an ideal tool for the real-time, non-invasive, quantitative detection of the number and amount of the species present during the electrodeposition process. This has been so far the exclusive domain of an expensive and very complex EXAFS and PNG-NMR techniques.[33] Therefore, this chapters' third objective is the application of PBD-EQCM in metal ion complexation studies. This is achieved through the study of systems with known complexation patterns.

It must be mentioned here that optical deflection analysis is unable to provide any structural information about the metal ion solvation shell and therefore PBD can only be used as a complementary tool in the studies of metal ion speciation.

Co-deposition of metals is an important part of the plating industry, particularly for the automotive industry. Complexity and number of species formed in the electrolyte during the plating process has a tremendous impact on the process efficiency and therefore on the quality of the coatings formed. Thus, the fourth and final objective of this chapter is the optical analysis of the metals co-deposition from DES. The aim of this objective was to provide an insight into the kinetics and relative magnitudes of the individual ionic fluxes present during the process and to test feasibility of PBD to study this type of reactions in ionic media.

5.5 Results and discussion

5.5.1 Formulation of the analytical standard. EQCM-PBD study of a mass transport during the electrodeposition-dissolution of silver from $AgNO_3$ in $HClO_4$ aq.

The process of silver deposition/dissolution in an aqueous solution of perchloric acid has been the subject of the first quantitative PBD – EQCM analysis.[23] Simplicity of the process results from its uncomplicated redox chemistry ($Ag^+ \rightarrow Ag^0$) as well as high refractivity of silver, its high molar mass, and ease of plating. Henderson and co-workers have proved that Ag^+ is the only significant charge carrier in this process and that the data from i, Δm and θ signals are fully consistent and are in fact different manifestations of the same process.

The goal of this analysis was then to repeat Henderson's original study but at a reduced distance of approach. The optical deflection reported in the original study was delayed by 2 – 3 s (in comparison to the instantaneous electric and gravimetric signals). This was a result of the relatively large beam-electrode distance of 155 μm. Another detrimental effect of the large electrode-beam gap was the open form (i.e. the end value of the optical deflection signal was different from the initial one) of the cyclic deflectograms obtained, being in stark contrast with closed forms of both voltammograms and massograms (i. e. the end values of these signals were equal to the initial ones). This undoubtedly resulted in reported difficulties of the data quantification. Hence, the original experiments were reproduced using a modified experimental setup (see Chapter II – experimental) with the distance of approach reduced by half. The

simultaneously recorded *i*, Δm and θ responses to silver deposition/dissolution are shown in figure 2.

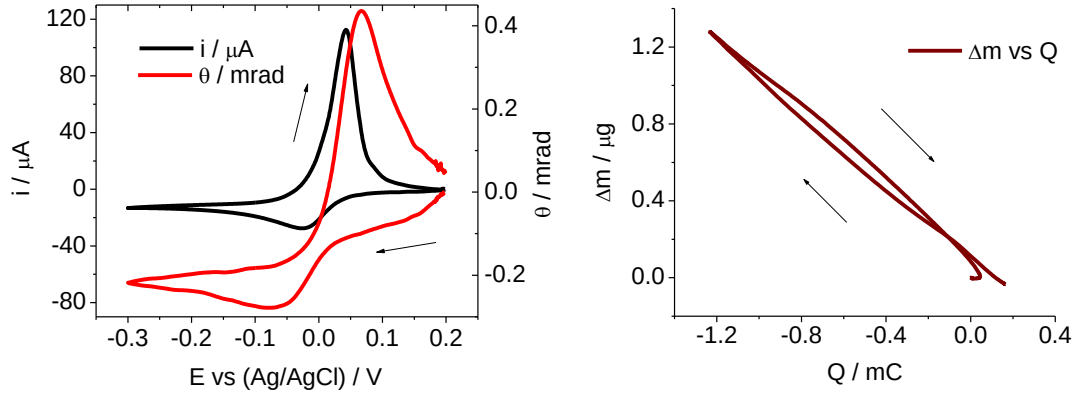

Figure 2. Left panel: cyclic voltammogram (black line) and cyclic deflectogram (red line) recorded during redox deposition-dissolution of elemental Ag from 0.001 M $AgNO_3$ in 0.2 M $HClO_4$ aq. ν = 5 mV s^{-1}, potential window applied 0.2 V → - 0.3 V → 0.2 V. $\mathbf{Q_{dep}}$ = 5.65 mC cm^{-2}. Right panel: corresponding mass change (Δm) versus charge (Q) plot.

The mass changes were calculated using the Sauerbrey equation, therefore assuming the rigidity of the deposited metal.[34] The deposit thickness was calculated to be ca 2.8 μm. Considering the average roughness of the AT-cut Au plated polished quartz resonators (used throughout this study) being on the order of 1 μm[35] one can safely assume that this deposit morphology will closely follow the one of the underlying quartz resonator. The current response (figure 2, left panel) displays typical reversible Ag^+/Ag^0 couple. Reduction of both the sweep rate (10 and 20 mV s^{-1} in the original experiments as opposed to 5 mV s^{-1} used here) and the beam-electrode distance (155 → 74 μm) resulted in a significantly improved optical signal of a closed form and bearing a very close resemblance of the current. Deflection profile (figure 2, left panel) is symmetrical showing clear negative deflection peak during reduction (result of a diminished silver ions concentration in the point of focus being a result of silver deposition) and a clear positive deflection peak during oxidation (a result of silver ion concentration increase during metal deposit dissolution into the electrolyte).

Correlation of mass and charge are shown in the right panel of figure 2. Faraday's law implies that an exchange of a single ion (in this case, electrodeposition from single metal specie) will always result in linearity of a Δm/Q profile. Any

deviation from this is then considered to be an evidence of other contributors. The gradient of Δm/Q plot allowed for the calculation of mobile species mass (henceforth abbreviated as MS_M) as 95 g mol $^{-1}$ (+ in the reduction part, - in the oxidation part) which is in a good agreement with molar mass of silver (107.62 g mol $^{-1}$). Small hysteresis visible in the plot can be assigned to the movement of the other species present (H^+, NO_3^- and ClO_4^-) in the electrolyte. Another possible reason for the hysteresis present even at this low sweep rate was previously described by Henderson as possibly originating from rapid changes in the electrolyte local density.[23] Upon dissolution, the *circa* 2.8 μm thick layer of metal is released into the solution within approximately 60 s. This results in a concentration increase, and considering silver mass, significant change in liquid density within the acoustic wave penetration depth. The penetration depth is described by the following equation as:

$$Depth = \sqrt{\frac{\upsilon_L}{\pi f_0}} \qquad \textbf{[1]}$$

Where υ_L is the kinematic viscosity of the solution (i.e. viscosity multiplied by density) and f_0 is the quartz resonator initial frequency. Simple calculation, assuming f_o = 10 MHz and viscosity of 1 cP, returns the value of the penetration depth as *circa* 178 nm. Rapid dissolution of the silver deposit followed by the subsequent increase in density and viscosity may result in a change of the resonator oscillation frequency (process colloquially known as 'damping').

The propagation delay was removed by an application of the convolution protocol (see Chapter IV). Using the experimental optical data (single peak recorded upon dissolution infers only one metal ion speciation being present), charge passed in the redox process (Q_{pas}) and gravimetric signal (Δm/Q plot indicating that Ag^+ is the only mobile specie) the following assumptions were formed:

1. The flux of Ag^+ species is the major (i.e the only significant one) species exchanged between the electrode and the bathing electrolyte as this is the only specie which can be deposited on the electrodes' surface. Therefore the reaction proceeds as follows:

$$\mathbf{Ag^+ + e^- \rightarrow Ag^0}$$

and

$$\mathbf{Ag^0 - e^- \rightarrow Ag^+ + NO_3^- \rightarrow AgNO_3}$$

2. The flux of Ag^+ species in the optical deflection zone is related to the Ag^+ flux at the electrode by the following equation:

$$J_{Ag^+NO_3^-(x,t)} = F_{(x,t)} \times J_{Ag^+NO_3^-(0,t)} \quad \textbf{[2]}$$

Where F is the mass transfer function through the equation 3:

$$F_{(x,t)} = \left(\frac{x}{2\sqrt{\pi D t^3}}\right) e^{\frac{-x^2}{4Dt}} \quad \textbf{[3]}$$

Where D is the diffusion coefficient of the mobile species (here treated as a coupled diffusion for $AgNO_3$ specie. Concentration gradient induced beam deviation is usually described by the following expression[36]:

$$\theta = -\frac{l}{n}\frac{\delta n}{\delta c}\frac{1}{D} J_{(x,t)} \quad \textbf{[4]}$$

Where θ denotes the beam deviation. The experimental arrangement used in this study (see Chapter II) resulted in the positive deflection indicating metal dissolution (decay of the concentration profile into the electrolyte) and negative deflection indicating metal deposition (decrease in Ag^+ concentration in the electrode vicinity). Thus, the application of Fick's 1st law of diffusion[37] (which relates the measured current to the resulting mass transport) allows for the beam deviation to be expressed as:

$$\theta_{(x,t)} = -\frac{h_{Ag^+}L}{z_{Ag^+}FA} F_{(x,t)} \times i_{(x,t)} \quad \textbf{[5]}$$

Where *h* is the convolution factor which can be calculated the following way:

$$h = -\left(\frac{1}{n}\frac{\delta n}{\delta c}\frac{1}{D}\right) \quad \textbf{[6]}$$

As it was already mentioned in Chapter IV, a general indicator for a successful quantitative optical analysis requires the form of the electrochemically generated optical signal to resemble the current. Analysis of the left panel of figure 2 revealed the evident similarity of the electric and optical profiles. This forms a firm footing for a quantitative analysis. Comparison of the differential form of the signals (convolved current ($i_{(x,t)}$hL/zFA) and convolved mass variation (($dM_{(x,t)}$/dt)zFAhl/mAg^+) superimposed onto the experimental optical response displays good correlation (see left panel of figure 3) although the convolved current deviates slightly form θ during the deposition process while matching it more closely during the dissolution.

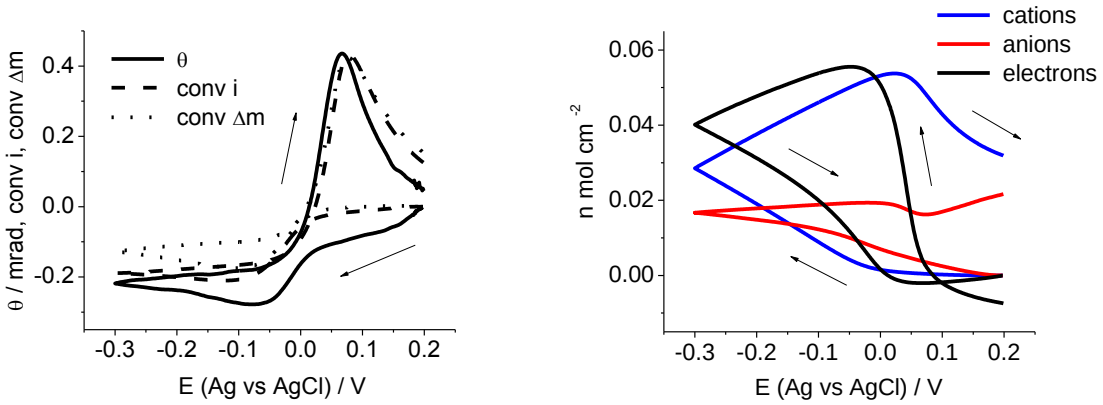

Figure 3. Left panel: solid line - experimental beam deflection (θ), dashed line - convolved current ($i_{(x,t)}$hL/zFA) and dotted line - convolved mass variation (($dM_{(x,t)}$/dt)zFAhl/m_{Ag^+}. Right panel: Comparison of the convolved signal integrals.

As for the convolved mass the same effect is even more profound. Such effects have previously been assigned to the effects of the supporting electrolyte (0.2 M $HClO_4$ aq.) [23] The integral form of the signals is shown in the right panel of figure 3. The equal in magnitude and opposite in directions fluxes of the metal cations (blue line) and of the electrons (black line) confirm the overall reaction as:

$$\mathbf{M^+ + e^- \rightarrow M^0}$$

Although two anionic species are present, NO_3^- and ClO_4^-, the latter concentration is 200 times higher (0.2 M vs. 0.001 M), thus, it is the perchlorate anion that is treated as anion is the convolution analysis) and solvent movements are consistent with the differential form of the signal. Figure 4 contains the plot of x/√D values (see equation 3) calculated at various approach distances. From this plot the

beam electrode distance was calculated as 73.9 μm and the coupled diffusion coefficient for silver nitrate as D_{AgNO_3} = 2.83 × 10^{-5} cm^2 s^{-1}. This value is in agreement with result obtained by Henderson et al.[23] as well as the value reported by Barbero et al. for a study of $AgClO_4$ in $HClO_4$ aq.[38]

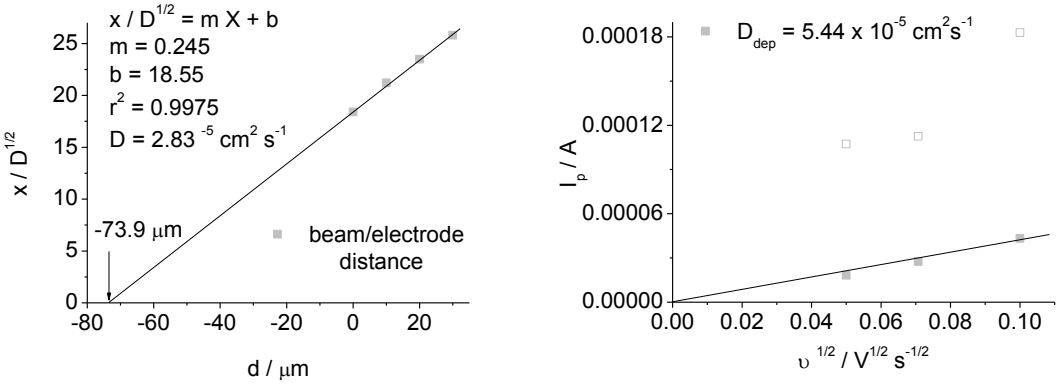

Figure 4. Plot of the convolution parameter (x/√D) expressed as a function of the relative beam deflection. Extrapolation of the linearity reveals absolute beam electrode distance (here 73.9 μm). Right panel: I_p – ν ½ linear plots for cathodic deposition (grey squares) and anodic dissolution (white squares) of Ag from Ag films deposited on Au-plated electrode (0.23 cm^2) from 0.001 $AgNO_3$ in 0.2 M $HClO_4$ aq.

Decrease of the electrode beam distance resulted in a closed form of the optical signal, unlike the signal obtained in the original study. This is a desired result as the current signal also has a closed from and good quality optical signal is expected to have the same pattern. The kinetics of silver deposition-dissolution were also probed through plotting I_p – ν ½ dependencies. Although an increase of peak current with the square root of the scan rate was found for all scan rates upon both deposition as well as dissolution, linear correlation of I_p vs √ν was observed only upon the deposition process. The diffusional control observed during deposition allowed for the application of Randles-Sevcik equation for a reversible metal deposition:

$$I_p = 0.6104\, nFAc\sqrt{\frac{nF}{RT}}\,vD \qquad \textbf{[7]}$$

Rearrangement of equation 7 allowed to calculate the diffusion coefficient of D_{AgNO_3} = 5.44 × 10^{-5} cm^2 s^{-1}

Good correlation between the experimental and convolved signals as well as the excellent signal-to-noise ratio confirmed the validity and robustness of the original experimental protocol, while improving the experimental setup sensitivity. Thus, a solid foundation was formed for the more challenging optical analysis in DES.

5.5.2 Application of the PBD-EQCM in the novel environment of Deep Eutectic Solvents.

Transition of the optical deflection analysis from a low viscosity, aqueous or organic solvent based electrolytes to a high viscosity, low diffusivity ionic liquids proved to be a challenging task

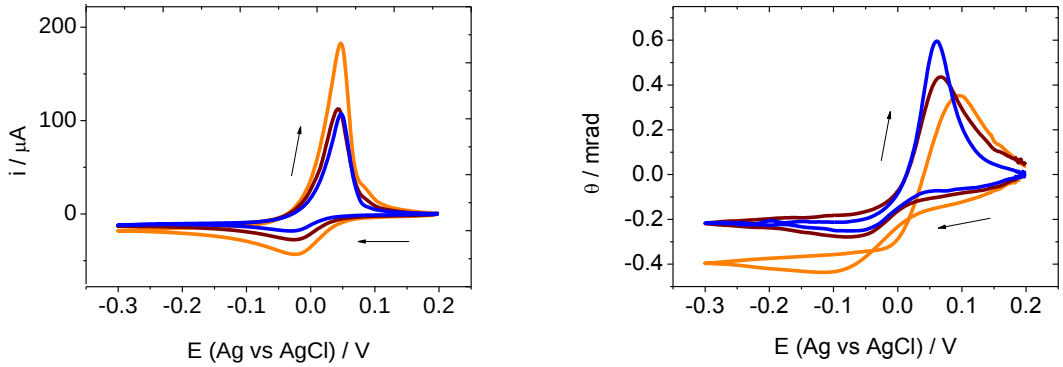

Figure 5. Left panel: Cyclic voltammograms of 0.001 M $AgNO_3$ in 0.2 M $HClO_4$. Potential window applied 0.2 V → – 0.3 V → 0.2 V. ν = 10 mV s^{-1} (orange line), 5 mV s^{-1} (blue line), 2.5 mV s^{-1} (black line). Right panel: corresponding deflectograms, x_0 = 73.9 μm.

The *i/θ* correlation for an aqueous solution is presented in figure 5 above. It can be noted that the magnitudes of both current and optical deflection increase with ν and all optical profiles recorded (at 10, 5 and 2.5 mV s^{-1}) resemble the electrochemical (i.e. current) profiles. Figure 6 contains the optical transients recorded during silver deposition/dissolution from 0.01 M AgCl dissolved in Ethaline 200 (1 mole Ch^+Cl^- + 2 moles of EG), at 39.9 μm distance of approach using five different sweep rates. The reducible silver species in this DES were previously found to be co-ordinately unsaturated $AgCl_2^-$ and $AgCl_3^{2-}$.[6] Due to the different shape and local density of ligand shells of these two speciations it is reasonable to expect them to possess different refractive indexes. No previous work on this subject has ever been published but it was

thought reasonable to expect double peak in a deflectogram of AgCl in Ethaline 200, with each peak assigned to individual species. The progressive diminishing of the scan rate revealed (at 0.25 mV s^{-1}) a poorly resolved double peak in the oxidation (i.e. dissolution) regime. Further sweep rate reduction (to 0.0625 mV s^{-1}) revealed a well-defined double peak present in the deflectogram.

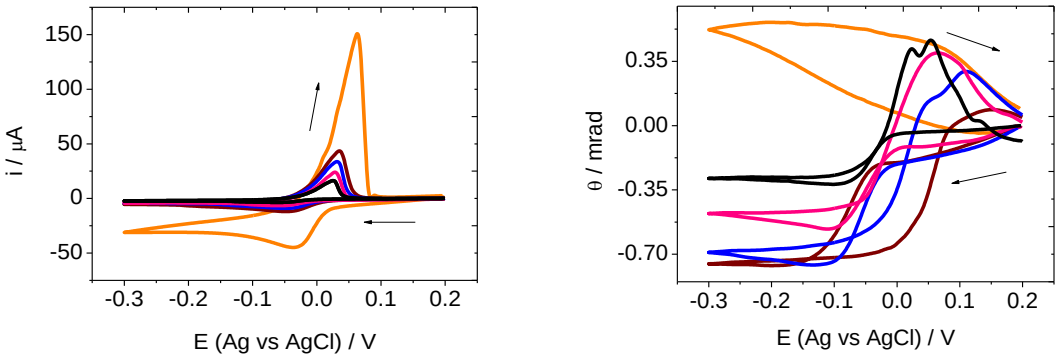

Figure 6. Left panel: Cyclic voltammograms of 0.01 M AgCl in Ethaline 200. Potential window applied 0.2 V → – 0.3 V → 0.2 V. ν = 5 mV s^{-1} (orange line), 0.5 mV s^{-1} (brown line), 0.25 mV s^{-1} (blue line), 0.125 mV s^{-1} (pink line) and 0.0625 mV s^{-1} (black line). Right panel: corresponding deflectograms, x_0 = 39.9 μm.

The above result is an indicator of the viscosity barrier present in ionic liquids, being overcome at a low sweep rate (i.e. optical sampling rate matches the slow deposition rate). The correlation of viscosity increase and the necessary sweep rate decrease was found to be linear. For an aqueous solution of silver nitrate (cP *circa* 1) the 2.5 mV s^{-1} sweep rate yielded high quality deflectogram, obtaining comparable quality of signal in the solution of silver chloride in Ethaline (cP *circa* 40) required a 40 fold decrease of the scan rate (2.5 → 0.0625 mV s^{-1}). This allows forming preliminary assumptions about the scan rate modifications necessary for the optical analysis in more viscous DES. In this study, $AgCl_{2/3}^{-/-2}$, $CuCl_{2/4}^{-/-2}$, $SnCl_4^{-2}$ and $BiCl_4^-$ complex species were formed by dissolution of AgCl, $CuCl_2$, $SnCl_2$ and $BiCl_3$ precursors in chlorine rich ionic liquid. Therefore, it seems reasonable to assume for the metal ions to display similar behaviour as in a highly concentrated aqueous solutions of chlorine. Then, the following electron transfer process may describe the direct discharge of ions to yield elementary metals:

$$\mathbf{MCl_n^- + m\,e^- \rightarrow M + nCl^-}$$

As the number of chloride ligands depends on the metal oxidation state, the identity of metal determines metal-chloride complex (MCl_n^-) mass, shape and thus its refractive index as well as its' mobility. This principle allows observing *in situ* changes of different oxidation states.

5.5.3 EQCM-PBD study of mass transport during the electrodeposition-dissolution of silver from AgCl in Ethaline 200.

Choline chloride based DES display excellent solubility for metal halides.[39] Metal nitrates however are not very soluble in these solvents. For this reason and due to the previous research on this subject deposition/dissolution of silver from silver chloride dissolved in Ethaline 200 was chosen as a proof of concept for the feasibility of PBD-EQCM in ionic liquids. High viscosity of the ionic media inevitably results in a diminished mass transport as compared to diffusion rates observed in molecular solvents. Hillman et al have already reported this effect in a recent study of PEDOT films redox dynamics in DES.[40] In order to make optical analysis achievable the electrode-beam distance was reduced further to *circa* 40 µm. Simultaneously recorded optical and electrochemical signals are shown in the left panel of figure 7.

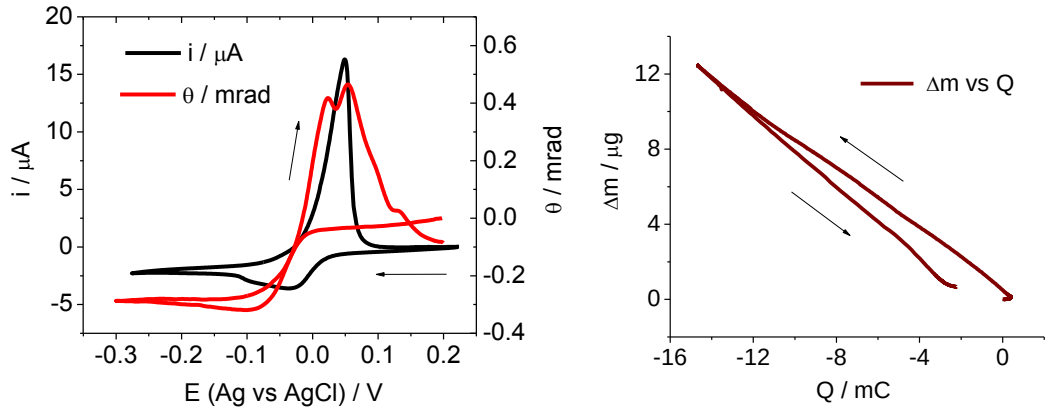

Figure 7. Left panel: cyclic voltammogram (black line) and cyclic deflectogram (red line) recorded during redox deposition-dissolution of elemental Ag from 0.01 M AgCl in Ethaline 200. ν = 0.0625 mV s^{-1}, potential window applied 0.2 V → - 0.3 V → 0.2 V. $\mathbf{Q_{dep}}$ = 53 mC cm^{-2}. Right panel: corresponding mass change (Δm) versus charge (Q) plot.

Low diffusion rate, observed in DES, results in a delay of *circa* 800 sec during the deposition part of the CV. In the aqueous solvent, this delay was *circa* 3 sec so simple calculation reveals that (considering the different distances of approach used) the diffusion in Ethaline is approximately 500 times slower as compared to the aqueous solution. This is possibly not only the effect of the increase in viscosity but also of the different speciation of silver in ChCl based DES. An EXAFS study has previously mentioned silver speciation as an average of 2.5 chlorine ions per silver cationThese results suggest a mixture of $AgCl_2^-$ and $AgCl_3^{2-}$. Analysis of the deflectogram (figure 7, left panel) shows two clear peaks present in the anodic regime. Although the complete baseline separation has not been achieved, the doublet's mere presence confirms the existence of two silver speciations. Abbott et al have applied EXAFS in studies of AgCl/Ethaline system in a static mode (i.e. metal speciation was observed in a static environment, without the application of any potential). PBD is a quantitative technique that is by default applied in a dynamic mode (i.e. upon application of a potential). Integration of the respective optical signals reveals that the silver speciations are in 1:1.15 ratios. Since EXAFS experiments were conducted on the metal salt solution *ex-sitiu* (i.e. in the absence of any electrochemical process), no direct comparison of the optical and X- ray data can be made. It can be however reasoned that the first peak observed during the oxidation (i.e. during the dissolution of the silver layer) phase represents $AgCl_3^{2-}$ and the second one $AgCl_2^-$. This is based on the assumption that upon the release of silver ions from the quartz oscillator electrode's surface three chloride specie forms first as its formation is initially favourable (requires only 1 Ag + 3Cl) as the relatively small amount of silver is confronted by an excess of chloride. This is followed by a formation of two chloride specie. This process is more favourable at the later stage of metal layer dissolution as the concentration of silver increases while one of chloride remains constant. Presence of more than one species in the silver deposition/dissolution process was confirmed by the hysteresis visible in the m/Q plot (figure 7, right panel). Gradient of this graph indicates that during the deposition the MS_M is 78.4 g mol $^{-1}$ and during the dissolution - 93 g mol $^{-1}$. The latter result is in good agreement with the $AgCl_2^-/AgCl_3^{2-}$ ratio obtained from the integration of optical signal. The thickness of the silver deposit was calculated as 12.5 μm. By inference from work published by Abbott et al . this is assumed to be the effect of the formation of nanoporous silver film of a much larger thickness than the one that can be obtained in the aqueous solutions. Formation of this type of morphology suggests the possibility of

electrolyte entrapment in the porous metallic layer. This effect might explain the discrepancy between MS_M observed upon the dissolution process (- 93 g mol^{-1}) and the value expected from the molar mass of silver (- 107.6 g mol^{-1}). Good agreement obtained between the recorded current (*i*) and experimental optical signal (θ) allowed for the convolution protocol to be applied. Presence of the two speciations of metal ions presented difficulties as to the formal identification of the mobile species. This was resolved through assumption of two/three chloride species being present in experimentally determined ratio. Thus, the following set of conditions was used in the setup of the convolution protocol:

1. No adsorption/desorption of chlorocomplexes on the Au plated electrode was observed. Therefore, it can be assumed that the Ag^+ is the only charged specie being exchanged between the electrode and the bathing electrolyte. Thus, the reaction proceeds as follows:

$$\mathbf{Ag^+ + e^- \rightarrow Ag^0}$$

and

$$\mathbf{Ag^0 - e^- \rightarrow Ag^+ + nCl^- \rightarrow AgCl_3^{-2} + AgCl_2^-}$$

2. The flux of Ag^+ species in the optical deflection zone can be quantified using the following equation:

$$J_{Ag^+Cl^-(x,t)} = F_{(x,t)} \times J_{Ag^+Cl^-(0,t)} \quad \textbf{[8]}$$

and by inference from an aqueous system:

$$F_{(x,t)} = \left(\frac{x}{2\sqrt{\pi D t^3}}\right) e^{\frac{-x^2}{4Dt}} \quad \textbf{[9]}$$

Where D is the coupled diffusion coefficient for $AgCl_2^-/AgCl_3^{2-}$ being present in the solution in 1:1.15 ratio. Results of the convolution analysis are visible in figure 8 (left

panel – differential form, right panel – integrated from). Convolved current (dashed line, figure 8, left panel) is superimposed over the experimental optical signal during the deposition (reduction) phase as well as during the most of the oxidation phase.

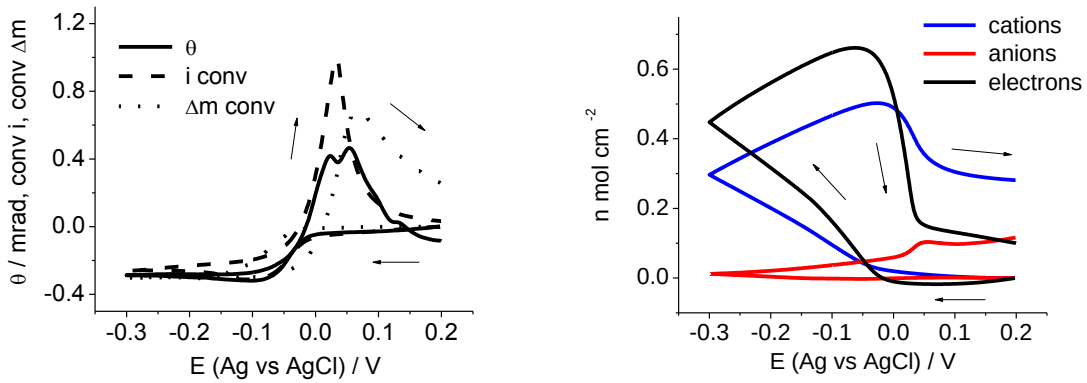

Figure 8. Left panel: solid line - experimental beam deflection (θ), dashed line - convolved current $i_{(x,t)}hL/zFA$, dotted line - convolved mass variation $((dM_{(x,t)}/dt)zFAhl/m_{Ag^+}$. Right panel: Comparison of the convolved signal integrals.

This result can be considered to be a successful validation of the convolution protocol applied. The only discrepancy between the optical signal and convolved current is observed during the maxima of the oxidation phase. This is attributed to the convolution software failing to accommodate the multiple speciations observed. Possible temporal variations in the speciations ratio further complicate analysis. The convolved mass l shows large delay (*circa* 400 s) in the dissolution phase. Such large propagation delay is a result of the diminished diffusion rate in DES. The convolved mass in the reduction phase precedes the flux detection by optical means; in the dissolution phase, a large delay is present. Since convolution protocol uses both PBD (temporally delayed) and EQCM (instantaneous) signals, this indicates that the discrepancy observed is an obvious effect of the diffusional delay. Lack of double peaks in both $i_{(x,t)}hL/zFA$ and $(dM_{(x,t)}/dt)zFAhl/m_{Ag^+}$ values is a result of a sum of both speciations contributing to the convolved signals.

Analysis of the integrated signals (figure 8, right panel) revealed the ratio of the exchanged electrons per silver chloride complexes as 1:1.3. This number, although slightly lower than obtained from the experimental optical response, was compared to it using the following calculations:

Integration of the experimental deflection:

	$AgCl_3^{2-}$	$AgCl_2^-$
electrons	1 e^-	1 e^-
(needed to reduce $Ag^+ \rightarrow Ag^0$)		
experimental signal	1	1.15
(intensity of each complexation)		
convoluted signal	1	1.3
(ratio of electrons exchanged per AgCl complex)		
total (determined experimentally)	1.0 e^- per	1.075 species

integration of convolved mass and current signals (see figure 8, right panel):

1.3 e^- per 1 species

The discrepancy between the numbers of electrons exchanged calculated from the integration of the convoluted signal and the rather qualitative approach of the 'raw' optical signal integration is most likely the result of the propagation delay.

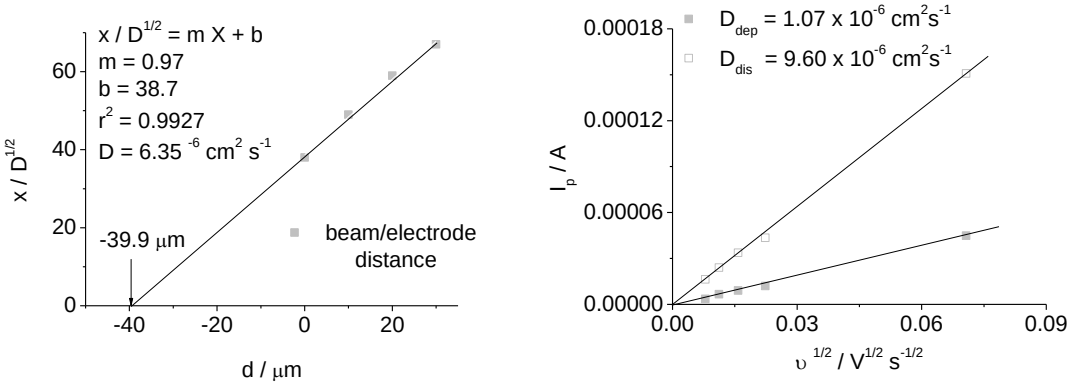

Figure 9. Plot of the convolution parameter ($x/\sqrt{D}$) expressed as a function of the relative beam deflection. Extrapolation of the linearity reveals real beam electrode distance (here 39.9 μm). Right panel: Right panel: $I_p/\nu^{1/2}$ linear plots for cathodic deposition (full squares) and anodic dissolution (empty squares) of Ag from Ag films deposited on Au-plated electrode (0.23 cm^2) from 0.01 M AgCl in Ethaline 200.

In this particular case, the data from raw signal integration is considered more valuable as the convolution protocol has been designed for low viscosity media; additionally, the convolution software in its current form it is unable to accommodate multiple metal ion speciations.[23]

The diffusion coefficient was obtained from $x/\sqrt{D}$ (figure 9, left panel). The gradient of the plot reveals the diffusion coefficient as 6.35×10^{-6} cm^2 s^{-1}. This has been compared to the value of 1.07×10^{-6} cm^2 s^{-1} which has been obtained from the Randles-Sevcik plots obtained for electrochemical transient's recorded at 4 sweep rates (see figure 9, right panel). It is noteworthy that, unlike in aqueous solution of perchloric acid, in Ethaline both cathodic and anodic processes display full linearity of $I_p/v^{½}$ dependences. This indicates diffusion control of both the deposition and dissolution processes with the dissolution proceeding faster ($D = 9.60 \times 10^{-7}$ cm^2 s^{-1}) than the deposition ($D = 1.07 \times 10^{-7}$ cm^2 s^{-1}) as expected.

The AFM image (figure 10), displays evident porous morphology, and a loose packing of the layer structure. This is in a good agreement with the results observed previously by Gu and co-workers.[7] Abbott et al has also previously described the growth of silver deposits from Ethaline to result in a formation of nano-porous Ag layer.[6]

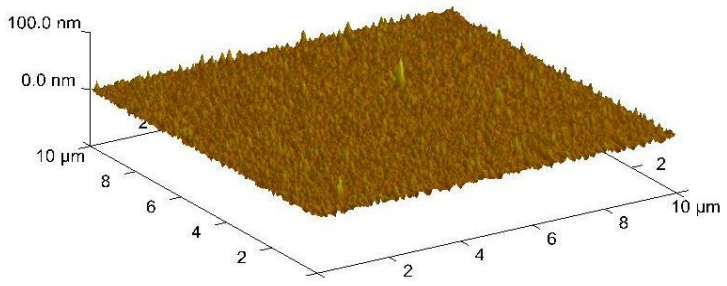

Figure 10. Ex-situ, dry Ag film electrodeposited on Au coated glass slide (A = 1.75 cm^{-2}) from 0.01 M AgCl dissolved in Ethaline 200. Potentiodynamic deposition (3 successive cycles) 0.2 V → - 0.3 V → 0.2 V, ν = 0.0625 mV s^{-1}. $\mathbf{Q_{dep}}$ = 53 mC cm^{-2}.

The optical analysis of the silver electrodepositon from AgCl in Ethaline confirmed the qualitative results of EXAFS study and provided quantitative data on the metal ion speciation. Morphology of the depostis obtained was very similar to the ones

previously reported for the depostion of silver from ChCl based DES. Thickness of the depostis obtained was considered to be a direct result of the silver layer porous nature.

5.5.4 EQCM-PBD study of a mass transport during the electrodeposition-dissolution of copper from $CuCl_2$ in Ethaline.

Being an essential industrial process, electrodeposition of copper has been conducted from a variety of solvents. Choline chloride based eutectics were previously reported to display an excellent solubility for copper salts and oxides and were also described as being capable (with or without the use of additives) of forming stable, copper plating solutions.[10] This has resulted in many ChCl based DES being applied to electrodeposition of copper. Previous research had highlighted the importance of understanding the speciation of metal ions during the electroplating in IL's as well as DES. Analytical tools used previously are either both complex and very expensive (dynamic EXAFS) or produce ambiguous results (FAB – MS). Application of relatively inexpensive, highly sensitive technique like optical deflection allows for the detailed study of the complexation patterns and their influence on the overall plating process. The electrochemistry of copper solutes in ionic liquids has already been reported by Gu, Abbott and other researchers as radically different than the one encountered in aqueous solutions. In the ionic media, copper ions are stabilized only by counter ions from ionic solvent and do not posses solvation shell of the type encountered in aqueous environment.

Experimental optical (θ) and electric (*i*) signals are shown in figure 11. Current displays the well described[8,41] $Cu_I \rightarrow Cu_0$ redox couple ($Cu_I \rightarrow Cu_{II}$ redox couple was deliberately omitted from this study in order to simplify the analysis). The possible presence of Cu^{2+} in this potential region can be most likely attributed to Cu^{+} ions in Ethaline oxidising to Cu^{2+} over time due to the reaction with atmospheric oxygen.

The electrochemically generated optical signal follows the electrochemical signal throughout the deposition phase (figure 11, left panel). In the dissolution phase however, two very well defined peaks (with peaks separation close to a baseline level) are clearly visible.

The reducible species of copper in Ethaline 200 were previously reported to exist as $CuCl_4^{2-}$ and $CuCl_2^{-}$.[10] However, the potential window applied in this experiment deliberately omits higher oxidation state of copper (Cu^{II}), hence $CuCl_2^{-}$

should theoretically be the only speciation present. By inference from Ag complexation process in Ethaline 200, the optical deflection peaks were assigned to metal ion speciations as follows. Upon the release of Cu^{+} from the metal deposit the complexation of copper cations with chloride results in the formation of $CuCl_2^{-}$. Unlike in silver process, here there are two metal speciations present and at more negative potentials Cu^{+} is the only available copper specie. Additionally, at the onset of the oxidation there is relatively little amount of copper exposed to the abundance of chloride (4.8 M in Ethaline 200). The result of this process is visible as the leftmost peak in the deflectogram. At the more positive potentials, the concentration gradient in the electrode vicinity changes in favour of copper ions. Hence, it is possible that $CuCl_3^{2-}$ becomes the dominant specie. Its formation is visible as a rightmost peak in the deflectogram.

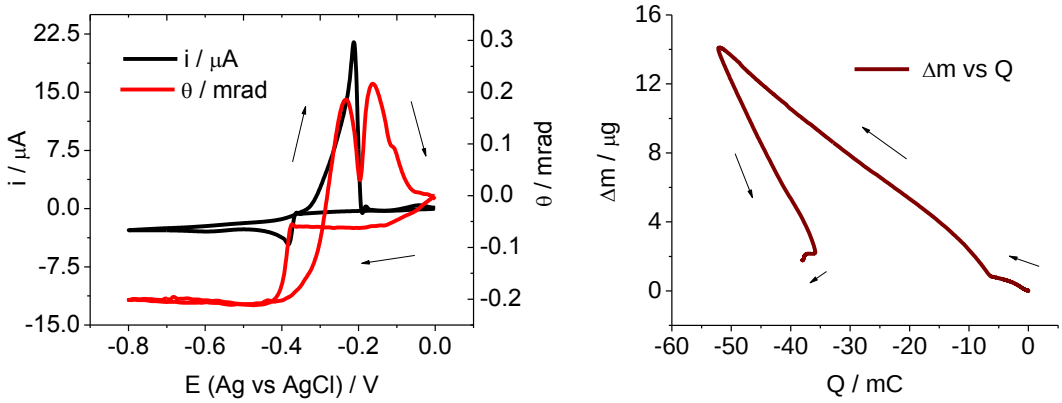

Figure 11. Left panel: cyclic voltammogram (black line) and cyclic deflectogram (red line) recorded during redox deposition-dissolution of elemental Cu from 0.01 M $CuCl_2$ in Ethaline 200. ν = 0.0625 mV s^{-1}, potential window applied 0.0 V → - 0.8 V → 0.0 V. $\mathbf{Q_{dep}}$ = 228.6 mC cm^{-2}. Right panel: corresponding mass change (Δm) versus charge (Q) plot.

Integration of the respective optical deflection peaks reveals the ratio of these two complexes as 1:1.22. Presence of more than one mobile specie is confirmed by the significant hysteresis visible in the Δm/Q plot (figure 11, right panel). Δm/Q gradient recorded during the deposition phase unravels the MS_M being as low as 26.6 g mol^{-1}. This indicates that, although the $Cu^{+} \rightarrow Cu^{0}$ is the major specie balancing the charge on the electrode there is a major involvement from other species as this value is significantly different from molar mass of copper (63.5 g mol^{-1}). Gradient of the

dissolution phase ($Cu^0 \rightarrow Cu^+$) reveals MS_M value as 74.7 g mol $^{-1}$ and this is consistent with the suggested mixture of metal ion complexes. Based on the above predilections, the following assumptions were used in the convolution protocol:

1. Cu^+ is the only charged specie exchanged between the electrode and the bathing electrolyte (copper underpotential deposition which has previously[10] been reported to occur in Ethaline was eliminated through the careful choice of the potential window). Therefore, the reaction proceed as follows:

$$\mathbf{Cu^+ + e^- \rightarrow Cu^0}$$

and

$$\mathbf{Cu^0 - e^- \rightarrow Cu^+ + nCl \rightarrow + CuCl_2^- + CuCl_3^{2-}}$$

2. The copper species flux observed is best described by the following equations

$$J_{Cu^+Cl^-(x,t)} = F_{(x,t)} \times J_{Cu^+Cl^-(0,t)} \quad \textbf{[10]}$$

$$F_{(x,t)} = \left(\frac{x}{2\sqrt{\pi D t^3}}\right) e^{\frac{-x^2}{4Dt}} \quad \textbf{[11]}$$

Where D is the coupled diffusion coefficient of both copper ion speciations being in a ratio specified above (1:1.22). Results of the convolution analysis are visible in figure 12 (left panel – differential form, right panel – integrated from). The convolved mass and current signals show good agreement between each other. However, both of these calculated signals deviate significantly from the experimental optical deflection signal. The difference is most prominent during the deposition phase.

This observation can be attributed mainly to diffusional delay, which in the case of this system is even more prominent than in AgCl/Ethaline system. Integration of the $i_{(x,t)}hL/zFA$ and $(dM_{(x,t)}/dt)zFAhl/m_{Cu^+}$ peaks areas, returns values very similar to the integration of the experimental optical signal. This is expected as the convolution

software returns the total current and mass values without accounting for the specific metal ion speciations that are contained within the signals.

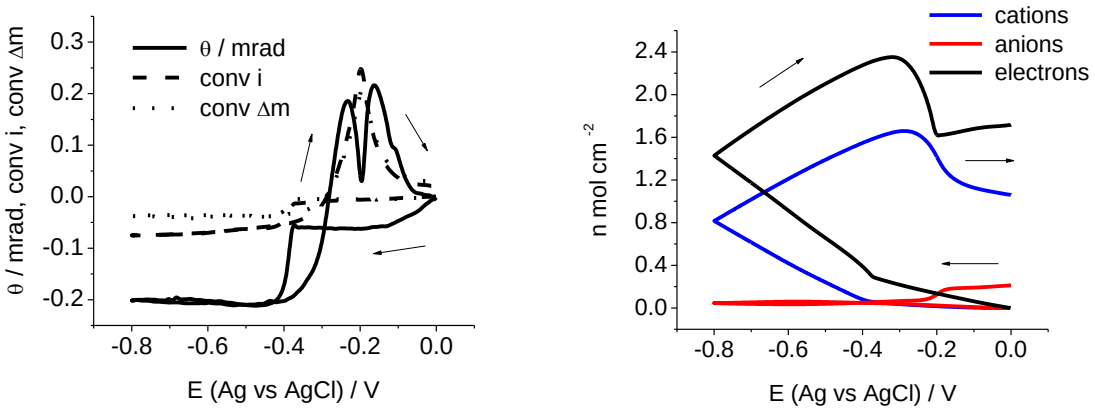

Figure 12. Left panel: solid line - experimental beam deflection (θ), dashed line - convolved current $i_{(x,t)}hL/zFA$, dotted line - convolved mass variation $((dM_{(x,t)}/dt)zFAhl/m_{Cu^+}$. Right panel: Comparison of the convolved signal integrals.

Analysis of the integrated form of the signal (figure 12, right panel) reveals the ratio of electrons-to-cations exchanged in the process as 1:1.4. By inference from silver based process this value was compared to the integration values of the experimental optical deflection signal in the following calculations':

Integration of the experimental deflection:

	$CuCl_2^{2-}$	$CuCl_3^-$
electrons	1 e^-	1 e^-
(needed to reduce $Cu^+ \rightarrow Cu^0$)		
experimental signal	1.22	1
(intensity of each complexation)		
convoluted signal	1	1.4
(ratio of electrons exchanged per $CuCl_n$ complex)		
total (determined experimentally)	1.4 e^- per	1.0 species

integration of convolved mass and current signals (see figure 8, right panel):

1.45 e^- per 1 species

The value obtained from the integration of the convoluted signal is higher than 1.4 e^- per specie resulting from the integration of the convolved signals. However, considering the effects observed for Ag^0/Ag^+ redox behaviour in Ethaline the discrepancy between the θ signal integration and the results obtained from the integration of the convolved current and mass values might also be an effect of the propagation delay. The diffusion coefficient for copper complexes in Ethaline has previously been reported as 3.01×10^{-7} cm^2 s^{-1} (calculated values from ref 10). These are in agreement with the value obtained from the x/√D plots (figure 13, left panel) and the application Randles – Sevcik equation (figure 13, right panel). Similarly to silver, both deposition and dissolution of copper in Ethaline is a diffusion-controlled process.

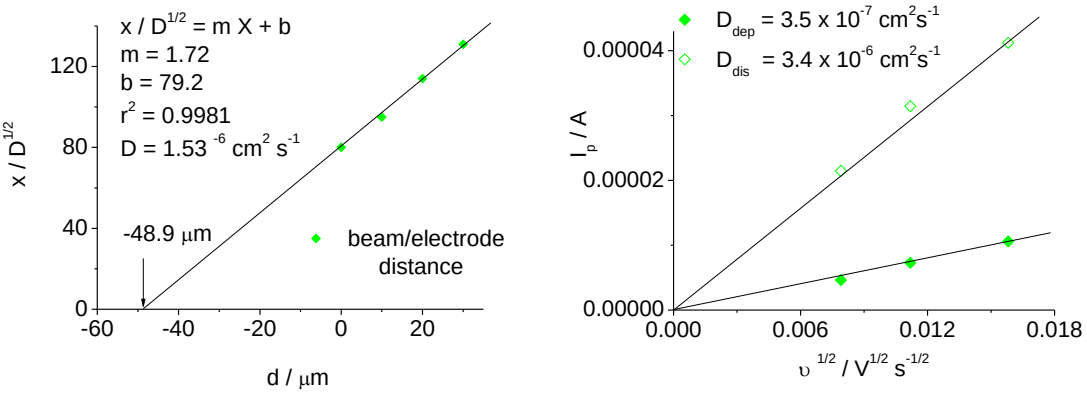

Figure 13. Plot of the convolution parameter (x/√D) expressed as a function of the relative beam deflection. Extrapolation of the linearity reveals real beam electrode distance (here denoted as x_0). Right panel: Right panel: $I_p/ \nu^{½}$ linear plots for cathodic deposition (full rhombs) and anodic dissolution (empty rhombs) of Cu from Cu films deposited on Au-plated electrode (0.23 cm^2) from 0.01 M $CuCl_2$ in Ethaline 200.

Morphology of the deposits obtained is visible in figure 14. Brightly coloured deposits similar to the one obtained in this study were previously reported for the electrodeposition of Cu from Ethaline at concentrations ≥ 0.01 M.[10]

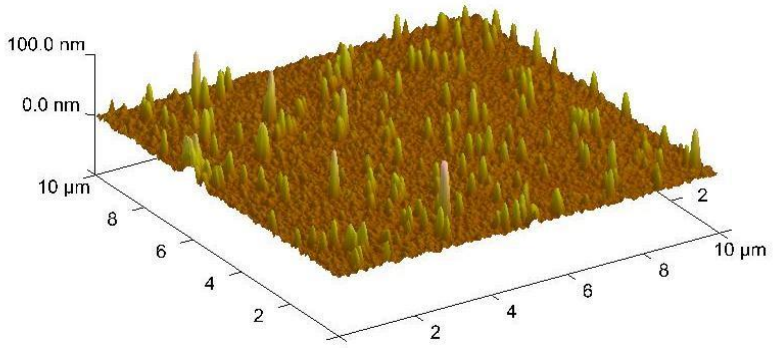

Figure 14. Ex-situ, dry Cu film electrodeposited on Au coated glass slide (A = 1.75 cm^{-2}) from 0.01 M $CuCl_2$ dissolved in Ethaline 200. Potentiodynamic deposition (3 successive cycles) 0.0 V → - 0.8 V → 0.0 V, ν = 0.0625 mV s^{-1}. $\mathbf{Q_{dep}}$ = 228 mC cm^{-2}.

5.5.5 EQCM-PBD study of a mass transport during the electrodeposition-dissolution of tin from $SnCl_2$ in Ethaline.

Electrodeposition of tin from DES in general and Ethaline in particular has been the subject of recent studies.[12,13,16,42] Many of these emphasized the importance of metal ion speciation in the overall process and the ambiguity of the current (FAB – MS derived) data on the subject. Thus, the purpose of the present study was to expand the current knowledge of tin electroplating from Ethaline 200.

Left panel of figure 15 shows the voltammetric and the experimental optical profiles for deposition/dissolution of tin from $SnCl_2$/Ethaline 200 electrolyte. As the rate of the tin electroplating in Ethaline has been reported to be hampered by low diffusion coefficient,[13] in order to obtain good quality of the optical signal this particular experiment was conducted at lower sweep rate (0.03125 mV s^{-1}) than the silver and copper cyclic voltammetry experiments (which were conducted at 0.0625 mV s^{-1}).

In a current signal, a well-defined peak is observed in the cathodic scan which originates from tin deposition through $Sn^{2+} \rightarrow Sn^{0}$ redox couple. The electrochemically generated optical signal follows the current profile closely throughout the reduction phase. The oxidation phase of the deflectogram however, shows an unusual discrepancy. While the current signal displays well defined oxidation peak the optical deflection signal fails to follow it to any reasonable degree.

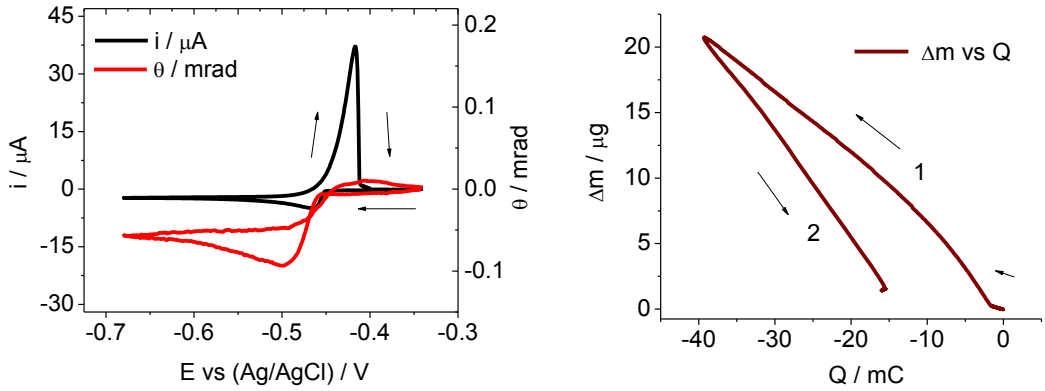

Figure 15. Left panel: cyclic voltammogram (black line) and cyclic deflectogram (red line) recorded during redox deposition-dissolution of elemental Sn from 0.01 $SnCl_2$ in Ethaline 200. ν = 0.03125 mV s^{-1}, potential window applied - 0.34 V → - 0.68 V → - 0.34 V. $\mathbf{Q_{dep}}$ = 170.6 mC cm^{-2}. Right panel: corresponding mass change (Δm) versus charge (Q) plot.

The reason for this lies in the solubility threshold for $SnCl_2$ in Ethaline being exceeded which has been separately calculated as 0.2 M.[30] Upon oxidation, ca. 20 μg of Sn (which equates to 0.17 μmol) is released into the electrolyte immediately adjacent to the electrode's surface. At the scan rate applied this process takes place over an interval of ca. 3000 s. During this period, tin species are able to diffuse 100 – 200 μm from the electrode's surface into (and beyond) the focal zone (i.e. optical deflection zone). Diffusion of tin in this case can be visualized as an injection of metal ions into a cylinder which base is the electrode area and height is the electrode-beam distance (ca. 50 μm). Based on these dimensions, cylinder volume has been calculated as ca. 1 μl. Thence, during the metal stripping process, an average concentration of Sn in the imaginary cylinder is approaching 0.17 M, noticeably close to the solubility limit. Furthermore, nature of the diffusion means that the localized concentration of metal ions will be significantly higher close to the electrode's surface. These factors resulted in un-dissolved metal precipitating to the bottom of the electrochemical cell without causing any noticeable change in concentration. Thus, no change in refractive index could be observed.

Good agreement between the current and optical signal was nevertheless obtained in the majority of the redox cycle allowing for the application of the

convolution protocol. The predominant Sn reductive specie in Ethaline was previously proposed to be $SnCl_3^-$, this result has been based on FAB – MS data.[12] The hysteresis present in Δm/Q plot indicates that this may not be the only tin speciation present in Ethaline and the presence of $Sn_2Cl_5^-$ cannot be completely excluded. The MS_M derived from the deposition phase (52.4 g mol $^{-1}$) of Δm/Q plot (figure 15, right panel) does not match the tin ion molar mass (118.7 g mol $^{-1}$), the difference was still significant during the dissolution phase, where the MS_M has been calculated as 78.6 g mol $^{-1}$. This is an unequivocal evidence of the heterogeneous mass transfer. Salomé and co-workers have previously suggested possible adsorption of the organic component of the ionic liquid on the electrode surface.[13] Upon Sn deposition organic molecules would form a counter flux explaining the observed $MS_M < Sn_{MW}$ effect. Based on the relative charge density of the two possible tin speciations it was speculated that $SnCl_3^-$ is the major specie (due to its higher charge density) in phase 1 (see figure 15, right panel). $Sn_2Cl_5^-$ (having lower charge density) might be the dominant specie in phase 2. Integration of the Δm/Q signal indicates that 27% of the species might be two-metal ion complexes ($Sn_2Cl_5^-$) with the remaining 63% being one-metal ion complexes ($SnCl_3^-$).

Based on the above, the following assumptions were formed for the convolution protocol:

1. Sn^{2+} is the only charged specie exchanged between the electrode and the bathing electrolyte. Therefore, the reaction proceed as follows:

$$\mathbf{Sn^{2+} + 2e^- \rightarrow Sn^0}$$

and

$$\mathbf{Sn^0 - 2e^- \rightarrow Sn^{2+} + nCl \rightarrow + SnCl_3^- + Sn_2Cl_5^-}$$

2. The following equation describes the flux of species in the electrode vicinity:

$$J_{Sn^{2+}2Cl^-(x,t)} = F_{(x,t)} \times J_{Sn^{2+}2Cl^-(0,t)} \qquad \textbf{[12]}$$

Where F is calculated like in the case of silver and copper and D is the coupled diffusion coefficient of $SnCl_3^-$ and $Sn_2Cl_5^-$. Differential form of the convolution results

is shown in the left panel of the figure 16. It can be noted that both the convolved current as well as convolved mass are almost completely superimposed on the experimental optical signal in the reduction phase and deviate from it significantly only in the oxidation phase.

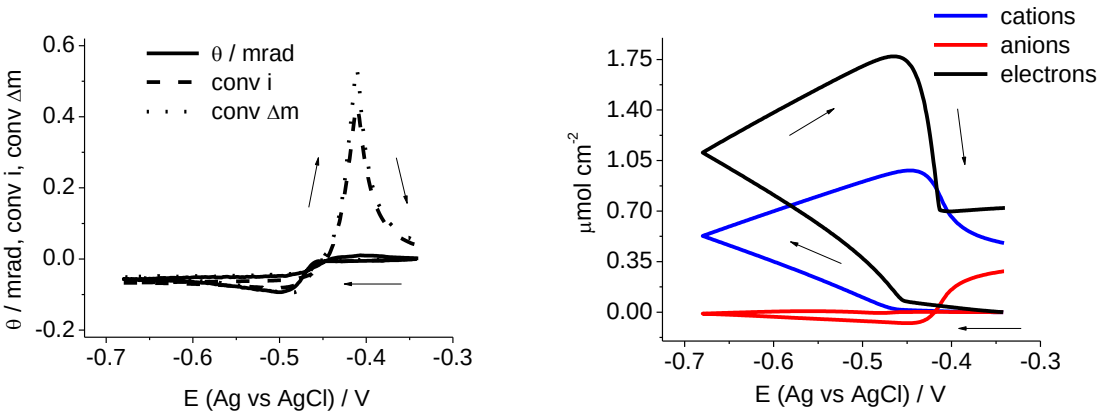

Figure 16. Left panel: solid line - experimental beam deflection (θ), dashed line - convolved current $i_{(x,t)}hL/zFA$, dotted line - convolved mass variation $((dM_{(x,t)}/dt)zFAhl/m_{Sn^{2+}}$. Right panel: Comparison of the convolved signal integrals.

Very good agreement of $i_{(x,t)}hL/zFA$ and $((dM_{(x,t)}/dt)zFAhl/m_{Sn^{2+}}$ achieved during the reduction phase allows for prediction of the current and mass transferred in the dissolution phase despite the complications described above. Unfortunately, the detection of possible metal ion speciations proved impossible as the convolved signal returns only the total, non-specific mass and current values. Integrated form of the convolved signals is shown in the right panel of figure 16. The overall ratio of cations to electrons exchanged has been calculated as 1:1.78. Since no optical signal was recorded for the oxidation phase, no information is available about the identity and the amounts of possible speciations could be derived from it. Hence, it was assumed that $SnCl_3^-$ might be the only mobile specie and then the charge balancing process at the electrode/electrolyte interface would proceeds as follows:

Integration of the experimental deflection:

$$SnCl_3^{2-}$$

electrons

(needed to reduce $Sn^{2+} \rightarrow Sn^0$) $2\ e^-$

experimental signal

(intensity of each complexation) 1

convoluted signal 2

(ratio of electrons exchanged per $SnCl_n$ complex)

total (determined experimentally) 2 e^- per 1 species

integration of convolved mass and current signals (see figure 16, right panel):

1.78 e^- per 1 species

The observed discrepancy of the calculated and experimental values has been assigned to the possible presence of di – tin species.

$$SnCl_3^- + 2e^- \rightarrow Sn^0 + 3Cl^-$$

and/or

$$Sn_2Cl_5^- + 4e^- \rightarrow 2Sn^0 + 5Cl^-$$

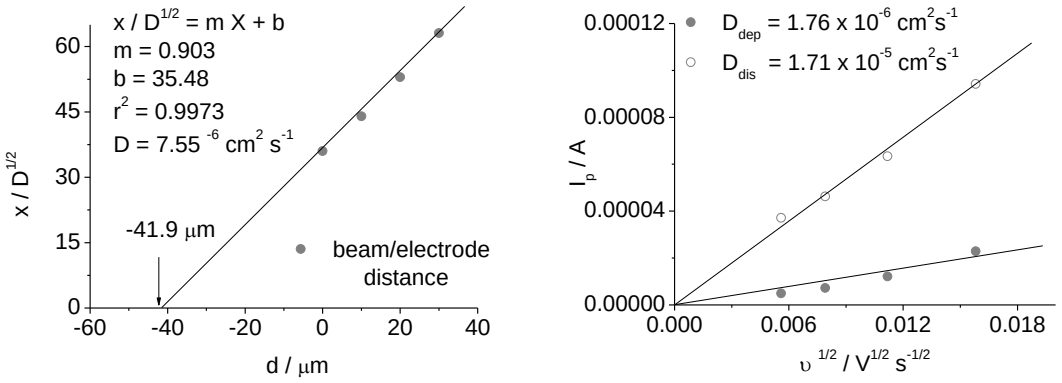

Figure 17. Plot of the convolution parameter ($x/\sqrt{D}$) expressed as a function of the relative beam deflection. Extrapolation of the linearity reveals real beam electrode distance (here 41.9 μm). Right panel: $I_p/\nu^{1/2}$ linear plots for cathodic deposition (full circles) and anodic dissolution (empty circles) of Sn from Sn films deposited on Au-plated electrode (0.23 cm^2) from 0.01 M $SnCl_2$ in Ethaline 200.

Diffusion coefficient was obtained from x/√D plot (figure 17, left panel). The obtained value of 7.55 $\times 10^{-7}$ $cm^2\ s^{-1}$ is in agreement with the result obtained by Salomé et al (D = 1.12 $\times 10^{-6}$ $cm^2\ s^{-1}$) considering the fact that their experiments were conducted at 348 K (Ethaline viscosity = 16 cP) and the experiments described in this thesis were conducted at 293 K (Ethaline viscosity = 40 cP). Quality of the data obtained from the convolution protocol was further evaluated by comparing this value to the one calculated from the Randles-Sevcik equation. Linearity of the $I_p/v^{½}$ plots (figure 17, right panel) confirms diffusive control in both the deposition (D = 1.76 $\times 10^{-7}$ $cm^2\ s^{-1}$) and dissolution processes (D = 1.71 $\times 10^{-7}$ $cm^2\ s^{-1}$).

Morphology of the deposits obtained is shown in figure 18. The profound influence of the electrochemical technique applied in the electrodepositing process has been emphasized previously.[2,10] Potentiodynamic tin deposition is a diffusion controlled process (see $I_p/v^{½}$ plots) and deposit morphology reveals homogeneous surface with very few crystalline particles. Dominance of regular particles is a possible indicator of progressive nucleation, which has previously been reported for this process.[13]

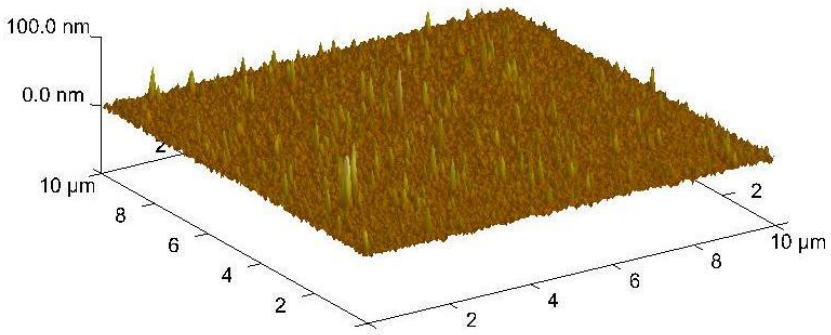

Figure 18. Ex-situ, dry Sn film electrodeposited on Au coated glass slide (A = 1.75 cm^{-2}) from 0.01 M $SnCl_2$ dissolved in Ethaline 200. Potentiodynamic deposition (3 successive cycles) - 0.34 V → - 0.68 V → - 0.34 V., ν = 0.03125 mV s^{-1}. $\mathbf{Q_{dep}}$ = 169.6 mC cm^{-2}.

5.5.6 EQCM-PBD study of a mass transport during the electrodeposition-dissolution of bismuth from $BiCl_3$ in Ethaline.

Electrodeposition of bismuth has been historically conducted in aqueous media with the UPD reported as far back as 1933.[43] Recent publication by Mao et al. reported

UPD during Bismuth deposition from $BMIBF_4$ ionic liquid on an Au plated electrode. [44] Mao et al reported the existence of neutral $BiCl_3$ molecule in $BMIBF_4$ ionic liquid. Authors described the UPD of bismuth as a reduction of absorbed $BiCl_3$ monolayer residing on the electrode's surface. The formation and stability of the $BiCl_3$ monolayer prior to its reduction was assigned to the strong ionic strength of the $BMIBF_4$ liquid protecting the absorbed structure through electrostatic interactions. Since DES, unlike classic IL, have highly coordinating constituents, Bi speciation in these novel solvents is expected to be significantly different. Hartley noted UPD during redox cycling of Bi films in Ethaline 200.[22]

Underpotential deposition of metals at noble surfaces has been observed for a variety of metals.[2] As the name implies this process occurs in a potential region positive of the expected Nernst potential and results in the formation of a usually very thin metallic deposit. The origins of this process is the competition between metal and ad atoms of the deposited metal with the latter forming a metal – substrate bond.

As proved by Henderson and co-workers in a lead UPD study PBD provides an excellent means for the *in-situ* detection of this process.[24] It was already shown by Hartley that bismuth trichloride dissolves readily in Ethaline 200. Therefore, in this study, PBD has been applied in a quantitative manner to study the possible occurrence of the UPD during deposition/dissolution of Bismuth from $BiCl_3$/Ethaline 200 solution.

Electrochemical and optical signals of the process are shown in the left panel of figure 19. The current signal displays clear pair of deposition (reduction at -0.13 V) and dissolution (oxidation at 0.05 V) peaks. This is in agreement with results reported by Hartley (reduction and oxidation peaks at -0.27 V and -0.18 respectively). The experimental optical signal however, shows a positive peak at - 0.2 V in the cathodic scan later followed by a negative deflection at -0.4 V. It is, clear (by comparison from other systems like AgCl or $SnCl_2$ in Ethaline) that the latter peak originates from the metal deposition (because negative deflection results from the *decrease* in concentration of $BiCl_4^-$ in the electrode vicinity as the metal is deposited). The only possible origin of the first positive peak is an *increase* in concentration in the optical deflection zone. Since UPD of bismuth in Ethaline occurs at 0.1 V, its occurrence in the studied system has been eliminated. In the anodic scan clear positive optical deflection peak can be seen shortly (~ 12 s) after the current oxidation peak. In order to elucidate the origin of the initial positive θ signal in the cathodic scan it was necessary to compare it to the gravimetric signal (figure 19 – right panel). At the onset of the cycle a rapid loss of

mass is recorded (low charge regime 0 → - 2 mC, marked as phase 1). This is followed by a mass increase (phase 2) which is a result of bismuth cathodic deposition. Phase 3 (mass decrease) represents an anodic stripping of the deposited metal. This is consistent with the recorded optical signal. Hartley reported the existence of an additional oxidation peak at 0.25 V without any corresponding reduction peak. Since the potential window applied here does not reach such positive potentials, UPD of bismuth can be excluded here. Therefore, the possibility of the gravimetric signal in the phase one (i.e. rapid mass decrease) can most probably be attributed to the removal of chlorocomplexes from the (Au plated) electrode surface prior to the deposition of metallic bismuth.

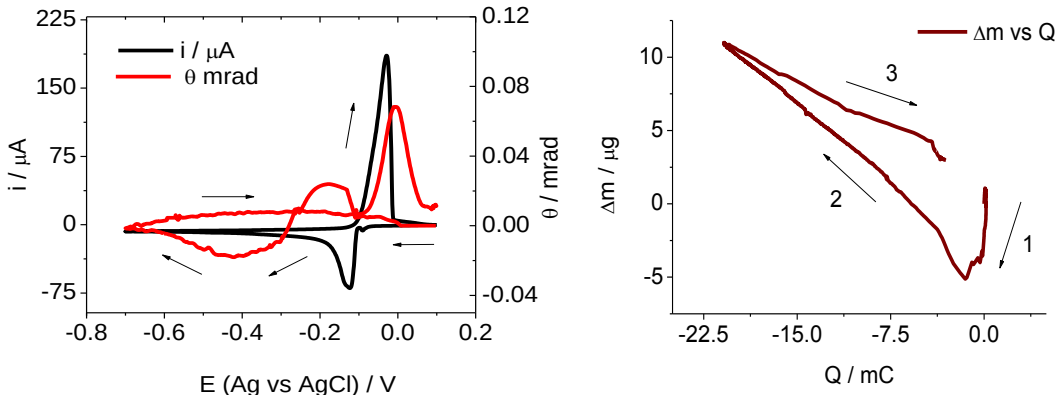

Figure 19. Left panel: cyclic voltammogram (black line) and cyclic deflectogram (red line) recorded during redox deposition-dissolution of elemental Bi from 0.01 $BiCl_3$ in Ethaline 200. ν = 0.5 mV s^{-1}, potential window applied 0.1 V → - 0.7 V → 0.1 V. $\mathbf{Q_{dep}}$ = 90.5 mC cm^{-2}. Right panel: corresponding mass change (Δm) versus charge (Q) plot. Numbers indicate the separate phases of the process.

Integration of the respective initial mass loss (phase 1) and cathodic deposition (phase 2) optical signals, allows for estimating of the amounts deposited during the spontaneous adhesion of species and the subsequent cathodic electrodeposition as 1:2. The Δm/Q dynamics of the overall process can be separated into three clear parts. Upon the application of the cathodic potential the MS_M in phase 1 is - 664 g mol^{-1}. Since this value extraordinarily exceeds molar weight of bismuth (Bi_{MW} = 208.98 g mol^{-1}), the only possibility for this rapid mass loss is a flux of different species (considering the environment, chlorocomplexes are the most probable candidates). Notably, in Bi redox process *mass decrease* occurs in the first part of the cathodic couple. This is presumed

to be a result of the removal of chlorocomplexes deposited on the electrode upon immersion in Ethaline. Phase 1 is followed by (starting at - 0.12 V) phase 2, (cathodic deposition) when *mass increase* is observed. However, MS_M of 70 g mol $^{-1}$ recorded during this phase is unexpectedly, below bismuth molar mass. This is assigned to the phase 1 process (i.e. removal of chlorocomplexes) still being present (it is confirmed by the delayed and irregular – i.e. not resembling the electrochemical profile, optical profile recorded during the cathodic deposition – see figure 19, left panel). Phase 3 has the lowest MS_M of 42.6 g mol $^{-1}$. The overall conclusion from the gravimetric point of view is that the very significant amount of chlorocomplexes present on the electrode prior to the commencement of Bi redox cycle distorts the EQCM signal outward appearance making elucidation of the process rather difficult. This signifies the demand for a complimentary technique.

Application of the convolution protocol has been based on the following assumptions:

1. Bi^{3+} is the only charge carrying specie being exchanged in the electrodeposition process between the electrode and the bathing solution. Therefore, the reaction is presumed to proceed as follows:

$$\mathbf{Bi^{3+} + 3e^- \rightarrow Bi^0}$$

and

$$\mathbf{Bi^0 - 3e^- \rightarrow Bi^{3+} + nCl \rightarrow BiCl_4^-}$$

2. The following equation describes the flux of species in the electrode vicinity:

$$J_{Bi^{3+}3Cl^-(x,t)} = F_{(x,t)} \times J_{Bi^{2+}3Cl^-(0,t)} \qquad \textbf{[13]}$$

Where F is obtained as before and D is the coupled diffusion coefficient D_{BiCl_3}. Differential form of the convoluted signal is shown in the left panel of figure 20. Difficulties in the convolution analysis of the more complicated electrochemical processes had been previously highlighted by Henderson et al.[24] Comparison of the convolved current and convolved mass signals versus the experimental optical signal

displays almost complete lack of signals superimposition. The projected current and mass do not superimpose onto the θ signal during the deposition phase, during dissolution their resemblance improves, however it is still far from full superimposition.

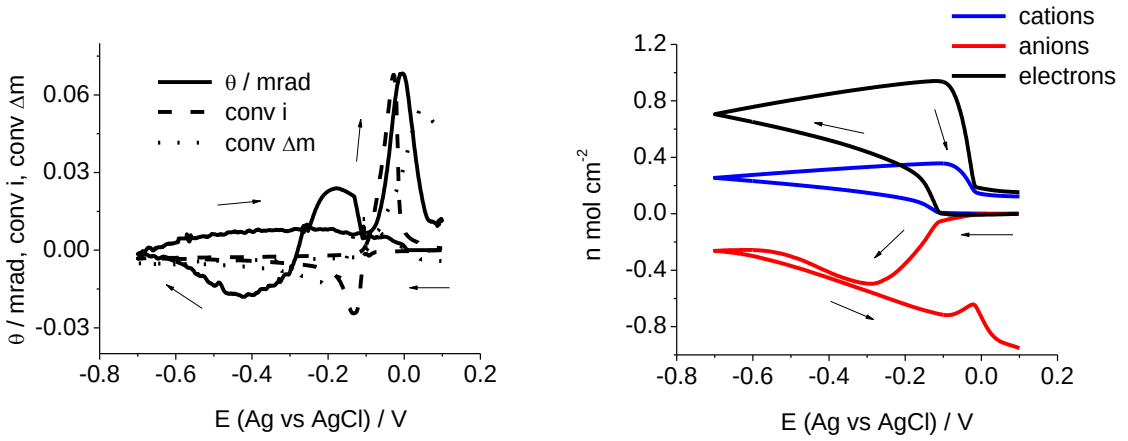

Figure 20. Left panel: solid line - experimental beam deflection (θ), dashed line - convolved current $i_{(x,t)}hL/zFA$, dotted line - convolved mass variation $((dM_{(x,t)}/dt)zFAhl/ m_{Sn^{2+}}$. Right panel: Comparison of the convolved signal integrals.

It is also noteworthy that the propagation delay is approximately four times larger in the reduction phase than in the oxidation phase. The reason for that most likely lies in the removal of pre-deposited layer of chlorocomplexes resulting in a flux of species *away* from the electrode. This opposes the flux of Bi^{3+} *towards* the electrode, which precedes the metal deposition. The exact nature of the chlorocomplexes present in the electrolyte is not yet known. Considering the presence of strong coordinating species such as chloride (high content in Ethaline 200), it is possible that bismuth metal complexes with chloride anions in an analogous fashion to silver, copper and tin. During oxidation, the reaction is more straightforward with the metal layer being dissolved into the bating electrolyte solution in the following reaction $Bi^0 \rightarrow Bi^{3+}$. The exact origin and identity of the species adhering to the electrode, prior to the redox process, have not yet been elucidated. Considering DES high chloride content the formation of chlorocomplexes seems to be the most plausible explanation. Single optical deflection peak, visible during the dissolution of the electrodeposited layer indicates single metal ion speciation being present in the solution. Applying this knowledge to the integrated form of the convoluted signal allows elucidating the whole redox process as follows:

$$nCl^- \rightarrow \text{adhered layer of chlorocomplexes}$$

$$\text{adhered layer of chlorocomplexes} \rightarrow nCl^-$$

$$BiCl_4^- + 3e^- \rightarrow Bi^0 \text{ [electrodepostion]}$$

$$Bi^0 - 3e^- \rightarrow Bi^{3+} + nCl^- \rightarrow BiCl_4^- \text{ [electrodissolution]}$$

The above reaction implies the 1:3 electron/cation ratio which considering the difficulty of this particular analysis is in good agreement with the calculated value of 1:2.45 obtained from the integrated convolved signals (figure 20, right panel). Electrodeposition of bismuth from chloroaluminate ionic liquids (BuPyCl-$AlCl_3$[45] and MBIC-$AlCl_3$[46]) was previously reported as a two-stage process. Pan et al reported two different UPD processes at 1.2V and 0.9 V, each resulting in a formation of a layer with a distinctly different morphology.

Heerman and D'Oileslager investigated the electrochemistry of bismuth in $AlCl_3$ - N(n-butyl) Pyridinium Chloride RTIL. Authors concluded that the electrochemical reduction of Bi^{3+} (on a glassy carbon electrode) initially resulted in formation of a Bi_5^{3+} cluster ion. Application of further cathodic potential resulted in reduction of this unstable intermediate to the Bi^0 metal. No direct evidence of similar processes was found in Ethaline 200. In this solvent, the deposition process seems to follow a straightforward $Bi^{3+} \rightarrow Bi^0$ pathway.

The diffusion coefficient was obtained from $x/\sqrt{D}$ plots (figure 21, left panel) with the value of $D = 5.79 \times 10^{-7}$ $cm^2\ s^{-1}$. This value is not in good agreement with $I_p - \nu^{1/2}$ plots (see figure 21, right panel) and the discrepancy is assigned to the difficulties in processing of the complex optical deflection signal.

The linear relationship observed in the $I_p/\nu^{1/2}$ plots (figure 21, right panel), indicates diffusion control of the system during both deposition ($D = 2.32 \times 10^{-7}$ $cm^2\ s^{-1}$) and dissolution processes ($D = 1.92 \times 10^{-7}$ $cm^2\ s^{-1}$). Similar effects of diffusion control and full reversibility of bismuth deposition were observed by Salomé and co-workers.[12]

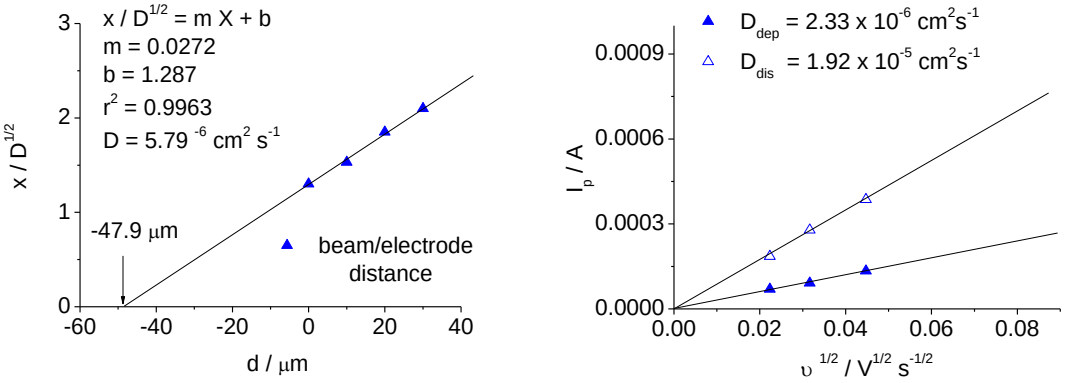

Figure 21. Plot of the convolution parameter ($x/\sqrt{D}$) expressed as a function of the relative beam deflection. Extrapolation of the linearity reveals real beam electrode distance (here 47.9 μm). Right panel: $I_p/v^{½}$ linear plots for cathodic deposition (full triangles) and anodic dissolution (empty triangles) of Bi from Bi films deposited on Au-plated electrode (0.23 cm^2) from 0.01 M $BiCl_3$ in Ethaline 200.

The morphology of the obtained deposits is shown in figure 22. The dense, uniform coating obtained is in good agreement with results reported by Agapescu and co-workers who conducted deposition of bismuth films from ChCl-Oxalic acid DES as resulting in similar morphologies.[19] These researchers have also reported improvement of the coatings during prolonged potentiostatic deposition at highly negative potentials – here the same effect has been achieved using slow sweep rate voltammetry.

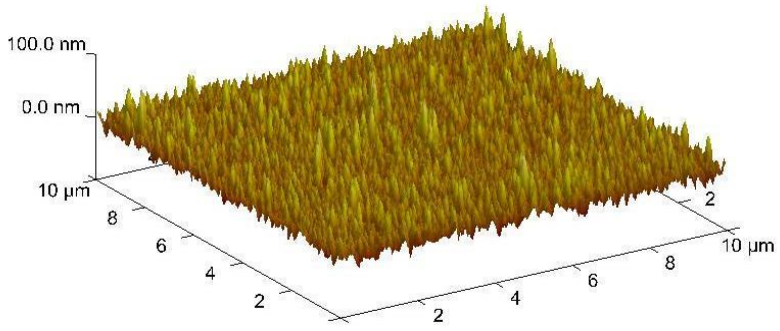

Figure 22. Ex-situ, dry Bi film electrodeposited on Au coated glass slide (A = 1.75 cm^{-2}) from 0.01 M $BiCl_3$ dissolved in Ethaline 200. Potentiodynamic deposition (3 successive cycles) 0.1 V → - 0.7 V → 0.1 V. ν = 0.5 mV s^{-1}. $\mathbf{Q_{dep}}$ = 90 mC cm^{-2}.

Additionally, Freyland et al. reported that the application of the potential sweep resulted in a formation of needle-like bismuth films while potential jump (from 1.3 V → 0.4 V) yielded ultrathin Bi films. Bi film presented here has large surface roughness being approximately 10 times larger than the Au surface roughness (50 nm vs 5 nm). The exact effects of the electrode morphology on the deposited material were not studied yet and will be a subject of further study.

5.5.7 EQCM-PBD study of a mass transport during the co-electrodeposition-dissolution of metals. Silver and copper co-deposition from AgCl/ $CuCl_2$ in Ethaline 200

Co-deposition of metals is an important industrial process.[2] Simultaneous deposition of silver and copper from Ethaline had previously been a subject of an electrochemical and acoustic impedance study.[5] Here PBD-EQCM has been applied to study the metal ion complexations present in the process and their influence on the final deposit. Silver had previously been reported to form porous deposits while being electrodeposited from Ethaline (see section 5.5.2). This kind of morphology enables a subsequent deposition of other metals. In this study, this effect has been exploited through subsequent electrodeposition of copper.

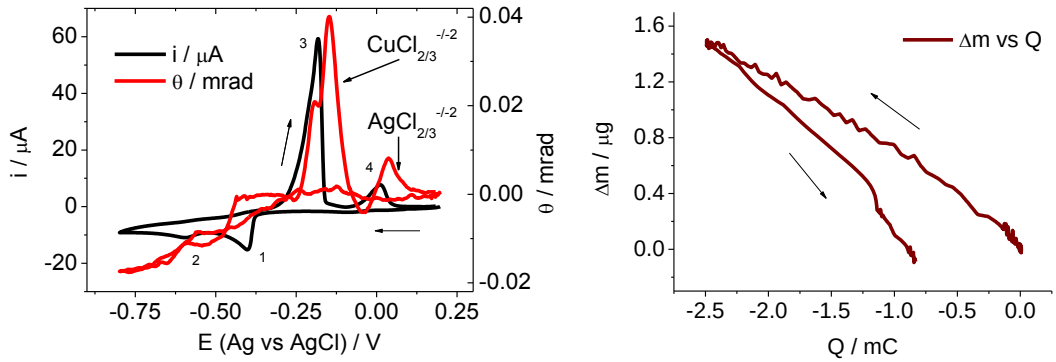

Figure 23. Left panel: cyclic voltammogram (black line) and cyclic deflectogram (red line) recorded during redox deposition-dissolution of elemental Ag and Cu from 0.005 M AgCl/0.005 M $CuCl_2$ in Ethaline 200. ν = 2.5 mV s^{-1}, potential window applied 0.2 V → - 0.8 V → 0.2 V. $\mathbf{Q_{dep}}$ = 10.8 mC cm^{-2}. Right panel: corresponding mass change (Δm) versus charge (Q) plot.

Left panel of the figure 23 contains the recorded current and experimental optical signals. Cyclic voltammogram displays two peaks in the cathodic direction. Comparison of the separate silver/Ethaline (figure 7, left panel) and copper/Ethaline (figure 11, left panel) voltammograms with the data presented in the figure 23, indicates significant shift of the deposition potentials during the co-deposition process with a prominent cathodic peak at -0.4 V, a feature not observed in both of the single metal redox couples. This cathodic peak at – 0.4 V is followed by two oxidation peaks in the anodic scan with first copper (- 0.26 V) and then silver (0.05 V) being dissolved from the electrode. The voltammetry results are in agreement with work reported by Abbott et al.[5] The optical signal reveals the previously encountered (see figure 11, left panel) double peak representing the formation of two copper speciations. At 0.06 V in the anodic direction, lies less clearly defined but nevertheless noticeable optical deflection doublet resulting from silver layer dissolution (see figure 23, left panel). The gradient of the $\Delta m/Q$ plot (figure 23, right panel), reveals the average MS_M during deposition as 57.5 g mol $^{-1}$. Considering molar masses of silver (107.87 g mol $^{-1}$) and copper (63.5 g mol $^{-1}$) the average mobile mass at 1:1 Ag/Cu ratio would return MS_M of 85.7 g mol $^{-1}$. However, the value obtained is lower than that and even lower than the molar mass of copper. There are two most plausible explanations of this observation. The first one is the counter-flux of chlorocomplexes during the Ag/Cu co-deposition. The second possible explanation is the presence of parasitic processes resulting in less than 100 % Faradic efficiency of the Ag/Cu deposition process. It has to be noted that the EQCM signal was not accompanied by any concomitant viscoelastic losses. This allows for the deduction that rigid, thin metallic layer was formed upon the Ag/Cu deposition. The MS_M recorded upon dissolution was 89.6 g mol $^{-1}$. Simple calculation (based on molar masses of Cu = 63.5 g mol^{-1} and Ag = 107.6 g mol^{-1}) reveals the composition of the outward flux as having approximately 1:1 silver and copper ratio. Since the origin of this flux lies entirely in the metallic deposit, the composition obtained can be treated as the composition of the Ag-Cu layer deposited on the electrode during the cathodic scan.

Based on the above, the following principles were formed for the convolution protocol:

1. Cu^+ and Ag^+ are the only charged species exchanged between the electrode and the bathing electrolyte. Therefore, the reaction proceed

as follows:

$$\mathbf{Ag^{+} + Cu^{+} + 2\ e^{-} \rightarrow Ag^{0} + Cu^{0}}$$

and

$$\mathbf{Cu^{0} - e^{-} \rightarrow Cu^{+} + nCl \rightarrow + CuCl_2^{-} + CuCl_3^{2-}}$$

$$\mathbf{Ag^{0} - e^{-} \rightarrow Ag^{+} + nCl^{-} \rightarrow AgCl_3^{-2} + AgCl_2^{-}}$$

2. The following equation describes the flux of species in the electrode vicinity:

$$J_{Ag^{+}Cl^{-}/\,Cu^{+}\,Cl^{-}(x,t)} = F_{(x,t)} \times J_{Ag^{+}Cl^{-}/\,Cu^{+}\,Cl^{-}(0,t)} \qquad \textbf{[14]}$$

Where F is obtained like for the other metals but with two separate diffusion coefficients: D_{AgCl} is the coupled diffusion coefficient of $AgCl_2^{-}/AgCl_3^{2-}$ and D_{CuCl} is the coupled diffusion coefficient of $CuCl_2^{-}/CuCl_3^{2-}$. Differential form of the convolved optical signals is shown in the left panel of the figure 24.

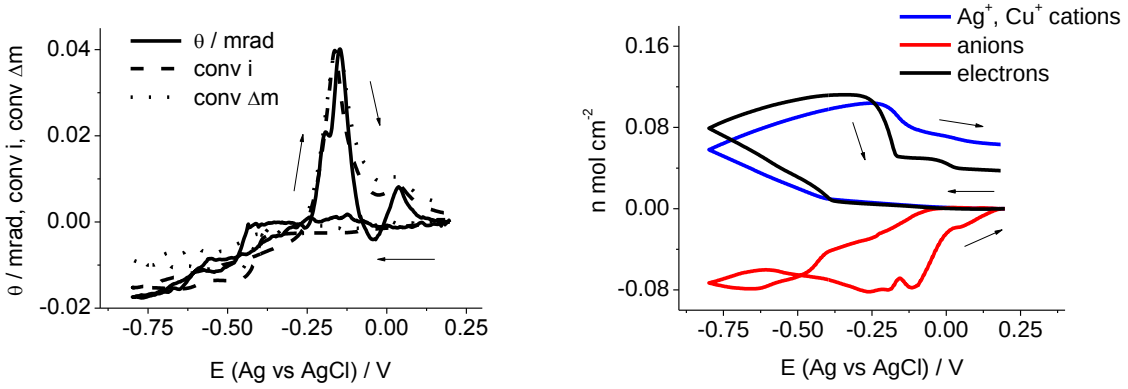

Figure 24. Left panel: solid line - experimental beam deflection (θ), dashed line - convolved current ($i_{(x,t)}$hL/zFA) and dotted line - convolved mass variation (($dM_{(x,t)}$/dt)zFAhl/$m_{Ag/Cu}$). Right panel: Comparison of the convolved signal integrals.

Both $i_{(x,t)}$hL/zFA and (($dM_{(x,t)}$/d*t*)zFA*h*l/$m_{Ag/Cu}$) deviate from the experimental optical signal (θ) in the cathodic scan. This is attributed to the simultaneous deposition of both metals at *circa* - 0.4 V and the presence of counter flux of chlorocomplexes (see

Δm/Q calculations above). In the anodic scan, the agreement between the convolved and experimental signals is much closer probably due to the high selectivity of the dissolution process. Analysis of the integrated form of the convolved signal (figure 24, right panel) reveals the ratio of electrons-to-cations exchanged in the process as 1:1.1.

Both $Ag^+ \rightarrow Ag^0$ and $Cu^+ \rightarrow Cu^0$ reductions require 1 electron per 1 metal cation. The discrepancy between the experimentally derived and theoretical ratio of electrons is attributed to parasitic losses during the deposition process. Integration of the copper deflectographic peaks (figure 23, left panel) indicates that the presence of silver has a profound effect on the $CuCl_2^-/CuCl_3^{2-}$ ratio, which in this system is 1:2.5 as opposed to 1/1.22 in a copper/Ethaline system.

The diffusion coefficient for both metals was obtained from x/√D plots (figure 25, left panel) with the value of $D = 2.16 \times 10^{-6}$ cm^2 s^{-1} . It must be noted that the optically determined diffusion coefficient applies to a co-deposition/dissolution process and therefore should be treated as an average of D_{AgCl} and D_{CuCl}.

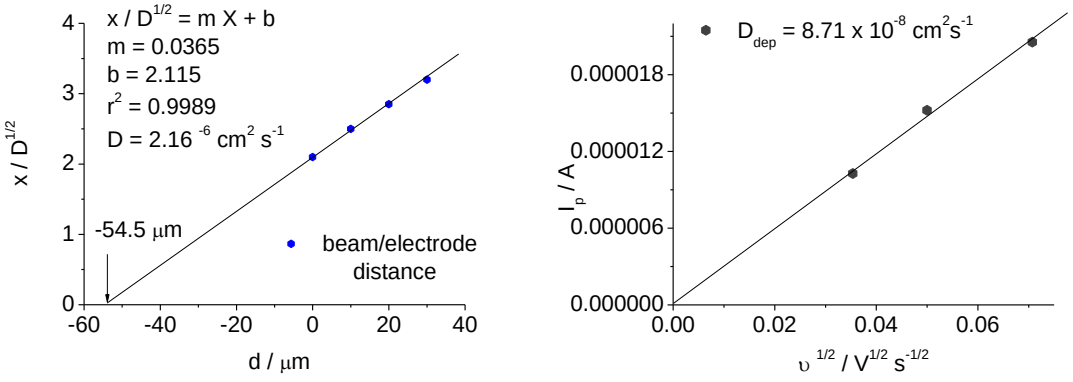

Figure 25. Plot of the convolution parameter (x/√D) expressed as a function of the relative beam deflection. Extrapolation of the linearity reveals absolute beam electrode distance (here 54.5 μm). Right panel: $I_p/v^{½}$ linear plots for cathodic deposition (full symbols) of Ag/Cu couple from Ag/Cu films deposited on Au-plated electrode (0.23 cm^2) from 0.005 M $AgCl/CuCl_2$ in Ethaline 200.

The optically determined D value is very distant from the $D = 8.71 \times 10^{-8}$ cm^2 s^{-1} obtained from Randles-Sevcik equation (see figure 25, right panel). The $I_p/v^{½}$ analysis of the deposition process proved rather difficult due to the cathodic peaks being merged (note large cathodic peak at – 0.4 V, figure 23, left panel). Therefore, the I_p derived value was treated as more of an estimate as the optical data seems to be closer to values

previously reported by Abbott and co-workers for $Cu^{2+/+}$ diffusion in Ethaline 200.[10] Clear anodic peak separation (see figure 23, left panel) allowed for the calculation of separate diffusion coefficient for the dissolution of copper ($D = 7.84 \times 10^{-7}$ cm^2 s^{-1}) and silver ($D = 2.18 \times 10^{-7}$ cm^2 s^{-1}) (see figure 26).

Due to different Nernst potentials of silver and copper in Ethaline 200 ($Ag^+ \rightarrow Ag^0$ = - 0.06 V, $Cu^+ \rightarrow Cu^0$ = - 0.4 V, both vs. silver pseudoreference electrode), the co-deposition of these two metals could theoretically be envisaged as a deposition of silver layer followed by a subsequent deposition of copper. However, the optical data obtained (figure 23, left panel) indicates that the presence of copper ions results in a transfer of the silver deposition process to more cathodic potentials (from - 0.06 V → to - 0.4 V). Therefore, it is likely that the majority of silver and copper metal ions are co-deposited at ca. - 0.4 V.

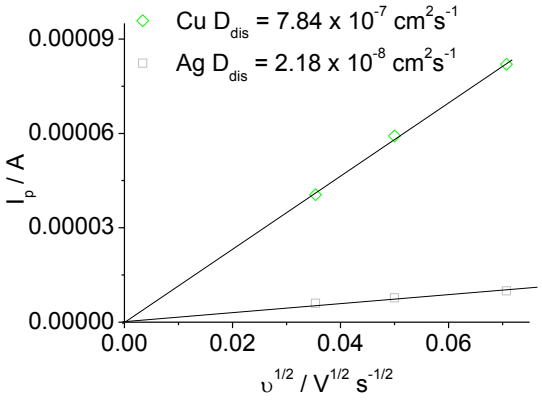

Figure 26.: $I_p/v^{½}$ linear plots for of Ag (empty squares) and Cu (empty rhombs) couple from Ag/Cu films deposited on Au-plated electrode (0.23 cm^2) from 0.005 M AgCl/ 0.005 M $CuCl_2$ in Ethaline 200.

The last peak visible in the cathodic part of the deflectogram (at *circa* - 0.7 V) is attributed to the deposition of the remaining copper ions. Dissolution of these two metals seems to be a more selective process with Cu(I) and Ag(I) departing from the electrode surface at the potentials similar to those observed for the single metal process.

Underpotential deposition of Ag on Cu, Cu on Au as well as Ag on Cu undoubtedly plays a major role in the Ag/Cu co-deposition on Au electrodes. Both metals are known to undergo chemical reduction in Ethaline 200 (not counting other DES) and this effect was already applied in the immersion coating processes. Abbott et al. have already reported Ag^+ ion reduction being thermodynamically favoured upon

immersing Cu electrodes into the AgCl/DES solution.[47] Since Au is a more noble metal than both Ag and Cu, it does not readily dissolve upon immersion into Ethaline 200. Therefore it can be assumed that with Au^+ concentration being 0, the following reaction can take place:

$$Au^0 + Ag+ \rightarrow Au^+ + Ag^0$$

This possibility is supported by an application of the Nernst equation which in the case of silver is:

$$E = E_0 + \frac{nF}{RT} ln\left(\frac{0.005\ M}{1}\right) \quad \textbf{[15]}$$

In the case of gold (since there is none of this metal in the solution) the Nernst equation is:

$$E = E_0 + \frac{nF}{RT} ln\left(\frac{0.0\ M}{1}\right) \quad \textbf{[16]}$$

Thence, it can be reasoned that there is a possibility of Ag layer being present on the surface of Au electrode prior to the commencement of the redox process. Further deposition then would take place on Ag modified Au surface instead of a bare Au crystal.

5.6 Conclusions

The main goal of this chapter; elucidation of metal electrodeposition in Ethaline by means of combined PBD-EQCM technique has been achieved. As the magnitude of the optical deflection depends on the concentration gradient, inherent high concentration of the ionic media (be it IL's or DES) requires minimization of the beam-electrode distance to compensate for this (the flux magnitude increases in the electrode proximity). It must be mentioned that the application of the optical deflection to study metal ion speciation in ionic media (or indeed, any other process) is a completely novel approach, therefore not without some teething problems.

Initially, the original (i.e. reported by Henderson et al) silver deposition-dissolution PBD-EQCM experiment has been reproduced at the reduced distance of approach in order to obtain a closed form of the optical signal. The profile of the signal

recorded had a closed form and displayed a very close resemblance of the electrode current.

The thus obtained, experimental protocol was then used as an analytical standard. The optical analysis in DES proved challenging and could only be conducted at a very slow sweep rate (in the case of potentiodynamic experiments) or an elongated steps (in the case of potentiostatic experiments). This was shown to be the only present possibility of overcoming the viscosity barrier, which is the main hindrance in performing quantitative optical deflection analysis in these high viscosity media. This is due to the slow diffusion processes which in DES and IL's result in a diffusion coefficients' being orders of magnitude lower than in aqueous or organic plating solutions. The decrease of sweep rate necessary for obtaining a deflectogram representing the nature of the electrode processes was found to be linear to the increase in the electrolyte viscosity (i.e. ν/η displayed inverse correlation).

In the case of Ag/Ethaline redox system two speciations were implied as $AgCl_3^{2-}$ and $AgCl_2^-$. This was deduced from the presence of two optical deflection peaks in the oxidation phase of AgCl/Ethaline 200 deflectogram. Presence of more than one optical deflection peak is an indicator of two possibilities. First one is the occurrence of the same process separated temporally into the two phases. This is unlikely in the case of silver oxidation. Second possibility is the existence of two species with different refractive indexes – this is very plausible as $AgCl_2^-$ and $AgCl_3^{2-}$ would display this due to structural differences. Thus, the structural differences resulted in specific refractive indexes yielding separate peaks in the deflectogram. This enabled the quantification of the data (unlike the previous EXAFS based qualitative study).[6]

In the redox cycling of copper (II) chloride in Ethaline 200 two optical deflection peaks were also observed. By inference from the silver process described above, these peaks were assigned to Cu(I) (present as $CuCl_2^-$ and $CuCl_3^{2-}$). Presence of Cu(II) species had been excluded through the careful choice of the potential window. Quantification revealed the relative and absolute amounts of the silver and copper speciations as well as their pattern of formation during the redox cycle.

Potential driven deposition/dissolution of tin proved to be a more difficult system to analyze. Application of the slow sweep rate (which for this particular system was reduced even further to compensate for low diffusion coefficient) resulted in a concentration threshold being exceeded and the subsequent loss of the optical deflection signal. However, the excellent agreement obtained between the electrode current and

the electrochemically generated optical signal during the reduction phase allowed for the calculation of the convolved signals and thus shed light on the possible tin speciations in Ethaline. Presence of $SnCl_3^-$ has been unequivocally confirmed while the presence of $Sn_2Cl_5^-$ still remains highly questionable.

Previously reported[39,40,41] underpotential deposition of bismuth on a noble (here – Au plated quartz resonator) surface during redox cycling in Ethaline has not been detected in the potential window applied. Quantification of the gravimetric signal suggests that the deposited layer is significantly thicker than a monolayer and probably consist of chlorocomplexes adhered to the electrodes' surface. Bismuth (III) was found to be the only oxidation state of this metal in Ethaline 200.

In co-deposition of metals, the deflectogram confirmed the presence of two silver and two copper speciations. It also indicated their relative ratios. Presence of different metal ions was found to have a profound effect on both deposition potentials as well as the concentrations of each specific metal ion speciation. Silver/copper chloride solution in Ethaline displayed twice as high $CuCl_2^-$ concentration as the one of pure copper chloride dissolved in Ethaline 200. Both metals were co-deposited at overlapping potentials but during the dissolution process the potential were clearly separated. The technique has also been successfully applied to study co-deposition of Bi and Ag.[48]

A common feature for all of the analysed redox couples in Ethaline was a linear increase of the both cathodic and anodic measured peak currents with the square root of the sweep rate. This indicates that the process is diffusion controlled.

This chapter presents completely novel approach to studies of metal ion complexation and redox processes in a fully ionic media. The sensitivity and even more importantly, non-invasive nature of this type of analysis (local heating effects originating from the passage of the laser beam can be dismissed as the thermal gradients dissipate much faster than the concentration gradients) opens many possibilities for the further studies of the rapidly growing ionic liquids field. Affordability of beam deflection instrumentation provides additional advantage. An ability to track metal oxidation states in a dynamic environment could prove very useful in the area of ionometallurgy and electroplating/electropolishing. This is because metal deposits morphology, thickness and other important properties like hardness are strongly dependant on the nucleation processes (instantaneous versus progressive) and the rate of deposition. This is turn is directly dependent on the magnitude and direction of the ionic

fluxes at the cathode proximity. EQCM-PBD is an affordable, versatile analytical tool to monitor these fluxes.

5.7 References

[1] Q. Zhang, K. D. O. Vigier, S. Royer and F. Jérôme, *Chemical Society Reviews*, 2012, **41**, 7108-7146.

[2] D. A. MacInnes, *The Principles of Electrochemistry*, New York, 1939

[3] F. Enders, D. MacFarlane, A. P .Abbott, (Eds), *Electrodepostion from Ionic Liquids*, WILEY-VCH Verlag GmbH & Co. KGaA.

[4] E. Gómez, P. Cojocaru, L. Magagnin, E. Valles, *Journal of Electroanalytical Chemistry*, 2011, **658**, 18-24.

[5] S. Zein El Abedin, A. Y. Saad, H. K. Farag, N .Borisenko, Q. X. Liu, F .Enders, *Electrochmica Acta*, 2007, 52, 2746-2754.

[6] A. P. Abbott, S. Nandhra, S. Postlethwaite, E. L. Smith and K. S. Ryder, *Physical Chemistry Chemical Physics*, 2007, **9**, 3735-3743.

[7] A. P. Abbott, K. El Ttaib, G. Frisch, K. S. Ryder and D. Weston, *Physical Chemistry Chemical Physics*, 2012, **14**, 2443-2449.

[8] C. D. Gu, X. J. Xu and J. P. Tu, *Journal of Physical Chemistry C*, 2010, **114**, 13614-13619.

[9] D. Grujicic, B. Pesic, *Electrochimica Acta*, 2002, **47**, 2901-2912.

[10] C. D. Gu, Y. H. You, X. L. Wang, J. P. Tu, *Surface & Coatings Technology*, 2012, **209**, 117-123.

[11] A. P. Abbott, K. El Ttaib, G .Frisch, K. J. McKenzie and K. S. Ryder, *Physical Chemistry Chemical Physics*, 2009, **11**, 4269-4277.

[12] K. Haerens, E. Matthijs, A. Chmielarz, B. Van der Bruggen, *Journal of Environmental Management*, 2009, **90**, 3245-3252.

[13] A. P. Abbott, G. Capper, D. L. Davies, K. J. McKenzie and S. U. Obi, *Journal of Chemical and Engineering data*, 2006, **51**, 1280-1282.

[14] S. Salomé, N. M. Pereira, E. S. Ferreira, C. M. Pereira, A. F. Silva, *Journal of Electroanalytical Chemistry*, 2013, **703**, 80-87.

[15] A. P. Abbott, G. Capper, K. J. McKenzie, K. S. Ryder, *Journal of Electroanalytical Chemistry*, 2007, **599**, 288-294.

[16] St. Vitkova, V. Ivanova, G. Raichevsky, *Surface Coating Technology*, 1996, **82**, 226.

[17] C. Rousse, S. Beaufils, P. Fricoteaux, *Electrochimica Acta*, 2013, **107**, 624-631.

[18] S. M. Sayed, K. Jüttner, *Electrochimica Acta*, 1983, **28**, 1635-1641.

[19] F. Golgovici, A. Cojocaru, M. Nedelcu, T. Visan, *Chalcogenide Letters*, 2009, **6**, 323-333.

[20] C. Agapescu, A. Cojocaru, A. Cotarta, T. Visan, *Journal of Applied Electrochemistry*, 2013, **43**, 309-321.

[21] C. Agapescu, A. Cojocaru, F. Golgovici, A. D. Manea, A. Cotarta, *Revistadechimie*, 2012, **9**, 911-920

[22] D. Lincot, *Thin Solid Films*, 2005, **487**, 40-48.

[23] J. M Hartely, PhD thesis, University of Leicester, 2013.

[24] T. Kekesi, M. Isshiki, *Journal of Applied Electrochemistry*, 1997, **27**, 982-990.

[25] M. J. Henderson, A. R. Hillman, E. Vieil, C. Lopez, *Journal of Electroanalytical Chemistry*, 1998, **458**, 214-248.

[26] M. J. Henderson, E. Bitziou, A. R. Hillman, E. Vieil, *Journal of the Electrochemical Society*, 2001, **148**, 105-111.

[27] H. M. French, M. J. Henderson, A. R. Hillman, E. Vieil, *Solid State Ionics*, 2002, **150**, 27-37.

[28] L. M. Abrantes, M. C. Oliveira, E. Vieil, *Electrochimica Acta*, 1996, **41**, 1515.

[29] R .Eriksson, *Electrochimica Acta*, 1996, **41**, 871.

[30] A. R. Hillman, K. S. Ryder, C. J. Zaleski, V. Ferreira, C. A. Beasley, E. Vieil, *ElectrochimicaActa*, 2014, accepted manuscript.

[31] A. R. Hillman, K. S. Ryder, V. C. Ferreira, C.J. Zaleski, E.Vieil, *Electrochimica Acta*, 2013, **110**, 418-427.

[32] A. P. Abbott, G. Capper, D. L. Davies, R. K. Rasheed and V. Tambyrajah, *Chemical Communications*, 2003, 70-71

[33] C. D'Agostino, R. C. Harris, A. P. Abbott, L. F. Gladden and M. D. Mantle, *Physical Chemistry Chemical Physics*, 2011, **13**, 21383-21391.

[34] Sauerbrey G, *Zeitschrift Physikalishe*, 1959, **155**, 202–222.

[35] S.Bruckenstein , A.Fensore , Z. Li , A. R. Hillman, *Journal of Electroanalytical Chemistry*,1994, **370**, 189–195.

[36] G. G. Lang, C. A. Barbero, *Laser Techniques for the Study of Electrode Processes*, Berlin, 2012

[37] C. A Barbero, M. C. Miras, *The Journal of the Argentine Chemical Society*, 2003, **91**, 1-40.

[38] C. Barbero, M. C. Miras and R. Kötz, *Electrochimica Acta*, 1991, **37**, 429-437.

[39] Q. Zhang, K. D. O. Vigier, S. Royer and F. Jérôme, *Chemical Society Reviews*, 2012, **41**, 7108-7146.

[40] A.R. Hillman, K.S. Ryder, C.J. Zaleski, C. Fullarton and E. L. Smith, *Z. Phys. Chem.* 2012, **226**, 1049-1068

[41] A. Ramos, M. Miranda-Hernández, I. González, *Journal of the Electrochemical Society*, 2001, **148**, 315-321.

[42] L. Anicai, A. Petica, S. Costovici, P. Prioteasa, T. Visan, *Electrochimica Acta*, 2013, **114**, 868-877.

[43] M. Harbaugh, F. C. Mathers, *Journal of the Electrochemical Society*, 1933, **64**, 293-298.

[44] Y-C Fu, Y-Z Su, H-M Zhang, J-W Yan, Z-X Xie, B-W Mao, *Electrochimica Acta*, 2010, **55**, 8105-8110.

[45] L.Herman, W. D'Olieslager, *Journal of the Electrochemical Society*, 1991, **138**, 1372.

[46] G. B. Pan, W. Freyland, *Electrochimica Acta*, 2007, **52**, 7254.

[47] A. P. Abbott, J. Griffith, S. Nandhra, C. O'Connor, S. Postlethwaite, K. S. Ryder, E. L. Smith, *Surface & Coatings Technology*, 2008, **202**, 2033-2039.

[48] A. R. Hillman, K. S. Ryder, C. J. Zaleski, V. Ferreira, C. A. Beasley, E. Vieil, manuscript in preparation.

Chapter VI

Conclusions and future work

6.1 Conclusions

An observation of the processes occurring at the electrode/electrolyte interface is usually considered to be the ultimate goal of the electrochemical analytical techniques. Transient concentration profiles determine the interfacial mass transport. The electrode/electrolyte mass transport is a key factor in any electrochemical charge storage device, as well as in important industrial processes like electroplating and electropolishing. Interface mass transport also plays a major role in redox reactions that occur in redox enzymes. [1]

Therefore, a plethora of techniques had been developed to monitor the interface concentration changes. As any incursion of any kind of a physical probe (be it a SECM or AFM tip) into this dynamic environment would unavoidably alter it, non-invasive techniques seem to be an obvious choice. Despite their undoubted advantages, optical methods are not widely represented in electrochemical studies. Difficult set–up, instrumental limitations and particularly prominent in the multi-flux systems, unambiguous data analysis all contribute to this fact. Additionally, optical deflection method has some inherent limitations due to the nature of the diffusion process, for example, the optical window is always smaller than the electrochemical one due to the diffusional delay and this may prohibit observation of some processes. Feasibility of the optical deflection analysis in the ionic solvents has not yet been studied. Therefore, the study presented in this thesis was considered both novel and important.

Chemistry and electrochemistry of DES is a rapidly growing field with a variety of processes (mainly focused on electrodeposition) currently under study. Since these liquids offer radically different environment when compared to molecular solvents any insight into their molecular identities and system dynamics of the DES is considered to

be highly valuable. For example, speciation of metal ions determines the morphology of the deposit and therefore its important properties like porosity and hardness,[2] while dopant ions type and its diffusion rate determine the performance of both primary and secondary charge storage devices.[3] Thus, optical deflection studies in a fully ionic environment described in this thesis was considered to be important, novel landmark, potentially opening up an entirely new field of analysis.

In case of the electroacitve polymer films, results presented in this thesis are complimentary to previous studies of PANI[4] and POT[5] redox chemistry conducted in aqueous solution, as well as PPy redox chemistry in Ethaline 200[6] with the distinction of this being the first published optical deflection study conducted in a fully ionic environment. Extensive work on the application of PBD to study the redox behaviour has been conducted in the past by Henderson, Barbero, Haas and others.[7] In this study, due to the slow diffusion observed in DES (as compared to diffusion rates observed in molecular solvents) not all experimental approaches (i.e. fast scan rate cyclic voltammetry) successfully applied in a low viscosity media could be replicated. However, a combination of carefully selected experimental conditions (extended steps chronoammperometry experiments) as well as optimization of the instrumental set-up (beam-electrode distance was minimized to the lowest physically possible value) allowed for unique, *in-situ* insight into the redox chemistry in these novel solvents. These results allowed for the complete determination of the mobile species population in PEDOT/Ethaline and PEDOT/Propaline systems. Used in conjunction with microgravimetry, optical deflection analysis enabled confirmation of the previously proposed theory that the electroneutrality during the charge transfer processes of PEDOT films in both of the solvents studied was maintained predominantly by cations ingress/egress. Additionally, the diffusion coefficients of charged species (envisaged as a $Ch^+/(EG)_2Cl^-$ couple or $Ch^+/(PG)_2Cl^-$ couple) were determined using the time dependence of the laser beam deflection delay[8] and were found to be in a good agreement with values previously determined using nuclear magnetic resonance.[9]

In case of metal deposition/dissolution processes, the long transit time of species travelling through viscous electrolyte between the electrode's surface and the focal point has been successfully overcame through an application of cyclic voltammetry at a very slow scan rates combined with reduction of the beam/electrode distance. The

experimental set-up has been validated using the experimental approach pioneered by Henderson et al.[5] As compared to the original work, reduction of electrode/beam distance allowed to obtain the optical deflection profile resembling the cyclic voltammogram more closely as both of the signals had a closed form. The PBD-EQCM technique was then successfully implemented to study AgCl/Ethaline redox chemistry. The $Ag^{+/0}$ redox system displayed a single optical deflection peak during the deposition of elemental silver from AgCl/Ethaline 200. Upon the dissolution however, the presence of two different silver speciations became apparent. Presence of doublet in an optical deflection signal is an evidence for the interplay between $(AgCl_3)^{2-}$ and $(AgCl_2)^-$. This interaction is thought to be a result of variations in local concentration of Cl^- being challenged by an increasing concentration of Ag^+ ions being released from WE during the oxidation phase of the redox cycle.

In case of copper, cyclic voltammetry/deflectometry experiments were deliberately limited to a relatively narrow (0 V $\rightarrow$ -0.8V) electrochemical window in order to focus on $Cu^+ \rightarrow Cu^0$ redox couple. Unexpectedly, in the oxidation phase of the process, two very clear peaks were observed in the optical signal. These peaks have been assigned to $(CuCl_2)^-$ and $(CuCl_3)^{-2}$. Comparison of the integrated peaks areas indicated that in Ethaline both proposed copper speciations exist in almost equal amounts. Optical deflection analysis of DES electrochemistry presented here is complimentary to EXAFS data published by Abbott et al. on copper and silver ions speciation in Ethaline 200.[2] The origins of the two copper (I) speciations in Ethaline (in the Cu(I) potential window) is thought to be the same as in the case of silver.

The tin(II)chloride/Ethaline 200 system also involves the formation of metal chloro-complexes. However, in the case of tin, the optical analysis of the oxidation part of the redox cycle has been hampered by the metal ion concentration locally (i.e in the very confined space extending from the working electrode to the focal point) exceeding the solubility limit. Excess amount of tin, unable to complex with chloride, was presumed to form a precipitate which could not be detected by the optical deflection analysis.

Analysis of the bismuth(III)chloride/Ethaline 200 system excluded the possibility of underpotential deposition (UPD) which was previously reported for this

metal redox chemistry conducted in aqueous solvents. Prominent positive deflection of the optical signal has been observed at the commencement of the *cathodic* part of the cycle. Considering the experimental set-up used in this study, this type of signal is associated with the increase in the concentration of redox species and is typically observed in the *anodic* part of the cycle. Its occurrence prior to the reduction of bismuth ions to elemental metal is a strong evidence for the process of material removal. Considering high chloride concentration, this material is thought to be composed of chlorocomplexes. Single optical deflection peak observed upon dissolution of bismuth indicated that in Ethaline 200, this metal exist only as a single speciation. Based on the previous work on the subject, this speciation has been proposed to be $(BiCl_4)^-$.

Finally, the applicability of PBD to study co-deposition of metals from ChCl based DES has been investigated using systems of $AgCl/CuCl_2$ in Ethaline and $AgCl/BiCl_3$ in Ethaline as model examples due to these metals ease of plating combined with clearly separated redox potentials. During the electrodeposition of silver-copper alloy, both speciations of silver ($(AgCl_2)^-$ and $(AgCl_3)^{2-}$) as well as those of copper (proposed to be (($CuCl_2$)- and $(CuCl_3)^{2-}$) were observed in the oxidation phase. A considerable shift in the plating potentials of both metals has also been detected. Bi/Ag alloys have been historically electrodeposited from toxic, cyanide based plating baths. [10] Therefore, a successful deposition of Bi/Ag metallic layer from a benign and affordable electrolyte, like Ethaline can be considered to be a very valuable achievement.

Gravimetric experiments were preformed over a range of eutectics. All solvents tested shared choline chloride as the Quaternary Ammonium Salt (QAS) while the other component of the solvent, Hydrogen Bond Donor, was varied. The study allowed to determine the suitability of these novel solvents as electrolytes in conducting polymer based charge storage devices. Results highlighted Ethaline's potential for this application, particularly for charge storage devices operating at slow discharge rate. Redox dynamics of the PEDOT/DES systems seem to be controlled by the relative mobility of ions with PEDOT films displaying cation exchange, anion exchange and most interestingly, a mixture of both processes. This last effect was observed in PEDOT/Propaline and, although to somewhat lesser extent, in PEDOT/Acetaline systems. Symmetry of the process combined with the excellent stability, displayed by the first of these systems, holds great promise for a DES based actuators.

6.2 Future work

PBD has historically been combined with EQCM and although this approach yielded some very valuable data, unresolved issues remain particularly when analysing electrochemical reactions in novel type of solvent like DES. The biggest hindrance seems to be optical deflection method inherent lack of specificity which has already been mentioned. This can represent serious issues in data analysis if simultaneous flux of many species occurs. Additionally, in order to convolve the PBD data, assumptions have to be made as of the ions identity. This however could be resolved through the combination of the PBD with surface plasmon resonance or confocal Raman spectroscopy. Both of these techniques have been previously described to be suitable for monitoring the concentration changes in front of the working electrode but as working separately not in conjunction with the optical deflection methods. SPR is based on the measurement of the change in oscillations of surface electromagnetic waves (plasmons). When propagating on the boundary of metal and an external medium (for example on the electrode/electrolyte interface) these oscillations frequency changes with the gradient of refractive index.[11] The advantage of SPR lies in its ability to measure total concentration change including that of the solvent – this cannot be achieved by PBD acting on its own. However, the method is not without possible drawbacks as SPR is a highly surface specific technique.

Amatore et al. reported the use of confocal Raman spectroscopy to monitor the fluxes of the electroacitve species and proposed the existence of two separate layers in the diffusion layer, each with its own, exclusive ion population.[12] Raman spectroscopy technique is based on the measurements of changes in the vibrational states of the molecules and because of this feature the signal is not significantly affected by the absorption in the solvent. As the method is non- invasive and very well suited to probe composition of spatially resolved micrometric volumes inside a limited space (i.e diffusion layer) it may offer unique insight into the electrode/electrolyte dynamics. While the instrumental set-up may indeed be rather complex, a possible combination of Raman with PBD-EQCM could allow for the identification of specific ionic fluxes. Implementation of this technique would allow for the identification of multi-ion fluxes.

This would have a particular impact on the analysis of redox chemistry of Layer-by-Layer (LbL) electrodes where multi ion fluxes abound.

Application of ultra-microelectrodes (operating either in potentiometric or amperometric modes) to probe the diffusion layer of a larger electrode has already been explored in molecular electrolytes[13,14] but not in IL/DES and certainly not in conjunction with PBD. Application of WE/sensor electrode system may yield valuable data. Amatore and co-workers have confirmed that physical placement of an ultra-microelectrode inside the WE diffusion layer did not result in a significant alternation of the diffusion pattern.[7] Since ultra-microelectrodes operate in a different mode to WE they are often used to search for evidence of conproportionation reactions. Combination of this approach with PBD would allow observing the concentration profiles in two different layers of the diffusion layer possibly yielding an *in-situ*, full concentration profile. Another, yet unexplored but possibly simpler approach would be the use of ion specific electrodes, combined with or used exclusively as the working electrode.

To expand the technique to studies of the deposits morphology studies (for example polymer film thickness change observed during redox cycling due to ingress and egress of dopants) interferometric microscopy or ellipsometry could be combined with PBD. Interferometric microscope however, has been reported to have resolution of ca. 5 μm[7] which is insufficient to conduct a detailed morphology studies (with surface features usually being in the nm range) and thus would require significant improvements. Rishpon and co-workers have reported the application of ellipsometry/EQCM in the study of PANI films electrodeposition.[15] However, application of ellipsometry to study deposition from DES still awaits implementation. If developed, this technique would form an affordable, non-invasive alternative to SECM or electrochemical AFM.

FTIR-PBD combination has been used previously to study redox chemistry of polynaphtol and poly (o-aminophenol) films.[16] Application of this technique to observe DES and IL electrochemistry could provide much needed information about metal ion speciation (assuming a defined IR signature for each metal ion could be obtained prior to the electrochemical experiment). Therefore, since FTIR is a structural probe (and its

combination with EQCM has already been reported elsewhere[17]) it could be used to probe the dynamics of CP films solvation state upon redox cycling as well as detecting possible degradation signs. As of now, a possible FTIR-EQCM-PBD combination still awaits development and any kind of instrumental approach would have to overcome the different timescales used by FTIR and PBD.

Since optical deflection experiments rely on the data received from the position sensing detector located on the opposite side of the electrochemical cell than the laser, it is imperative that the electrolyte must not absorb at the wavelength used. Since most PBD experiments are conducted using He-Ne lasers (λ = 632.8 nm) any solution that absorbs wavelengths within this range (for example $CoCl_2$/Ethaline 200) cannot be analysed. To overcome this limitation and broaden the analysis range, use of UV or near-IR lasers would have to be implemented. McCreery and co-workers reported simultaneous PBD/UV-Vis spectroscopy studies. In their approach not only the deflection of the laser beam upon undergoing diffraction was monitored but also light absorption was measured allowing for the calculation of the real time concentration gradient. Combined with UV-Vis this methodology enabled also the spectroscopic analysis of the species present in the flux thus overcoming the non-selectivity issue of optical deflection when implemented on its own.[18]

Electrochemical Impedance Spectroscopy (also known as resistometry) is a very sensitive technique widely used in electrochemistry.[19] This method is based on the use of electrical equivalent circuit to model the reaction, which takes place at the electrode/electrolyte interface. Its application allows for the separation of faradaic and non-faradaic currents. The technique was initially applied to study electrodes capacitance in different polarization states to then progress into the studies of impedance. It has also been combined with SECM[14] as well as AFM[14] allowing for the simultaneous mapping of samples topography and its impedance. EIS has been so far applied to study biosensors design, dissolution and deposition of metals, monitoring of corrosion rates and corrosion inhibition studies, electrodeposition of conducting polymers and their redox chemistry, design of dye-sensitized solar cells, characterization of electron transport properties of various materials and the design of batteries and fuel cells. Aurbach and co-workers have reported a combined Probe Beam Deflection/Resistometry/X-ray Diffraction study of graphite sulphates redox chemistry

conducted in an aqueous electrolyte.[20] Graphite materials studied were modelled on composite powder electrodes, which are widely used in Li-ion secondary batteries. Improvement of such batteries performance can only be achieved by thorough understanding of the intercalation mechanism and capacity fading processes. Authors have successfully determined the degree of electrode's material intercalation using resistometry measurements. Graphite sulphate electrode'selectrical performance was monitored by cyclic voltammetry, system concentration changes by optical deflection and the electrode intercalation was observed by resistometry. The latter signal showed significant delay indicating that the structural changes influencing the intercalation were occurring on a much slower timescale than the electrochemical processes. As of now (2015) there are no known publications of PBD/EIS studies conducted in IL/DES environment therefore its application may reveal some previously unknown phenomena and give valuable insight into the performance of DES based systems like Zn/PEDOT/Ethaline 200 secondary batteries.[3]

Finally, areas that seem to be an excellent field for non-invasive techniques like PBD are still awaiting investigation. Liquid/liquid phase transport as well as ion transport across membranes (the latter usually monitored by conductivity measurements) both seem to be an obvious choice. These areas have not yet been a subject of optical deflection studies and the application of this technique could allow observing new, interesting phenomena.

6.3 References

1 Q. Zhang, K. D. O.Vigier, S. Royer and F. Jérôme, *Chemical Society Reviews*, 2012, **41**, 7108-7146.

2 A. P. Abbott, S. Nandhra, S. Postlethwaite, E. L. Smith and K. S. Ryder,*Physical Chemistry Chemical Physics*, 2007, **9**, 3735-3743.

3 A.R. Hillman, K.S. Ryder, C.J. Zaleski, C. Fullarton and E. L. Smith, *Z. Phys. Chem.* 2012, **226**, 1049-1068.

[4] C. A Barbero, M. C. Miras, *The Journal of the Argentine Chemical Society*, 2003, **91**, 1-40.

[5] M. J. Henderson, A. R. Hillman, E. Vieil, *Journal of Electroanalytical Chemistry*, 1998, **454**, 1-8.

[6] M. A. Skopek, M. A. Mohamoud, K. S. Ryder and A. R. Hillman, *Chemical Communications*, 2009, 935-937.

[7] G. G. Lang, C. A. Barbero, *Laser Techniques for the Study of Electrode Processes*, Berlin, 2012.

[8] A. R. Hillman, K. S. Ryder, V. C. Ferreira, C.J. Zaleski, E.Vieil, *Electrochimica Acta*, 2013, **110**, 418-427.

[9] C. D'Agostino, R. C. Harris, A. P. Abbott, L. F. Gladden and M. D. Mantle, *Physical Chemistry Chemical Physics*, 2011, **13**, 21383-21391.

[10] I. Krastev, T. Valkova and A. Zielonka, *Journal of Applied Electrochemistry*, 2004, **34**, 79-85.

[11] A. Raitman, E. Katz, A. F. Bückmann, I. Willner, Journal of the American Chemical Society, 2002, **124**, 6487-6496.

[12] C. Amatore, F. Bonhomme, J-L Bruneel, L. Servant, L. Thouin, *Electrochemistry Commuincations*, 2000, **2**, 235-239.

[13] C. Amatore, S. Szunerits, L. Thouin, *Electrochemistry Commuincations*, 2000, **2**, 248-253.

[14] C. Amatore, S. Szunerits, L. Thouin, J-S Warkocz, *Electrochemistry Commuincations*, 2000, **2**, 353-358.

[15] J. Rishpon, A. Redondo, C. Derouin and S. Gotttesfeld, *Journal of Electroanalytical Chemistry*, 1990, **294**, 73-85.

[16] H. J. Salavagione, J. Arias-Pardilla, J. M. Pèrez, J. L. Vázquez, E. Morallón, M. C. Miras, C. Barbero, *Journal of Electroanalytical Chemistry*, 2004,

[17] K. Shimazu, S. Ye, Y. Sato, K. Uosaki, *Journal of Electroanalytical Chemistry*, 1994, **375**, 409-413.

[18] C-C Jan, R. L. Mc Creery, *Analytical Chemistry*, 1986, **58**, 2771-2777.

[19] B-Y Chang, S-M Park, *Annual Review of Analytical Chemistry*, 2010, **3**, 207-229.

[20] M. D. Levi, E. Levi, Y. Gofer, D. Aurbach, E. Vieil, J. Serose, *Journal of Physical Chemistry B*, 1999, **103**, 1499-1508.